NASA/TM—2009-215524

Jet Noise Modeling for Suppressed and Unsuppressed Aircraft in Simulated Flight

James R. Stone, Eugene A. Krejsa, and Bruce J. Clark
Modern Technologies Corporation, Middleburg Heights, Ohio

Jeffrey J. Berton
Glenn Research Center, Cleveland, Ohio

March 2009

NASA STI Program . . . in Profile

Since its founding, NASA has been dedicated to the advancement of aeronautics and space science. The NASA Scientific and Technical Information (STI) program plays a key part in helping NASA maintain this important role.

The NASA STI Program operates under the auspices of the Agency Chief Information Officer. It collects, organizes, provides for archiving, and disseminates NASA's STI. The NASA STI program provides access to the NASA Aeronautics and Space Database and its public interface, the NASA Technical Reports Server, thus providing one of the largest collections of aeronautical and space science STI in the world. Results are published in both non-NASA channels and by NASA in the NASA STI Report Series, which includes the following report types:

- TECHNICAL PUBLICATION. Reports of completed research or a major significant phase of research that present the results of NASA programs and include extensive data or theoretical analysis. Includes compilations of significant scientific and technical data and information deemed to be of continuing reference value. NASA counterpart of peer-reviewed formal professional papers but has less stringent limitations on manuscript length and extent of graphic presentations.

- TECHNICAL MEMORANDUM. Scientific and technical findings that are preliminary or of specialized interest, e.g., quick release reports, working papers, and bibliographies that contain minimal annotation. Does not contain extensive analysis.

- CONTRACTOR REPORT. Scientific and technical findings by NASA-sponsored contractors and grantees.

- CONFERENCE PUBLICATION. Collected papers from scientific and technical conferences, symposia, seminars, or other meetings sponsored or cosponsored by NASA.

- SPECIAL PUBLICATION. Scientific, technical, or historical information from NASA programs, projects, and missions, often concerned with subjects having substantial public interest.

- TECHNICAL TRANSLATION. English-language translations of foreign scientific and technical material pertinent to NASA's mission.

Specialized services also include creating custom thesauri, building customized databases, organizing and publishing research results.

For more information about the NASA STI program, see the following:

- Access the NASA STI program home page at *http://www.sti.nasa.gov*

- E-mail your question via the Internet to *help@sti.nasa.gov*

- Fax your question to the NASA STI Help Desk at 301–621–0134

- Telephone the NASA STI Help Desk at 301–621–0390

- Write to:
  NASA Center for AeroSpace Information (CASI)
  7115 Standard Drive
  Hanover, MD 21076–1320

NASA/TM—2009-215524

Jet Noise Modeling for Suppressed and Unsuppressed Aircraft in Simulated Flight

James R. Stone, Eugene A. Krejsa, and Bruce J. Clark
Modern Technologies Corporation, Middleburg Heights, Ohio

Jeffrey J. Berton
Glenn Research Center, Cleveland, Ohio

National Aeronautics and
Space Administration

Glenn Research Center
Cleveland, Ohio 44135

March 2009

Acknowledgments

The authors were funded by contract NAS3–00178 and Task Order Number 10.

This work was sponsored by the Fundamental Aeronautics Program
at the NASA Glenn Research Center.

Level of Review: This material has been technically reviewed by technical management.

Available from

NASA Center for Aerospace Information
7115 Standard Drive
Hanover, MD 21076–1320

National Technical Information Service
5285 Port Royal Road
Springfield, VA 22161

Available electronically at http://gltrs.grc.nasa.gov

Contents

Jet Noise Modeling for Suppressed and Unsuppressed Aircraft in Simulated Flight

James R. Stone, Eugene A. Krejsa, and Bruce J. Clark
Modern Technologies Corporation
Middleburg Heights, Ohio 44130

Jeffrey J. Berton
National Aeronautics and Space Administration
Glenn Research Center
Cleveland, Ohio 44135

Summary

This document describes the development of further extensions and improvements to the jet noise model developed by Modern Technologies Corporation (MTC) for the National Aeronautics and Space Administration (NASA). The noise component extraction and correlation approach, first used successfully by MTC in developing a noise prediction model for two-dimensional mixer ejector (2DME) nozzles under the High Speed Research (HSR) Program, has been applied to dual-stream nozzles, then extended and improved in earlier tasks under this contract. Under Task 6, the coannular jet noise model was formulated and calibrated with limited scale model data, mainly at high bypass ratio, including a limited-range prediction of the effects of mixing-enhancement nozzle-exit chevrons on jet noise. Under Task 9 this model was extended to a wider range of conditions, particularly those appropriate for a Supersonic Business Jet, with an improvement in simulated flight effects modeling and generalization of the suppressor model. In the present task further comparisons are made over a still wider range of conditions from more test facilities. The model is also further generalized to cover single-stream nozzles of otherwise similar configuration. So the evolution of this prediction/analysis/correlation approach has been in a sense backward, from the complex to the simple; but from this approach a very robust capability is emerging. Also from these studies, some observations emerge relative to theoretical considerations.

The purpose of this task is to develop an analytical, semi-empirical jet noise prediction method applicable to takeoff, sideline and approach noise of subsonic and supersonic cruise aircraft over a wide size range. The product of this task is an even more consistent and robust model for the *Footprint/Radius (FOOTPR)* code than even the Task 9 model. The model is validated for a wider range of cases and statistically quantified for the various reference facilities. The possible role of facility effects will thus be documented. Although the comparisons that can be accomplished within the limited resources of this task are not comprehensive, they provide a broad enough sampling to enable NASA to make an informed decision on how much further effort should be expended on such comparisons.

The improved finalized model is incorporated into the *FOOTPR* code. MTC has also supported the adaptation of this code for incorporation in NASA's *Aircraft Noise Prediction Program (ANOPP)*.

Nomenclature

2DME	Two-dimensional mixer ejector nozzle
A	Nozzle area, m^2
ANOPP	Aircraft Noise Prediction Program
AR	Nozzle outer-to-inner area ratio, dimensionless
AST	Advanced Subsonic Technology
b	Empirical term in correlation of noise components at high velocity, dimensionless
BPR	Bypass ratio
C	Noise component coefficient, dB
c	Sonic velocity, m/s
C-D	Convergent-divergent
D	Characteristic diameter, m
DOD	Department of Defense
F	Empirical factor in shock noise relation, dB/deg
f	1/3rd-Octave-band center frequency, Hz
FAA	Federal Aviation Administration
FOOTPR	NASA GRC's Fortran code for noise prediction
GE	General Electric
GRC	NASA Glenn Research Center
HSR	High Speed Research
k	Convection coefficient
L	Length (axial distance), m
L_I	Axial length from secondary nozzle exit plane to primary nozzle exit plane, m
L_P	Axial length from primary nozzle exit plane to plug tip, m
LaRC	NASA Langley Research Center
LeRC	NASA Lewis Research Center
LSF	Linear scale factor, full-scale dimension divided by model-scale dimension
M	Mach number
$\dot{m}$	Mass flow rate, kg/s
MAR	Mixer area ratio (Ref. 1), dimensionless
MTC	Modern Technologies Corporation
N	Slope of component noise versus effective velocity
NASA	National Aeronautics and Space Administration

n_c	Convection velocity coefficient
OASPL	Overall sound pressure level, dB re 20 μPa
P	Total pressure, Pa
PR_I	Suppressed-to-unsuppressed wetted perimeter ratio of the inner (primary) stream of a coannular nozzle; this is defined as the wetted exit perimeter for the primary stream *with* chevrons (i.e., the sum of the center plug perimeter – if any – and the outer, chevron-serrated, perimeter of the of the primary stream annulus), divided by the wetted exit perimeter of the annular primary stream *without* chevrons (note this quantity is dimensionless, and is always greater than unity for nozzles with chevrons; and equal to unity for nozzles without chevrons)
PR_O	Suppressed-to-unsuppressed wetted perimeter ratio of the outer (bypass) stream of a coannular nozzle; this is defined as the wetted exit perimeter for the bypass stream *with* chevrons (i.e., the sum of the inner perimeter and the outer, chevron-serrated, perimeter of the of the bypass stream annulus), divided by the wetted exit perimeter of the annular bypass stream *without* chevrons (note this quantity is dimensionless, and is always greater than unity for nozzles with chevrons; and equal to unity for nozzles without chevrons)
R	Source-to-observer distance, m, or gas constant, m^2/s^2-K
RMS	Root-mean-square average
r_{pt}	Plug tip radius, m
S	Strouhal number, dimensionless
SAR	Suppressor area ratio (Ref. 1), dimensionless
SPL	1/3rd-Octave-band sound pressure level, dB re 20 μPa
T	Total temperature, K
t	Static temperature, K
UOL	Overall sound pressure level uncorrected for refraction, dB re 20 μPa
V	Characteristic velocity, m/s
V_e	Effective velocity for noise generation, m/s
$V_{I/O}$	Higher of inner stream or outer stream velocity, m/s
X_C	Empirical length scaling factor, m
X_s	Axial source location relative to outer stream nozzle exit, m
α	Turbulence convection correlation length factor, dimensionless
β	Shock strength
Δ	Difference in variable
ε	Root-mean-square error, dB
θ	Directivity angle (Fig. 2), deg (“thet” on some figures)
θ′	Effective directivity angle, accounting for refraction, deg
θ_F	Empirical angle scaling factor

θ_M	Mach angle, deg
ρ	Fully-expanded jet density, kg/m^3
ω	Density exponent

Subscripts	(Note that on some figures subscripts appear as regular text)
1	Inner boundary
2	Outer boundary
amb	Ambient conditions
c	Convection
comp	Noise component
cor	Corrected for source location
D	Downstream of plug
d	Design value
EE	Experimental/extracted
eff	Effective value, including perimeter ratio effect
eq	Equivalent
ex	Exit of nozzle
exp	Experimental value
f	Flight (or simulated flight)
h	Hydraulic
I	Inner stream
ISA	International Standard Atmosphere
j	Jet (single stream)
L	Large-scale turbulent mixing noise generated well downstream of nozzle exit (previously called merged mixing noise – subscript M)
M	Merged mixing noise (terminology of Task 9 and earlier)
mix	Isentropic mixed flow
Norm	Normalized
O	Outer stream (previously also used for outer shear layer mixing noise)
P	Inner stream plug separation
Pred	Predicted
S	Small-scale turbulent mixing noise generated near nozzle exit (previously called outer shear layer mixing noise – subscript O)
sh	Shock
supr	Suppressed

T	Transitional/intermediate-scale turbulent mixing noise generated in vicinity of end of potential core (previously called inner stream mixing noise – subscript O; analogous to premerged mixing noise of 2DME and internal mixer nozzles; subscript T no longer used for total noise)
th	Throat of nozzle

Introduction

The National Aeronautics and Space Administration (NASA) has long been involved in aircraft noise research and technology development and has on some occasions carried these activities to the level of engine system tests and even flight tests. The Department of Defense (DOD) and the Federal Aviation Administration (FAA) have traditionally looked to NASA for technology advancement in noise that may be applicable to DOD's needs. With the termination of the High Speed Research (HSR) and Advanced Subsonic Technology (AST) programs, NASA has been directed to focus on relatively advanced concepts that have high risk, but potentially high payoff. The nature of this work does not at present include significant near-term design effort building on the development engine system and flight tests of the past. Key experienced personnel are retiring without having the opportunity to work on design/development projects with their younger colleagues. Much of the practical knowledge and experience acquired in the 1970s and 1980s is in danger of being lost.

The Modern Technologies Corporation (MTC) has been supporting NASA and the aircraft propulsion industry by developing practical and easy-to-use semi-empirical predictive models for jet noise since 1995. MTC's efforts started with the very complicated two-dimensional mixer ejector (2DME) nozzles of the HSR program (Ref. 1), which had so many complicated features that the semi-empirical approach was necessitated. The product of this effort is now a part of the design and data reduction software of General Electric (GE) and is included in the Aircraft Noise Prediction Program (ANOPP) of NASA Langley Research Center (LaRC) and the NASA Glenn Research Center (GRC) *Footprint/Radius (FOOTPR)* code.

Of perhaps as much value as the predictive code itself are the methods and experience acquired in analyzing and correlating noise data involving multiple sources. This methodology involves first using a relatively crude model to predict the *relative* levels of the various noise components, using this model to deduce individual components and then correlating those components; iteration results in rapidly improving predictive models. As MTC has applied this approach to relatively simpler coannular nozzle configurations, the value of this approach has been demonstrated with accurate predictive models developed first for high bypass ratio (BPR) nozzles, including suppression features, for subsonic aircraft (Refs. 2 to 4) and then generalized to cover low BPR supersonic cruise applications (Refs. 5 and 6). The approach used in developing this model might be called "hybrid experimental/empirical," but relevant elements of theory are utilized to the extent considered practical. As this work has evolved, in reverse, from complex to simple, MTC has attempted to relate the empirical relations as much as possible to theory.

In the current task the approach is applied to the even simpler single stream nozzles, and further comparisons of the empirical relations with theoretical relations are made. Progress in relating the empirical/applied models to theory indicates that the development of a fundamentally-sound jet noise reduction design guide is now feasible.

NASA uses state-of-the-art system noise prediction codes to analytically calculate the noise levels of aircraft. FAA certification noise levels, airport-vicinity noise footprints, climbout, and en route noise levels all may be calculated with these computer models using a variety of noise metrics. These analysis tools (namely the LaRC *Aircraft Noise Prediction Program (ANOPP)* (Ref. 7) and GRC *FOOTPR* (Ref. 8) codes) compute spectral, one-third octave band sound pressure levels from several aircraft noise sources for both static and in-flight conditions. The source noise models are generally semi-empirical, using real physical scaling laws that are calibrated with measured test data. The coded prediction structure is flexible enough that new methods may easily be added to the system. A new source noise model that more accurately predicts both subsonic and supersonic jet noise and that incorporates new noise suppression features for single-stream and dual-stream nozzles is the focus of this report.

The approach MTC has employed in these tasks, summarized in Reference 6, is to use an initial predictive model based on analogy to relatively simple semi-empirical expressions derived mainly from the theory of Lighthill (Refs. 9 and 10) for circular jets. We assume that even for complex geometries subsonic jet noise will correlate in a manner analogous to the classical model (also taking into account the

theoretical developments of Ffowcs-Williams (Ref. 11) and Goldstein and Howes (Ref. 12)), if the proper characteristic velocity and characteristic length can be established. For supersonic jet cases, we assume that the subsonic mixing noise relations may be extrapolated and that the additional shock/turbulence interaction noise can be correlated with a model similar to that of Harper-Bourne and Fisher (Ref. 13), again assuming that characteristic velocity and characteristic length can be established.

A persistent problem in developing predictive models is in obtaining good quality experimental data. Noise generated in the experimental facility upstream of the test nozzle: valves, elbows, obstructions, and especially the combustor can contribute significant noise, and much of this noise is of a broadband nature, easily confused with jet noise. Muffling of these sources is costly in terms of size as well as expense, and it is particularly difficult in flight simulation facilities, where compactness of hardware is very important, as discussed by Viswanathan (Ref. 14). Ahuja (Ref. 15) has recently documented the difficulties in obtaining good quality data even for static testing. Another feature of our approach is that all the analyses are conducted with *lossless,* rather than Standard Day spectra, as is often done in industry. We feel that it is important to isolate the effects of as many physical processes as practical.

Free-jet flight simulation facilities are very useful, and can provide meaningful data so long as that data can be analytically transformed to the flight frame of reference. The different methodologies used by NASA and industry to perform this transformation produce very different results, especially in the rear quadrant; this compelled us to rely largely on static data to develop our model, but we showed reasonable agreement with simulated flight data when these transformation issues are considered (Refs. 3 to 6).

Based on recent analyses and past experience, seven potential source mechanisms must be assessed and preliminary models are available from Task 9 (Ref. 6), as discussed in the following section.

Predictive Model

The general dual-stream nozzle geometry and the mixing noise generation regions modeled are illustrated in Figure 1. Inner stream flow separation from the plug was also found to be a significant source (Refs. 3 to 6). When the exhaust conditions of either or both streams are supersonic, shock noise becomes significant, and we use an updated model structurally similar to that currently in *FOOTPR* (Ref. 6). In generalizing the predictive model to include single stream cases, this terminology becomes awkward and should be replaced by a more fundamental description as follows.

The lowest frequency component, previously called “merged mixing noise” (subscript M) for multiple-stream nozzles and generated well downstream of the nozzle exit, is most likely due to the mixing of the coherent large-scale turbulent structures of the jet with the ambient; so it is now called “large scale mixing noise,” denoted by the subscript L. The relatively high frequency mixing noise generated near the nozzle exit, previously called “outer shear layer mixing noise” (subscript O) is likely due to the small-scale turbulent mixing in the initial shear layer(s); so it is now called simply “small scale mixing noise,” denoted by the subscript S. The most difficult to characterize mixing noise component, needed to completely correlate dual-stream mixing noise (Refs. 4 to 6) and also identified by Fisher, et al. (Refs. 16 and 17), occurs primarily at middle-to-high frequency and was previously called “inner stream mixing noise” (subscript I). Comparisons and discussion to follow support the notion that this is analogous to what has been termed “premerged mixing noise” in many analyses of suppressor nozzles (e.g., Ref. 1) and internal mixer nozzles (e.g., Ref. 18). We now label this component “transitional/intermediate scale mixing noise,” denoted by the subscript T. The large scale mixing and small scale mixing components may very well be amenable to theoretical/computational modeling in the near future, and the empirical models herein may be replaced, but it is more likely that for system design purposes the computationally faster empirical approach will be retained in as close to theoretically-based formulation as possible. In contrast, the transitional/intermediate scale turbulent mixing noise is likely to be very difficult to characterize from first principles in the near term although some progress was made for the 2DME in relating the noise characteristics to the measured flow field characteristics (Ref. 19), which may be predictable by Computational Fluid Mechanics. Also potentially contributing is “inner-stream plug separation noise” (Refs. 4 to 6, 20) at high frequency, denoted by the subscript P. The shock

noise relations are essentially as in Reference 6, but with some renaming: the module that was called inner stream shock noise (subscript I,sh) is now also applied to single-stream shock noise (subscript sh); outer-stream shock noise (subscript O,sh) and downstream merged (beyond plug tip) shock noise (subscript D,sh) (e.g., Ref. 21) are used only for dual-stream configurations under specific circumstances.

Source Locations

Experimental jet noise measurements are typically made at a distance far enough from the nozzle to be in the far field of any individual noise source region, but not far enough away to treat the entire exhaust plume as a point source at the center of the nozzle exit plane, as is usually assumed in determining the directivity angle. The prediction procedures must take this difference into account. A simple method is used (Refs. 3 to 6) herein to approximate these source location effects for the different sources. The geometric relations for noise sources downstream of the nozzle exit plane (the outer stream exit plane is used for dual stream nozzles) are given in Figure 2. The relationship of the actual (corrected) source-to-observer distance, R_{cor}, to its apparent value, R, for a source at distance, X_s, downstream of the exit plane is as follows

$$(R_{cor}/R)^2 = 1 + (X_s/R)^2 + 2\,(X_s/R)\cos\theta \tag{1}$$

The relationship of the corrected angle, θ_{cor}, to its apparent value, θ, is then

$$\theta_{cor} = \cos^{-1}[(R/R_{cor})\cos\theta + X_s/R_{cor}] \tag{1a}$$

$$\Delta\theta = \theta_{cor} - \theta \tag{1b}$$

$$\Delta SPL = -\,20 \log (R_{cor}/R) \tag{1c}$$

In reality the noise received at any point in the far field comes from multiple locations within the source region as a function of frequency, but reasonably accurate predictions can be made with a simple model wherein the source location variation with frequency is assumed to be less important than the variation with angle. Essentially the model accounts for the location, for each component, from which the peak of the noise spectrum at that angle appears to radiate. These corrections differ for each component, because the source positions are different. The simplification of assuming no change in source location as a function of frequency at each far field angle is generally adequate because each component contributes only over a limited frequency range; however, it is quite feasible to introduce frequency dependence if needed, as it might very well be to deal with airframe installation effects. Such an approach was used for ejector internal sources in Reference 1. These source locations must be accounted for in the correction for free jet shear layer effects (Ref. 22), as shown in References 4 to 6.

Mixing Noise Components

Any jet mixing noise source region is treated as a round jet of appropriate nozzle exit area at the appropriate conditions. Similar reasoning is used for all the mixing noise components. For a general mixing region the overall level, uncorrected for refraction, UOL, is given by the following

$$\begin{aligned} UOL = {} & C + 10 \log [(\rho_{amb}/\rho_{ISA})^2\,(c_{amb}/c_{ISA})^4] + 10 \log (A/R_{cor}^2) + 10\,\omega \log (\rho/\rho_{amb}) \\ & + 10 \log [(V_e/c_{amb})^N/\{1 + b\,(V_e/c_{amb})^{N-3}\}] - 5\,k \log [(1 + M_c \cos\theta_{cor})^2 + \alpha^2\,M_c^2] \end{aligned} \tag{2}$$

Where C is the coefficient and N the velocity slope, both determined experimentally and then correlated, A is the appropriate nozzle exit area, and ρ is the fully-expanded jet density for that region. The convection coefficient k has been taken as 3 in our past work based on the theory of Goldstein and Howes (Ref. 12); whereas according to Ffowcs Williams (Ref. 11) it should be 5; our current model uses k = 4. In the past $\alpha = 0.2$ has been assumed, but this will be investigated. Note that the Doppler term, $-10 \log [1 - M_f \cos \theta_{cor}]$ has been eliminated; this results from comparisons with the data of Reference 23. The repeatability and consistency of those data is such that it can be deduced that better agreement between static and simulated flight data is obtained if this term is eliminated. The simulated flight transformation includes a Doppler correction, so it appears that the relations presented herein do model the flight situation, but this should be validated by comparison with actual flight data. Note that the velocity term now features a limiting behavior, producing a 30 slope versus the logarithmic velocity parameter at very high velocity, while retaining the N slope, where N is on the order of 8, at low velocity, resulting in an 80 slope. This change of slope at high velocity is somewhat consistent with our recent correlations using different slopes at high and low velocity, but it is further motivated by our intent to develop relationships of very wide applicability now, and is consistent with the correlation of von Glahn (Ref. 24), which included rocket data. Essentially the same relation, but with N = 7.5 was used in the initial ANOPP jet noise model (Ref 25). Note that angle of attack effects are not yet included. The effective velocity for noise generation, V_e, is in most cases calculated as follows

$$V_e = V [1 - M_f (c_{amb}/V)]^{1/2} \tag{2a}$$

Where V is the characteristic velocity for this region. This expression has evolved from earlier relations wherein jet noise was assumed to vary with relative jet velocity to a relatively high power, typically 5th or 6th, times absolute jet velocity to a somewhat lesser power, typically 2nd or 3rd, preserving the overall 8th power expected (Refs. 9 and 10). Most of our earlier relations (e.g., Ref. 26) split the velocity effect as 2/3 relative and 1/3 absolute; the current even split is somewhat more conservative, yielding a smaller in-flight reduction of jet noise than the earlier relations.

The effect of jet temperature or density on noise has also been a matter of contention, and is rather complicated even for a single subsonic static round jet. It is generally accepted that in the case of the hot jet the noise generated is due to two source terms quadrupole and dipole, with the dipole term contributing more strongly as jet temperature increases (or as density decreases) and as jet velocity is reduced. Thus for cold jets the 8th power velocity effect is observed even to low velocity, while for hot jets at low velocity the jet velocity dependence reduces to a 5th or 6th power. Although such behavior can be explained on a theoretical basis, in an experiment it is difficult to separate this relative increase in noise with increasing temperature at low velocity from the contamination from upstream noise sources. This problem has long been recognized (Ref. 27) and must still be considered (Ref. 3). The approach to quantifying this effect, as suggested by Ahuja and Bushell (Ref. 27), has been to assume that the density effect on noise can be correlated by a variable exponent ω as a function of velocity, i.e., OASPL $\propto 10\ \omega \log (\rho/\rho_{amb})$, where ω is tabulated as a function of nondimensionalized jet velocity, V/c_{amb}. In our work (e.g., Refs. 1 and 26) we have used a simple algebraic expression for this density exponent, as follows

$$\omega = 3 (V_e/c_{amb})^{3.5}/[0.6 + (V_e/c_{amb})^{3.5}] - 1 \tag{2b}$$

However, in some of our recent work (Refs. 4 to 6) we considered other approaches where ω might be constant for some source regions. The resulting expressions are different for the different components.

The convective Mach number, M_c, is calculated from the following relation

$$M_c = n_c [(V/c_{amb}) - M_f] \tag{2c}$$

In our recent work (Refs. 4 to 6) initially n_c was assumed constant at 0.62, as has been assumed in many early models. We found that using a variable n_c was quite helpful. Such variations could be related to flow-acoustic interaction, or "flow shielding." These considerations are explored more thoroughly by Gliebe, et al (Ref. 28).

The effect of refraction is incorporated in the spectral directivity relations in an empirical manner, but crudely in the direction suggested by theory. The relative sound pressure level, SPL – UOL, is correlated as a function of the effective directivity angle, θ', and the logarithmic Strouhal number, log S, where the Strouhal number is calculated as follows

$$S = (f\,D/V_e)\,(T/T_{amb})^{0.4\,(1\,+\,\cos\,\theta')} \tag{3}$$

Where D is the characteristic diameter, typically $(4A/\pi)^{0.5}$, and T is the region total temperature. Analogously to the level relation (Eq. (2)), the Doppler factor, $[1 - M_f \cos\,\theta_{cor}]$, is no longer included, except for the plug separation noise component; flight comparisons will determine whether it should be or not. The effective angle, to account for refraction effects, is calculated as follows

$$\theta' = \theta_{cor}\,(V/c_{amb})^{0.1} \tag{3a}$$

It is by use of this effective directivity angle that, in a very simple and approximate way, refraction is accounted for. It is assumed that the spectra for widely differing jet velocities are similar at this adjusted angle rather than at the same geometric angle. This approach, in conjunction with the analytically modeled convection effect in Equation (2), correlates the variation of SPL with frequency and angle rather well, as shown later herein. The resulting spectral directivity tables are developed iteratively as further discussed later in this report.

The source location for a mixing region noise, X_s, is as follows

$$X_s = [L + (X_C + \theta/\theta_F)\,D]/LSF \tag{4}$$

L is the displacement of the start of the mixing region from the fan nozzle exit plane, while X_C and θ_F are empirical length and angle scaling factors. LSF is the linear scale factor, full-scale dimension divided by model-scale dimension. The uncorrected angle, θ, is used here to start the correction process in closed form. Even though the experimental data are scaled to the correct size for comparisons, the linear scale factor is used in conjunction with the experiment geometry to correct the predictions for the effect of source location.

Shock Noise Components

The relationships used to predict any shock noise component $OASPL_{sh,}$ for $M \geq 1.0$, is as follows

$$\begin{aligned} OASPL_{sh} = C_{sh} &+ 10\,\log\,[(\rho_{amb}/\rho_{ISA})^2(c_{amb}/c_{ISA})^4] + 10\,\log\,(A/R_{cor}{}^2) \\ &+10\,\log\,\{\beta^4/(1+\beta^4)\} - 40\,\log\,(1 - M_f \cos\,\theta_{cor}) - F\,(\theta_{cor} - \theta_M) \end{aligned} \tag{5}$$

Where β is the shock strength and the ambient property and area/distance terms also used in the internal mixing noise relations have the same meaning. The shock strength parameter β is calculated as follows

$$\beta = [(M^2 - M_d{}^2)^2 + 0.01\,M_d/(1 - D_1/D_2)]^{1/4} \tag{5a}$$

Where M is the particular stream Mach number expanded to ambient conditions and M_d is the design Mach number. D_1 is the inner diameter and D_2 is the outer diameter for the stream under consideration. The term $0.01\ M_d/(1 - D_1/D_2)$ is included to prevent a singularity at $M = M_d$, where β is at its minimum. The intercept C_{sh} may be dependent on geometry. The Mach angle is denoted by θ_M, calculated as follows

$$\theta_M = 180 - \sin^{-1}(1/M) \text{ (in degrees)} \tag{5b}$$

(Note on terminology: θ_M will always have an additional subscript; otherwise the subscript M on other variables refers to the merged region.) The term $F(\theta_{cor} - \theta_M)$ is calculated as follows

$$\left.\begin{aligned} F(\theta_{cor} - \theta_M) &= 0.0 && \text{for } \theta_{cor} < \theta_M \\ F(\theta_{cor} - \theta_M) &= 0.75(\theta_{cor} - \theta_M) && \text{for } \theta_{cor} \geq \theta_M \end{aligned}\right\} \tag{5c}$$

Spectral directivity effects are calculated next. The relative sound pressure level, $SPL_{sh} - OASPL_{sh}$, is given in tabular form as a function of the directivity angle θ and the logarithmic Strouhal number $\log S_{sh}$. The Strouhal number is calculated as follows

$$S_{sh} = [f\beta D_h/(0.7V)]\,(1 - M_f \cos\theta_{cor})\{[1 + (0.7\ V/c_{amb})\cos\theta_{cor}]^2 + \alpha^2(0.7\ V/c_{amb})^2\}^{1/2} \tag{6}$$

It may very well be that the tables eventually developed will be different for under-expanded and over-expanded cases, but at present this is not the case.

The source location for shock noise, $X_{s,sh}$, is as follows

$$X_{s,sh} = [L + 2\ D_h\,(M^2-1)^{1/2}]/LSF \tag{7}$$

Since the characteristic dimensions for shock noise components are typically the exit dimensions of a convergent-divergent nozzle, while the characteristic dimensions for mixing noise are typically those of the nozzle throat, up to eight diameters are needed to fully describe the geometry of a nozzle as complex as a coannular, convergent-divergent plug nozzle.

Component Extraction Examples

The process of component noise separation and coefficient adjustment is illustrated in the following. Examples are shown here and in References 4 to 6 for a wide enough range of situations to give the reader an appreciation of the power of this approach and the issues that must be addressed in its application. The experimental/extracted component SPLs are obtained from the following relation for each component: $SPL_{comp,EE} = SPL_{exp} - (SPL_{Pred} - SPL_{comp,Pred})$. There are adjustments made; the component coefficients are adjusted, generally by a small amount to minimize errors, but no adjustments are made to the spectral directivity relations. Since several examples of this sort have been shown for coannular nozzles in the previous task (Ref. 6) and the predicted spectral directivity relations are only slightly different (and those differences mainly confined to extremes in angle and frequency), the examples shown here are for single-stream nozzles. The cases shown in Reference 6 include subsonic and supersonic cases with both inverted and conventional velocity profiles and also include suppression modifications to both streams.

Shock-Free Conical Nozzle

A near-static case for a small model in the Lockheed Georgia anechoic chamber (Ref. 29) for a relatively high subsonic jet velocity, $V_j/c_{amb} = 0.98$ is shown in Figure 3 for four far-field locations: forward quadrant, $\theta = 90$ deg (Fig. 3(a)), $\theta = 120$ deg (Fig. 3(b)), $\theta = 135$ deg (Fig. 3(c)), and near the

peak noise angle in aft quadrant at θ = 150 deg (Fig. 3(d)). (The low M_f is the result of the pumping effect of the small model jet on the facility free jet. Because of the very low M_f no shear layer corrections are made.) The coannular nozzle relations (essentially Ref. 6) are used, but with the conical nozzle conditions and parameters used for each component. The measured noise spectra (SPL_{exp}) are shown by the heavy solid line (unsmoothed); the downstream/merged noise spectra ($SPL_{L,EE}$) are indicated by the ○ symbols connected by the dashed curve, the initial/outer shear layer noise spectra ($SPL_{S,EE}$) are indicated by the □ symbols connected by the dotted curve and the intermediate/transitional (inner stream) noise spectra ($SPL_{T,EE}$) are indicated by the ◇ symbols connected by the dot-dash curve. Data are not usually plotted if $SPL_{comp,EE} - SPL_{exp} \leq -10.0$ dB, since such data are not meaningful; where such low values are shown, it is simply to show that the particular component does not contribute significantly at that angle. Comparisons are only meaningful for the dominant component at each frequency and angle. It should be noted that regardless of whether or not component levels are plotted, using this method of extraction, the antilogarithmic sum of the components always equals the total SPL, whether experimental or predicted. Comparing the plots at the four angles shows that the various components have different directivity effects.

The magnitude of the adjustment applied to the total experimental SPLs to yield the component values can be seen by comparing the extracted component spectra with the total. At all angles for this test case the downstream/merged mixing noise is dominant over most of the spectrum, but the outer shear layer does contribute at high frequency. For other cases the other noise components can also become important, depending on test conditions and geometry. Where the extracted component SPL is within 4.0 dB of the total, the data are correlated in normalized spectral form, as discussed later herein. The values of the corrected effective directivity angles for each noise component are noted on these figures: for large scale (previously called merged) mixing noise, θ'_L = thet′L (on figure 3); for small scale (previously called outer shear layer) mixing noise, θ'_S = thet′S (on figure 3); and for transitional/intermediate scale (previously called inner stream) mixing noise, θ'_T = thet′T (on figure 3). Since for this particular case for all these components, the $(V_e/c)^{0.1}$ is close to 1.00, $\theta_{comp} \cong \theta'_{comp}$, and the magnitude of the correction due to source location can be seen.

Once the noise spectra have been broken down into their components, the experimental/extracted components can be compared with prediction, as shown in Figure 4, for the same case as in Figure 3. The same symbols are used for each component as in Figure 3, but now the corresponding curves are the predicted values. The coefficients for the various components, C_L, C_S, and C_T, are adjusted to minimize the average error (experimental minus predicted) at all angles where the data are considered valid, over the frequency range where that component is most important. The adjusted values of the component coefficients are shown on each such figure. (Note that as the coefficients change relative to each other, the correction $SPL_{comp,EE} - SPL_{exp}$ as a function of frequency and angle, also changes.) Fairly good agreement between experimental/extracted and predicted spectra can be seen, but not as good as seen in recent coannular nozzle cases. Considering that these 27-year-old data were obtained in a fairly small facility with a small (5-cm diameter) nozzle, these results are encouraging with regard to the likelihood that a "universal" correlation may be achievable.

Similar comparisons for a higher jet velocity, but still subsonic due to elevated temperature, are shown in Figures 5 and 6 for similar-vintage data from the NASA Lewis Research Center (LeRC, predecessor to GRC, Ref. 30) dual-stream hot-jet facility. These tests were made with a coannular nozzle having no flow in the outer stream. For this outdoor facility, both ground and pole-mounted (nozzle centerline level) microphones were used; both were corrected analytically and merged—low frequencies from the ground microphones and high frequencies from pole microphones, with variably-weighted averaging at middle frequencies. The conical nozzle was 10-cm diameter, twice the linear dimension and four times the area of the nozzle for which data are shown in Figures 3 and 4. With the larger size and higher jet velocity, the contributions of the small scale mixing and intermediate/transitional mixing are more significant although the large scale mixing is still the most important. In terms of full-scale perceived noise level, the intermediate/transitional contribution is probably significant.

Conical Nozzle With Shock Noise

Similar analyses for a static case from GE's anechoic free-jet facility, scaled to nominal full size on a 2400-ft sideline at takeoff conditions, $V_j/c_{amb} = 2.11$ and $M_f = 0.0$ (Ref. 31), are shown in Figures 7 and 8. The adjustments to the mixing noise components are C_L –1.0, C_T –2.0, C_S +4.5, with C_{Sh} exactly as predicted. Shock noise is very dominant at θ = 40 deg (Fig. 7(a)); shock noise is the controlling component from 100 to 1000 Hz. Shock noise is also dominant at θ = 70 deg (Fig. 7(b)), but not as dominant over mixing noises as at θ = 40 deg. Also apparent at θ = 70 deg is a tone in the vicinity of 159 Hz, probably due to shock "screech," a common problem with small nozzles. At θ = 100 deg (Fig. 7 (c)) the large-scale turbulent mixing noise is dominant up to 316 Hz, with shock noise dominant at 400 to 500 Hz, transitional-scale turbulent mixing noise dominant at 800 to 1590 Hz, and small-scale turbulent mixing noise dominant at 2512 to 5010 Hz. From about 251 to 2512 Hz, no individual component is within 2.0 dB of the total, which illustrates how difficult it can be to isolate and then correlate individual components. Similar results are seen at θ = 120 deg (Fig. 7(d)), but with shock noise becoming a less than significant contributor. At the aft angles, θ = 140 and 160 deg (Fig. 7(e) to (f)), large-scale turbulent mixing is dominant over most of the spectrum, but a hump can be seen in the 159 to 200 Hz range. Whether this hump is due to a tone, like the "screech" tone evident in the forward quadrant, or an additional mechanism such as large eddy Mach wave radiation, is uncertain. The level of agreement shown in Figure 8 was achieved by changing α from 0.2 to 0.3, which has a significant effect only in the rear quadrant. Note that for the cases previously analyzed in References 4 to 6 the change in α does have a small, but noticeable effect; experimental/extracted component coefficients typically change by a few tenths of a dB.

Component Correlations

The same extraction and coefficient adjustment approach demonstrated in the foregoing section was applied to an more extensive set of data from References 23, and 30 to 34 used in Reference 6 as well as single stream conic and convergent divergent (C-D) nozzle data from Reference 29. This includes reevaluation of representative cases previously analyzed in Reference 6 to assure that the changes made to the predictive model to cover a wider range of conditions and geometries do not degrade the agreement demonstrated in the earlier comparisons. The baseline (unsuppressed) configurations are considered first, with the expectation that the changes will be minor for the relatively dominant merged mixing and outer shear layer mixing noise components and that some further improvements and/or simplifications may be found for the less dominant components. The change of α from 0.2 to 0.3 is used throughout. New correlations for the coefficients are developed in this section.

For all the components, adjusted spectral directivity relations are developed, although these changes for most components are relatively small with respect to the relations of Reference 6. These tables are given for large scale mixing noise (formerly merged mixing noise) in Table I, for small scale mixing noise (formerly outer shear layer mixing noise) in Table II, for transitional/intermediate scale mixing noise (formerly inner stream mixing noise) in Table III, for inner stream plug separation noise in Table IV, for plug/downstream shock noise in Table V, for outer stream shock noise in Table VI, and for single stream or inner stream shock noise in Table VII. Since our previous reports have include a number of comparisons of the normalized experimental/extracted spectra with the tabulated values, further spectral comparisons herein will be limited to comparisons of total predicted spectra with experimental values, with predicted component levels shown to indicate the relative contributions of the different source mechanisms.

Note that, as in Reference 6, the effects of nozzle exit mixing enhancement modification are correlated only in terms of influence on levels and not the spectra, so simple "delta" correlations are all that is justified, at present, to represent the observed reductions in merged noise at the expense of small increases in the higher frequency components. However, there is some evidence of small spectral and

directivity effects, particularly on merged mixing noise, and an approach to modifying the relations is discussed. As in the previous model (Ref. 6), it is assumed, for correlation purposes, that the effects of outer nozzle chevrons is additive to that for inner nozzle chevrons. The chevron effects are correlated in terms of perimeter ratio, where the perimeter ratio for each stream is defined as the ratio of the total wetted perimeter for that stream (i.e., both inner and outer perimeters) divided by the total wetted perimeter for the unsuppressed annular passage.

Regarding statistics to be cited below, in comparing repeat tests for the nominal BPR = 5 external plug nozzle (Conf. 3BB, Ref. 23) at $V_{mix}/c_{amb} = 1.072 \pm 0.014$ and $M_f = 0.28$, 3BB-549 relative to 3BB-396, the following is observed: the average error in OASPL is –0.8 dB, while the standard deviation is 0.7 dB and RMS error is 0.8 dB. When the data at all frequencies and angles are considered, they show an average error of –0.9 dB, with standard deviation and RMS error both 1.2 dB. Breaking this down into low, middle and high frequency ranges, the corresponding error results are –0.8, 1.0 and 0.9 dB from 50 to 500 Hz (where large scale mixing is generally dominant); –0.9, 1.3 and 1.3 for 631 to 1995 Hz (where transitional and small scale mixing are generally dominant); and –1.0, 1.7 and 1.7 for 1995 to 3980 Hz (where small scale mixing and/or plug separation are generally dominant).

Large Scale Mixing Noise

In Reference 4 several different assumptions regarding the density exponent ω_L (ω_M in earlier models) were investigated. Because of the range of test conditions included there was a significant range of temperature and velocity, so the method of correlating density effects was quite significant. Considered were $\omega_L = 0.0$, 1.0, and 2.0, as well as the variable ω_L (from Equation (2b)). The variable ω_L was found to provide the most satisfactory correlation, yielding the simplest velocity effect. In Reference 6, a small effect of nozzle extension was included that now does not appear appropriate. With the generalized convection formulation, the normalized baseline (unsuppressed) large scale mixing noise overall level is defined as follows

$$\begin{aligned} UOL_{L,Norm} = UOL_L - 10 \log [(\rho_{amb}/\rho_{ISA})^2 (c_{amb}/c_{ISA})^4] - 10 \log (A_L/R_{cor,L}^2) - 10\, \omega_L \log (\rho_L/\rho_{amb}) \\ + 20 \log [(1 + M_{c,L} \cos \theta_{cor,L})^2 + 0.09\, M_{c,L}^2] \end{aligned} \quad (8)$$

Where, analogous to Reference 6

$$\omega_L = 3\, (V_{e,L}/c_{amb})^{3.5}/[0.6 + (V_{e,L}/c_{amb})^{3.5}] - 1 \quad (8a)$$

$$V_{e,L} = V_{mix}\, [1 - M_f\, (c_{amb}/V_{mix})]^{1/2} \quad (8b)$$

$$M_{c,L} = n_{c,L}\, [(V_{mix}/c_{amb}) - M_f] \quad (8c)$$

$$n_{c,L} = 0.4/(1 + 1.5\, \{V_O/V_I\}^4) + 0.3 \qquad \text{(Dual-stream nozzle)} \quad (8d)$$

$$n_{c,L} = 0.460 \qquad \text{(Single-stream nozzle)} \quad (8e)$$

$$A_L = A_I + A_O \qquad \text{(Dual-stream nozzle)} \quad (8f)$$

$$A_L = A_I \qquad \text{(Single-stream nozzle)} \quad (8g)$$

$$V_{mix} = (\dot{m}_I V_I + \dot{m}_O V_O)/(\dot{m}_I + \dot{m}_O) \qquad \text{(Dual-stream nozzle)} \quad (8h)$$

$$V_{mix} = V_I \qquad \text{(Single-stream nozzle)} \quad (8i)$$

$$\rho_L = P_{amb} / (R\, t_{mix}) \tag{8j}$$

$$t_{mix} = T_{mix} - (\gamma - 1)\, V_{mix}^2/(2\gamma R) \tag{8k}$$

$$T_{mix} = (\dot{m}_I T_I + \dot{m}_O T_O)/(\dot{m}_I + \dot{m}_O) \qquad \text{(Dual-stream nozzle)} \tag{8l}$$

$$T_{mix} = T_I \qquad \text{(Single-stream nozzle)} \tag{8m}$$

Note that the areas are isentropically fully-expanded and that jet properties are fully-expanded and mass averaged. In this case, the large scale merged density, ρ_L, is computed using the ideal gas state equation with the mass averaged specific heat ratio γ and gas constant R along with the merged static temperature t_{mix} (which is in turn computed with isentropic relations using the mass averaged total temperature and V_{mix}). Strictly, the mixed jet velocity should be computed via a bona fide thermodynamic mixing analysis rather than the simple averaging method specified above. A true velocity mixing analysis could improve the quality of the correlation and this effect could be explored in future studies. Of course for a single stream nozzle, the mass averaged conditions are simply those of that (inner) stream conditions with $A_O = V_O = \dot{m}_O = 0$. Also for the single-stream case, $n_{c,L}$ is calculated for $V_O/V_I = 1.00$, yielding $n_{c,L} = 0.460$; this is a significant change from the 0.620 value used in our earlier single-stream formulations, but it appears to be consistent with the new assumptions of $k = 4$ and $\alpha = 0.3$.

Values of this normalized large scale mixing noise level are plotted against the nondimensionalized effective jet velocity parameter log $(V_{e,L}/c_{amb})$ and found to correlate well. The two-segment approach used in References 4 to 6 would be adequate, but in attempting to make our relations as general as possible, the predicted values of UOL_L as a function of the velocity parameter for several different approaches are compared in Figure 9. The two-segment approach for dual-stream nozzle merged mixing noise from Task 9 (Ref. 6) is shown by the solid line connecting circle symbols; the relation for the 2DME merged mixing noise at sideline orientation (Ref. 1) is shown by the dashed line connecting square symbols; the original ANOPP jet noise relation for OASPL is shown by the dotted line connecting triangle symbols; and the conventional-profile coannular nozzle OASPL relation is shown by the dash-dot line connecting diamond symbols. Since the OASPL of these jets is controlled by the merged/large-scale contributions, these comparisons are valid. Since the formulation of the original ANOPP model was based partially on the correlation of von Glahn (Ref. 24) that included very high jet velocity rocket data, we now suggest the following relation, labeled "Trial" in Figure 9

$$UOL_{L,Norm} = 140.0 + 10 \log [(V_{e,L}/c_{amb})^8/\{1 + 0.02\, (V_{e,L}/c_{amb})^5\}] \tag{9}$$

This relationship is now compared with data from several unsuppressed dual-stream and single-stream configurations, as shown in Figure 10. Dual-stream comparisons are shown in Figure 10(a) for a large number of configurations from References 23, 30, 31, and 34. Only 3 of the 91 data points fall outside the ±3.0 dB band, and the average over-prediction is 0.1 dB. With this very small average error, the standard deviation and the RMS error are essentially equal at 1.6 dB, which we consider to be very good when consideration is given to the repeatability RMS error of 0.8 dB seen for OASPL. The single-stream data (Refs. 29 to 31) shown in Figure 10(b) agree reasonably, but on average the experimental values fall below the correlation based on the dual-stream configurations; however, all these single-stream data are rather old and so may not be as reliable in an absolute sense as the more recent data. The fact that one relationship does as well as it does for such a wide range of cases is quite encouraging.

In Figure 11 data for both suppressed and unsuppressed configurations at BPR ≅ 5 are shown, compared with the baseline correlation modified for suppression effects as in Reference 6

$$UOL_{L,Norm} + 45\, [\log (PR_I PR_O)]/(1 + BPR) = 140.0 + 10 \log [(V_{e,L}/c_{amb})^8/\{1 + 0.02\, (V_{e,L}/c_{amb})^5\}] \tag{10}$$

The experimental data agree reasonably well with the predicted trend versus velocity, but on average fall slightly the prediction. Note that the unsuppressed BPR ≅ 5 data (repeated from Figure 10(a)) also fall below the relation, but only by an average of 0.2 dB. The suppressed cases fall an average of 2.8 dB below the prediction; so this means that the current formulation somewhat (2.6 dB) under-predicts the suppression benefits. Because of this significant average error, the RMS error is rather large at 3.2 dB, whereas the standard deviation is only 1.5 dB. A revised correlation, along the lines suggested below, should lead to a relation with RMS error approaching 1.5 dB. Although this relationship works reasonably well, perhaps a better long-term approach is to modify the calculation to account for the reduction noise by assuming that it is the result of a reduction in V_{mix}, and consequently $V_{e,L}$, due to the mixing enhancement, in which case the relation might be, based on these limited comparisons

$$V_{mix,supr} = V_{mix} \{[\log (PR_I PR_O)]/(1 + BPR)\}^{0.5}$$

However, such a change in the characteristic velocity would result in a change in Strouhal relations, and furthermore, when considering a wider range of suppressor designs, we expect that an additional variable, most likely suppressor area ratio and/or mixer area ratio, will be required. Thus the more general approach we envision at present is as follows

$$V_{mix,supr}/V_{mix} = \text{Function of } (PR_I, PR_O, BPR, SAR, MAR)$$

Where SAR and MAR are the suppressor area ratio and mixer area ratio, respectively (Ref. 1). The relation developed must, of course, also give agreement with single-stream suppressor results. The magnitude of such an effort is beyond the scope of the current task, but should be considered in a follow-on effort.

The Strouhal relations of Reference 6 are retained. The relative sound pressure level, $SPL_L - UOL_L$, is correlated in Table I as a function of the effective directivity angle, θ'_L, and the logarithmic Strouhal number, $\log S_L$, where the Strouhal number is calculated as follows

$$S_L = (f D_L/V_{e,L}) (T_L/T_{amb})^{0.4 (1 + \cos \theta'L)} \tag{11}$$

Where for dual-stream configurations D_L is taken to be D_M, the equivalent diameter based on total fan plus core fully-expanded merged area, $[4(A_I + A_O)/\pi]^{1/2}$, while for a single-stream nozzle D_L is simply taken to be the equivalent diameter of the fully-expanded single jet: $(4A_I/\pi)^{1/2}$. Note that this is the only noise component that utilizes fully-expanded areas in computing the characteristic length for the Strouhal number; all others use hardware geometry. Analogously the temperature T_L is the total temperature of the single jet or for the dual-stream case T_L is taken to be T_{mix}, the mass-averaged total temperature.

The effective angle, to account for refraction effects, is calculated as follows

$$\theta'_L = \theta_{cor,L} (V_{mix}/c_{amb})^{0.1} \tag{11a}$$

Of course, for the single-stream case V_{mix} is replaced by the fully-expanded single jet velocity. It is by use of this effective directivity angle that in a very simple and approximate way refraction is accounted for. It is assumed that the spectra for widely differing jet velocities are similar at this adjusted angle rather than at the same geometric angle. This approach, in conjunction with the analytically modeled convection effect in Equation (8), correlates the variation of SPL with frequency and angle rather well, as shown herein.

The source location for merged region noise, $X_{s,L}$, is calculated from Equation (4) modified for this component specifically, including the effect of the mixing enhancement modifications, as follows

$$X_{s,L} = [L_I + (4 + \theta/30) D_L (PR_I PR_O)^{-0.25}]/LSF \tag{12}$$

Note that the uncorrected angle, θ, in degrees, is used here to start the correction process (Eqs. (1) to (1c)) in closed form.

Small Scale Mixing Noise

There is not enough independent variation of outer stream velocity and temperature in the experimental data for dual-stream exhausts to really determine the best approach to correlating density effects. Therefore, as in References 4 to 6, since the variable ω_M relation was found appropriate for merged mixing noise, the analogous assumption is made here, and the variable ω_S is calculated from Equation (2b). Based on these considerations, the normalized baseline (unsuppressed) outer shear layer mixing noise overall level is defined as follows

$$UOL_S = C_S + 10 \log [(\rho_{amb}/\rho_{ISA})^2 (c_{amb}/c_{ISA})^4] + 10 \log (A_S/R_{cor,S}^2) + 10\, \omega_S \log (\rho_S/\rho_{amb}) + 75 \log (V_{e,S}/c_{amb}) - 20 \log [(1 + M_{c,S} \cos \theta_{cor,S})^2 + 0.09\, M_{c,S}^2] \quad (13)$$

Where $\alpha = 0.3$, and as explained in References 4 to 6

$$\omega_S = 3\, (V_{e,S}/c_{amb})^{3.5}/[0.6 + (V_{e,S}/c_{amb})^{3.5}] - 1 \quad (13a)$$

$$V_{e,S} = V_S\, [1 - M_f\, (c_{amb}/V_S)]^{1/2} \quad (13b)$$

$$M_{c,S} = n_{c,S}\, [(V_S/c_{amb}) - M_f] \quad (13c)$$

$$n_{c,S} = 0.3/(1 + \{V_O/V_I\}^2) + 0.35 \qquad \text{(Dual-stream nozzle)} \quad (13d)$$

$$n_{c,S} = 0.500 \qquad \text{(Single-stream nozzle)} \quad (13e)$$

$$A_S = A_O \qquad \text{(Dual-stream nozzle)} \quad (13f)$$

$$A_S = A_I \qquad \text{(Single-stream nozzle)} \quad (13g)$$

$$V_S = V_O \qquad \text{(Dual-stream nozzle)} \quad (13h)$$

$$V_S = V_I \qquad \text{(Single-stream nozzle)} \quad (13i)$$

$$T_S = T_O \qquad \text{(Dual-stream nozzle)} \quad (13j)$$

$$T_S = T_I \qquad \text{(Single-stream nozzle)} \quad (13k)$$

$$\rho_S = P_{amb} / (R\, t_S) \quad (13l)$$

$$t_S = T_S - (\gamma - 1)\, V_S^2/(2\gamma R) \quad (13m)$$

Note that the area is fully expanded isentropic and that fully-expanded jet properties are used outer stream for a dual-stream nozzle, and inner stream for a single-stream nozzle. Also note that for a single-stream nozzle, $V_O/V_I = 1.0$, yielding $n_{c,S} = 0.500$. The small scale density, ρ_S, is computed using the ideal gas state equation with the specific heat ratio γ and gas constant R of the appropriate stream along with the static temperature t_S (which is in turn computed with isentropic relations using the total temperature and V_S). In Reference 6, the coefficient then labeled C_O was taken to be constant 133.0. For the wider range of conditions and configurations now considered, this assumption no longer appears valid.

Experimental/extracted coefficients C_S results are plotted against outer-stream/inner-stream velocity ration V_O/V_I for a wide range of unsuppressed dual-stream configurations are shown in Figure 12(a). An S-shaped correlation relation is currently used

$$C_S = 130.0 + [6/\{1 + 1.5\ (V_O/V_I)^{3.5}\}] \tag{14}$$

For single-stream nozzles with $V_O = 0$, $C_S = 136.0$. Single-stream results are also shown in Figure 12(a) to help establish proper limiting behavior. However, one approach to improve agreement for single-stream nozzles at high frequencies may be to evaluate C_S where V_O/V_I is unity, rather than zero, resulting in a value of 132.4 instead of 136.0. Conical nozzle results, arbitrarily plotted on the logarithmic scale at $V_O/V_I = 0.1$, agree well with the low velocity ratio dual-stream results. On the other hand, one annular nozzle result, arbitrarily plotted at $V_O/V_I = 9$, indicates agreement with high velocity ratio dual-stream results. Much of the scatter is due to the fact that this component is mainly observed at relatively high frequency, where the data are inherently more prone to error and where it is difficult to separate the competing contributions of intermediate/transitional-scale mixing along with plug separation and shock noises, when they are present. Recall that the repeatability of the experimental data is almost twice as poor at high frequency than at low frequency (standard deviation 0.9 dB for lows and 1.7 dB for highs). It is also likely that with further analysis and evolution of the model, the form of this relation may change considerably, though not much in magnitude, resulting ultimately in a model that is more accurate and aesthetically pleasing. Even so, for the dual-stream configurations the average error (predicted minus experimental) is—0.3 dB, the RMS error is 1.5 dB and the standard deviation is 1.5 dB. For the much more limited single-stream cases the average error is—0.5 dB, with 2.2 dB RMS error and 2.1 dB standard deviation.

As for the large-scale mixing noise, the assumption is made that the effect of noise suppression nozzle exit modifications is as found in Reference 6, $\Delta C_S = 3.37 \log (PR_I PR_O)$, so in Figure 12(b) the perimeter-ratio corrected coefficient, $C_S - 3.37 \log (PR_I PR_O)$ is plotted against V_O/V_I. This expression, in combination with that for large scale mixing, quantifies the finding that the suppression of low frequency noise with enhanced mixing must be traded against an increase, though smaller, in middle and higher frequency noise. In other words, nozzle exit modifications actually cause an *increase* in small scale mixing noise. On average, the suppressed level is under-predicted by 1.4 dB, with 1.7 dB RMS error and 1.0 dB standard deviation. For the BPR ≅ 5 baselines in comparison the under-prediction is 0.1, so the increase in high frequency noise due to the enhanced mixing is under-predicted by 1.3 dB. Recall that the low frequency benefit appears to under-predicted by 2.7 dB; it is apparent that the evolution of the model is indicating stronger effects, both positive and negative, for the mixing enhancement.

The relative sound pressure level, SPL_S —UOL_S, is correlated in Table II as a function of the effective directivity angle θ'_S and the logarithmic Strouhal number log S_S, where the Strouhal number is calculated as follows

$$S_S = (f\ D_S/V_{e,S})\ (T_S/T_{amb})^{0.4\ (1\ +\ \cos\ \theta'S)} \tag{15}$$

Where D_S is the outer throat physical diameter of the flow stream(s) ($D_{2,O,th}$ for dual-stream or $D_{2,I,th}$ for a single-stream nozzle), and T_S is the total temperature of the outer stream (T_O for dual-stream or T_I for single-stream nozzles). The effective angle, to account for refraction effects, is calculated as follows

$$\theta'_S = \theta_{cor,S}\ (V_S/c_{amb})^{0.1} \tag{15a}$$

These spectral directivity tables are developed iteratively as discussed in Reference 6.

No effect of the mixing devices is expected on the location for outer shear layer noise, $X_{s,S}$, calculated as follows

$$X_{s,S} = (\theta/45)\, D_S/LSF \tag{16}$$

Again, note that the uncorrected angle, θ, in degrees, is used here to start the correction process in closed form.

Transitional/Intermediate-Scale Mixing Noise

A significant change from the early model (Ref. 3) was made in References 4 to 6; it was found that much better agreement is obtained if the characteristic velocity $V_{I/O}$ is taken to be the larger of V_O and V_I, and that the overall level correlates reasonably well with $\omega_T = 0.0$. Our original attempts to correlate this component used a velocity difference term, $|V_O - V_I|$, but it was found that this component was present even as the difference term approached zero, so the more complicated form gradually evolved (Refs. 4 to 6). It is interesting to note that in developing a prediction procedure for conventional velocity profile coannular nozzles, Fisher, et al. (Refs. 16 and 17) found that a term dependent on V_I was needed.

$$UOL_T = C_T + 10 \log [(\rho_{amb}/\rho_{ISA})^2 (c_{amb}/c_{ISA})^4] + 10 \log (A_T/R_{cor,T}^2) + 10\, \omega_T \log (\rho_I/\rho_O)$$
$$+75 \log (V_{e,T}/c_{amb}) - 20 \log [(1 + M_{c,T} \cos \theta_{cor,T})^2 + 0.09\, M_{c,T}^2] \tag{17}$$

Where

$$V_{e,T} = V_{I/O} [1 - M_f (c_{amb}/V_{I/O})]^{1/2} \tag{17a}$$

$$M_{c,T} = n_{c,T} [(V_{I/O}/c_{amb}) - M_f] \tag{17b}$$

$$V_{I/O} = MAX (V_O, V_I) \tag{17c}$$

$$n_{c,T} = 0.3/(1 + 0.5 \{V_O/V_I\}^2) + 0.30 \qquad \text{(Dual-stream nozzle)} \tag{17d}$$

$$n_{c,T} = 0.500 \qquad \text{(Single-stream nozzle)} \tag{17e}$$

$$A_T = A_I \tag{17f}$$

Once again, the inner area is fully expanded isentropic and fully-expanded jet conditions are used. Note that in our earlier analyses the density ratio effect was found to be minor, $\omega_T = 0.0$. It would seem that for the single-stream case, (ρ_I/ρ_O) should be replaced by (ρ_I/ρ_{amb}), but so long as $\omega_T = 0.0$, this does not matter. Also for single-stream cases $n_{c,T}$ is calculated for $V_O/V_I = 1.00$, or $n_{c,T} = 0.500$.

This component is treated in a similar manner to the small-scale mixing noise, in that the coefficient C_T appears to be a function of velocity ratio, but here the fully expanded area ratio A_O/A_I appears to be a factor also, with the relationship otherwise as in Reference 6. The data and the resulting correlation are shown in Figure 13. This component is only marginally significant in most cases, so the scatter is large. It also may very well be that the issue of density effect should be reconsidered. Results for the unsuppressed dual-stream and single-stream nozzles are shown in Figure 13(a). As for the small-scale mixing noise, an S-shaped relationship is used, with rather weak justification in view of the scatter, but to assure less risky extrapolation to high and low values of the velocity-ratio and area-ratio parameter. The single-stream cases, both conical and annular appear to agree with the low velocity ratio, low area ratio limit exhibited by the dual stream cases. The resulting correlation expression is

$$C_T = 127.0 + 8.0/[1 + 0.25 \{(V_O/V_I)(A_O/A_I)\}^5] \tag{18}$$

For single-stream nozzles with $V_O = A_O = 0$, $C_T = 135.0$. For the dual-stream cases the average over-prediction is 1.2 dB, the RMS error is 3.3 dB, and the standard deviation is 3.1 dB. For the single-stream cases, the average over-prediction is 1.5 dB, the RMS error is 2.7 dB, and the standard deviation is 2.2 dB. So the model is somewhat conservative.

As for the large-scale and small-scale mixing noises, the assumption is made that the effect of noise suppression nozzle exit modifications is as found in Reference 6, $\Delta C_T = \Delta C_L = - 45 [\log (PR_I PR_O)]/(1 + BPR)$, so in Figure 13(b) the perimeter-ratio corrected coefficient, $C_T + 45 [\log (PR_I PR_O)]/(1 + BPR)$ is plotted against (V_O/V_I) (A_O/A_I). On average, the suppressed level is significantly over-predicted by 3.9 dB, with the RMS error 4.7 dB and the standard deviation 2.7 dB. With this component being a relatively minor contributor for the suppressed cases, the real impact of these poor statistics is not highly significant, but still it should be reevaluated as a more universally-applicable model is developed.

The relative sound pressure level, $SPL_T - UOL_T$, is correlated in Table III as a function of the effective directivity angle θ'_T and the logarithmic Strouhal number $\log S_T$, where the Strouhal number is calculated as follows

$$S_T = (f D_{2,I,th}/V_{e,T}) (T_I/T_O)^{0.4 (1 + \cos \theta'T)} \tag{19}$$

Where $D_{2,I,th}$ is the outer physical throat diameter of the inner stream nozzle and T_I is the core (inner stream) total temperature; for the single-stream case T_O is replaced by T_{amb}. The effective angle, to account for refraction effects, is calculated as follows

$$\theta'_T = \theta_{cor,I} (V_{e,T}/c_{amb})^{0.1} \tag{19a}$$

The spectral directivity comparisons for the suppressed configurations are not shown since the spectral range is very limited in most cases and the scatter relatively large. Comparisons for unsuppressed configurations are shown in References 4 to 6, and since the changes in spectral directivity correlations are so minor, they are not repeated herein.

No effect of the mixing devices is expected on the location for source location for inner stream mixing noise, $X_{s,T}$, calculated as follows

$$X_{s,T} = [L_I + (\theta/45) D_{h,I,th}]/LSF \tag{20}$$

The hydraulic diameter of the inner stream throat, $D_{h,I,th}$, is defined as $D_{2,I,th}$—$D_{1,I,th}$. Again, note that the uncorrected angle, θ, in degrees, is used here to start the correction process in closed form.

Inner Stream Plug Separation Noise

This component appears only on nozzles with relatively blunt-tipped plugs, and then strongly only for high bypass ratio and low mixed jet velocity. There is also a concern as to whether the high frequency noise is really due to flow separation from the plug or whether it might be due to upstream sources such as valve noise. The fact that the experimental/extracted component coefficients are on the order of 10 dB less for the LaRC facility (Ref. 34) than for the GRC facility (Ref. 23) supports this notion, as discussed in Reference 6. The modified relations developed in Reference 6 are now used, and the experimental/extracted normalized level is calculated as follows

$$\begin{aligned} UOL_{P,Norm} = UOL_P &- 10 \log [(\rho_{amb}/\rho_{ISA})^2 (c_{amb}/c_{ISA})^4] - 10 \log (A_I/R_{cor,P}^2) - 20 \log (\rho_I/\rho_O) \\ &+ 40 \log [1 - M_f \cos \theta_{cor,P}] \end{aligned} \tag{21}$$

$$\rho_I = P_{amb} / (R\, t_I) \tag{21a}$$

$$\rho_O = P_{amb} / (R\, t_O) \qquad \text{(Dual-stream nozzle)} \tag{21b}$$

$$\rho_O = \rho_{amb} \qquad \text{(Single-stream nozzle)} \tag{21c}$$

$$t_I = T_I - (\gamma - 1)\, V_I^2/(2\gamma R) \tag{21d}$$

$$t_O = T_O - (\gamma - 1)\, V_O^2/(2\gamma R) \qquad \text{(Dual-stream nozzle)} \tag{21e}$$

Once again, the inner area A_I is fully expanded isentropic and fully-expanded jet properties are used. Note that the convecting eddy directivity term is replaced by the 40 log [1 - $M_f \cos \theta_{cor,P}$] term used for sources moving with fixed position relative to the aircraft, e.g., shock noise. The following simple relation is currently employed for the effective velocity, $V_{e,P}$,

$$V_{e,P} = V_I \tag{21f}$$

Normalized levels (Eq. (21)) are plotted against the logarithmic velocity parameter, log ($V_{e,P}/c_O$) for the unsuppressed external plug nozzles of References 23 and 34 in Figure 14(a). For single-stream nozzles, c_O is replaced by the ambient sound speed and ρ_O is replaced by the ambient density. It is tempting to try to correlate the differences as a function of configuration, but in view of all the experimental problems, particularly the possible plug misalignment in some of the cases from Reference 23, we currently accept the scatter and use the crude relation

$$UOL_{P,Norm} = 140.0 + 35 \log (V_{e,P}/c_O) \tag{22}$$

This "eye-ball" relation produces an average under-prediction of 2.0 dB, an RMS error of 4.4 dB and a standard deviation of 4.0 dB. For the nominal BPR = 13 nozzle (Ref. 19), the experimental levels average 4.6 dB above the general correlation (Eq. (22)), with an RMS error of 4.6 dB, but a standard deviation of only 0.4 dB, so they would correlate with very little scatter for C_P = 144.6 dB. For the nominal BPR = 8, the reason not to try to correlate configuration effects becomes apparent. For very similar configurations the GE/GRC data (Ref. 23) indicate that the noise is under-predicted by an average of 5.6 dB with RMS error 5.7 dB and standard deviation 1.4 dB, while for the LaRC test (Ref. 34) the noise is over-predicted by 2.4 dB with RMS error 2.9 dB and standard deviation 1.5 dB. So on average, there is an 8.5 dB difference. Similar comparisons for the nominal BPR = 5 GE/GRC and LaRC tests of baseline and suppressed configurations (Fig. 14 (b)) show similar problems: over-prediction 0.2 dB, RMS error 3.6 dB, and standard deviation 3.6 dB for Reference 23; over-prediction 2.0 dB, RMS error 2.2 dB, and standard deviation 0.9 dB for Reference 34.

Strouhal-type scaling of the frequency spectra in terms of the plug separation parameter utilized herein is not very convincing. Therefore, we offer an alternative approach where the characteristic velocity is the geometric mean of $V_{e,P}$ and the ambient sonic velocity c_{amb}. The relative sound pressure level, SPL_P—UOL_P, is correlated in Table IV as a function of the effective directivity angle θ'_P and the modified logarithmic Strouhal number log S_P, where the Strouhal number is calculated as follows

$$S_P = [2\, f\, r_{pt}/\{(V_{e,P})^{0.5}(c_{amb})^{0.5}\}]\, [1 - M_f \cos \theta_{cor,P}] \tag{23}$$

Where r_{pt} is the inner stream nozzle physical plug tip radius. The temperature ratio term is omitted. The effective angle, to account for refraction effects, is calculated as follows

$$\theta'_P = \theta_{cor,P}\, (V_{e,P}/c_{amb})^{0.1} \tag{23a}$$

No effect of the mixing devices is expected on the source location. The source location for inner stream plug separation noise, $X_{s,P}$, with θ once again in degrees, is as follows

$$X_{s,P} = [L_I + L_P + 2\, (\theta/45)\, r_{pt}]/LSF \tag{24}$$

Plug/Downstream Shock Noise

For the cases investigated to the present, it appears that this noise component only occurs when there is a plug present, both streams are fully-expanded supersonic with total pressures $P_O \geq P_I$, and there are no noise suppression modifications to the nozzle exit planes that might prevent this shock interaction process. At present, such a component is not included for single-stream plug nozzles, but this may need to be reconsidered in the future. Equation (5) is made specific to this source, as follows

$$OASPL_{D,sh} = C_{D,sh} + 10 \log [(\rho_{amb}/\rho_{ISA})^2 (c_{amb}/c_{ISA})^4] + 10 \log (A_M/R_{cor,D}^2) + 10 \log \{\beta_D^4/(1 + \beta_D^4)\} - 40 \log (1 - M_f \cos \theta_{cor,D}) - F (\theta_{cor,D} - \theta_{M,D}) \quad (25)$$

Where A_M is the fully expanded merged area, $A_I + A_O$. If in the future the method for this shock noise source is modified to include extensions for single-stream plug nozzles, A_M would be simply A_I. Also,

$$\beta_D = [(M_D^2 - M_{d,D}^2)^2 + 0.01\, M_{d,D} / (1 - D_{1,I,ex}/D_{2,O,ex})]^{1/4} \quad (25a)$$

Where M_D is the isentropically-calculated Mach number based the mass-averaged specific heat ratio and the fully-expanded area-weighted pressure ratio, and $M_{d,D}$ is the overall nozzle design Mach number, calculated as follows:

$$M_D = \{[(P_D/P_{amb})^{(\gamma - 1)/\gamma} - 1][2/(\gamma - 1)]\}^{1/2} \quad (25b)$$

$$P_D = (P_I A_I + P_O A_O) / (A_O + A_I) \quad (25c)$$

$$M_{d,D} = (1 - 0.5\{1 - 2r_{pt}/D_{2,O,ex}\})(M_{d,I} + M_{d,O}\, BPR)/(1+BPR) + 0.5\{1 - 2r_{pt}/D_{2,O,ex}\} M_D \quad (25d)$$

This formulation accounts for the reduction in shock strength due to both C-D exits and a sharp plug tip. $D_{1,I,ex}$ is the inner diameter of the inner-stream nozzle exit and $D_{2,O,ex}$ is the outer diameter of the outer-stream nozzle exit. Note that the values for design Mach numbers $M_{d,I}$ and $M_{d,O}$ are unity for convergent inner and outer nozzles, respectively. As in the case of the large scale mixing noise, better statistical correlations may be achieved using a bona fide thermodynamic mixing analysis. The Mach angle is denoted by $\theta_{M,D}$, calculated as follows

$$\theta_{M,D} = 180 - \sin^{-1} (1/M_D) \text{ (in degrees)} \quad (25e)$$

The term $F (\theta_{cor,D} - \theta_{M,D})$ is calculated as follows

$$\left.\begin{array}{ll} F(\theta_{cor,D} - \theta_{M,D}) = 0.0 & \text{for } \theta_{cor,D} < \theta_{M,D} \\ F(\theta_{cor,D} - \theta_{M,D}) = 0.75(\theta_{cor,D} - \theta_{M,D}) & \text{for } \theta_{cor,D} \geq \theta_{M,D} \end{array}\right\} \quad (25f)$$

The relation found appropriate for the coefficient $C_{D,Sh}$ is as follows

$$C_{D,sh} = 164.5 - 50 \log [1 + (D_{1,I,ex} / D_{2,O,ex})^2] \quad (25g)$$

The spectral directivity relations are given in Table V. The Strouhal number is calculated from Equation (6) with the appropriate variables, as follows

$$S_{D,sh} = [f\beta_D D_{h,D,ex} /(0.7V_D)] (1 - M_f \cos \theta_{cor,D}) \{[1 + (0.7V_D/c_{amb}) \cos\theta_{cor,D}]^2 + 0.04 (0.7V_D/c_{amb})^2\}^{1/2} \quad (26)$$

Where $D_{h,D,ex}$ is the "total" hydraulic nozzle exit diameter, $D_{2,O,ex} - D_{1,I,ex}$, and V_D is calculated from M_D and the mass-averaged total temperature

$$V_D = M_D (\gamma R t_D)^{1/2} \quad (26a)$$

$$t_D = T_D / [1 + M_D^2 (\gamma - 1) / 2] \quad (26b)$$

$$T_D = (\dot{m}_I T_I + \dot{m}_O T_O)/(\dot{m}_I + \dot{m}_O) \quad (26c)$$

The source location for downstream shock noise, $X_{s,D,sh}$, is taken to be as follows

$$X_{s,D,sh} = [L_P + L_I + 2 D_M (M_D^2 - 1)^{1/2}]/LSF \quad (27)$$

Where D_M is the equivalent diameter based on total fan plus core fully-expanded merged area, $[4(A_I + A_O)/\pi]^{1/2}$.

Outer Stream Shock Noise

Outer stream shock noise is present only for dual-stream nozzles when the outer stream is fully-expanded supersonic and plug/downstream shock noise is absent. To calculate outer stream shock noise, Equation (5) is made specific to this source, as follows

$$OASPL_{O,sh} = C_{O,sh} + 10 \log [(\rho_{amb}/\rho_{ISA})^2 (c_{amb}/c_{ISA})^4] + 10 \log (A_O/R_{cor,O}^2) + 10 \log \{\beta_O^4/(1 + \beta_O^4)\} - 40 \log (1 - M_f \cos \theta_{cor,O}) - F (\theta_{cor,O} - \theta_{M,O}) \quad (28)$$

Where the subscript O refers to the outer stream. A_O is the fully-expanded area of the outer stream. The shock strength parameter β_O is calculated as follows

$$\beta_O = [(M_O^2 - M_{d,O}^2)^2 + 0.01 M_{d,O}/(1 - D_{1,O,ex}/D_{2,O,ex})]^{1/4} \quad (28a)$$

Where M_O is the outer stream Mach number fully expanded to ambient conditions and $M_{d,O}$ is the outer stream nozzle design Mach number. Note that the value of the design Mach number $M_{d,O}$ is unity for convergent outer stream nozzles. $D_{1,O,ex}$ is the outer stream nozzle exit inner diameter and $D_{2,O,ex}$ is the outer stream nozzle exit outer diameter. The Mach angle is denoted by $\theta_{M,O}$, calculated as follows

$$\theta_{M,O} = 180 - \sin^{-1} (1/M_O) \quad \text{(in degrees)} \quad (28b)$$

The term $F (\theta_{cor,O} - \theta_{M,O})$ is calculated as follows

$$\left.\begin{aligned} F(\theta_{cor,O} - \theta_{M,O}) &= 0.0 && \text{for } \theta_{cor,O} < \theta_{M,O} \\ F(\theta_{cor,O}) &= 0.75(\theta_{cor,O} - \theta_{M,O}) && \text{for } \theta_{cor,O} \geq \theta_{M,O} \end{aligned}\right\} \quad (28c)$$

Results recently reported by Viswanathan (Ref. 35) indicate that outer stream shock noise may remain a significant contributor in the rear quadrant, so this term may need reevaluation in the future, but this is not surprising since this term was developed arbitrarily to give proper limiting behavior.

The relation found appropriate for the coefficient $C_{O,sh}$ is dependent on geometry and whether or not the inner stream is supersonic, as follows (as in Refs. 5 and 6)

$$\left.\begin{aligned} C_{O,sh} &= 168.0 - 60\log\left[1+\left(D_{1,O,ex}/D_{2,O,ex}\right)^2\right] \quad \text{for } M_I \geq 1.0 \\ C_{O,sh} &= 163.5 - 45\log\left[1+\left(D_{1,O,ex}/D_{2,O,ex}\right)^2\right] \quad \text{for } M_I < 1.0 \end{aligned}\right\} \tag{28d}$$

The spectral directivity relations are given in Table VI. The Strouhal number is calculated from Equation (6) modified and with the appropriate variables, as follows

$$_{O,sh} = [f\beta_O(D_{h,O,ex}{}^{0.9}D_{eq,O,ex}{}^{0.1})/(0.7V_O)](1 - M_f \cos\theta_{cor,O}) \{[1 + (0.7\ V_O/c_{amb})\cos\theta_{cor,O}]^2 + 0.04\ (0.7\ V_O/c_{amb})^2\}^{1/2} \tag{29}$$

Where V_O is the fully-expanded jet velocity of the outer stream. The source location for the outer stream shock noise, $X_{s,O,sh}$, is taken to be as follows

$$X_{s,O,sh} = [2\ D_{h,O,ex}\ (M_O{}^2 - 1)^{1/2}]/LSF \tag{30}$$

In both of the above equations, the hydraulic diameter of the outer stream nozzle exit, $D_{h,O,ex}$, is defined as $D_{2,O,ex} - D_{1,O,ex}$, while the equivalent diameter of the outer stream nozzle exit, $D_{eq,O,ex}$, is defined as $(D_{2,O,ex}{}^2 - D_{1,O,ex}{}^2)^{1/2}$.

Inner Stream (or Single Stream) Shock Noise

Inner stream shock noise is present only for nozzles whose inner stream (or single stream) is fully-expanded supersonic. To calculate inner stream shock noise for single-stream or dual-stream nozzles, Equation (5) is made specific to this source, as follows:

$$OASPL_{I,sh} = C_{I,sh} + 10\log[(\rho_{amb}/\rho_{ISA})^2(c_{amb}/c_{ISA})^4] + 10\log(A_I/R_{cor,I}{}^2) + 10\log\{\beta_I{}^4/(1+\beta_I{}^4)\} - 40\log(1 - M_f\cos\theta_{cor,I}) - F(\theta_{cor,I} - \theta_{M,I}) \tag{31}$$

Where the subscript I refers to the inner stream. A_I is the fully-expanded area of the inner stream. The shock strength parameter β_I is calculated as follows

$$\beta_I = [(M_I{}^2 - M_{d,I}{}^2)^2 + 0.01\ M_{d,I}/(1 - D_{1,I,ex}/D_{2,I,ex})]^{1/4} \tag{31a}$$

Where M_I is the inner stream Mach number fully expanded to ambient conditions and $M_{d,I}$ is the inner stream nozzle design Mach number. Note that the value for the design Mach number $M_{d,I}$ is unity for convergent inner stream nozzles. $D_{1,I,ex}$ is the inner stream nozzle exit inner diameter and $D_{2,I,ex}$ is the inner stream nozzle exit outer diameter. The Mach angle is denoted by $\theta_{M,I}$, calculated as follows

$$\theta_{M,I} = 180 - \sin^{-1}(1/M_I)\ \text{(in degrees)} \tag{31b}$$

The term $F(\theta_{cor,I} - \theta_{M,I})$ is calculated as follows

$$\left.\begin{aligned} F\left(\theta_{cor,I} - \theta_{M,I}\right) &= 0.0 && \text{for } \theta_{cor,I} < \theta_{M,I} \\ F\left(\theta_{cor,I} - \theta_{M,I}\right) &= 0.75\left(\theta_{cor,I} - \theta_{M,I}\right) && \text{for } \theta_{cor,I} \geq \theta_{M,I} \end{aligned}\right\} \quad (31c)$$

Inner stream shock noise is shown to correlate reasonably well with a constant coefficient for the plugless configurations (Ref. 30). Previous experience indicates that nozzle diameter ratio is a factor, so the relation recommended is as follows

$$C_{I,sh} = 158.0 - 50 \log \left[1 + (D_{1,I,ex}/D_{2,I,ex})^2\right] \quad (31d)$$

The spectral directivity relations are given in Table VII. The Strouhal number is calculated from Equation (6) modified and with the appropriate variables, as follows

$$S_{I,sh} = [f\beta_I D_{h,I,ex} / (0.7V_I)](1 - M_f \cos \theta_{cor,I})\{[1 + (0.7V_I/c_{amb}) \cos \theta_{cor,I}]^2 + 0.04\,(0.7V_I/c_{amb})^2\}^{1/2} \quad (32)$$

Where V_I is the fully-expanded jet velocity of the inner stream. The source location for the inner stream shock noise, $X_{s,I,sh}$, is taken to be as follows

$$X_{s,I,sh} = [L_I + 2\, D_{h,I,ex}\,(M_I^2 - 1)^{1/2}]/LSF \quad (33)$$

In both of the above equations, the hydraulic diameter of the inner stream nozzle exit, $D_{h,I,ex}$, is defined as $D_{2,I,ex} - D_{1,I,ex}$.

Comparisons With Finalized Model

A number of comparisons are presented for a wide range of geometries and test conditions to demonstrate the degree of agreement between the finalized model and experimental data. The statistical comparisons are summarized in Table VIII.

LaRC Free Jet Unsuppressed Cases

A statistical summary of experimental versus predicted levels for several configurations, including one suppressed (8 petal core nozzle), and test conditions in the LaRC free jet facility at $M_f = 0.10$ is given in Table VIII (a). Overall, the average under-prediction is 0.4 dB in OASPL and 0.7 dB at low frequency, while there is an average over-prediction of 0.2 dB in the mid-frequency range and 0.7 dB at high frequency; over all angles and frequencies not exhibiting obvious contamination the average under-prediction is 0.2 dB. The corresponding RMS error, $\varepsilon = 1.4$ dB for OASPL and range from 1.7 to 2.1 dB for the more difficult measures summing over various frequency ranges. Such agreement is certainly encouraging, but more insight can be obtained by some more detailed graphical comparisons.

A relatively high mixed velocity case for the BPR ≅ 5 external plug nozzle (very similar to one of the GE/GRC configurations) is considered first. The experimental OASPL directivity is compared with the predicted total and component levels at $V_{mix}/c_{amb} = 0.989$ in Figure 15. The experimental levels are not edited in any way except to be corrected from the measurement sideline to a constant arc distance from the fan nozzle exit plane. Note that at this relatively high mixed velocity, the large-scale mixing noise is the dominant term. The agreement is nearly perfect except in the forward quadrant, where contamination may be present, and very near the peak in the rear quadrant. Note that there is a kink in the large-scale mixing, and therefore the total, noise; this is due to the shear layer correction procedure breaking down

for the far-forward region with θ = 62 deg being the smallest angle where the correction was applied. (The actual angle where the correction should terminate is lower, ~ 25 deg for M_f = 0.10.) From 72 deg≤θ≤157 deg, there is an average over-prediction of 0.2 dB and ε = 0. 7 dB. Still more can be seen from the spectral comparisons in Figure 16. Contamination at low frequency is very evident at θ = 48 deg (Fig. 16(a)). At θ = 72 and 92 deg (Fig. 16(b) and (c)) any contamination is minimal and the agreement is fairly good across the spectrum except at the highest frequencies, where the predicted plug separation noise is not indicated by the experimental results. At θ = 117 and 130 deg (Fig. 16(d) and (e)) the predicted plug separation noise is less and the agreement is better. At the more aft angles of θ = 151 and 157 deg (Fig. 16(f) and (g)) the agreement is good at the lowest frequencies, but there is a wide mid-frequency range where the noise is over-predicted; at the highest frequencies there is a turn-up as might be expected for plug separation noise, but the predicted levels for this component are significantly lower.

The apparent influence of facility/background noise contamination is much more evident at low mixed jet velocity, specifically for V_{mix}/c_{amb} = 0.591 and BPR = 10.4 with internal plug. The OASPL directivity comparison, in Figure 17, shows experimental levels significantly above predicted except for θ≥133, and there are anomalous-looking peaks at θ = 67, 122 and 130 deg. On average the OASPL is under-predicted by 2.4 dB, and ε = 3.1 dB. This is clearly not the kind of agreement desired, but examination of the spectra (Fig. 18) confirms that these data are too contaminated to place much weight on. The contamination is most evident at θ = 67 deg (Fig. 18(a)) where there is a strong relatively narrow band peak that is almost 14 dB above the prediction at 501 Hz, and there is also a turn-up at high frequency even though there is no external plug to supply a source for separation noise. At θ = 92 deg (Fig. 18(b)) the low and mid-frequency levels are not too far above prediction, but the problems at high frequency are worse. Similar comments are appropriate at θ = 130 deg (Fig. 18(c)), but the 501 Hz tone is evident here, though not quite at obviously as at θ = 67 deg (Fig. 18(a)). At θ = 151 (Fig. 18(d)) the agreement is good except for the high frequency problem; this is believed to be due to the fact that the jet noise is high enough at this angle to exceed the contaminating sources. Note that even this case is included in the statistical comparison (Table VIII (a)), eliminating only the most obviously contaminated data.

The effect of increasing free jet Mach number is to increase the relative contamination; for otherwise the same conditions the relative jet velocities are decreased, so the jet noise levels are reduced, while any free-jet generated background noise increases. Because of the facility/background noise problems evident even at M_f = 0.10 at low jet velocity, the lowest mixed jet velocity cases at M_f = 0.20 are not included in the statistical summary in Table VIII (b).

Figure 19 shows the OASPL comparison for M_f = 0.201 for the same nozzle and essentially the same jet conditions, V_{mix}/c_{amb} = 0.971, as in Figure 15. The comparison is relatively good, with an average (58≤θ≤161 deg) under-prediction of 0.8 dB with ε = 1.2 dB, but the M_f = 0.10 agreement was significantly better. The spectrum at θ = 51 deg (Fig. 20(a)) shows strong evidence of contamination, with a sharp peak at 400 Hz. At θ = 71, 90 and 117 deg (Fig. 20(b) to (d)) the agreement is fairly good except at high frequencies, where the predicted plug separation noise is not observed. At θ = 131 deg (Fig. 20(e)) the agreement is quite good across the spectrum, and at θ = 151 and 161 deg (Fig. 20(f) and (g)) the agreement is almost as good.

GE/GRC Free Jet Unsuppressed Cases

There is a fairly large set of data available from Reference 23, so the comparisons are broken down by configuration and free jet Mach number. For the highest BPR (~13) only one case each was reported at M_f = 0.00 and 0.28, so the entire set is lumped together in Table VIII (c). On average, the OASPL is over-predicted by 1.1 dB; the low frequency and mid-frequency ranges also show over-predictions of 1.7 and 1.6 dB, respectively, while at the high frequencies the noise (mainly plug separation) is under-predicted by 1.2 dB; over all angles and frequencies not exhibiting obvious contamination the average over-

prediction is 1.1 dB. The corresponding root-mean-square errors, ε, are 1.6 dB for OASPL and range from 2.1 to 2.4 dB for the more difficult measures summing over various frequency ranges.

Graphical comparisons are shown for the only static ($M_f = 0.00$) case, where shear layer corrections are not an issue, at $V_{mix}/c_{amb} = 0.766$. Figure 21 shows the OASPL comparison with very good agreement in trend, although the levels are consistently over-predicted, by an average of 1.2 dB, and ε = 1.3 dB. Spectral comparisons are shown in Figure 22. At θ = 60 deg (Fig. 22(a)), the agreement at low frequency is near perfect, with a modest over-prediction at f ≥ 160 Hz. For θ = 90 deg (Fig. 22(b)) the low frequency is good, with a slight over-prediction that increases with increasing frequency up to 2500 Hz, beyond which it appears that the plug separation noise is under-predicted. At θ = 120 and 135 deg (Fig. 22(c) and (d)) the observations are similar to those at θ = 90 deg (Fig. 22(b)). At the more aft angles of θ = 150 and 160 deg (Fig. 22(e) and (f)) the levels are somewhat over-predicted, but the spectral shapes are reasonably in agreement.

For the next-lower bypass ratio configuration (BPR ≅ 8) a significant number of comparisons were made, and the statistical results are summarized in Table VIII (d) for $M_f = 0.00$, Table VIII (e) for $M_f = 0.20$ and Table VIII (f) for $M_f = 0.28$. In terms of OASPL there is an average under-prediction of 0.6 dB for the static cases and an over-prediction of 0.7 dB in simulated flight; the corresponding RMS errors, ε, are good at 1.1 and 1.3 dB, respectively. When all frequencies not exhibiting obvious contamination and all angles, the average agrees to 0.0 dB for the static tests, and there is an average over-prediction of 0.3 dB in simulated flight, and the corresponding ε values are 1.5 and 2.2 dB for static and simulated flight conditions, respectively. The increased scatter in simulated flight may be due at least in part to the crudeness of the source location and shear layer correction models.

For, the lowest bypass ratio configuration (BPR ≅ 5) analyzed from Reference 23, the statistical results are shown in Table VIII (g), (h) and (i) for $M_f = 0.00$, 0.20 and 0.28, respectively. Agreement is very similar to the BPR ≅ 8 configuration, with an average under-prediction of 0.6 dB for the static cases and an over-prediction of 0.9 dB in simulated flight; the corresponding RMS errors, ε, are good at 1.0 and 1.5 dB, respectively. When all frequencies not exhibiting obvious contamination and all angles, the average agrees to 0.0 dB for the static tests, and there is an average over-prediction of 0.4 dB in simulated flight; the corresponding ε values are 1.2 and 1.7 dB for static and simulated flight conditions, respectively, a little better than for the BPR ≅ 8 configuration.

Graphical comparisons are shown in Figures 23 and 24 for a case very closely approximating the external plug nozzle configuration and test conditions of the LaRC case shown in Figures 15 and 16. The OASPL directivity agreement (Fig. 23) is comparable to that for the LaRC, but the aft-angle discrepancies go in opposite directions. It is in this aft-angle region where the source location and shear layer effects are most significant. The OASPL is under-predicted by 0.3 dB, with ε = 0.9 dB, very comparable to the LaRC values of 0.2 and 0.7, respectively. The spectral agreement at the smallest angle, θ = 55 deg (Fig. 24(a)) is somewhat better than for the LaRC case, although there is definite evidence of contamination at low frequency. Essentially the same observations can be made at θ = 70 deg (Fig. 24(b)), but the low frequency contamination is less, and at high frequency the plug separation noise is over-predicted. At θ = 90 and 115 deg (Fig. 24(c) and (d)), as in the LaRC case, the agreement is good at low frequency, and there is some over-prediction at middle and high frequencies. The agreement is excellent at θ = 130 and 150 deg (Fig. 24(e) and (f)), somewhat better than for the LaRC case. At θ = 165 deg (Fig. 24(g)), beyond the angular range of the LaRC results, the spectral shape agrees well except at very high frequencies where the experimental results appear anomalous, but the experimental levels are under-predicted by 1 to 2 dB.

LeRC Outdoor Facility

Statistical comparisons (Table VIII (j)) are not as impressive for the old LeRC outdoor test facility reported in 1979 (Ref. 30), but this is not surprising since free-field spectra were approximated by a weighted averaging of ground and centerline level microphones, each analytically corrected. Also, these

experiments were conducted at some extreme conditions to establish limiting behavior. On average the OASPL is under-predicted by 0.8 dB with ε = 2.4 dB, while for all frequencies at all angles the under-prediction is 0.9 dB with ε = 3.0 dB.

Conical Nozzle in Lockheed-Georgia Anechoic Chamber

Comparisons are also made with data obtained in the mid-1970s for a small conical nozzle at near-static conditions in the Lockheed-Georgia anechoic free jet facility, wherein data were obtained in the rear quadrant (θ≤90 deg) only. The statistical results are given in Table VIII (k) for a limited sample; on average the OASPL is over-predicted by 1.3 dB with ε = 1.9 dB, while for all frequencies at all angles, the over-prediction is 0.6 dB with ε = 2.3 dB. For intermediate jet velocity, V_j/c_{amb} = 0.74, spectral comparisons are shown in Figure 25. At θ = 90 deg (Fig. 25(a)) the agreement is excellent from 200 to 12600 Hz, but at higher frequency the noise is over-predicted due to the small-scale and intermediate mixing components. At θ = 120 deg (Fig. 25(b)) the good agreement extends to higher frequency. At θ = 135 deg (Fig. 25(c)) the agreement is good at high and low frequencies, with over-prediction of about 2.5 dB at middle frequencies. At θ = 150 deg (Fig. 25(d)) there is reasonable agreement in spectral shape over most of the spectrum, but the level is over-predicted by as much as 5 dB.

Conical Nozzle at Supersonic Conditions in GE Anechoic Chamber

Further conical nozzle comparisons are now made for very high velocity supersonic exhaust conditions in GE's facility. The statistical results are given in Table VIII (l) for a very limited sample, one test condition, V_j/c_{amb} = 2.11, M_j = 1.38. On average the OASPL is over-predicted by 1.5 dB with ε = 3.6 dB; while for all frequencies at all angles, the over-prediction is 1.1 dB and ε = 3.5 dB. The OASPL directivity comparison is shown in Figure 26, where it can be seen that the accuracy problem is mainly in the rear quadrant; the empirical spectral directivity tables, as well as the empirical convection velocity relations are based on very little data at these extreme conditions and may require more work. Spectral comparisons are shown in Figure 27. In the far forward quadrant at θ = 40 deg (Fig. 27(a)) shock noise is the dominant contributor, and considering the steep SPL versus f gradient at low frequency the agreement is fairly good. At θ = 70 deg (Fig. 27(b)) shock noise is dominant, but less so than at θ = 40 deg, and there appears to be a "screech" tone in the 159 Hz band; except for this tone a 2 dB under-prediction of the peak SPL, the agreement is very good. At θ = 90 deg (Fig. 27(c)) the situation becomes very complicated, with large-scale and transitional-scale mixing becoming more important at low and high frequencies, respectively, and shock noise dominant only in a small range near the peak. The screech tone may again be present, elevating the SPLs in the 126 and 159 Hz bands; in general the agreement is fairly good. At θ = 120 deg (Fig. 27(d)) the shock noise is no longer predicted to be a significant contributor. At low frequencies where the large-scale mixing noise is predicted to dominate, the agreement is very good, while at middle frequencies it appears that the transitional-scale mixing noise is somewhat over-predicted, and at high frequencies where the small-scale and transitional-scale mixing noises are predicted to contribute, rough agreement is seen. At θ = 140 deg (Fig. 27(e)) the observations at middle and high frequencies are similar to those at θ = 120 deg, but the low frequency (predicted to be large-scale mixing noise) there is an over-prediction of a few dB; there is also a narrow peak that could be tone-related or, more speculatively, this could be evidence of Mach wave noise. At θ = 160 deg (Fig. 27(f)) the agreement is not good, and there is some evidence of the same type of low frequency narrow peak seen at θ = 140 deg. While the agreement show here is not as good as hoped for, at least reasonable behavior of the model under these extreme conditions is encouraging.

LaRC Free Jet Suppressed Case

The statistical summary in Table VIII (a) and (b) includes results for a BPR ≅ 5 internal plug nozzle with 8 core petals, a configuration that provides modest suppression benefits. Comparison of OASPL prediction with the experimental results is shown in Figure 28 for $V_{mix}/c_{amb} = 0.954$ and $M_f = 0.201$. On average the OASPL is under-predicted by 2.2 dB, with $\varepsilon = 2.2$ dB. Spectral comparisons are shown in Figure 29; there is an average under-prediction for all frequencies and all angles of 1.5, with $\varepsilon = 2.3$ dB. At $\theta = 62$ deg (Fig. 29(a)) there is a significant apparent under-prediction at low and middle frequencies, but comparisons with results at other conditions, particularly for lower power support our convention that this is due to contamination from free jet background noise and/or upstream sources. At $\theta = 90$ deg (Fig. 29(b)) the agreement is fairly good, with modest under-prediction (or excess noise) at low to middle frequencies, a region of modest over-prediction from 7940 to 39800 Hz and a flattening of the experimental data at high frequency that could be due to a number of problems: excess noise, over-correction for atmospheric attenuation, and/or instrumentation. Similar observations can be made for $\theta = 111$ and 125 deg (Fig. 29(c) and (d)) and to some extent at $\theta = 141$ and 151 deg (Fig. 29(e) and (f)), but instead of a range of over-prediction at moderately high frequencies, there are regions of nearly exact agreement. At $\theta = 161$ deg (Fig. 29(g)) the noise is under-predicted at all frequencies, but except for the high frequency turn-up of the experimental data, the spectral shape is reasonably good.

GE/GRC Free Jet Suppressed Cases

There are significant sets of data available from Reference 23 for two suppressed BPR ≅ 5 external plug nozzle configurations, one with 12 "in-flip" core chevrons (Configuration 3IB) and one with the same core chevrons and with 24 fan nozzle chevrons (Configuration 3IC).

For the core chevrons (Conf. 3IB, Table VIII (m)) there is only one case each for $M_f = 0.00$ and 0.20, with the rest at $M_f = 0.28$; the average over-prediction is 1.5 dB, with $\varepsilon = 1.9$ dB. Over all angles and frequencies, the average under-prediction is 0.8 dB, with $\varepsilon = 1.8$ dB.

The OASPL directivity comparison for the static case at $V_{mix}/c_{amb} = 1.047$ is shown in Figure 30; the average over-prediction is 0.2 dB, with $\varepsilon = 1.0$ dB. Spectral comparisons for this case are shown in Figure 31. At $\theta = 60$ deg and 90 deg (Fig. 31(a) and (b)) the agreement is quite good except at low frequency; whether this is an actual under-prediction or excess noise exposed because of the suppression of the large-scale turbulent mixing noise is uncertain. Except for a small under-prediction at low frequency, the agreement at $\theta = 120$ deg (Fig. 31(c)) is excellent. The agreement is good at $\theta = 135$ deg (Fig. 31(d)) with small under-prediction at low frequency slightly greater over-prediction at middle-to-high frequency. The tendency to over-predict at high frequency is more pronounced at $\theta = 150$ deg and 160 deg (Fig. 31(e) and (f)). Over all angles and frequencies, the average under-prediction is 0.2 dB, with $\varepsilon = 1.7$ dB.

For essentially the same nozzle conditions in simulated flight at $M_f = 0.28$, the OASPL directivity comparison is shown in Figure 32. Note that the experimental data do not exhibit a peak, but continue to increase with increasing angle; this problem appears unique to the simulated flight data of Reference 23. The average over-prediction is 1.4 dB, with $\varepsilon = 1.7$ dB. Spectral comparisons at $\theta = 60$ deg (Figs 33(a)) exhibit a low-frequency apparent under-prediction similar to that seen in the static case, which again may be due to excess noise exposed because of the suppression of the large-scale turbulent mixing noise. At $\theta = 90$ to 150 deg (Fig. 33(b) to (e)) the agreement is not as good as that in the static case. At $\theta = 165$ deg (Fig. 33(f)) the agreement is good at low and middle frequencies, while at high frequencies the experimental values are about 3 dB above the prediction. Over all angles and frequencies, the average over-prediction is 0.8 dB, with $\varepsilon = 1.8$ dB, which is very comparable to the static statistics.

Comparisons for the combined core and fan chevrons are summarized in Table VIII (n), (o), and (p) for $M_f = 0.00$, 0.20, and 0.28, respectively. The statistical agreement is actually significantly better for the

simulated flight cases. Combining the results for all M_f the average over-prediction is 1.1 dB, with $\varepsilon = 1.7$ dB. Over all angles and frequencies, the average over-prediction is 0.2 dB, with $\varepsilon = 2.2$ dB.

The OASPL directivity comparison at $V_{mix}/c_{amb} = 1.087$ and $M_f = 0.28$ is shown in Figure 34. Note that the experimental data, as for the core chevrons, do not exhibit a peak, but continue to increase with increasing angle. The average over-prediction is 1.0 dB, with $\varepsilon = 1.7$ dB. The spectral comparisons shown in Figure 35 are not quite as good as for the core chevrons alone, which appears to be mainly due to an under-prediction of the increase in small-scale turbulent mixing noise with the added fan chevrons. Over all angles and frequencies, the average over-prediction is 0.1 dB, with $\varepsilon = 2.3$ dB.

Concluding Remarks

The predictive tool developed herein provides reasonably accurate prediction of jet mixing and shock noise for single-stream and dual-stream nozzles over a very wide range of geometries and test conditions, including suppression modifications on either or both streams. The correlation of suppression device effects is only demonstrated over a limited range, but it appears that a very general approach is within reach with a modest change of approach. We believe that the methodology can be formulated to blend smoothly with the model for more aggressive suppression approaches, such as the two-dimensional mixer ejector predictive model is available in NASA Langley's *Aircraft Noise Prediction Program (ANOPP)* and in NASA Glenn's *FOOTPR* code.

The approach used in developing this model might be called "hybrid experimental/empirical," but relevant elements of theory are utilized to the extent considered practical. Of perhaps as much value as the predictive code itself are the methods and experience acquired in analyzing and correlating noise data involving multiple sources. This methodology involves first using a relatively crude model to predict the *relative* levels of the various noise components, using this model to deduce individual components and then correlating those components; iteration results in rapidly improving predictive models. As this work has evolved, in reverse, from complex to simple, MTC has attempted to relate the empirical relations as much as possible to theory. We also believe that the breakdown of mixing noise into large-scale, transitional/intermediate and small-scale turbulent mixing components provides the long-range hope of transitioning to more theoretically-based models, especially for the large-scale mixing noise where significant progress has been made recently.

This progress in relating the empirical/applied models to theory indicates that the development of a fundamentally-sound jet noise reduction design guide is now feasible. The "design guide" approach we now envision would provide users with a noise prediction model for jet and shock noise for nozzles with a wide range of potential design options, rather than requiring the user to identify the model appropriate for the type of nozzle being considered. In addition to the predictive models, the design guide documentation would include quantitative comparisons with the available base of experimental data. Building this up would be a significant effort, but will provide the needed credibility for the design guide. The design guide would also be a powerful tool for research users, who would use the models capabilities for comparisons with experimental data, to evaluate a concept of interest against the available database and, by comparisons with previous comparisons with similar configurations, assess experimental data quality and facility issues. Research users willing to share the results of their analyses with NASA would aid in the continued development of the design guide database. These research comparisons would span the range from small model tests to full-scale ground and flight tests. Results from continuing research on noise reduction concepts could be incorporated to allow competing concepts to be evaluated against consistent baselines; the benefits of many noise reduction approaches have in the past been overstated due to comparisons with inappropriate baselines. Periodic updates of the predictive model, perhaps yearly, would continue the to be made as comparative results accumulate.

This design guide approach could very well be extended beyond acoustics and include nozzle weight and performance models. Furthermore, the approach could be extended to other engine components and their noise characteristics.

References

1. Stone, J.R., and Clark, B.J., "Development of a Noise Prediction Code for 2-D Mixer Ejector Nozzle Systems, I—Effects of Principal Geometric Variables," Modern Technologies Corporation Report to General Electric Aircraft Engines, December 30, 1996.
2. Stone, J.R., Krejsa, E.A. and Clark, B.J., "Jet Noise Source Separation and Improved Correlation Using Separate Flow Nozzle Data," MTC Report to GE Aircraft Engines, June 15, 2001. (Correction of October 6, 2000 Report).
3. Stone, J.R., "Separate Flow Nozzle Jet Noise Source Separation and Correlation Extension to Enhanced Mixing Configurations," MTC Report to GE Aircraft Engines, June 22, 2001.
4. Stone, J.R., Krejsa, E.A. and Clark, B.J., "Jet Noise Modeling for Coannular Nozzles Including the Effects of Chevrons," Contract NAS3–00178, Task Order No. 6, NASA/CR—2003-212522, September, 2003.
5. Stone, J.R., Krejsa, E.A. and Clark, B.J., "Semi-Empirical Model for Coannular Nozzle Component Noise Extraction and Correlation Including the Effects of Noise Reduction Devices," AIAA–2003–1060, January 2003.
6. Stone, J.R., Krejsa, E.A. and Clark, B.J., "Jet Noise Modeling For Supersonic Business Jet Application," Contract NAS3-00178, Task Order No. 9, NASA/CR—2004-212984, March 2004.
7. Zorumski, W.E., "Aircraft Noise Prediction Program Theoretical Manual," NASA TM-83199, Parts 1 and 2, February 1982.
8. Clark, B.J., "Computer Program to Predict Aircraft Noise Levels," NASA TP-1913, September 1981.
9. Lighthill, M.J., "On Sound Generated Aerodynamically. I. General Theory," Proc. Roy. Soc. (London), Ser. A, vol. 211, no. 1107, March 1952, pp. 564–587.
10. Lighthill, M.J., "On Sound Generated Aerodynamically. II. Turbulence as a Source of Sound," Proc. Roy. Soc. (London), Ser. A, vol. 222, no. 1148, February 1954, pp. 1–32.
11. Ffowcs Williams, J.E., "Some Thoughts on the Effects of Aircraft Motion and Eddy Convection on the Noise from Air Jets," USAA Report 155, Southampton University, Great Britain, 1960.
12. Goldstein, M.E. and Howes, W.L., "New Aspects of Subsonic Aerodynamic Noise Theory," NASA TN D-7158, 1973.
13. Harper-Bourne, M. and Fisher, M.J., "The Noise from Shock Waves in Supersonic Jets," Noise Mechanisms, AGARD Conference Proceedings No. 131, 1974, Paper No. 11.
14. Viswanathan, K., "Quality of Jet Noise Data: Issues, Implications and Needs," AIAA–2002–0365, January 2002.
15. Ahuja, K.K., "Designing Clean Jet Noise Facilities and Making Accurate Jet Noise Measurements," AIAA–2003–0706, January 2003.
16. Fisher, M.J., Preston, G.A. and Bryce, W.D., "A Modelling of the Noise from Simple Co-axial Jets," AIAA–93–4413, October 1993.
17. Fisher, M.J., Preston, G.A. and Mead, C.J., "A Modelling of the Noise From Simple Coaxial Jets, Part II—With Heated Primary Flow," AIAA–96–1666, 1996.
18. Stone, J.R. and Clark, B.J., "Development of a Noise Prediction Code for Internal Mixer Nozzle Systems," MTC Report to GE under Contract NAS3–26617, March 1997.
19. Stone, J.R. and Clark, B.J., "Enhancement to Noise Prediction Code for 2-D Mixer Ejector Nozzle System," Final Report from MTC to GE under Contract NAS3–27235, January 1998.
20. Olsen, W. and Karchmer, A., "Lip Noise Generated by Flow Separation From Nozzle Surfaces," AIAA–76–3, January 1976. (Also NASA TM X–71859)
21. Stone, J.R., "Supersonic Jet Shock Noise Reduction," AIAA Paper 84–2278, October 1984 (also NASA TM-83799).
22. Ahuja, K.K., Tester, B.J. and Tanna, H.K., "The Free Jet as a Simulator of Forward Velocity Effects on Jet Noise," NASA CR-3056, October 1978.
23. Janardan, B.A., Hoff, G.E., Barter, J.W., Martens, S., and Gliebe, P.R. (GEAE), and Mengle, V. and Dalton, W.N. (Allison Engine Co.), "AST Critical Propulsion and Noise Reduction Technologies for

Future Commercial Subsonic Engines – Separate-Flow Exhaust System Noise Reduction Evaluation," Final Report: NAS3–27720, Area of Interest 14.3, General Electric Report R98AEB152, May 1998.
24. von Glahn, U.H., "Correlation of Total Sound Power and Peak Sideline OASPL From Jet Exhausts," AIAA–71–582, June 1971.
25. Stone, J.R., "Interim Prediction Method for Jet Noise," NASA TM X-71618, November 1974.
26. Stone, J.R., Zola, C.L. and Clark, B.J., "An Improved Model for Conventional and Inverted-Velocity-Profile Coannular Jet Noise," AIAA–99–0078, January 1999.
27. Ahuja, K.K. and Bushell, K.W., "An Experimental Study of Subsonic Jet noise and Comparison with Theory," J. Sound Vibration, vol. 30, no. 3, 1973, pp. 317–341.
28. Gliebe, P.R., Brausch, J.F., Majjigi, R.K., and Lee, R., "Jet Noise Suppression," in Aeroacoustics of Flight Vehicles: Theory and Practice, Volume 2: Noise Control, NASA RP-1258, vol. 2 (WRDC TR 90-3052), August 1991, pp. 207–269.
29. Plumblee, H.E. (Ed.), "Effects of Forward Velocity on Turbulent Jet Mixing Noise," Lockheed Georgia Co., NASA CR-2702, 1976.
30. Goodykoontz, J.H. and Stone, J.R., "Experimental Study of Coaxial Nozzle Exhaust Noise," AIAA Paper 79-0631, March 1979.
31. Knott, P.R., Janardan, B.A., Majjigi, R.K., Bhutiani, P.K. and Vogt, P.G., "Free-Jet Acoustic Investigation of High-Radius-Ratio Coannular Plug Nozzles," NASA CR-3818, October 1984 (Date for General Release November 1, 1985).
32. Janardan, B.A., Yamamoto, K., Majjigi, R.K., and Brausch, J.F., "Experimental Investigation of Shock-Cell Noise Reduction for Dual-Stream Nozzles in Simulated Flight," NASA CR-3846, November 1984.
33. Janardan, B.A., Majjigi, R.K., Brausch, J.F. and Knott, P.R., "Free-Jet Investigation of Mechanically Suppressed, High-Radius-Ratio Coannular Plug Model Nozzles," NASA CR-3596, May 1985 (Date for General Release May 1987).
34. Posey, J.W., Norum, T.D., Brown, M.G. and Bhat, T.R.S., "Jet Noise from Ultra-High Bypass Turbofan Engines," 143rd Meeting of the Acoustical Society of America, Pittsburgh, PA, June 3–7, 2002.
35. Viswanathan, K., "Parametric Study of Noise from Dual-Stream Nozzles," AIAA–2003–1198, January 2003.

Table I - Spectral Directivity Relations for Large-Scale Turbulent Mixing Noise
(a) Corrected Effective Directivity Angle, $\theta'_{L,cor}$, from 0 to 100 deg

Frequency parameter,	Normalized sound pressure level, SPL_L-UOL_L, dB vs. corrected effective directivity angle										
	Corrected effective directivity angle, $\theta'_{L,cor}$, deg										
log S_L	0	10	20	30	40	50	60	70	80	90	100
-3.6	-92.9	-92.9	-92.9	-92.9	-92.9	-92.9	-92.9	-92.9	-92.9	-92.9	-92.9
-2.2	-50.9	-50.9	-50.9	-50.9	-50.9	-50.9	-50.9	-50.9	-50.9	-50.9	-50.9
-2.1	-47.9	-47.9	-47.9	-47.9	-47.9	-47.9	-47.9	-47.9	-47.9	-47.9	-47.9
-2.0	-44.9	-44.9	-44.9	-44.9	-44.9	-44.9	-44.9	-44.9	-44.9	-44.9	-44.9
-1.9	-41.9	-41.9	-41.9	-41.9	-41.9	-41.9	-41.9	-41.9	-41.9	-41.9	-41.9
-1.8	-39.1	-39.1	-39.1	-39.1	-39.1	-39.1	-39.1	-39.1	-39.1	-39.1	-39.1
-1.7	-36.5	-36.5	-36.5	-36.5	-36.5	-36.5	-36.5	-36.5	-36.5	-36.5	-36.5
-1.6	-34.0	-34.0	-34.0	-34.0	-34.0	-34.0	-34.0	-34.0	-34.0	-34.0	-34.0
-1.5	-31.6	-31.6	-31.6	-31.6	-31.6	-31.6	-31.6	-31.6	-31.6	-31.6	-31.6
-1.4	-29.3	-29.3	-29.3	-29.3	-29.3	-29.3	-29.3	-29.3	-29.3	-29.3	-29.3
-1.3	-27.1	-27.1	-27.1	-27.1	-27.1	-27.1	-27.1	-27.1	-27.1	-27.1	-27.1
-1.2	-24.9	-24.9	-24.9	-24.9	-24.9	-24.9	-24.9	-24.9	-24.9	-24.9	-24.9
-1.1	-22.7	-22.7	-22.7	-22.7	-22.7	-22.7	-22.7	-22.7	-22.7	-22.7	-22.7
-1.0	-20.6	-20.6	-20.6	-20.6	-20.6	-20.6	-20.6	-20.6	-20.6	-20.6	-20.6
-0.9	-18.5	-18.5	-18.5	-18.5	-18.5	-18.5	-18.5	-18.5	-18.5	-18.5	-18.5
-0.8	-16.5	-16.5	-16.5	-16.5	-16.5	-16.5	-16.5	-16.5	-16.5	-16.5	-16.5
-0.7	-14.6	-14.6	-14.6	-14.6	-14.6	-14.6	-14.6	-14.6	-14.6	-14.6	-14.6
-0.6	-13.1	-13.1	-13.1	-13.1	-13.1	-13.1	-13.1	-13.1	-13.1	-13.1	-13.1
-0.5	-12.0	-12.0	-12.0	-12.0	-12.0	-12.0	-12.0	-12.0	-12.0	-12.0	-12.0
-0.4	-11.2	-11.2	-11.2	-11.2	-11.2	-11.2	-11.2	-11.2	-11.2	-11.2	-11.2
-0.3	-10.7	-10.7	-10.7	-10.7	-10.7	-10.7	-10.7	-10.7	-10.7	-10.7	-10.7
-0.2	-10.4	-10.4	-10.4	-10.4	-10.4	-10.4	-10.4	-10.4	-10.4	-10.4	-10.4
-0.1	**-10.2**	**-10.2**	**-10.2**	**-10.2**	**-10.2**	**-10.2**	**-10.2**	**-10.2**	**-10.2**	**-10.2**	**-10.2**
0.0	-10.4	-10.4	-10.4	-10.4	-10.4	-10.4	-10.4	-10.4	-10.4	-10.4	-10.4
0.1	-10.8	-10.8	-10.8	-10.8	-10.8	-10.8	-10.8	-10.8	-10.8	-10.8	-10.8
0.2	-11.4	-11.4	-11.4	-11.4	-11.4	-11.4	-11.4	-11.4	-11.4	-11.4	-11.4
0.3	-12.3	-12.3	-12.3	-12.3	-12.3	-12.3	-12.3	-12.3	-12.3	-12.3	-12.3
0.4	-13.5	-13.5	-13.5	-13.5	-13.5	-13.5	-13.5	-13.5	-13.5	-13.5	-13.5
0.5	-15.0	-15.0	-15.0	-15.0	-15.0	-15.0	-15.0	-15.0	-15.0	-15.0	-15.0
0.6	-16.6	-16.6	-16.6	-16.6	-16.6	-16.6	-16.6	-16.6	-16.6	-16.6	-16.6
0.7	-18.2	-18.2	-18.2	-18.2	-18.2	-18.2	-18.2	-18.2	-18.2	-18.2	-18.2
0.8	-19.8	-19.8	-19.8	-19.8	-19.8	-19.8	-19.8	-19.8	-19.8	-19.8	-19.8
0.9	-21.4	-21.4	-21.4	-21.4	-21.4	-21.4	-21.4	-21.4	-21.4	-21.4	-21.4
1.0	-23.0	-23.0	-23.0	-23.0	-23.0	-23.0	-23.0	-23.0	-23.0	-23.0	-23.0
1.1	-24.6	-24.6	-24.6	-24.6	-24.6	-24.6	-24.6	-24.6	-24.6	-24.6	-24.6
1.2	-26.2	-26.2	-26.2	-26.2	-26.2	-26.2	-26.2	-26.2	-26.2	-26.2	-26.2
1.3	-27.8	-27.8	-27.8	-27.8	-27.8	-27.8	-27.8	-27.8	-27.8	-27.8	-27.8
1.4	-29.4	-29.4	-29.4	-29.4	-29.4	-29.4	-29.4	-29.4	-29.4	-29.4	-29.4
1.5	-31.0	-31.0	-31.0	-31.0	-31.0	-31.0	-31.0	-31.0	-31.0	-31.0	-31.0
1.6	-32.6	-32.6	-32.6	-32.6	-32.6	-32.6	-32.6	-32.6	-32.6	-32.6	-32.6
1.7	-34.2	-34.2	-34.2	-34.2	-34.2	-34.2	-34.2	-34.2	-34.2	-34.2	-34.2
1.8	-35.8	-35.8	-35.8	-35.8	-35.8	-35.8	-35.8	-35.8	-35.8	-35.8	-35.8
1.9	-37.4	-37.4	-37.4	-37.4	-37.4	-37.4	-37.4	-37.4	-37.4	-37.4	-37.4
2.0	-39.0	-39.0	-39.0	-39.0	-39.0	-39.0	-39.0	-39.0	-39.0	-39.0	-39.0
3.6	-61.4	-61.4	-61.4	-61.4	-61.4	-61.4	-61.4	-61.4	-61.4	-61.4	-61.4
$OASPL_L$-UOL_L	0.0	0.0	0.0	0.0	0.0	0.0	0.0	0.0	0.0	0.0	0.0

Table I (Concluded) - Spectral Directivity Relations for Large-Scale Turbulent Mixing Noise
(b) Corrected Effective Directivity Angle, $\theta'_{L,cor}$, from 110 to 250 deg

Frequency parameter,	Normalized sound pressure level, SPL_L-UOL_L, dB vs. corrected effective directivity angle										
	Corrected effective directivity angle, $\theta'_{L,cor}$, deg										
log S_L	110	120	130	140	150	160	170	180	190	200	250
-3.6	-93.4	-91.3	-93.0	-88.4	-86.9	-88.9	-90.5	-94.5	-99.5	-104.5	-129.5
-2.2	-51.4	-49.3	-51.0	-46.4	-44.9	-46.9	-49.9	-53.9	-58.9	-63.9	-88.9
-2.1	-48.4	-46.3	-48.0	-43.4	-41.9	-43.9	-46.9	-50.9	-55.9	-60.9	-85.9
-2.0	-45.4	-43.3	-45.0	-40.4	-38.9	-40.9	-43.9	-47.9	-52.9	-57.9	-82.9
-1.9	-42.4	-40.3	-42.0	-37.4	-35.9	-37.9	-40.9	-44.9	-49.9	-54.9	-79.9
-1.8	-39.6	-37.6	-39.0	-34.4	-32.9	-34.9	-37.9	-41.9	-46.9	-51.9	-76.9
-1.7	-37.0	-35.0	-36.0	-31.4	-29.9	-31.9	-34.9	-38.9	-43.9	-48.9	-73.9
-1.6	-34.5	-32.5	-33.0	-28.4	-26.9	-28.9	-31.9	-35.9	-40.9	-45.9	-70.9
-1.5	-32.1	-30.1	-30.0	-25.4	-24.0	-26.0	-29.0	-33.0	-38.0	-43.0	-68.0
-1.4	-29.8	-27.8	-27.0	-22.5	-21.2	-23.2	-26.2	-30.2	-35.2	-40.2	-65.2
-1.3	-27.6	-25.5	-24.1	-19.7	-18.5	-20.5	-23.5	-27.5	-32.5	-37.5	-62.5
-1.2	-25.4	-23.2	-21.3	-17.0	-15.9	-17.9	-20.9	-24.9	-29.9	-34.9	-59.9
-1.1	-23.2	-21.0	-18.6	-14.4	-13.4	-15.4	-18.4	-22.4	-27.4	-32.4	-57.4
-1.0	-21.1	-18.9	-16.0	-11.9	-11.2	-13.2	-16.2	-20.2	-25.2	-30.2	-55.2
-0.9	-19.0	-16.9	-13.5	-9.7	-9.4	-11.4	-14.4	-18.4	-23.4	-28.4	-53.4
-0.8	-17.0	-15.0	-11.3	-7.9	-7.9	-9.9	-12.9	-16.9	-21.9	-26.9	-51.9
-0.7	-15.2	-13.4	-9.5	-6.4	-6.7	-8.7	-11.7	-15.7	-20.7	-25.7	-50.7
-0.6	-13.6	-11.9	-8.0	-5.2	-5.9	-7.9	-10.9	-14.9	-19.9	-24.9	-49.9
-0.5	-12.2	-10.6	-6.8	-4.4	**-5.5**	**-7.5**	**-10.5**	**-14.5**	**-19.5**	**-24.5**	**-49.5**
-0.4	-11.0	-9.7	-6.0	**-4.0**	-6.3	-8.3	-11.3	-15.3	-20.3	-25.3	-50.3
-0.3	-10.2	-9.0	**-5.6**	-4.8	-7.8	-9.8	-12.6	-16.6	-21.6	-26.6	-51.6
-0.2	-9.8	**-8.7**	-6.2	-6.3	-10.2	-12.2	-15.0	-19.0	-24.0	-29.0	-54.0
-0.1	**-9.5**	-9.1	-7.1	-8.3	-13.1	-15.1	-17.9	-21.9	-26.9	-31.9	-56.9
0.0	-9.8	-9.7	-8.3	-10.5	-16.0	-18.1	-20.9	-24.9	-29.9	-34.9	-59.9
0.1	-10.4	-10.4	-9.8	-12.7	-18.9	-21.1	-23.9	-27.9	-32.9	-37.9	-62.9
0.2	-11.1	-11.4	-11.4	-14.9	-21.8	-24.1	-26.9	-30.9	-35.9	-40.9	-65.9
0.3	-12.3	-12.5	-13.1	-17.1	-24.7	-27.1	-29.9	-33.9	-38.9	-43.9	-68.9
0.4	-13.6	-13.8	-15.1	-19.4	-27.6	-30.1	-32.9	-36.9	-41.9	-46.9	-71.9
0.5	-15.1	-15.4	-17.1	-21.7	-30.5	-33.1	-35.9	-39.9	-44.9	-49.9	-74.9
0.6	-16.7	-17.2	-19.2	-24.0	-33.4	-36.1	-38.9	-42.9	-47.9	-52.9	-77.9
0.7	-18.3	-19.1	-21.3	-26.3	-36.3	-39.1	-41.9	-45.9	-50.9	-55.9	-80.9
0.8	-19.9	-21.0	-23.4	-28.6	-39.2	-42.1	-44.9	-48.9	-53.9	-58.9	-83.9
0.9	-21.6	-22.9	-25.5	-30.9	-42.1	-45.1	-47.9	-51.9	-56.9	-61.9	-86.9
1.0	-23.3	-24.8	-27.6	-33.2	-45.0	-48.1	-50.9	-54.9	-59.9	-64.9	-89.9
1.1	-25.0	-26.7	-29.7	-35.5	-47.9	-51.1	-53.9	-57.9	-62.9	-67.9	-92.9
1.2	-26.7	-28.6	-31.8	-37.9	-50.8	-54.1	-56.9	-60.9	-65.9	-70.9	-95.9
1.3	-28.4	-30.5	-33.9	-40.3	-53.7	-57.1	-59.9	-63.9	-68.9	-73.9	-98.9
1.4	-30.1	-32.5	-36.0	-42.7	-56.6	-60.1	-62.9	-66.9	-71.9	-76.9	-101.9
1.5	-31.8	-34.5	-38.2	-45.1	-59.5	-63.1	-65.9	-69.9	-74.9	-79.9	-104.9
1.6	-33.5	-36.5	-40.4	-47.5	-62.4	-66.1	-68.9	-72.9	-77.9	-82.9	-107.9
1.7	-35.2	-38.5	-42.6	-49.9	-65.3	-69.1	-71.9	-75.9	-80.9	-85.9	-110.9
1.8	-37.0	-40.5	-44.8	-52.3	-68.2	-72.1	-74.9	-78.9	-83.9	-88.9	-113.9
1.9	-38.8	-42.5	-47.0	-54.7	-71.1	-75.1	-77.9	-81.9	-86.9	-91.9	-116.9
2.0	-40.6	-44.5	-49.2	-57.1	-74.0	-78.1	-80.9	-84.9	-89.9	-94.9	-119.9
3.6	-69.4	-72.5	-80.0	-90.7	-120.4	-126.1	-128.9	-132.9	-137.9	-142.9	-167.9
$OASPL_L$-UOL_L	0.2	0.9	3.2	4.2	2.6	0.6	-2.4	-6.4	-11.4	-16.4	-41.4

Table II - Spectral Directivity Relations for Small-Scale Turbulent Mixing Noise
(a) Corrected Effective Directivity Angle, $\theta'_{S,cor}$, from 0 to 100 deg

Frequency parameter,	Normalized sound pressure level, SPL_S-UOL_S, dB vs. corrected effective directivity angle Corrected effective directivity angle, $\theta'_{S,cor}$, deg										
log S_S	0	10	20	30	40	50	60	70	80	90	100
-3.6	-253.5	-253.5	-253.5	-253.5	-253.5	-253.5	-253.5	-253.5	-253.5	-253.8	-253.6
-2.2	-169.5	-169.5	-169.5	-169.5	-169.5	-169.5	-169.5	-169.5	-169.5	-169.8	-169.6
-2.1	-163.5	-163.5	-163.5	-163.5	-163.5	-163.5	-163.5	-163.5	-163.5	-163.8	-163.6
-2.0	-157.5	-157.5	-157.5	-157.5	-157.5	-157.5	-157.5	-157.5	-157.5	-157.8	-157.6
-1.9	-151.5	-151.5	-151.5	-151.5	-151.5	-151.5	-151.5	-151.5	-151.5	-151.8	-151.6
-1.8	-145.5	-145.5	-145.5	-145.5	-145.5	-145.5	-145.5	-145.5	-145.5	-145.8	-145.6
-1.7	-139.5	-139.5	-139.5	-139.5	-139.5	-139.5	-139.5	-139.5	-139.5	-139.8	-139.6
-1.6	-133.5	-133.5	-133.5	-133.5	-133.5	-133.5	-133.5	-133.5	-133.5	-133.8	-133.6
-1.5	-127.5	-127.5	-127.5	-127.5	-127.5	-127.5	-127.5	-127.5	-127.5	-127.8	-127.6
-1.4	-121.5	-121.5	-121.5	-121.5	-121.5	-121.5	-121.5	-121.5	-121.5	-121.8	-121.6
-1.3	-115.5	-115.5	-115.5	-115.5	-115.5	-115.5	-115.5	-115.5	-115.5	-115.8	-115.6
-1.2	-109.5	-109.5	-109.5	-109.5	-109.5	-109.5	-109.5	-109.5	-109.5	-109.8	-109.6
-1.1	-103.5	-103.5	-103.5	-103.5	-103.5	-103.5	-103.5	-103.5	-103.5	-103.8	-103.6
-1.0	-97.5	-97.5	-97.5	-97.5	-97.5	-97.5	-97.5	-97.5	-97.5	-97.8	-97.6
-0.9	-91.5	-91.5	-91.5	-91.5	-91.5	-91.5	-91.5	-91.5	-91.5	-91.8	-91.6
-0.8	-85.5	-85.5	-85.5	-85.5	-85.5	-85.5	-85.5	-85.5	-85.5	-85.8	-85.6
-0.7	-79.5	-79.5	-79.5	-79.5	-79.5	-79.5	-79.5	-79.5	-79.5	-79.8	-79.6
-0.6	-73.5	-73.5	-73.5	-73.5	-73.5	-73.5	-73.5	-73.5	-73.5	-73.8	-73.6
-0.5	-67.5	-67.5	-67.5	-67.5	-67.5	-67.5	-67.5	-67.5	-67.5	-67.8	-67.6
-0.4	-61.5	-61.5	-61.5	-61.5	-61.5	-61.5	-61.5	-61.5	-61.5	-61.8	-61.6
-0.3	-55.5	-55.5	-55.5	-55.5	-55.5	-55.5	-55.5	-55.5	-55.5	-55.8	-55.6
-0.2	-49.5	-49.5	-49.5	-49.5	-49.5	-49.5	-49.5	-49.5	-49.5	-49.8	-49.6
-0.1	-43.5	-43.5	-43.5	-43.5	-43.5	-43.5	-43.5	-43.5	-43.5	-43.8	-43.6
0.0	-37.6	-37.6	-37.6	-37.6	-37.6	-37.6	-37.6	-37.6	-37.6	-37.8	-37.6
0.1	-32.6	-32.6	-32.6	-32.6	-32.6	-32.6	-32.6	-32.6	-32.6	-32.8	-32.6
0.2	-28.1	-28.1	-28.1	-28.1	-28.1	-28.1	-28.1	-28.1	-28.1	-28.3	-28.1
0.3	-24.1	-24.1	-24.1	-24.1	-24.1	-24.1	-24.1	-24.1	-24.1	-24.3	-24.1
0.4	-20.6	-20.6	-20.6	-20.6	-20.6	-20.6	-20.6	-20.6	-20.6	-20.8	-20.6
0.5	-17.5	-17.5	-17.5	-17.5	-17.5	-17.5	-17.5	-17.5	-17.5	-17.6	-17.6
0.6	-15.0	-15.0	-15.0	-15.0	-15.0	-15.0	-15.0	-15.0	-15.0	-15.1	-15.1
0.7	-13.0	-13.0	-13.0	-13.0	-13.0	-13.0	-13.0	-13.0	-13.0	-13.1	-13.1
0.8	-11.5	-11.5	-11.5	-11.5	-11.5	-11.5	-11.5	-11.5	-11.5	-11.6	-11.6
0.9	-10.5	-10.5	-10.5	-10.5	-10.5	-10.5	-10.5	-10.5	-10.5	-10.6	-10.6
1.0	-9.8	-9.8	-9.8	-9.8	-9.8	-9.8	-9.8	-9.8	-9.8	-9.9	-9.9
1.1	**-9.5**	**-9.5**	**-9.5**	**-9.5**	**-9.5**	**-9.5**	**-9.5**	**-9.5**	**-9.5**	**-9.6**	**-9.6**
1.2	-9.7	-9.7	-9.7	-9.7	-9.7	-9.7	-9.7	-9.7	-9.7	-9.8	-9.8
1.3	-10.0	-10.0	-10.0	-10.0	-10.0	-10.0	-10.0	-10.0	-10.0	-10.1	-10.1
1.4	-10.4	-10.4	-10.4	-10.4	-10.4	-10.4	-10.4	-10.4	-10.4	-10.5	-10.6
1.5	-11.0	-11.0	-11.0	-11.0	-11.0	-11.0	-11.0	-11.0	-11.0	-11.1	-11.3
1.6	-11.7	-11.7	-11.7	-11.7	-11.7	-11.7	-11.7	-11.7	-11.7	-11.8	-12.2
1.7	-12.6	-12.6	-12.6	-12.6	-12.6	-12.6	-12.6	-12.6	-12.6	-12.7	-13.2
1.8	-13.6	-13.6	-13.6	-13.6	-13.6	-13.6	-13.6	-13.6	-13.6	-13.7	-14.2
1.9	-14.7	-14.7	-14.7	-14.7	-14.7	-14.7	-14.7	-14.7	-14.7	-14.8	-15.4
2.0	-15.8	-15.8	-15.8	-15.8	-15.8	-15.8	-15.8	-15.8	-15.8	-15.9	-16.6
3.6	-33.4	-33.4	-33.4	-33.4	-33.4	-33.4	-33.4	-33.4	-33.4	-33.5	-35.8
$OASPL_S$-UOL_S	0.4	0.4	0.4	0.4	0.4	0.4	0.4	0.4	0.4	0.3	0.2

Table II (Concluded) - Spectral Directivity Relations for Small-Scale Turbulent Mixing Noise
(b) Corrected Effective Directivity Angle, $\theta'_{S,cor}$, from 110 to 250 deg

Frequency parameter,	Normalized sound pressure level, SPL_S-UOL_S, dB vs. corrected effective directivity angle										
	Corrected effective directivity angle, $\theta'_{S,cor}$, deg										
$\log S_S$	110	120	130	140	150	160	170	180	190	200	250
-3.6	-253.6	-255.1	-257.6	-254.0	-256.0	-258.0	-261.0	-265.0	-270.0	-275.0	-300.0
-2.2	-169.6	-171.1	-173.6	-170.0	-172.0	-174.0	-177.0	-181.0	-186.0	-191.0	-216.0
-2.1	-163.6	-165.1	-167.6	-164.0	-166.0	-168.0	-171.0	-175.0	-180.0	-185.0	-210.0
-2.0	-157.6	-159.1	-161.6	-158.0	-160.0	-162.0	-165.0	-169.0	-174.0	-179.0	-204.0
-1.9	-151.6	-153.1	-155.6	-152.0	-154.0	-156.0	-159.0	-163.0	-168.0	-173.0	-198.0
-1.8	-145.6	-147.1	-149.6	-146.0	-148.0	-150.0	-153.0	-157.0	-162.0	-167.0	-192.0
-1.7	-139.6	-141.1	-143.6	-140.0	-142.0	-144.0	-147.0	-151.0	-156.0	-161.0	-186.0
-1.6	-133.6	-135.1	-137.6	-134.0	-136.0	-138.0	-141.0	-145.0	-150.0	-155.0	-180.0
-1.5	-127.6	-129.1	-131.6	-128.0	-130.0	-132.0	-135.0	-139.0	-144.0	-149.0	-174.0
-1.4	-121.6	-123.1	-125.6	-122.0	-124.0	-126.0	-129.0	-133.0	-138.0	-143.0	-168.0
-1.3	-115.6	-117.1	-119.6	-116.0	-118.0	-120.0	-123.0	-127.0	-132.0	-137.0	-162.0
-1.2	-109.6	-111.1	-113.6	-110.0	-112.0	-114.0	-117.0	-121.0	-126.0	-131.0	-156.0
-1.1	-103.6	-105.1	-107.6	-104.0	-106.0	-108.0	-111.0	-115.0	-120.0	-125.0	-150.0
-1.0	-97.6	-99.1	-101.6	-98.0	-100.0	-102.0	-105.0	-109.0	-114.0	-119.0	-144.0
-0.9	-91.6	-93.1	-95.6	-92.0	-94.0	-96.0	-99.0	-103.0	-108.0	-113.0	-138.0
-0.8	-85.6	-87.1	-89.6	-86.0	-88.0	-90.0	-93.0	-97.0	-102.0	-107.0	-132.0
-0.7	-79.6	-81.1	-83.6	-80.0	-82.0	-84.0	-87.0	-91.0	-96.0	-101.0	-126.0
-0.6	-73.6	-75.1	-77.6	-74.0	-76.0	-78.0	-81.0	-85.0	-90.0	-95.0	-120.0
-0.5	-67.6	-69.1	-71.6	-68.0	-70.0	-72.0	-75.0	-79.0	-84.0	-89.0	-114.0
-0.4	-61.6	-63.1	-65.6	-62.0	-64.0	-66.0	-69.0	-73.0	-78.0	-83.0	-108.0
-0.3	-55.6	-57.1	-59.6	-56.0	-58.0	-60.0	-63.0	-67.0	-72.0	-77.0	-102.0
-0.2	-49.6	-51.1	-53.6	-50.0	-52.0	-54.0	-57.0	-61.0	-66.0	-71.0	-96.0
-0.1	-43.6	-45.1	-47.6	-44.0	-46.0	-48.0	-51.0	-55.0	-60.0	-65.0	-90.0
0.0	-37.6	-39.1	-41.6	-39.0	-41.0	-43.0	-46.0	-50.0	-55.0	-60.0	-85.0
0.1	-32.6	-34.1	-36.6	-34.5	-36.5	-38.5	-41.5	-45.5	-50.5	-55.5	-80.5
0.2	-28.1	-29.6	-32.1	-30.5	-32.5	-34.5	-37.5	-41.5	-46.5	-51.5	-76.5
0.3	-24.1	-25.6	-28.1	-27.0	-29.0	-31.0	-34.0	-38.0	-43.0	-48.0	-73.0
0.4	-20.6	-22.1	-24.6	-24.0	-26.0	-28.0	-31.0	-35.0	-40.0	-45.0	-70.0
0.5	-17.6	-19.1	-21.6	-21.5	-23.5	-25.5	-28.5	-32.5	-37.5	-42.5	-67.5
0.6	-15.1	-16.6	-19.1	-19.5	-21.5	-23.5	-26.5	-30.5	-35.5	-40.5	-65.5
0.7	-13.1	-14.6	-17.1	-18.0	-20.0	-22.0	-25.0	-29.0	-34.0	-39.0	-64.0
0.8	-11.6	-13.1	-15.6	-17.0	-19.0	-21.0	-24.0	-28.0	-33.0	-38.0	-63.0
0.9	-10.6	-12.1	-14.6	-16.3	-18.3	-20.3	-23.3	-27.3	-32.3	-37.3	-62.3
1.0	-9.9	-11.4	-13.9	**-16.0**	**-18.0**	**-20.0**	**-23.0**	**-27.0**	**-32.0**	**-37.0**	**-62.0**
1.1	**-9.6**	**-11.1**	**-13.6**	-16.3	-18.3	-20.3	-23.3	-27.3	-32.3	-37.3	-62.3
1.2	-9.8	-11.3	-13.8	-16.9	-18.9	-20.9	-23.9	-27.9	-32.9	-37.9	-62.9
1.3	-10.2	-11.8	-14.4	-17.8	-19.8	-21.8	-24.8	-28.8	-33.8	-38.8	-63.8
1.4	-10.8	-12.4	-15.1	-19.0	-21.0	-23.0	-26.0	-30.0	-35.0	-40.0	-65.0
1.5	-11.6	-13.2	-16.0	-20.4	-22.4	-24.4	-27.4	-31.4	-36.4	-41.4	-66.4
1.6	-12.7	-14.4	-17.2	-21.8	-23.8	-25.8	-28.8	-32.8	-37.8	-42.8	-67.8
1.7	-13.8	-15.6	-18.5	-23.2	-25.2	-27.2	-30.2	-34.2	-39.2	-44.2	-69.2
1.8	-15.0	-16.8	-19.8	-24.6	-26.6	-28.6	-31.6	-35.6	-40.6	-45.6	-70.6
1.9	-16.2	-18.1	-21.1	-26.0	-28.0	-30.0	-33.0	-37.0	-42.0	-47.0	-72.0
2.0	-17.4	-19.4	-22.5	-27.4	-29.4	-31.4	-34.4	-38.4	-43.4	-48.4	-73.4
3.6	-36.6	-40.2	-44.9	-49.8	-51.8	-53.8	-56.8	-60.8	-65.8	-70.8	-95.8
$OASPL_S$-UOL_S	0.0	-1.6	-4.2	-6.7	-8.7	-10.7	-13.7	-17.7	-22.7	-27.7	-52.7

Table III - Spectral Directivity Relations for Transitional-Scale Turbulent Mixing Noise
(a) Corrected Effective Directivity Angle, $\theta'_{T,cor}$, from 0 to 100 deg

Frequency parameter,	Normalized sound pressure level, SPL_T-UOL_T, dB vs. corrected effective directivity angle Corrected effective directivity angle, $\theta'_{T,cor}$, deg										
log S_T	0	10	20	30	40	50	60	70	80	90	100
-3.6	-206.0	-205.2	-204.6	-204.2	-204.0	-204.4	-204.8	-205.3	-205.8	-198.5	-194.0
-2.2	-122.0	-121.2	-120.6	-120.2	-120.0	-120.4	-120.8	-121.3	-121.8	-114.5	-110.0
-2.1	-116.0	-115.2	-114.6	-114.2	-114.0	-114.4	-114.8	-115.3	-115.8	-108.5	-104.0
-2.0	-110.0	-109.2	-108.6	-108.2	-108.0	-108.4	-108.8	-109.3	-109.8	-102.5	-98.0
-1.9	-104.0	-103.2	-102.6	-102.2	-102.0	-102.4	-102.8	-103.3	-103.8	-96.5	-92.0
-1.8	-98.0	-97.2	-96.6	-96.2	-96.0	-96.4	-96.8	-97.3	-97.8	-90.5	-86.0
-1.7	-92.0	-91.2	-90.6	-90.2	-90.0	-90.4	-90.8	-91.3	-91.8	-84.5	-80.0
-1.6	-86.0	-85.2	-84.6	-84.2	-84.0	-84.4	-84.8	-85.3	-85.8	-78.5	-74.0
-1.5	-80.0	-79.2	-78.6	-78.2	-78.0	-78.4	-78.8	-79.3	-79.8	-72.5	-68.0
-1.4	-74.0	-73.2	-72.6	-72.2	-72.0	-72.4	-72.8	-73.3	-73.8	-66.5	-62.0
-1.3	-68.0	-67.2	-66.6	-66.2	-66.0	-66.4	-66.8	-67.3	-67.8	-60.5	-56.0
-1.2	-62.0	-61.2	-60.6	-60.2	-60.0	-60.4	-60.8	-61.3	-61.8	-54.5	-50.0
-1.1	-56.0	-55.2	-54.6	-54.2	-54.0	-54.4	-54.8	-55.3	-55.8	-48.5	-44.0
-1.0	-50.0	-49.2	-48.6	-48.2	-48.0	-48.4	-48.8	-49.3	-49.8	-42.5	-38.0
-0.9	-44.0	-43.2	-42.6	-42.2	-42.0	-42.4	-42.8	-43.3	-43.8	-37.5	-33.0
-0.8	-38.0	-37.2	-36.6	-36.2	-36.0	-36.4	-36.8	-37.3	-37.8	-32.5	-28.5
-0.7	-33.0	-32.2	-31.6	-31.2	-31.0	-31.4	-31.8	-32.3	-32.8	-28.0	-24.5
-0.6	-28.5	-27.7	-27.1	-26.7	-26.5	-26.9	-27.3	-27.8	-28.3	-24.0	-21.0
-0.5	-24.5	-23.7	-23.1	-22.7	-22.5	-22.9	-23.3	-23.8	-24.3	-20.5	-18.0
-0.4	-21.0	-20.2	-19.6	-19.2	-19.0	-19.4	-19.8	-20.3	-20.8	-17.5	-15.5
-0.3	-18.0	-17.2	-16.6	-16.2	-16.0	-16.4	-16.8	-17.3	-17.8	-15.0	-13.5
-0.2	-15.5	-14.7	-14.1	-13.7	-13.5	-13.9	-14.3	-14.8	-15.3	-13.0	-12.0
-0.1	-13.5	-12.7	-12.1	-11.7	-11.5	-11.9	-12.3	-12.8	-13.3	-11.5	-11.0
0.0	-12.0	-11.2	-10.6	-10.2	-10.0	-10.4	-10.8	-11.3	-11.8	-10.5	-10.5
0.1	-11.0	-10.2	-9.6	-9.2	-9.0	-9.4	-9.8	-10.3	-10.8	-10.0	**-10.3**
0.2	-10.5	-9.7	-9.1	-8.7	-8.5	-8.9	-9.3	-9.8	-10.3	**-9.8**	-10.5
0.3	**-10.3**	**-9.5**	**-8.9**	**-8.5**	**-8.3**	**-8.7**	**-9.1**	**-9.6**	**-10.1**	-10.0	-10.9
0.4	-10.5	-9.7	-9.1	-8.7	-8.5	-8.9	-9.3	-9.8	-10.3	-10.4	-11.5
0.5	-10.9	-10.1	-9.5	-9.1	-8.9	-9.3	-9.7	-10.2	-10.7	-11.0	-12.7
0.6	-11.5	-10.7	-10.1	-9.7	-9.5	-9.9	-10.3	-10.8	-11.3	-12.2	-13.9
0.7	-12.7	-11.9	-11.3	-10.9	-10.7	-11.1	-11.5	-12.0	-12.5	-13.4	-15.1
0.8	-14.0	-13.2	-12.6	-12.2	-12.0	-12.4	-12.8	-13.2	-13.7	-14.6	-16.3
0.9	-15.4	-14.6	-14.0	-13.6	-13.4	-13.8	-14.1	-14.4	-14.9	-15.8	-17.5
1.0	-16.8	-16.0	-15.4	-15.0	-14.8	-15.2	-15.4	-15.6	-16.1	-17.0	-18.7
1.1	-18.2	-17.4	-16.8	-16.4	-16.2	-16.6	-16.7	-16.8	-17.3	-18.2	-19.9
1.2	-19.6	-18.8	-18.2	-17.8	-17.6	-18.0	-18.0	-18.0	-18.5	-19.4	-21.1
1.3	-21.0	-20.2	-19.6	-19.2	-19.0	-19.4	-19.3	-19.2	-19.7	-20.6	-22.3
1.4	-22.4	-21.6	-21.0	-20.6	-20.4	-20.8	-20.6	-20.4	-20.9	-21.8	-23.5
1.5	-23.8	-23.0	-22.4	-22.0	-21.8	-22.2	-21.9	-21.6	-22.1	-23.0	-24.7
1.6	-25.2	-24.4	-23.8	-23.4	-23.2	-23.6	-23.2	-22.8	-23.3	-24.2	-25.9
1.7	-26.6	-25.8	-25.2	-24.8	-24.6	-25.0	-24.5	-24.0	-24.5	-25.4	-27.1
1.8	-28.0	-27.2	-26.6	-26.2	-26.0	-26.4	-25.8	-25.2	-25.7	-26.6	-28.3
1.9	-29.4	-28.6	-28.0	-27.6	-27.4	-27.8	-27.1	-26.4	-26.9	-27.8	-29.5
2.0	-30.8	-30.0	-29.4	-29.0	-28.8	-29.2	-28.4	-27.6	-28.1	-29.0	-30.7
3.6	-50.4	-49.6	-49.0	-48.6	-48.4	-48.8	-46.6	-44.4	-44.9	-45.8	-47.5
$OASPL_T$-UOL_T	-0.6	0.2	0.8	1.2	1.4	1.0	0.6	0.2	-0.3	0.0	-0.5

Table III (Concluded) - Spectral Directivity Relations for Transitional-Scale Turbulent Mixing Noise
(b) Corrected Effective Directivity Angle, $\theta'_{T,cor}$, from 110 to 250 deg

Frequency parameter,	Normalized sound pressure level, SPL_T-UOL_T, dB vs. corrected effective directivity angle Corrected effective directivity angle, $\theta'_{T,cor}$, deg										
log S_T	110	120	130	140	150	160	170	180	190	200	250
-3.6	-194.3	-189.3	-184.3	-179.3	-174.3	-173.3	-171.5	-173.0	-174.0	-174.5	-195.0
-2.2	-110.3	-105.3	-100.3	-95.3	-90.3	-89.3	-87.5	-89.0	-90.0	-90.5	-111.0
-2.1	-104.3	-99.3	-94.3	-89.3	-84.3	-83.3	-81.5	-83.0	-84.0	-84.5	-105.0
-2.0	-98.3	-93.3	-88.3	-83.3	-78.3	-77.3	-75.5	-77.0	-78.0	-78.5	-99.0
-1.9	-92.3	-87.3	-82.3	-77.3	-72.3	-71.3	-69.5	-71.0	-72.0	-72.5	-93.0
-1.8	-86.3	-81.3	-76.3	-71.3	-66.3	-65.3	-63.5	-65.0	-66.0	-66.5	-87.0
-1.7	-80.3	-75.3	-70.3	-65.3	-60.3	-59.3	-57.5	-59.0	-60.0	-60.5	-81.0
-1.6	-74.3	-69.3	-64.3	-59.3	-54.3	-53.3	-53.0	-55.0	-56.5	-57.5	-75.0
-1.5	-68.3	-63.3	-58.3	-53.3	-48.3	-47.3	-48.5	-51.0	-53.0	-54.5	-73.5
-1.4	-62.3	-57.3	-52.3	-47.3	-42.3	-42.3	-44.0	-47.0	-49.5	-51.5	-72.0
-1.3	-56.3	-51.3	-46.3	-41.3	-37.3	-37.8	-40.0	-43.5	-46.5	-49.0	-70.5
-1.2	-50.3	-45.3	-40.3	-36.3	-32.8	-33.8	-36.5	-40.5	-44.0	-47.0	-69.5
-1.1	-44.3	-39.3	-35.3	-31.8	-28.8	-30.3	-33.5	-38.0	-42.0	-45.5	**-69.0**
-1.0	-38.3	-34.3	-30.8	-27.8	-25.3	-27.3	-31.0	-36.0	-40.5	-44.5	-69.3
-0.9	-33.3	-29.8	-26.8	-24.3	-22.3	-24.8	-29.0	-34.5	-39.5	**-44.0**	-70.1
-0.8	-28.8	-25.8	-23.3	-21.3	-19.8	-22.8	-27.5	-33.5	**-39.0**	-44.3	-71.3
-0.7	-24.8	-22.3	-20.3	-18.8	-17.8	-21.3	-26.5	**-33.0**	-39.3	-45.1	-72.8
-0.6	-21.3	-19.3	-17.8	-16.8	-16.3	-20.3	**-26.0**	-33.3	-40.1	-46.3	-74.6
-0.5	-18.3	-16.8	-15.8	-15.3	-15.3	**-19.8**	-26.3	-34.1	-41.3	-47.8	-76.4
-0.4	-15.8	-14.8	-14.3	-14.3	**-14.8**	-20.1	-27.1	-35.3	-42.8	-49.6	-78.2
-0.3	-13.8	-13.3	-13.3	**-13.8**	-15.1	-20.9	-28.3	-36.8	-44.6	-51.4	-80.0
-0.2	-12.3	-12.3	**-12.8**	-14.1	-15.9	-22.1	-29.8	-38.6	-46.4	-53.2	-81.8
-0.1	-11.3	**-11.8**	-13.1	-14.9	-17.1	-23.6	-31.6	-40.4	-48.2	-55.0	-83.6
0.0	**-10.8**	-12.1	-13.9	-16.1	-18.6	-25.4	-33.4	-42.2	-50.0	-56.8	-85.4
0.1	-11.1	-12.9	-15.0	-17.6	-20.4	-27.2	-35.2	-44.0	-51.8	-58.6	-87.2
0.2	-11.8	-14.0	-16.6	-19.4	-22.2	-29.0	-37.0	-45.8	-53.6	-60.4	-89.0
0.3	-12.8	-15.6	-18.2	-21.4	-24.0	-30.8	-38.8	-47.6	-55.4	-62.2	-90.8
0.4	-14.3	-17.3	-20.0	-23.4	-25.8	-32.6	-40.6	-49.4	-57.2	-64.0	-92.6
0.5	-15.8	-19.1	-21.9	-25.4	-27.6	-34.4	-42.4	-51.2	-59.0	-65.8	-94.4
0.6	-17.3	-20.9	-23.9	-27.4	-29.4	-36.2	-44.2	-53.0	-60.8	-67.6	-96.2
0.7	-18.8	-22.7	-25.9	-29.4	-31.2	-38.0	-46.0	-54.8	-62.6	-69.4	-98.0
0.8	-20.3	-24.5	-27.9	-31.4	-33.0	-39.8	-47.8	-56.6	-64.4	-71.2	-99.8
0.9	-21.8	-26.3	-29.9	-33.4	-34.8	-41.6	-49.6	-58.4	-66.2	-73.0	-101.6
1.0	-23.3	-28.1	-31.9	-35.4	-36.6	-43.4	-51.4	-60.2	-68.0	-74.8	-103.4
1.1	-24.8	-29.9	-33.9	-37.4	-38.4	-45.2	-53.2	-62.0	-69.8	-76.6	-105.2
1.2	-26.3	-31.7	-35.9	-39.4	-40.2	-47.0	-55.0	-63.8	-71.6	-78.4	-107.0
1.3	-27.8	-33.5	-37.9	-41.4	-42.0	-48.8	-56.8	-65.6	-73.4	-80.2	-108.8
1.4	-29.3	-35.3	-39.9	-43.4	-43.8	-50.6	-58.6	-67.4	-75.2	-82.0	-110.6
1.5	-30.8	-37.1	-41.9	-45.4	-45.6	-52.4	-60.4	-69.2	-77.0	-83.8	-112.4
1.6	-32.3	-38.9	-43.9	-47.4	-47.4	-54.2	-62.2	-71.0	-78.8	-85.6	-114.2
1.7	-33.8	-40.7	-45.9	-49.4	-49.2	-56.0	-64.0	-72.8	-80.6	-87.4	-116.0
1.8	-35.3	-42.5	-47.9	-51.4	-51.0	-57.8	-65.8	-74.6	-82.4	-89.2	-117.8
1.9	-36.8	-44.3	-49.9	-53.4	-52.8	-59.6	-67.6	-76.4	-84.2	-91.0	-119.6
2.0	-38.3	-46.1	-51.9	-55.4	-54.6	-61.4	-69.4	-78.2	-86.0	-92.8	-121.4
3.6	-59.3	-71.3	-79.9	-83.4	-79.8	-86.6	-94.6	-103.4	-111.2	-118.0	-146.6
$OASPL_T$-UOL_T	-2.0	-3.2	-4.2	-5.2	-6.2	-11.2	-17.4	-24.4	-30.4	-35.4	-60.4

Table IV - Spectral Directivity Relations for Inner Stream Plug Separation Noise
(a) Corrected Effective Directivity Angle, $\theta'_{P,cor}$, from 0 to 100 deg

Frequency parameter	Normalized sound pressure level, SPL_P-UOL_P, dB vs. corrected effective directivity angle										
	Corrected effective directivity angle, $\theta'_{P,cor}$, deg										
log S_P	0	10	20	30	40	50	60	70	80	90	100
-3.6	-194.1	-191.6	-188.6	-185.1	-181.1	-176.6	-170.8	-165.4	-162.8	-161.5	-161.7
-2.2	-138.1	-135.6	-132.6	-129.1	-125.1	-120.6	-114.8	-109.4	-106.8	-105.5	-105.7
-2.1	-134.1	-131.6	-128.6	-125.1	-121.1	-116.6	-110.8	-105.4	-102.8	-101.5	-101.7
-2.0	-130.1	-127.6	-124.6	-121.1	-117.1	-112.6	-106.8	-101.4	-98.8	-97.5	-97.7
-1.9	-126.1	-123.6	-120.6	-117.1	-113.1	-108.6	-102.8	-97.4	-94.8	-93.5	-93.7
-1.8	-122.1	-119.6	-116.6	-113.1	-109.1	-104.6	-98.8	-93.4	-90.8	-89.5	-89.7
-1.7	-118.1	-115.6	-112.6	-109.1	-105.1	-100.6	-94.8	-89.4	-86.8	-85.5	-85.7
-1.6	-114.1	-111.6	-108.6	-105.1	-101.1	-96.6	-90.8	-85.4	-82.8	-81.5	-81.7
-1.5	-110.1	-107.6	-104.6	-101.1	-97.1	-92.6	-86.8	-81.4	-78.8	-77.5	-77.7
-1.4	-106.1	-103.6	-100.6	-97.1	-93.1	-88.6	-82.8	-77.4	-74.8	-73.5	-73.7
-1.3	-102.1	-99.6	-96.6	-93.1	-89.1	-84.6	-78.8	-73.4	-70.8	-69.5	-69.7
-1.2	-98.1	-95.6	-92.6	-89.1	-85.1	-80.6	-74.8	-69.4	-66.8	-65.5	-65.7
-1.1	-94.1	-91.6	-88.6	-85.1	-81.1	-76.6	-70.8	-65.4	-62.8	-61.5	-61.7
-1.0	-90.1	-87.6	-84.6	-81.1	-77.1	-72.6	-66.8	-61.4	-58.8	-57.5	-57.7
-0.9	-86.1	-83.6	-80.6	-77.1	-73.1	-68.6	-62.8	-57.4	-54.8	-53.5	-53.7
-0.8	-82.1	-79.6	-76.6	-73.1	-69.1	-64.6	-58.8	-53.4	-50.8	-49.5	-49.7
-0.7	-78.1	-75.6	-72.6	-69.1	-65.1	-60.6	-54.8	-49.4	-46.8	-45.5	-45.7
-0.6	-74.1	-71.6	-68.6	-65.1	-61.1	-56.6	-50.8	-45.4	-42.8	-41.5	-41.7
-0.5	-70.1	-67.6	-64.6	-61.1	-57.1	-52.6	-46.8	-41.4	-38.8	-37.5	-37.7
-0.4	-66.1	-63.6	-60.6	-57.1	-53.1	-48.6	-42.8	-37.4	-34.8	-33.5	-33.7
-0.3	-62.1	-59.6	-56.6	-53.1	-49.1	-44.6	-38.8	-33.4	-30.8	-29.5	-29.7
-0.2	-58.1	-55.6	-52.6	-49.1	-45.1	-40.6	-34.8	-29.4	-26.8	-25.5	-25.7
-0.1	-54.1	-51.6	-48.6	-45.1	-41.1	-36.6	-30.8	-25.4	-22.8	-21.5	-21.7
0.0	-50.1	-47.6	-44.6	-41.1	-37.1	-32.6	-26.8	-21.4	-18.8	-17.5	-17.7
0.1	-46.6	-44.1	-41.1	-37.6	-33.6	-29.1	-23.3	-17.9	-15.3	-14.0	-14.2
0.2	-43.8	-41.3	-38.3	-34.8	-30.8	-26.3	-20.5	-15.1	-12.5	-11.2	-11.4
0.3	-42.0	-39.5	-36.5	-33.0	-29.0	-24.5	-18.7	-13.3	-10.7	-9.4	-9.6
0.4	**-41.0**	**-38.5**	**-35.5**	**-32.0**	**-28.0**	**-23.5**	**-17.7**	**-12.3**	**-9.7**	**-8.4**	**-8.6**
0.5	-41.4	-38.9	-35.9	-32.4	-28.4	-23.9	-18.1	-12.7	-10.1	-8.8	-9.0
0.6	-42.0	-39.5	-36.5	-33.0	-29.0	-24.5	-18.7	-13.3	-10.7	-9.4	-9.6
0.7	-43.2	-40.7	-37.7	-34.2	-30.2	-25.7	-19.9	-14.5	-11.9	-10.6	-10.8
0.8	-44.4	-41.9	-38.9	-35.4	-31.4	-26.9	-21.1	-15.7	-13.1	-11.8	-12.0
0.9	-45.6	-43.1	-40.1	-36.6	-32.6	-28.1	-22.3	-16.9	-14.3	-13.0	-13.2
1.0	-46.8	-44.3	-41.3	-37.8	-33.8	-29.3	-23.5	-18.1	-15.5	-14.2	-14.4
1.1	-48.0	-45.5	-42.5	-39.0	-35.0	-30.5	-24.7	-19.3	-16.7	-15.4	-15.6
1.2	-49.2	-46.7	-43.7	-40.2	-36.2	-31.7	-25.9	-20.5	-17.9	-16.6	-16.8
1.3	-50.4	-47.9	-44.9	-41.4	-37.4	-32.9	-27.1	-21.7	-19.1	-17.8	-18.0
1.4	-51.6	-49.1	-46.1	-42.6	-38.6	-34.1	-28.3	-22.9	-20.3	-19.0	-19.2
1.5	-52.8	-50.3	-47.3	-43.8	-39.8	-35.3	-29.5	-24.1	-21.5	-20.2	-20.4
1.6	-54.0	-51.5	-48.5	-45.0	-41.0	-36.5	-30.7	-25.3	-22.7	-21.4	-21.6
1.7	-55.2	-52.7	-49.7	-46.2	-42.2	-37.7	-31.9	-26.5	-23.9	-22.6	-22.8
1.8	-56.4	-53.9	-50.9	-47.4	-43.4	-38.9	-33.1	-27.7	-25.1	-23.8	-24.0
1.9	-57.6	-55.1	-52.1	-48.6	-44.6	-40.1	-34.3	-28.9	-26.3	-25.0	-25.2
2.0	-58.8	-56.3	-53.3	-49.8	-45.8	-41.3	-35.5	-30.1	-27.5	-26.2	-26.4
3.6	-78.0	-75.5	-72.5	-69.0	-65.0	-60.5	-54.7	-49.3	-46.7	-45.4	-45.6
$OASPL_P$-UOL_P	-32.6	-30.1	-27.1	-23.6	-19.6	-15.1	-9.3	-3.9	-1.3	0.0	-0.2

Table IV (Concluded) - Spectral Directivity Relations for Inner Stream Plug Separation Noise
(b) Corrected Effective Directivity Angle, $\theta'_{P,cor}$, from 110 to 250 deg

Frequency	Normalized sound pressure level, SPL_P-UOL_P, dB vs. corrected effective directivity angle										
parameter	Corrected effective directivity angle, $\theta'_{P,cor}$, deg										
$\log S_P$	110	120	130	140	150	160	170	180	190	200	250
-3.6	-158.3	-160.1	-163.1	-166.1	-168.1	-170.1	-171.1	-172.6	-174.1	-176.1	-186.1
-2.2	-102.3	-104.1	-107.1	-110.1	-112.1	-114.1	-115.1	-116.6	-118.1	-120.1	-130.1
-2.1	-98.3	-100.1	-103.1	-106.1	-108.1	-110.1	-111.1	-112.6	-114.1	-116.1	-126.1
-2.0	-94.3	-96.1	-99.1	-102.1	-104.1	-106.1	-107.1	-108.6	-110.1	-112.1	-122.1
-1.9	-90.3	-92.1	-95.1	-98.1	-100.1	-102.1	-103.1	-104.6	-106.1	-108.1	-118.1
-1.8	-86.3	-88.1	-91.1	-94.1	-96.1	-98.1	-99.1	-100.6	-102.1	-104.1	-114.1
-1.7	-82.3	-84.1	-87.1	-90.1	-92.1	-94.1	-95.1	-96.6	-98.1	-100.1	-110.1
-1.6	-78.3	-80.1	-83.1	-86.1	-88.1	-90.1	-91.1	-92.6	-94.1	-96.1	-106.1
-1.5	-74.3	-76.1	-79.1	-82.1	-84.1	-86.1	-87.1	-88.6	-90.1	-92.1	-102.1
-1.4	-70.3	-72.1	-75.1	-78.1	-80.1	-82.1	-83.1	-84.6	-86.1	-88.1	-98.1
-1.3	-66.3	-68.1	-71.1	-74.1	-76.1	-78.1	-79.1	-80.6	-82.1	-84.1	-94.1
-1.2	-62.3	-64.1	-67.1	-70.1	-72.1	-74.1	-75.1	-76.6	-78.1	-80.1	-90.1
-1.1	-58.3	-60.1	-63.1	-66.1	-68.1	-70.1	-71.1	-72.6	-74.1	-76.1	-86.1
-1.0	-54.3	-56.1	-59.1	-62.1	-64.1	-66.1	-67.1	-68.6	-70.1	-72.1	-82.1
-0.9	-50.3	-52.1	-55.1	-58.1	-60.1	-62.1	-63.1	-64.6	-66.1	-68.1	-78.1
-0.8	-46.3	-48.1	-51.1	-54.1	-56.1	-58.1	-59.1	-60.6	-62.1	-64.1	-74.1
-0.7	-42.3	-44.1	-47.1	-50.1	-52.1	-54.1	-55.1	-56.6	-58.1	-60.1	-70.1
-0.6	-38.3	-40.1	-43.1	-46.1	-48.1	-50.1	-51.1	-52.6	-54.1	-56.1	-66.1
-0.5	-34.3	-36.1	-39.1	-42.1	-44.1	-46.1	-47.1	-48.6	-50.1	-52.1	-62.1
-0.4	-30.3	-32.1	-35.1	-38.1	-40.1	-42.1	-43.1	-44.6	-46.1	-48.1	-58.1
-0.3	-26.3	-28.1	-31.1	-34.1	-36.1	-38.1	-39.1	-40.6	-42.1	-44.1	-54.1
-0.2	-22.3	-24.1	-27.1	-30.1	-32.1	-34.1	-35.1	-36.6	-38.1	-40.1	-50.1
-0.1	-18.3	-20.1	-23.1	-26.1	-28.1	-30.1	-31.1	-32.6	-34.1	-36.1	-46.1
0.0	-14.8	-16.6	-19.6	-22.6	-24.6	-26.6	-27.6	-29.1	-30.6	-32.6	-42.6
0.1	-12.0	-13.8	-16.8	-19.8	-21.8	-23.8	-24.8	-26.3	-27.8	-29.8	-39.8
0.2	-10.2	-12.0	-15.0	-18.0	-20.0	-22.0	-23.0	-24.5	-26.0	-28.0	-38.0
0.3	**-9.2**	**-11.0**	**-14.0**	**-17.0**	**-19.0**	**-21.0**	**-22.0**	**-23.5**	**-25.0**	**-27.0**	**-37.0**
0.4	-9.6	-11.4	-14.4	-17.4	-19.4	-21.4	-22.4	-23.9	-25.4	-27.4	-37.4
0.5	-10.2	-12.0	-15.0	-18.0	-20.0	-22.0	-23.0	-24.5	-26.0	-28.0	-38.0
0.6	-11.4	-13.2	-16.2	-19.2	-21.2	-23.2	-24.2	-25.7	-27.2	-29.2	-39.2
0.7	-12.6	-14.4	-17.4	-20.4	-22.4	-24.4	-25.4	-26.9	-28.4	-30.4	-40.4
0.8	-13.8	-15.6	-18.6	-21.6	-23.6	-25.6	-26.6	-28.1	-29.6	-31.6	-41.6
0.9	-15.0	-16.8	-19.8	-22.8	-24.8	-26.8	-27.8	-29.3	-30.8	-32.8	-42.8
1.0	-16.2	-18.0	-21.0	-24.0	-26.0	-28.0	-29.0	-30.5	-32.0	-34.0	-44.0
1.1	-17.4	-19.2	-22.2	-25.2	-27.2	-29.2	-30.2	-31.7	-33.2	-35.2	-45.2
1.2	-18.6	-20.4	-23.4	-26.4	-28.4	-30.4	-31.4	-32.9	-34.4	-36.4	-46.4
1.3	-19.8	-21.6	-24.6	-27.6	-29.6	-31.6	-32.6	-34.1	-35.6	-37.6	-47.6
1.4	-21.0	-22.8	-25.8	-28.8	-30.8	-32.8	-33.8	-35.3	-36.8	-38.8	-48.8
1.5	-22.2	-24.0	-27.0	-30.0	-32.0	-34.0	-35.0	-36.5	-38.0	-40.0	-50.0
1.6	-23.4	-25.2	-28.2	-31.2	-33.2	-35.2	-36.2	-37.7	-39.2	-41.2	-51.2
1.7	-24.6	-26.4	-29.4	-32.4	-34.4	-36.4	-37.4	-38.9	-40.4	-42.4	-52.4
1.8	-25.8	-27.6	-30.6	-33.6	-35.6	-37.6	-38.6	-40.1	-41.6	-43.6	-53.6
1.9	-27.0	-28.8	-31.8	-34.8	-36.8	-38.8	-39.8	-41.3	-42.8	-44.8	-54.8
2.0	-28.2	-30.0	-33.0	-36.0	-38.0	-40.0	-41.0	-42.5	-44.0	-46.0	-56.0
3.6	-47.4	-49.2	-52.2	-55.2	-57.2	-59.2	-60.2	-61.7	-63.2	-65.2	-75.2
$OASPL_P$-UOL_P	-0.8	-2.6	-5.6	-8.6	-10.6	-12.6	-13.6	-15.1	-16.6	-18.6	-28.6

Table V - Spectral Directivity Relations for Plug/Downstream Shock Noise
(a) Corrected Directivity Angle, $\theta_{D.sh,cor}$, 0 to 90 deg

Frequency parameter	Normalized sound pressure level, $SPL_{D,sh}$-$UOL_{D,sh}$, dB vs. corrected directivity angle Corrected directivity angle, $\theta_{D,sh,cor}$, deg									
log $S_{D,sh}$	0	10	20	30	40	50	60	70	80	90
-3.6	-174.2	-173.0	-171.8	-170.6	-169.4	-168.2	-166.0	-165.3	-159.8	-159.6
-2.2	-104.2	-103.0	-101.8	-100.6	-99.4	-98.2	-96.0	-95.3	-89.8	-89.6
-2.1	-99.2	-98.0	-96.8	-95.6	-94.4	-93.2	-91.0	-90.3	-84.8	-84.6
-2.0	-94.2	-93.0	-91.8	-90.6	-89.4	-88.2	-86.0	-85.3	-79.8	-79.6
-1.9	-89.2	-88.0	-86.8	-85.6	-84.4	-83.2	-81.0	-80.3	-74.8	-74.6
-1.8	-84.2	-83.0	-81.8	-80.6	-79.4	-78.2	-76.0	-75.3	-69.8	-69.6
-1.7	-79.2	-78.0	-76.8	-75.6	-74.4	-73.2	-71.0	-70.3	-64.8	-64.6
-1.6	-74.2	-73.0	-71.8	-70.6	-69.4	-68.2	-66.0	-65.3	-59.8	-59.6
-1.5	-69.2	-68.0	-66.8	-65.6	-64.4	-63.2	-61.0	-60.3	-54.8	-54.6
-1.4	-64.2	-63.0	-61.8	-60.6	-59.4	-58.2	-56.0	-55.3	-49.8	-49.6
-1.3	-59.2	-58.0	-56.8	-55.6	-54.4	-53.2	-51.0	-50.3	-44.8	-44.6
-1.2	-54.2	-53.0	-51.8	-50.6	-49.4	-48.2	-46.0	-45.3	-39.8	-39.6
-1.1	-49.2	-48.0	-46.8	-45.6	-44.4	-43.2	-41.0	-40.3	-34.8	-34.6
-1.0	-44.2	-43.0	-41.8	-40.6	-39.4	-38.2	-36.0	-35.3	-29.8	-29.6
-0.9	-39.2	-38.0	-36.8	-35.6	-34.4	-33.2	-31.0	-30.3	-24.8	-24.6
-0.8	-34.2	-33.0	-31.8	-30.6	-29.4	-28.2	-26.0	-25.3	-19.8	-19.6
-0.7	-29.2	-28.0	-26.8	-25.6	-24.4	-23.2	-21.0	-20.3	-14.8	-14.6
-0.6	-24.2	-23.0	-21.8	-20.6	-19.4	-18.2	-16.0	-15.3	-9.8	-9.6
-0.5	-19.2	-18.0	-16.8	-15.6	-14.4	-13.2	-11.0	-10.3	**-7.3**	**-7.6**
-0.4	**-14.2**	**-13.0**	**-11.8**	**-10.6**	**-9.4**	**-8.2**	**-7.0**	**-7.3**	-9.3	-8.6
-0.3	-16.2	-15.0	-13.8	-12.6	-11.4	-10.2	-9.0	-9.3	-10.3	-9.6
-0.2	-18.2	-17.0	-15.8	-14.6	-13.4	-12.2	-11.0	-10.3	-11.3	-10.6
-0.1	-20.2	-19.0	-17.8	-16.6	-15.4	-14.2	-12.0	-11.3	-12.3	-11.6
0.0	-22.2	-21.0	-19.8	-18.6	-16.4	-15.2	-13.0	-12.3	-13.3	-12.6
0.1	-23.2	-22.0	-20.8	-19.6	-17.4	-16.2	-14.0	-13.3	-14.3	-13.6
0.2	-24.2	-23.0	-21.8	-20.6	-18.4	-17.2	-15.0	-14.3	-15.3	-14.6
0.3	-25.2	-24.0	-22.8	-21.6	-19.4	-18.2	-16.0	-15.3	-16.3	-15.6
0.4	-26.2	-25.0	-23.8	-22.6	-20.4	-19.2	-17.0	-16.3	-17.3	-16.6
0.5	-27.2	-26.0	-24.8	-23.6	-21.4	-20.2	-18.0	-17.3	-18.3	-17.6
0.6	-28.2	-27.0	-25.8	-24.6	-22.4	-21.2	-19.0	-18.3	-19.3	-18.6
0.7	-29.2	-28.0	-26.8	-25.6	-23.4	-22.2	-20.0	-19.3	-20.3	-19.6
0.8	-30.2	-29.0	-27.8	-26.6	-24.4	-23.2	-21.0	-20.3	-21.3	-20.6
0.9	-31.2	-30.0	-28.8	-27.6	-25.4	-24.2	-22.0	-21.3	-22.3	-21.6
1.0	-32.2	-31.0	-29.8	-28.6	-26.4	-25.2	-23.0	-22.3	-23.3	-22.6
1.1	-33.2	-32.0	-30.8	-29.6	-27.4	-26.2	-24.0	-23.3	-24.3	-23.6
1.2	-34.2	-33.0	-31.8	-30.6	-28.4	-27.2	-25.0	-24.3	-25.3	-24.6
1.3	-35.2	-34.0	-32.8	-31.6	-29.4	-28.2	-26.0	-25.3	-26.3	-25.6
1.4	-36.2	-35.0	-33.8	-32.6	-30.4	-29.2	-27.0	-26.3	-27.3	-26.6
1.5	-37.2	-36.0	-34.8	-33.6	-31.4	-30.2	-28.0	-27.3	-28.3	-27.6
1.6	-38.2	-37.0	-35.8	-34.6	-32.4	-31.2	-29.0	-28.3	-29.3	-28.6
1.7	-39.2	-38.0	-36.8	-35.6	-33.4	-32.2	-30.0	-29.3	-30.3	-29.6
1.8	-40.2	-39.0	-37.8	-36.6	-34.4	-33.2	-31.0	-30.3	-31.3	-30.6
1.9	-41.2	-40.0	-38.8	-37.6	-35.4	-34.2	-32.0	-31.3	-32.3	-31.6
2.0	-42.2	-41.0	-39.8	-38.6	-36.4	-35.2	-33.0	-32.3	-33.3	-32.6
3.6	-58.2	-57.0	-55.8	-54.6	-52.4	-51.2	-49.0	-48.3	-49.3	-48.6
$OASPL_{D,sh}$-$UOL_{D,sh}$	-8.8	-7.6	-6.4	-5.2	-3.7	-2.5	-0.8	-0.5	-0.4	0.0

Table V (Concluded) - Spectral Directivity Relations for Plug/Downstream Shock Noise
(b) Corrected Directivity Angle, $\theta_{D.sh,cor}$, 100 to 180 deg

Frequency parameter	Normalized sound pressure level, $SPL_{D,sh}$-$UOL_{D,sh}$, dB vs. corrected directivity angle								
	Corrected directivity angle, $\theta_{D,sh,cor}$, deg								
log $S_{D,sh}$	100	110	120	130	140	150	160	170	180
-3.6	-159.6	-159.6	-159.6	-159.6	-159.6	-159.6	-159.6	-159.6	-159.6
-2.2	-89.6	-89.6	-89.6	-89.6	-89.6	-89.6	-89.6	-89.6	-89.6
-2.1	-84.6	-84.6	-84.6	-84.6	-84.6	-84.6	-84.6	-84.6	-84.6
-2.0	-79.6	-79.6	-79.6	-79.6	-79.6	-79.6	-79.6	-79.6	-79.6
-1.9	-74.6	-74.6	-74.6	-74.6	-74.6	-74.6	-74.6	-74.6	-74.6
-1.8	-69.6	-69.6	-69.6	-69.6	-69.6	-69.6	-69.6	-69.6	-69.6
-1.7	-64.6	-64.6	-64.6	-64.6	-64.6	-64.6	-64.6	-64.6	-64.6
-1.6	-59.6	-59.6	-59.6	-59.6	-59.6	-59.6	-59.6	-59.6	-59.6
-1.5	-54.6	-54.6	-54.6	-54.6	-54.6	-54.6	-54.6	-54.6	-54.6
-1.4	-49.6	-49.6	-49.6	-49.6	-49.6	-49.6	-49.6	-49.6	-49.6
-1.3	-44.6	-44.6	-44.6	-44.6	-44.6	-44.6	-44.6	-44.6	-44.6
-1.2	-39.6	-39.6	-39.6	-39.6	-39.6	-39.6	-39.6	-39.6	-39.6
-1.1	-34.6	-34.6	-34.6	-34.6	-34.6	-34.6	-34.6	-34.6	-34.6
-1.0	-29.6	-29.6	-29.6	-29.6	-29.6	-29.6	-29.6	-29.6	-29.6
-0.9	-24.6	-24.6	-24.6	-24.6	-24.6	-24.6	-24.6	-24.6	-24.6
-0.8	-19.6	-19.6	-19.6	-19.6	-19.6	-19.6	-19.6	-19.6	-19.6
-0.7	-14.6	-14.6	-14.6	-14.6	-14.6	-14.6	-14.6	-14.6	-14.6
-0.6	-9.6	-9.6	-9.6	-9.6	-9.6	-9.6	-9.6	-9.6	-9.6
-0.5	**-7.6**	**-7.6**	**-7.6**	**-7.6**	**-7.6**	**-7.6**	**-7.6**	**-7.6**	**-7.6**
-0.4	-8.6	-8.6	-8.6	-8.6	-8.6	-8.6	-8.6	-8.6	-8.6
-0.3	-9.6	-9.6	-9.6	-9.6	-9.6	-9.6	-9.6	-9.6	-9.6
-0.2	-10.6	-10.6	-10.6	-10.6	-10.6	-10.6	-10.6	-10.6	-10.6
-0.1	-11.6	-11.6	-11.6	-11.6	-11.6	-11.6	-11.6	-11.6	-11.6
0.0	-12.6	-12.6	-12.6	-12.6	-12.6	-12.6	-12.6	-12.6	-12.6
0.1	-13.6	-13.6	-13.6	-13.6	-13.6	-13.6	-13.6	-13.6	-13.6
0.2	-14.6	-14.6	-14.6	-14.6	-14.6	-14.6	-14.6	-14.6	-14.6
0.3	-15.6	-15.6	-15.6	-15.6	-15.6	-15.6	-15.6	-15.6	-15.6
0.4	-16.6	-16.6	-16.6	-16.6	-16.6	-16.6	-16.6	-16.6	-16.6
0.5	-17.6	-17.6	-17.6	-17.6	-17.6	-17.6	-17.6	-17.6	-17.6
0.6	-18.6	-18.6	-18.6	-18.6	-18.6	-18.6	-18.6	-18.6	-18.6
0.7	-19.6	-19.6	-19.6	-19.6	-19.6	-19.6	-19.6	-19.6	-19.6
0.8	-20.6	-20.6	-20.6	-20.6	-20.6	-20.6	-20.6	-20.6	-20.6
0.9	-21.6	-21.6	-21.6	-21.6	-21.6	-21.6	-21.6	-21.6	-21.6
1.0	-22.6	-22.6	-22.6	-22.6	-22.6	-22.6	-22.6	-22.6	-22.6
1.1	-23.6	-23.6	-23.6	-23.6	-23.6	-23.6	-23.6	-23.6	-23.6
1.2	-24.6	-24.6	-24.6	-24.6	-24.6	-24.6	-24.6	-24.6	-24.6
1.3	-25.6	-25.6	-25.6	-25.6	-25.6	-25.6	-25.6	-25.6	-25.6
1.4	-26.6	-26.6	-26.6	-26.6	-26.6	-26.6	-26.6	-26.6	-26.6
1.5	-27.6	-27.6	-27.6	-27.6	-27.6	-27.6	-27.6	-27.6	-27.6
1.6	-28.6	-28.6	-28.6	-28.6	-28.6	-28.6	-28.6	-28.6	-28.6
1.7	-29.6	-29.6	-29.6	-29.6	-29.6	-29.6	-29.6	-29.6	-29.6
1.8	-30.6	-30.6	-30.6	-30.6	-30.6	-30.6	-30.6	-30.6	-30.6
1.9	-31.6	-31.6	-31.6	-31.6	-31.6	-31.6	-31.6	-31.6	-31.6
2.0	-32.6	-32.6	-32.6	-32.6	-32.6	-32.6	-32.6	-32.6	-32.6
3.6	-48.6	-48.6	-48.6	-48.6	-48.6	-48.6	-48.6	-48.6	-48.6
$OASPL_{D,sh}$-$UOL_{D,sh}$	0.0	0.0	0.0	0.0	0.0	0.0	0.0	0.0	0.0

Table VI - Spectral Directivity Relations for Outer Stream Shock Noise
(a) Corrected Directivity Angle, $\theta_{O.sh,cor}$, 0 to 90 deg

Frequency parameter	Normalized sound pressure level, $SPL_{O,sh}$-$UOL_{O,sh}$, dB vs. corrected directivity angle									
	Corrected directivity angle, $\theta_{O,sh,cor}$, deg									
log $S_{O,sh}$	0	10	20	30	40	50	60	70	80	90
-3.6	-186.6	-184.6	-182.6	-180.6	-178.6	-176.6	-174.6	-174.6	-174.6	-174.6
-2.2	-116.6	-114.6	-112.6	-110.6	-108.6	-106.6	-104.6	-104.6	-104.6	-104.6
-2.1	-111.6	-109.6	-107.6	-105.6	-103.6	-101.6	-99.6	-99.6	-99.6	-99.6
-2.0	-106.6	-104.6	-102.6	-100.6	-98.6	-96.6	-94.6	-94.6	-94.6	-94.6
-1.9	-101.6	-99.6	-97.6	-95.6	-93.6	-91.6	-89.6	-89.6	-89.6	-89.6
-1.8	-96.6	-94.6	-92.6	-90.6	-88.6	-86.6	-84.6	-84.6	-84.6	-84.6
-1.7	-91.6	-89.6	-87.6	-85.6	-83.6	-81.6	-79.6	-79.6	-79.6	-79.6
-1.6	-86.6	-84.6	-82.6	-80.6	-78.6	-76.6	-74.6	-74.6	-74.6	-74.6
-1.5	-81.6	-79.6	-77.6	-75.6	-73.6	-71.6	-69.6	-69.6	-69.6	-69.6
-1.4	-76.6	-74.6	-72.6	-70.6	-68.6	-66.6	-64.6	-64.6	-64.6	-64.6
-1.3	-71.6	-69.6	-67.6	-65.6	-63.6	-61.6	-59.6	-59.6	-59.6	-59.6
-1.2	-66.6	-64.6	-62.6	-60.6	-58.6	-56.6	-54.6	-54.6	-54.6	-54.6
-1.1	-61.6	-59.6	-57.6	-55.6	-53.6	-51.6	-49.6	-49.6	-49.6	-49.6
-1.0	-56.6	-54.6	-52.6	-50.6	-48.6	-46.6	-44.6	-44.6	-44.6	-44.6
-0.9	-51.6	-49.6	-47.6	-45.6	-43.6	-41.6	-39.6	-39.6	-39.6	-39.6
-0.8	-46.6	-44.6	-42.6	-40.6	-38.6	-36.6	-34.6	-34.6	-34.6	-34.6
-0.7	-41.6	-39.6	-37.6	-35.6	-33.6	-31.6	-29.6	-29.6	-29.6	-29.6
-0.6	-36.6	-34.6	-32.6	-30.6	-28.6	-26.6	-24.6	-24.6	-24.6	-24.6
-0.5	-31.6	-29.6	-27.6	-25.6	-23.6	-21.6	-19.6	-19.6	-19.6	-19.6
-0.4	-26.6	-24.6	-22.6	-20.6	-18.6	-16.6	-14.6	-14.6	-14.6	-14.6
-0.3	-21.6	-19.6	-17.6	-15.6	-13.6	-11.6	-9.6	-9.6	-9.6	-9.6
-0.2	**-19.6**	**-17.6**	**-15.6**	**-13.6**	**-11.6**	**-9.6**	**-7.6**	**-7.6**	**-7.6**	**-7.6**
-0.1	-20.6	-18.6	-16.6	-14.6	-12.6	-10.6	-8.6	-8.6	-8.6	-8.6
0.0	-21.6	-19.6	-17.6	-15.6	-13.6	-11.6	-9.6	-9.6	-9.6	-9.6
0.1	-22.6	-20.6	-18.6	-16.6	-14.6	-12.6	-10.6	-10.6	-10.6	-10.6
0.2	-23.6	-21.6	-19.6	-17.6	-15.6	-13.6	-11.6	-11.6	-11.6	-11.6
0.3	-24.6	-22.6	-20.6	-18.6	-16.6	-14.6	-12.6	-12.6	-12.6	-12.6
0.4	-25.6	-23.6	-21.6	-19.6	-17.6	-15.6	-13.6	-13.6	-13.6	-13.6
0.5	-26.6	-24.6	-22.6	-20.6	-18.6	-16.6	-14.6	-14.6	-14.6	-14.6
0.6	-27.6	-25.6	-23.6	-21.6	-19.6	-17.6	-15.6	-15.6	-15.6	-15.6
0.7	-28.6	-26.6	-24.6	-22.6	-20.6	-18.6	-16.6	-16.6	-16.6	-16.6
0.8	-29.6	-27.6	-25.6	-23.6	-21.6	-19.6	-17.6	-17.6	-17.6	-17.6
0.9	-30.6	-28.6	-26.6	-24.6	-22.6	-20.6	-18.6	-18.6	-18.6	-18.6
1.0	-31.6	-29.6	-27.6	-25.6	-23.6	-21.6	-19.6	-19.6	-19.6	-19.6
1.1	-32.6	-30.6	-28.6	-26.6	-24.6	-22.6	-20.6	-20.6	-20.6	-20.6
1.2	-33.6	-31.6	-29.6	-27.6	-25.6	-23.6	-21.6	-21.6	-21.6	-21.6
1.3	-34.6	-32.6	-30.6	-28.6	-26.6	-24.6	-22.6	-22.6	-22.6	-22.6
1.4	-35.6	-33.6	-31.6	-29.6	-27.6	-25.6	-23.6	-23.6	-23.6	-23.6
1.5	-36.6	-34.6	-32.6	-30.6	-28.6	-26.6	-24.6	-24.6	-24.6	-24.6
1.6	-37.6	-35.6	-33.6	-31.6	-29.6	-27.6	-25.6	-25.6	-25.6	-25.6
1.7	-38.6	-36.6	-34.6	-32.6	-30.6	-28.6	-26.6	-26.6	-26.6	-26.6
1.8	-39.6	-37.6	-35.6	-33.6	-31.6	-29.6	-27.6	-27.6	-27.6	-27.6
1.9	-40.6	-38.6	-36.6	-34.6	-32.6	-30.6	-28.6	-28.6	-28.6	-28.6
2.0	-41.6	-39.6	-37.6	-35.6	-33.6	-31.6	-29.6	-29.6	-29.6	-29.6
3.6	-57.6	-55.6	-53.6	-51.6	-49.6	-47.6	-45.6	-45.6	-45.6	-45.6
$OASPL_{O,sh}$-$UOL_{O,sh}$	-12.0	-10.0	-8.0	-6.0	-4.0	-2.0	0.0	0.0	0.0	0.0

Table VI (Concluded) - Spectral Directivity Relations for Outer Stream Shock Noise
(b) Corrected Directivity Angle, $\theta_{O.sh,cor}$, 100 to 180 deg

Frequency parameter	Normalized sound pressure level, $SPL_{o,sh}$-$UOL_{o,sh}$, dB vs. corrected directivity angle								
	Corrected directivity angle, $\theta_{O,sh,cor}$, deg								
log $S_{O,sh}$	100	110	120	130	140	150	160	170	180
-3.6	-174.6	-174.6	-174.6	-174.6	-179.6	-179.6	-179.6	-179.6	-179.6
-2.2	-104.6	-104.6	-104.6	-104.6	-109.6	-109.6	-109.6	-109.6	-109.6
-2.1	-99.6	-99.6	-99.6	-99.6	-104.6	-104.6	-104.6	-104.6	-104.6
-2.0	-94.6	-94.6	-94.6	-94.6	-99.6	-99.6	-99.6	-99.6	-99.6
-1.9	-89.6	-89.6	-89.6	-89.6	-94.6	-94.6	-94.6	-94.6	-94.6
-1.8	-84.6	-84.6	-84.6	-84.6	-89.6	-89.6	-89.6	-89.6	-89.6
-1.7	-79.6	-79.6	-79.6	-79.6	-84.6	-84.6	-84.6	-84.6	-84.6
-1.6	-74.6	-74.6	-74.6	-74.6	-79.6	-79.6	-79.6	-79.6	-79.6
-1.5	-69.6	-69.6	-69.6	-69.6	-74.6	-74.6	-74.6	-74.6	-74.6
-1.4	-64.6	-64.6	-64.6	-64.6	-69.6	-69.6	-69.6	-69.6	-69.6
-1.3	-59.6	-59.6	-59.6	-59.6	-64.6	-64.6	-64.6	-64.6	-64.6
-1.2	-54.6	-54.6	-54.6	-54.6	-59.6	-59.6	-59.6	-59.6	-59.6
-1.1	-49.6	-49.6	-49.6	-49.6	-54.6	-54.6	-54.6	-54.6	-54.6
-1.0	-44.6	-44.6	-44.6	-44.6	-49.6	-49.6	-49.6	-49.6	-49.6
-0.9	-39.6	-39.6	-39.6	-39.6	-44.6	-44.6	-44.6	-44.6	-44.6
-0.8	-34.6	-34.6	-34.6	-34.6	-39.6	-39.6	-39.6	-39.6	-39.6
-0.7	-29.6	-29.6	-29.6	-29.6	-34.6	-34.6	-34.6	-34.6	-34.6
-0.6	-24.6	-24.6	-24.6	-24.6	-29.6	-29.6	-29.6	-29.6	-29.6
-0.5	-19.6	-19.6	-19.6	-19.6	-24.6	-24.6	-24.6	-24.6	-24.6
-0.4	-14.6	-14.6	-14.6	-14.6	-19.6	-19.6	-19.6	-19.6	-19.6
-0.3	-9.6	-9.6	-9.6	-9.6	-14.6	-14.6	-14.6	-14.6	-14.6
-0.2	**-7.6**	**-7.6**	**-7.6**	**-7.6**	-9.6	-9.6	-9.6	-9.6	-9.6
-0.1	-8.6	-8.6	-8.6	-8.6	**-7.6**	**-7.6**	**-7.6**	**-7.6**	**-7.6**
0.0	-9.6	-9.6	-9.6	-9.6	-8.6	-8.6	-8.6	-8.6	-8.6
0.1	-10.6	-10.6	-10.6	-10.6	-9.6	-9.6	-9.6	-9.6	-9.6
0.2	-11.6	-11.6	-11.6	-11.6	-10.6	-10.6	-10.6	-10.6	-10.6
0.3	-12.6	-12.6	-12.6	-12.6	-11.6	-11.6	-11.6	-11.6	-11.6
0.4	-13.6	-13.6	-13.6	-13.6	-12.6	-12.6	-12.6	-12.6	-12.6
0.5	-14.6	-14.6	-14.6	-14.6	-13.6	-13.6	-13.6	-13.6	-13.6
0.6	-15.6	-15.6	-15.6	-15.6	-14.6	-14.6	-14.6	-14.6	-14.6
0.7	-16.6	-16.6	-16.6	-16.6	-15.6	-15.6	-15.6	-15.6	-15.6
0.8	-17.6	-17.6	-17.6	-17.6	-16.6	-16.6	-16.6	-16.6	-16.6
0.9	-18.6	-18.6	-18.6	-18.6	-17.6	-17.6	-17.6	-17.6	-17.6
1.0	-19.6	-19.6	-19.6	-19.6	-18.6	-18.6	-18.6	-18.6	-18.6
1.1	-20.6	-20.6	-20.6	-20.6	-19.6	-19.6	-19.6	-19.6	-19.6
1.2	-21.6	-21.6	-21.6	-21.6	-20.6	-20.6	-20.6	-20.6	-20.6
1.3	-22.6	-22.6	-22.6	-22.6	-21.6	-21.6	-21.6	-21.6	-21.6
1.4	-23.6	-23.6	-23.6	-23.6	-22.6	-22.6	-22.6	-22.6	-22.6
1.5	-24.6	-24.6	-24.6	-24.6	-23.6	-23.6	-23.6	-23.6	-23.6
1.6	-25.6	-25.6	-25.6	-25.6	-24.6	-24.6	-24.6	-24.6	-24.6
1.7	-26.6	-26.6	-26.6	-26.6	-25.6	-25.6	-25.6	-25.6	-25.6
1.8	-27.6	-27.6	-27.6	-27.6	-26.6	-26.6	-26.6	-26.6	-26.6
1.9	-28.6	-28.6	-28.6	-28.6	-27.6	-27.6	-27.6	-27.6	-27.6
2.0	-29.6	-29.6	-29.6	-29.6	-28.6	-28.6	-28.6	-28.6	-28.6
3.6	-45.6	-45.6	-45.6	-45.6	-44.6	-44.6	-44.6	-44.6	-44.6
$OASPL_{O,sh}$-$UOL_{O,sh}$	0.0	0.0	0.0	0.0	0.0	0.0	0.0	0.0	0.0

Table VII - Spectral Directivity Relations for Inner Stream Shock Noise
(a) Corrected Directivity Angle, $\theta_{l.sh,cor}$, 0 to 90 deg

Frequency parameter	Normalized sound pressure level, $SPL_{l,sh}$-$UOL_{l,sh}$, dB vs. corrected directivity angle									
	Corrected directivity angle, $\theta_{l,sh,cor}$, deg									
log $S_{l,sh}$	0	10	20	30	40	50	60	70	80	90
-3.6	-181.0	-181.0	-181.0	-181.0	-181.0	-181.5	-182.0	-182.5	-178.0	-178.4
-2.2	-111.0	-111.0	-111.0	-111.0	-111.0	-111.5	-112.0	-112.5	-108.0	-108.4
-2.1	-106.0	-106.0	-106.0	-106.0	-106.0	-106.5	-107.0	-107.5	-103.0	-103.4
-2.0	-101.0	-101.0	-101.0	-101.0	-101.0	-101.5	-102.0	-102.5	-98.0	-98.4
-1.9	-96.0	-96.0	-96.0	-96.0	-96.0	-96.5	-97.0	-97.5	-93.0	-93.4
-1.8	-91.0	-91.0	-91.0	-91.0	-91.0	-91.5	-92.0	-92.5	-88.0	-88.4
-1.7	-86.0	-86.0	-86.0	-86.0	-86.0	-86.5	-87.0	-87.5	-83.0	-83.4
-1.6	-81.0	-81.0	-81.0	-81.0	-81.0	-81.5	-82.0	-82.5	-78.0	-78.4
-1.5	-76.0	-76.0	-76.0	-76.0	-76.0	-76.5	-77.0	-77.5	-73.0	-73.4
-1.4	-71.0	-71.0	-71.0	-71.0	-71.0	-71.5	-72.0	-72.5	-68.0	-68.4
-1.3	-66.0	-66.0	-66.0	-66.0	-66.0	-66.5	-67.0	-67.5	-63.0	-63.4
-1.2	-61.0	-61.0	-61.0	-61.0	-61.0	-61.5	-62.0	-62.5	-58.0	-58.4
-1.1	-56.0	-56.0	-56.0	-56.0	-56.0	-56.5	-57.0	-57.5	-53.0	-53.4
-1.0	-51.0	-51.0	-51.0	-51.0	-51.0	-51.5	-52.0	-52.5	-48.0	-48.4
-0.9	-46.0	-46.0	-46.0	-46.0	-46.0	-46.5	-47.0	-47.5	-43.0	-43.4
-0.8	-41.0	-41.0	-41.0	-41.0	-41.0	-41.5	-42.0	-42.5	-38.0	-38.4
-0.7	-36.0	-36.0	-36.0	-36.0	-36.0	-36.5	-37.0	-37.5	-33.0	-33.4
-0.6	-31.0	-31.0	-31.0	-31.0	-31.0	-31.5	-32.0	-32.5	-28.0	-28.4
-0.5	-26.0	-26.0	-26.0	-26.0	-26.0	-26.5	-27.0	-27.5	-23.0	-23.4
-0.4	-21.0	-21.0	-21.0	-21.0	-21.0	-21.5	-22.0	-22.5	-18.0	-18.4
-0.3	-16.0	-16.0	-16.0	-16.0	-16.0	-16.5	-17.0	-17.5	-13.0	-13.4
-0.2	-11.0	-11.0	-11.0	-11.0	-11.0	-11.5	-12.0	-12.5	-8.0	-8.4
-0.1	-6.0	-6.0	-6.0	-6.0	-6.0	-6.5	-7.0	-7.5	**-6.0**	**-6.4**
0.0	**-4.0**	**-4.0**	**-4.0**	**-4.0**	**-4.0**	**-4.5**	**-5.0**	**-5.5**	-7.5	-7.9
0.1	-5.5	-5.5	-5.5	-5.5	-5.5	-6.0	-6.5	-7.0	-9.5	-9.4
0.2	-7.5	-7.5	-7.5	-7.5	-7.5	-8.0	-8.5	-9.0	-11.5	-10.9
0.3	-9.5	-9.5	-9.5	-9.5	-9.5	-10.0	-10.5	-11.0	-13.5	-12.4
0.4	-11.5	-11.5	-11.5	-11.5	-11.5	-12.0	-12.5	-13.0	-15.5	-13.9
0.5	-13.5	-13.5	-13.5	-13.5	-13.5	-14.0	-14.5	-15.0	-17.5	-15.4
0.6	-15.5	-15.5	-15.5	-15.5	-15.5	-16.0	-16.5	-17.0	-19.5	-16.9
0.7	-17.5	-17.5	-17.5	-17.5	-17.5	-18.0	-18.5	-19.0	-21.5	-18.4
0.8	-19.5	-19.5	-19.5	-19.5	-19.5	-20.0	-20.5	-21.0	-23.5	-19.9
0.9	-21.5	-21.5	-21.5	-21.5	-21.5	-22.0	-22.5	-23.0	-25.5	-21.4
1.0	-23.5	-23.5	-23.5	-23.5	-23.5	-24.0	-24.5	-25.0	-27.5	-22.9
1.1	-25.5	-25.5	-25.5	-25.5	-25.5	-26.0	-26.5	-27.0	-29.5	-24.4
1.2	-27.5	-27.5	-27.5	-27.5	-27.5	-28.0	-28.5	-29.0	-31.5	-25.9
1.3	-29.5	-29.5	-29.5	-29.5	-29.5	-30.0	-30.5	-31.0	-33.5	-27.4
1.4	-31.5	-31.5	-31.5	-31.5	-31.5	-32.0	-32.5	-33.0	-35.5	-28.9
1.5	-33.5	-33.5	-33.5	-33.5	-33.5	-34.0	-34.5	-35.0	-37.5	-30.4
1.6	-35.5	-35.5	-35.5	-35.5	-35.5	-36.0	-36.5	-37.0	-39.5	-31.9
1.7	-37.5	-37.5	-37.5	-37.5	-37.5	-38.0	-38.5	-39.0	-41.5	-33.4
1.8	-39.5	-39.5	-39.5	-39.5	-39.5	-40.0	-40.5	-41.0	-43.5	-34.9
1.9	-41.5	-41.5	-41.5	-41.5	-41.5	-42.0	-42.5	-43.0	-45.5	-36.4
2.0	-43.5	-43.5	-43.5	-43.5	-43.5	-44.0	-44.5	-45.0	-47.5	-37.9
3.6	-71.5	-71.5	-71.5	-71.5	-71.5	-72.0	-72.5	-73.0	-75.5	-65.9
$OASPL_{l,sh}$-$UOL_{l,sh}$	1.8	1.8	1.8	1.8	1.8	1.3	0.8	0.3	-0.2	0.0

Table VII (Concluded) - Spectral Directivity Relations for Inner Stream Shock Noise
(b) Corrected Directivity Angle, $\theta_{l.sh,cor}$, 100 to 180 deg

Frequency parameter	Normalized sound pressure level, SPL_{lsh}-$UOL_{l,sh}$, dB vs. corrected directivity angle								
	Corrected directivity angle, $\theta_{l,sh,cor}$, deg								
log $S_{l,sh}$	100	110	120	130	140	150	160	170	180
-3.6	-178.6	-178.8	-179.0	-179.2	-179.4	-179.6	-179.8	-180.0	-180.2
-2.2	-108.6	-108.8	-109.0	-109.2	-109.4	-109.6	-109.8	-110.0	-110.2
-2.1	-103.6	-103.8	-104.0	-104.2	-104.4	-104.6	-104.8	-105.0	-105.2
-2.0	-98.6	-98.8	-99.0	-99.2	-99.4	-99.6	-99.8	-100.0	-100.2
-1.9	-93.6	-93.8	-94.0	-94.2	-94.4	-94.6	-94.8	-95.0	-95.2
-1.8	-88.6	-88.8	-89.0	-89.2	-89.4	-89.6	-89.8	-90.0	-90.2
-1.7	-83.6	-83.8	-84.0	-84.2	-84.4	-84.6	-84.8	-85.0	-85.2
-1.6	-78.6	-78.8	-79.0	-79.2	-79.4	-79.6	-79.8	-80.0	-80.2
-1.5	-73.6	-73.8	-74.0	-74.2	-74.4	-74.6	-74.8	-75.0	-75.2
-1.4	-68.6	-68.8	-69.0	-69.2	-69.4	-69.6	-69.8	-70.0	-70.2
-1.3	-63.6	-63.8	-64.0	-64.2	-64.4	-64.6	-64.8	-65.0	-65.2
-1.2	-58.6	-58.8	-59.0	-59.2	-59.4	-59.6	-59.8	-60.0	-60.2
-1.1	-53.6	-53.8	-54.0	-54.2	-54.4	-54.6	-54.8	-55.0	-55.2
-1.0	-48.6	-48.8	-49.0	-49.2	-49.4	-49.6	-49.8	-50.0	-50.2
-0.9	-43.6	-43.8	-44.0	-44.2	-44.4	-44.6	-44.8	-45.0	-45.2
-0.8	-38.6	-38.8	-39.0	-39.2	-39.4	-39.6	-39.8	-40.0	-40.2
-0.7	-33.6	-33.8	-34.0	-34.2	-34.4	-34.6	-34.8	-35.0	-35.2
-0.6	-28.6	-28.8	-29.0	-29.2	-29.4	-29.6	-29.8	-30.0	-30.2
-0.5	-23.6	-23.8	-24.0	-24.2	-24.4	-24.6	-24.8	-25.0	-25.2
-0.4	-18.6	-18.8	-19.0	-19.2	-19.4	-19.6	-19.8	-20.0	-20.2
-0.3	-13.6	-13.8	-14.0	-14.2	-14.4	-14.6	-14.8	-15.0	-15.2
-0.2	-8.6	-8.8	-9.0	-9.2	-9.4	-9.6	-9.8	-10.0	-10.2
-0.1	**-6.6**	**-6.8**	**-7.0**	**-7.2**	**-7.4**	**-7.6**	**-7.8**	**-8.0**	**-8.2**
0.0	-8.1	-8.3	-8.5	-8.7	-8.9	-9.1	-9.3	-9.5	-9.7
0.1	-9.6	-9.8	-10.0	-10.2	-10.4	-10.6	-10.8	-11.0	-11.2
0.2	-11.1	-11.3	-11.5	-11.7	-11.9	-12.1	-12.3	-12.5	-12.7
0.3	-12.6	-12.8	-13.0	-13.2	-13.4	-13.6	-13.8	-14.0	-14.2
0.4	-14.1	-14.3	-14.5	-14.7	-14.9	-15.1	-15.3	-15.5	-15.7
0.5	-15.6	-15.8	-16.0	-16.2	-16.4	-16.6	-16.8	-17.0	-17.2
0.6	-17.1	-17.3	-17.5	-17.7	-17.9	-18.1	-18.3	-18.5	-18.7
0.7	-18.6	-18.8	-19.0	-19.2	-19.4	-19.6	-19.8	-20.0	-20.2
0.8	-20.1	-20.3	-20.5	-20.7	-20.9	-21.1	-21.3	-21.5	-21.7
0.9	-21.6	-21.8	-22.0	-22.2	-22.4	-22.6	-22.8	-23.0	-23.2
1.0	-23.1	-23.3	-23.5	-23.7	-23.9	-24.1	-24.3	-24.5	-24.7
1.1	-24.6	-24.8	-25.0	-25.2	-25.4	-25.6	-25.8	-26.0	-26.2
1.2	-26.1	-26.3	-26.5	-26.7	-26.9	-27.1	-27.3	-27.5	-27.7
1.3	-27.6	-27.8	-28.0	-28.2	-28.4	-28.6	-28.8	-29.0	-29.2
1.4	-29.1	-29.3	-29.5	-29.7	-29.9	-30.1	-30.3	-30.5	-30.7
1.5	-30.6	-30.8	-31.0	-31.2	-31.4	-31.6	-31.8	-32.0	-32.2
1.6	-32.1	-32.3	-32.5	-32.7	-32.9	-33.1	-33.3	-33.5	-33.7
1.7	-33.6	-33.8	-34.0	-34.2	-34.4	-34.6	-34.8	-35.0	-35.2
1.8	-35.1	-35.3	-35.5	-35.7	-35.9	-36.1	-36.3	-36.5	-36.7
1.9	-36.6	-36.8	-37.0	-37.2	-37.4	-37.6	-37.8	-38.0	-38.2
2.0	-38.1	-38.3	-38.5	-38.7	-38.9	-39.1	-39.3	-39.5	-39.7
3.6	-66.1	-66.3	-66.5	-66.7	-66.9	-67.1	-67.3	-67.5	-67.7
$OASPL_{l,sh}$-$UOL_{l,sh}$	-0.2	-0.4	-0.6	-0.8	-1.0	-1.2	-1.4	-1.6	-1.8

Table VIII - Statistical Summary

Nozzle/Plug	Suppression	BPR	M_f	V_O/V_J	V_{mix}/c_{amb}	Errors (experimental minus predicted) using predicted coefficients Δ{OASPL}	Δ{All f}	ε{OASPL}	ε{All f}
(a) LaRC data, M_f = 0.10									
Internal	None	5.0	0.10	0.81	0.814	0.4	0.0	0.9	1.7
Internal	None	5.1	0.10	0.69	0.965	0.3	-0.4	0.7	1.9
Internal	None	9.0	0.10	0.95	0.677	0.7	0.7	1.9	2.0
Internal	None	8.0	0.10	0.78	0.841	-0.3	-0.2	1.2	2.0
Internal	None	10.4	0.10	0.79	0.592	2.4	1.5	3.1	2.4
Internal	None	13.1	0.10	0.90	0.800	-0.4	-0.1	1.8	1.9
Internal	None	14.4	0.10	0.81	0.635	1.0	0.7	2.5	2.3
External	None	9.1	0.10	0.93	0.672	0.3	0.3	1.4	1.9
External	None	8.0	0.10	0.78	0.828	-0.1	-0.1	0.8	1.7
External	None	4.8	0.10	0.81	0.835	-0.2	-0.5	0.9	2.0
External	None	4.9	0.10	0.72	0.989	-0.3	-0.7	0.7	2.3
Internal	8 Core Petals	5.1	0.10	0.80	0.812	1.2	0.6	1.4	2.2
Internal	8 Core Petals	5.1	0.10	0.69	0.973	0.9	0.3	1.0	2.1
		Average for LaRC, M_f = 0.10:				**0.4**	**0.2**	**1.4**	**2.0**
(b) LaRC data, M_f = 0.20									
Internal	None	4.8	0.20	0.81	0.808	2.5	1.7	2.3	2.1
Internal	None	4.7	0.20	0.72	0.978	1.3	1.0	1.5	2.0
Internal	None	9.1	0.20	0.98	0.649	. . . . .	3.0	. . . . .	3.8
Internal	None	8.1	0.20	0.78	0.808	1.5	1.3	1.7	1.9
External	None	9.1	0.20	0.98	0.648	1.4	2.7	1.6	3.6
External	None	8.1	0.20	0.79	0.811	1.3	1.0	1.5	2.7
External	None	4.9	0.20	0.79	0.790	2.0	1.6	2.1	2.7
External	None	4.7	0.20	0.72	0.972	0.8	0.5	1.2	2.2
Internal	8 Core Petals	4.9	0.20	0.79	0.790	5.1	3.5	4.7	4.1
Internal	8 Core Petals	4.8	0.20	0.70	0.954	**2.2**	**1.5**	**2.2**	**2.3**
		Average for LaRC, M_f = 0.20:				**2.0**	**1.8**	**2.1**	**2.7**
(c) GE/GRC Configuration 7BB, M_f = 0.00 - 0.28									
External	None	14.9	0.20	0.84	0.591	1.0	0.7	2.0	3.9
External	None	13.3	0.20	0.74	0.654	-0.8	-0.6	1.2	2.0
External	None	13.1	0.20	0.71	0.707	-1.4	-1.3	1.6	2.1
External	None	12.9	0.20	0.69	0.760	-1.7	-1.6	1.8	2.2
External	None	12.3	0.20	0.65	0.801	-1.6	-1.5	1.7	2.2
External	None	13.3	0.28	0.70	0.769	-1.7	-1.4	2.0	2.6
External	None	13.3	0.00	0.70	0.766	-1.2	-1.6	1.3	1.9
		Average for Conf. 7BB, M_f = 0.00-0.28:				**-1.1**	**-1.0**	**1.6**	**2.4**
(d) GE/GRC Configuration 5BB, M_f = 0.00									
External	None	7.6	0.00	0.80	0.712	0.0	-0.1	0.7	1.4
External	None	7.3	0.00	0.73	0.804	0.4	-0.3	0.5	1.3
External	None	6.9	0.00	0.69	0.870	0.9	0.2	1.1	1.5
External	None	6.6	0.00	0.62	0.949	1.2	0.2	1.4	1.9
		Average for Conf. 5BB, M_f = 0.00:				**0.6**	**0.0**	**0.9**	**1.5**
(e) GE/GRC Configuration 5BB, M_f = 0.20									
External	None	7.9	0.20	0.82	0.709	-0.9	-0.4	1.2	2.0
External	None	9.5	0.20	0.97	0.709	-1.2	-0.4	2.0	2.6
		Average for Conf. 5BB, M_f = 0.20:				**-1.1**	**-0.4**	**1.6**	**2.3**
(f) GE/GRC Configuration 5BB, M_f = 0.28									
External	None	7.9	0.28	0.82	0.712	-0.3	0.2	1.5	2.5
External	None	6.9	0.28	0.68	0.869	-0.7	-0.4	0.9	2.1
External	None	6.6	0.28	0.62	0.945	-0.1	-0.1	0.9	2.0
		Average for Conf. 5BB, M_f = 0.28:				**-0.4**	**-0.1**	**1.1**	**2.2**
		Average for Conf. 5BB in simulated flight:				**-0.7**	**-0.2**	**1.3**	**2.3**

Table VIII (Continued) - Statistical Summary

Nozzle/Plug	Suppression	BPR	M_f	V_O/V_J	V_{mix}/c_{amb}	Errors (experimental minus predicted) using predicted coefficients Δ{OASPL}	Δ{All f}	ε{OASPL}	ε{All f}
(g) GE/GRC Configuration 3BB, M_f = 0.00									
External	None	4.8	0.00	0.65	1.088	1.1	0.5	1.5	1.8
External	None	5.0	0.00	0.67	1.048	0.8	0.1	1.3	1.8
External	None	5.3	0.00	0.75	0.957	0.6	-0.1	0.8	1.4
External	None	5.8	0.00	0.82	0.889	-0.1	-0.4	0.5	1.2
		Average for Conf. 3BB, M_f = 0.00:				**0.6**	**0.0**	**1.0**	**1.6**
(h) GE/GRC Configuration 3BB, M_f = 0.20									
External	None	5.0	0.20	0.68	1.047	0.3	0.0	0.9	1.3
External	None	6.0	0.20	0.88	0.826	-1.6	-1.0	1.8	1.7
External	None	6.4	0.20	0.95	0.759	-2.0	-1.0	2.3	2.1
External	None	6.6	0.20	1.02	0.636	-1.1	-0.1	1.7	2.3
		Average for Conf. 5BB, M_f = 0.20:				**-1.1**	**-0.5**	**1.7**	**1.8**
(i) GE/GRC Configuration 3BB, M_f = 0.28									
External	None	4.8	0.28	0.65	1.059	0.3	0.1	0.9	1.6
External	None	5.0	0.28	0.67	1.050	-0.2	-0.2	0.7	1.4
External	None	6.2	0.28	0.89	0.827	-1.8	-1.0	2.1	2.1
		Average for Conf. 3BB, M_f = 0.28:				**-0.6**	**-0.3**	**1.2**	**1.7**
		Average for Conf. 3BB in simulated flight:				**-0.9**	**-0.4**	**1.5**	
(j) LeRC Outdoor Dual-Stream Hot Jet, M_f = 0.00									
Ext. Core Coax.	None	1.8	0.00	0.37	1.040	0.3	1.0	1.8	2.4
Ext. Core Coax.	None	1.3	0.00	1.33	2.021	-2.2	-2.0	2.3	2.3
Ext. Core Coax.	None	1.1	0.00	0.45	1.041	0.8	0.8	2.9	2.4
		Average for AR = 1.3, M_f = 0.00:				**-0.4**	**0.0**	**2.3**	**2.4**
Coplanar Coax.	None	2.0	0.00	0.37	1.009	-0.7	-0.4	3.0	3.6
Coplanar Coax.	None	1.5	0.00	1.33	2.038	-0.3	-0.1	0.7	1.8
		Average for AR = 1.4, M_f = 0.00:				**-0.5**	**-0.2**	**1.8**	**2.7**
Coplanar Coax.	None	2.8	0.00	0.69	0.724	2.8	2.3	3.1	2.7
Coplanar Coax.	None	1.7	0.00	2.84	1.721	1.0	0.9	1.3	2.6
Coplanar Coax.	None	1.8	0.00	0.28	1.252	1.2	2.8	1.5	3.8
Coplanar Coax.	None	1.6	0.00	0.44	0.958	0.8	0.9	3.9	3.4
		Average for AR = 1.9, M_f = 0.00:				**1.5**	**1.7**	**2.4**	**3.1**
Coplanar Coax.	None	4.6	0.00	0.37	0.839	2.3	1.7	3.6	4.4
Coplanar Coax.	None	3.5	0.00	1.33	2.134	1.4	1.5	1.6	2.5
Coplanar Coax.	None	4.6	0.00	0.37	2.134	2.3	1.7	3.6	4.4
		Average for AR = 3.3, M_f = 0.00:				**2.0**	**1.7**	**2.9**	**3.8**
		Average for old LeRC tests, M_f = 0.00:				**0.8**	**0.9**	**2.4**	**3.0**
(k) Lockheed Conic, M_f = 0.02 - 0.05									
Conical	None	N/A	0.02	N/A	0.407	0.4	1.2	0.7	2.2
Conical	None	N/A	0.04	N/A	0.736	-1.3	-0.7	1.7	1.9
Conical	None	N/A	0.05	N/A	0.984	-3.1	-2.2	3.3	2.9
		Average for Lockheed Conic, M_f = 0.02 - 0.05:				**-1.3**	**-0.6**	**1.9**	**2.3**
(l) GE Cell 41 Conic, M_f = 0.00									
Conical	None	N/A	0.00	N/A	2.120	**-1.5**	**-1.1**	**3.6**	**3.5**

Table VIII (Concluded) - Statistical Summary

						Errors (experimental minus predicted) using predicted coefficients			
Nozzle/Plug	Suppression	BPR	M_f	V_O/V_J	V_{mix}/c_{amb}	Δ{OASPL}	Δ{All f}	ε{OASPL}	ε{All f}
(m) GE/GRC Suppressed Configuration 3IB, M_f = 0.0-0.28									
External	Core Chevrons	5.0	0.00	0.67	1.047	0.2	-0.2	1.0	1.7
External	Core Chevrons	5.0	0.20	0.68	1.046	-0.9	-0.5	1.2	1.3
External	Core Chevrons	4.8	0.28	0.65	1.087	-1.3	-0.7	1.6	1.7
External	Core Chevrons	4.8	0.28	0.65	1.070	-1.3	-0.6	1.7	2.0
External	Core Chevrons	6.1	0.28	0.88	0.814	-2.1	-0.7	2.6	2.7
External	Core Chevrons	5.0	0.28	0.67	1.049	-1.4	*-0.8*	1.7	*1.8*
External	Core Chevrons	5.4	0.28	0.74	0.979	-2.0	-1.2	2.3	2.2
External	Core Chevrons	5.9	0.28	0.83	0.891	-2.3	-1.0	2.7	2.6
External	Core Chevrons	6.1	0.28	0.87	0.828	-2.2	-0.8	2.6	2.6
		Average for Conf. 3IB, M_f = 0.0-0.28:				**-1.5**	**-0.7**	**1.9**	**2.1**
(n) GE/GRC Suppressed Configuration 3IC, M_f = 0.0									
External	Cr&Fn Chvs	4.9	0.00	0.65	1.087	0.2	0.0	1.0	1.9
External	Cr&Fn Chvs	5.1	0.00	0.68	1.048	0.2	0.2	0.8	1.6
External	Cr&Fn Chvs	5.4	0.00	0.74	0.978	0.1	0.3	0.7	1.5
External	Cr&Fn Chvs	6.0	0.00	0.83	0.892	-0.7	-0.1	0.9	1.5
External	Cr&Fn Chvs	6.8	0.00	1.03	0.637	-0.7	0.2	1.2	1.7
		Average for Conf. 3IC, M_f = 0.0:				**-0.2**	**0.1**	**0.9**	**1.6**
(o) GE/GRC Suppressed Configuration 3IC, M_f = 0.20									
External	Cr&Fn Chvs	5.1	0.20	0.68	1.057	-1.0	-0.4	1.6	1.9
External	Cr&Fn Chvs	6.2	0.20	0.87	0.833	-1.8	-0.5	2.1	2.6
External	Cr&Fn Chvs	6.5	0.20	0.93	0.762	-1.9	-0.6	2.3	2.6
		Average for Conf. 3IC, M_f = 0.20:				**-1.5**	**-0.5**	**2.0**	**2.4**
(p) GE/GRC Suppressed Configuration 3IC, M_f = 0.28									
External	Cr&Fn Chvs	4.9	0.28	0.65	1.087	-1.0	-0.1	1.7	2.3
External	Cr&Fn Chvs	5.1	0.28	0.68	1.053	-1.3	-0.3	1.8	2.2
External	Cr&Fn Chvs	5.4	0.28	0.74	0.987	-1.7	-0.6	2.2	2.3
External	Cr&Fn Chvs	6.0	0.28	0.84	0.896	-2.3	-0.9	2.7	2.9
External	Cr&Fn Chvs	6.1	0.28	0.87	0.834	-1.5	-0.2	2.1	2.7
External	Cr&Fn Chvs	7.1	0.28	0.98	0.823	-1.5	0.0	2.4	3.1
		Average for Conf. 3IC, M_f = 0.28:				**-1.5**	**-0.3**	**2.1**	**2.6**
		Average for Conf. 3IC, M_f = 0.0-0.28:				**-1.1**	**-0.2**	**1.7**	**2.2**

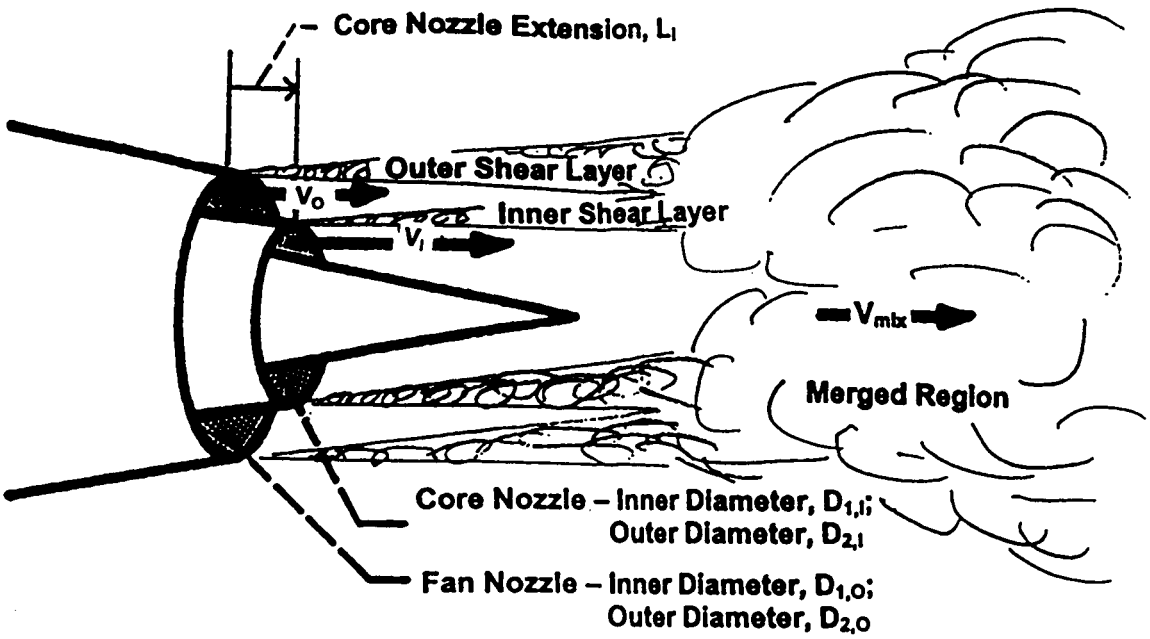

Figure 1.—Separate-Flow Coannular Plug Nozzle Geometry and Mixing Noise Generation Regions.

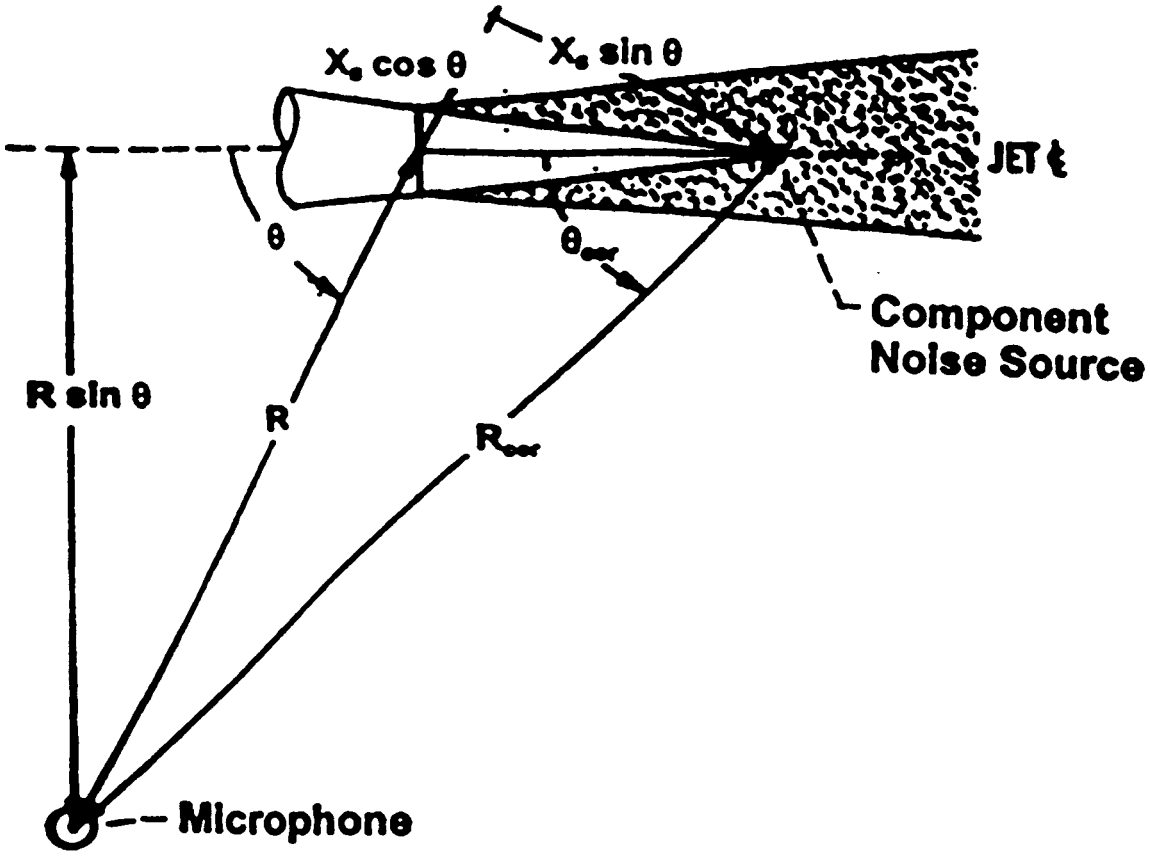

Figure 2.—Noise Source and Microphone Location Geometry.

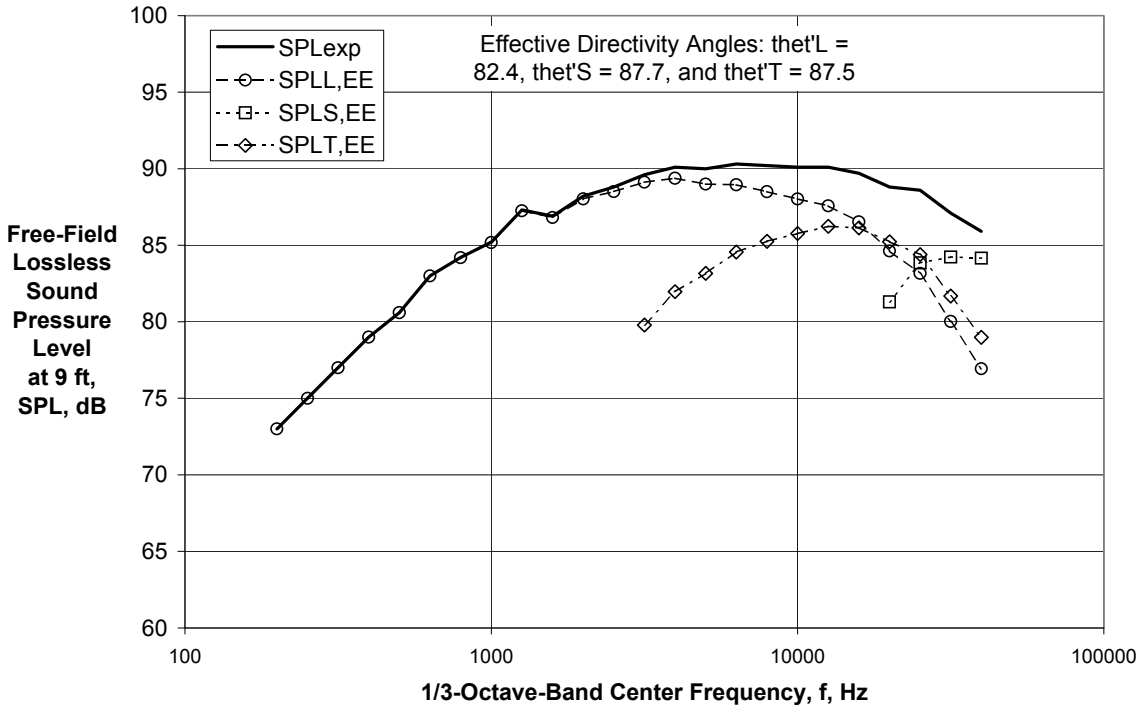

Directivity Angle = 90 deg

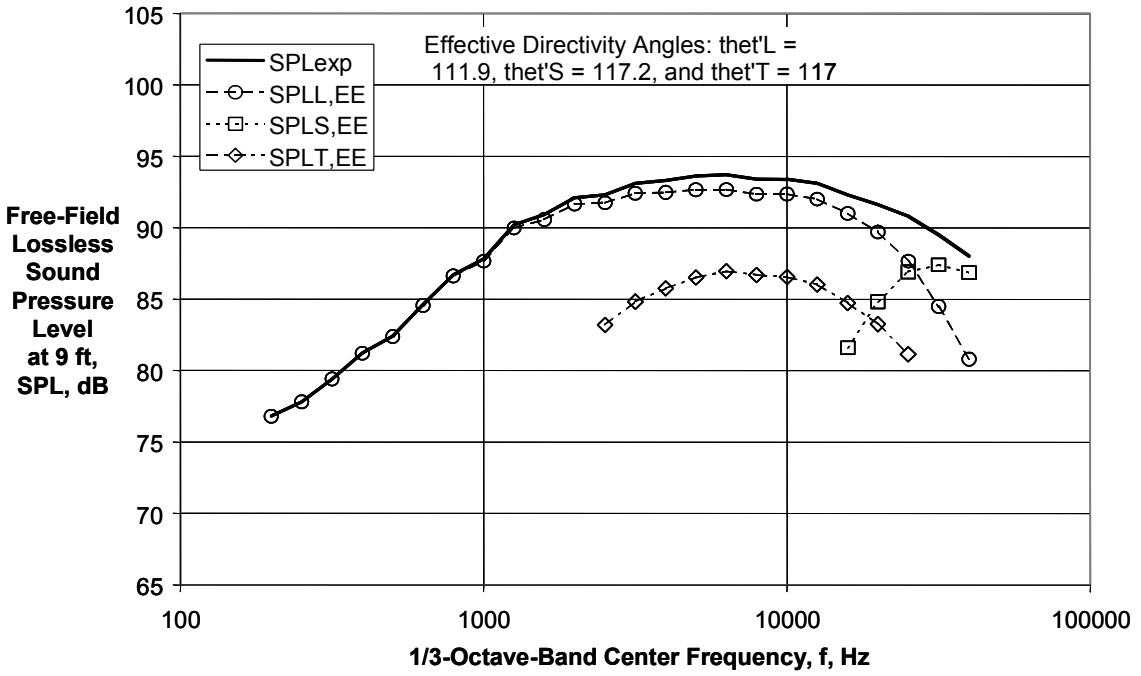

(b) Directivity Angle = 120 deg

Figure 3.—Component Spectral Extraction Using Predicted Spectral Directivities and Experimental Coefficients for Conical Nozzle with Vj/camb = 0.98 and Mf = 0.05 (Ref. 29).

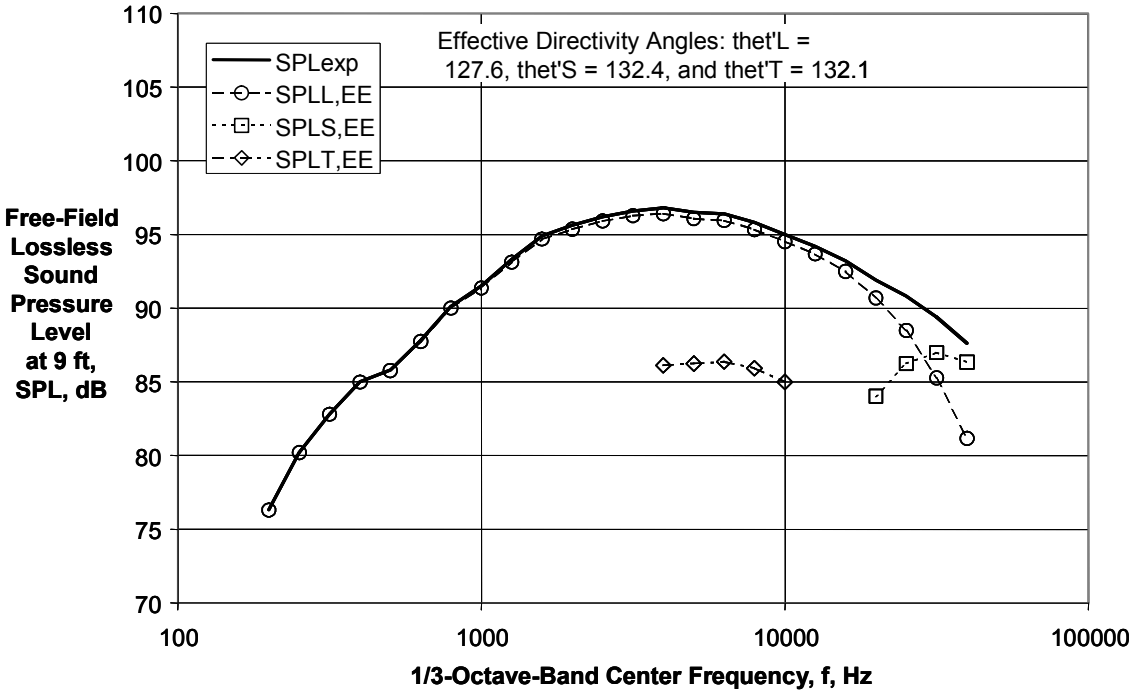

(c) Directivity Angle = 135 deg

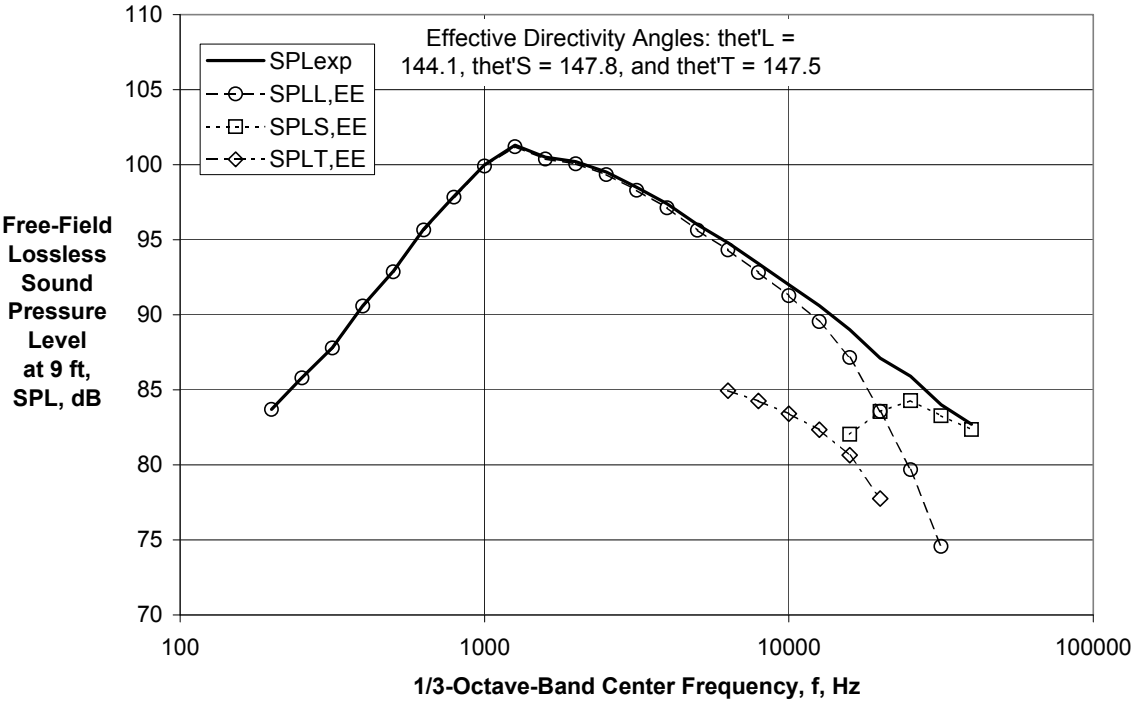

(d) Directivity Angle = 150 deg

Figure 3.—Concluded.

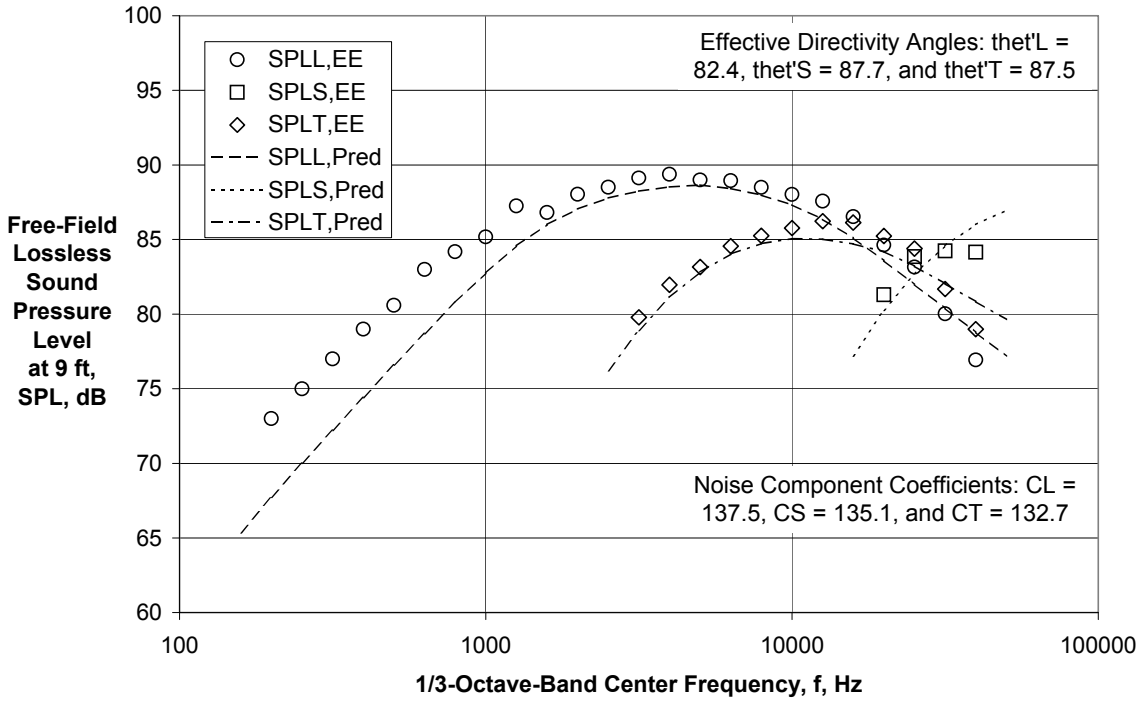

(a) Directivity Angle = 90 deg

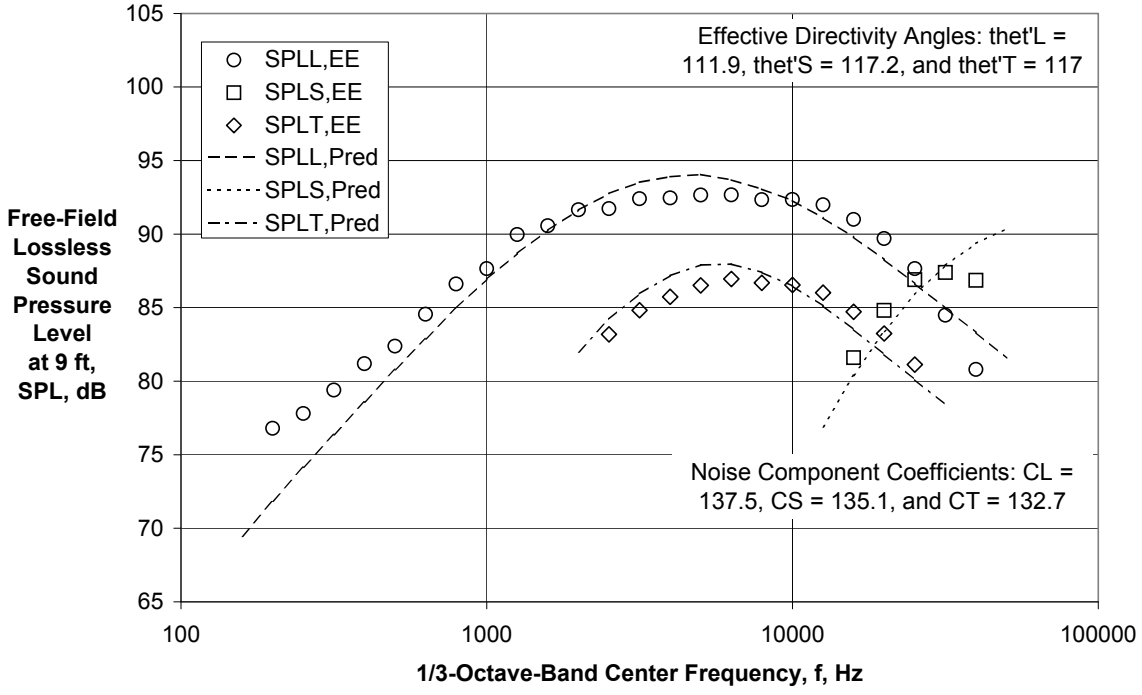

(b) Directivity Angle = 120 deg

Figure 4.—Comparison of Extracted and Predicted Component Spectral and Using Experimental Coefficients for Conical Nozzle with V_j/c_{amb} = 0.98 and M_f = 0.05 (Ref. 29).

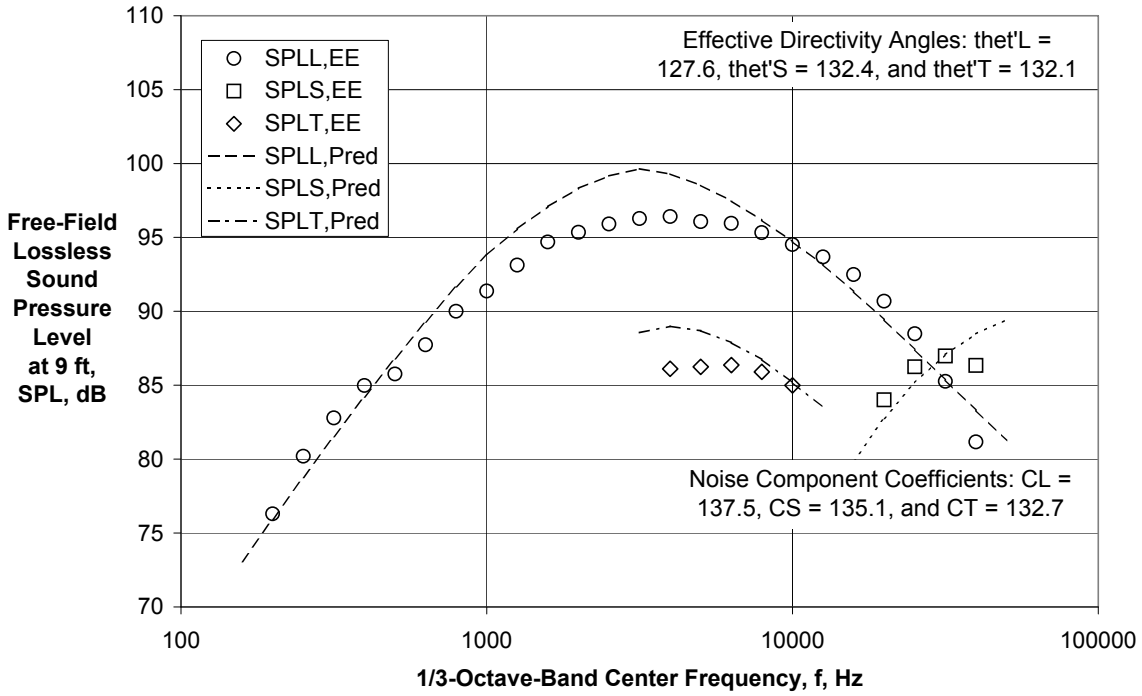

(c) Directivity Angle = 135 deg

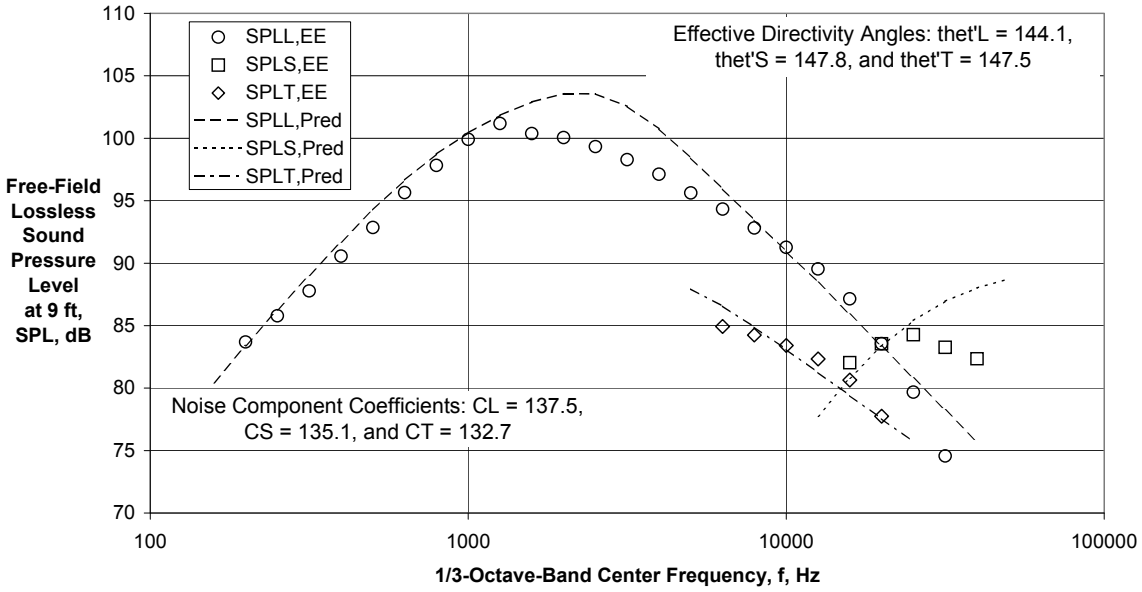

(d) Directivity Angle = 150 deg

Figure 4.—Concluded.

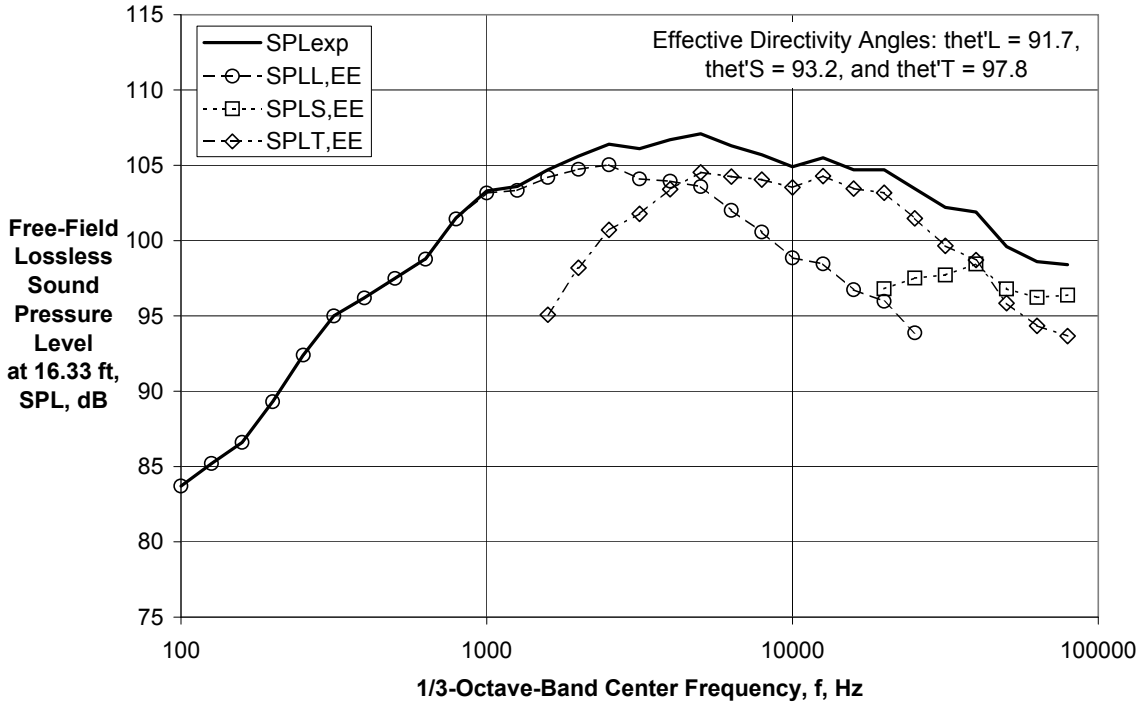

(a) Directivity Angle = 95 deg

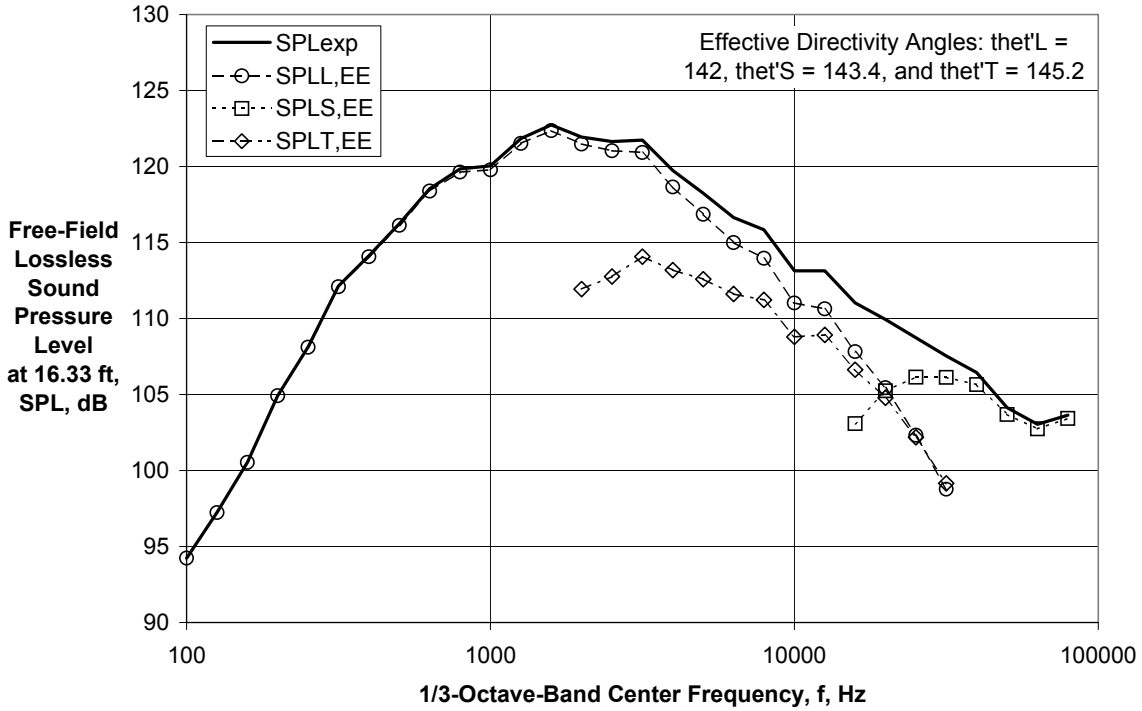

(b) Directivity Angle = 139 deg

Figure 5.—Component Spectral Extraction Using Predicted Spectral Directivities and Experimental Coefficients for Conical Nozzle with Vj/camb = 1.74 and Mf = 0.0 (Ref. 30).

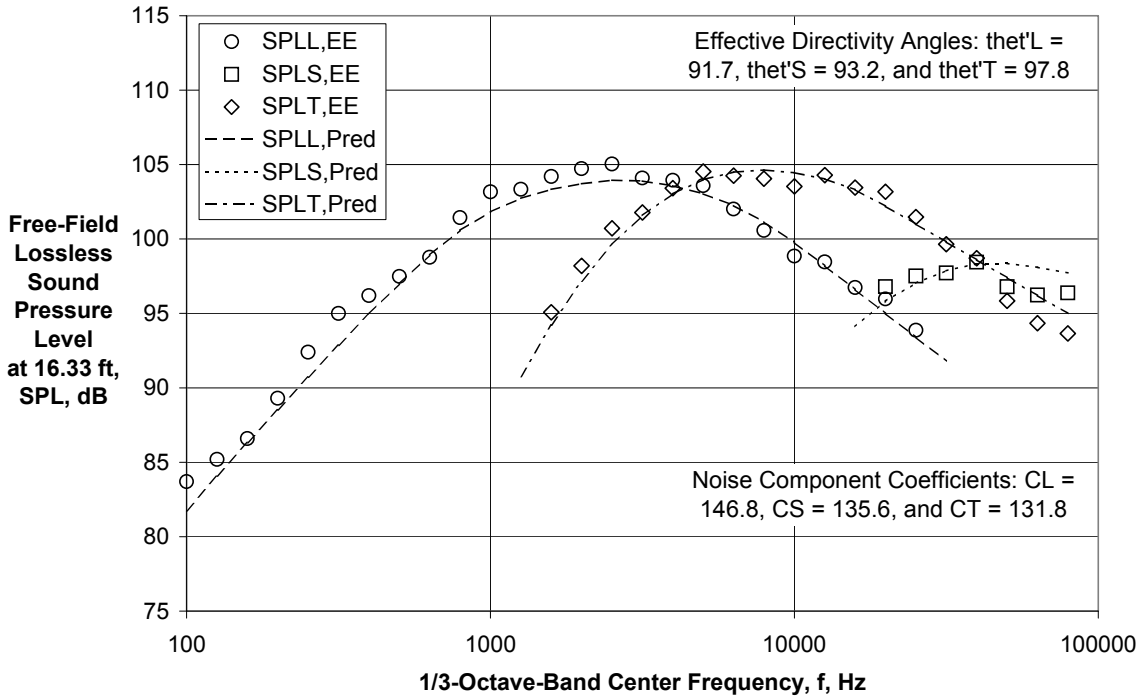

(a) Directivity Angle = 95 deg

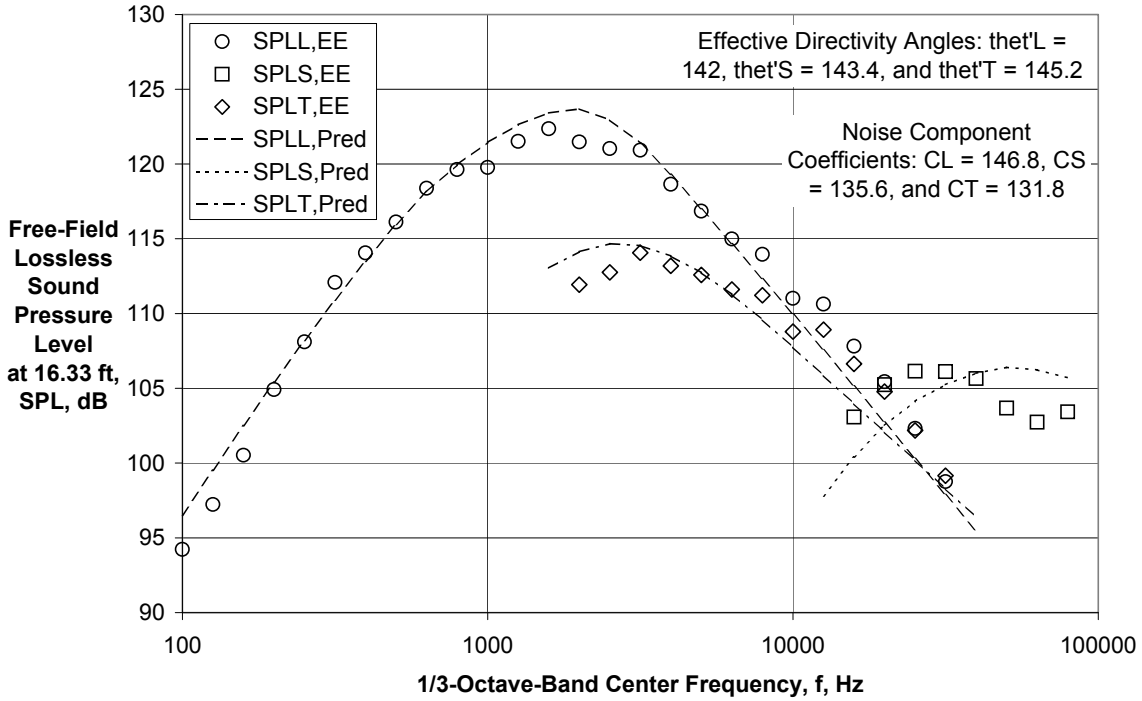

(b) Directivity Angle = 139 deg

Figure 6.—Comparison of Extracted and Predicted Component Spectral and Using Experimental Coefficients for Conical Nozzle with V_j/c_{amb} = 1.74 and M_f = 0.0 (Ref. 30).

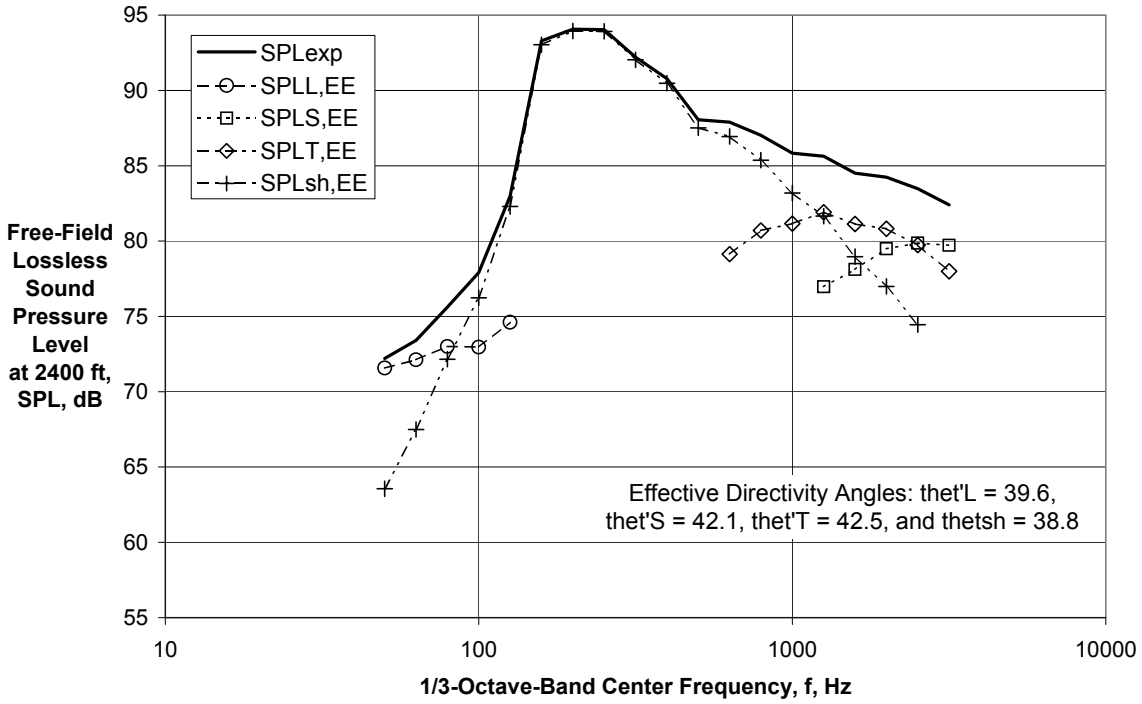

(a) Directivity Angle = 40 deg

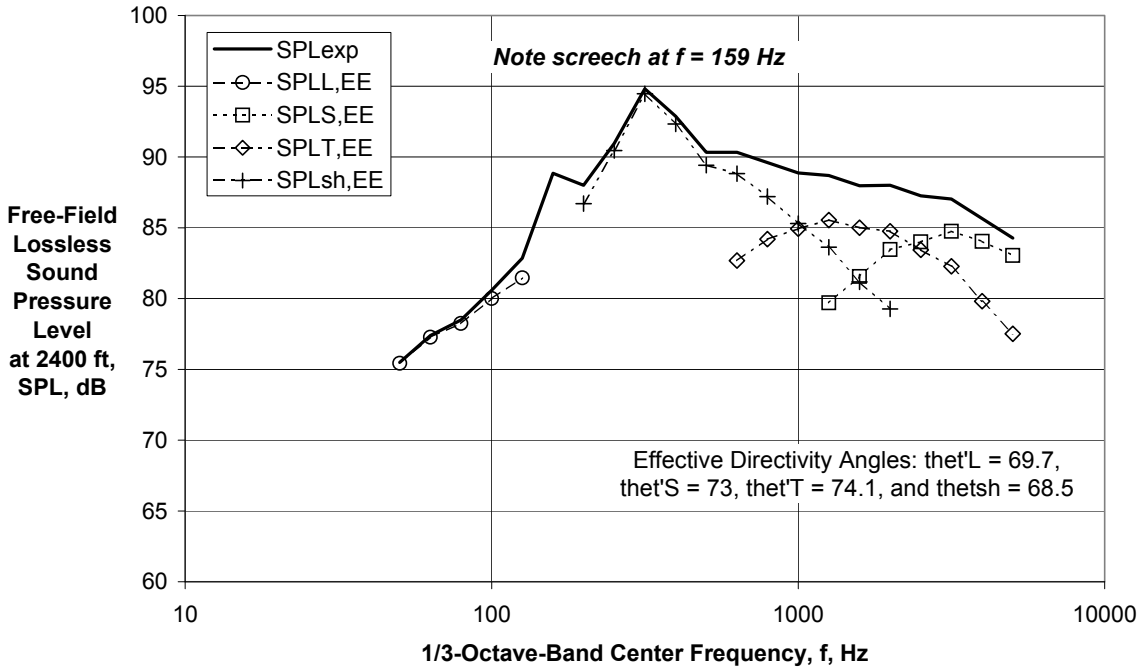

(b) Directivity Angle = 70 deg

Figure 7.—Component Spectral Extraction Using Predicted Spectral Directivities and Experimental Coefficients for Conical Nozzle with Vj/camb = 2.11 and Mf = 0.0 (Ref. 31).

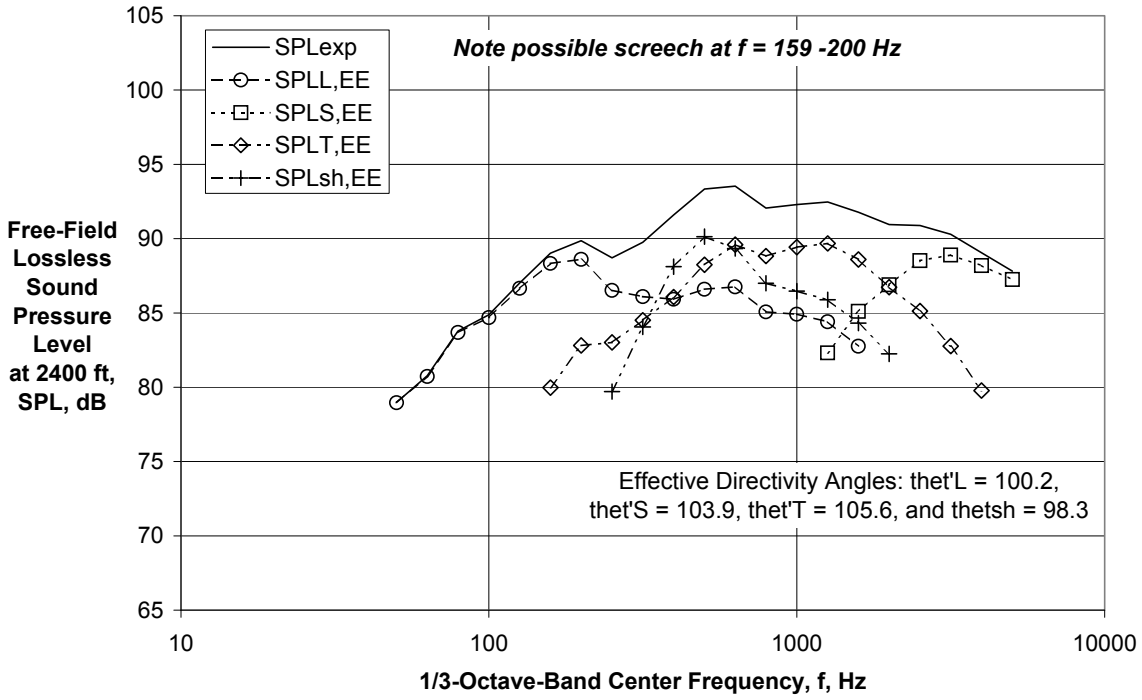

(c) Directivity Angle = 100 deg

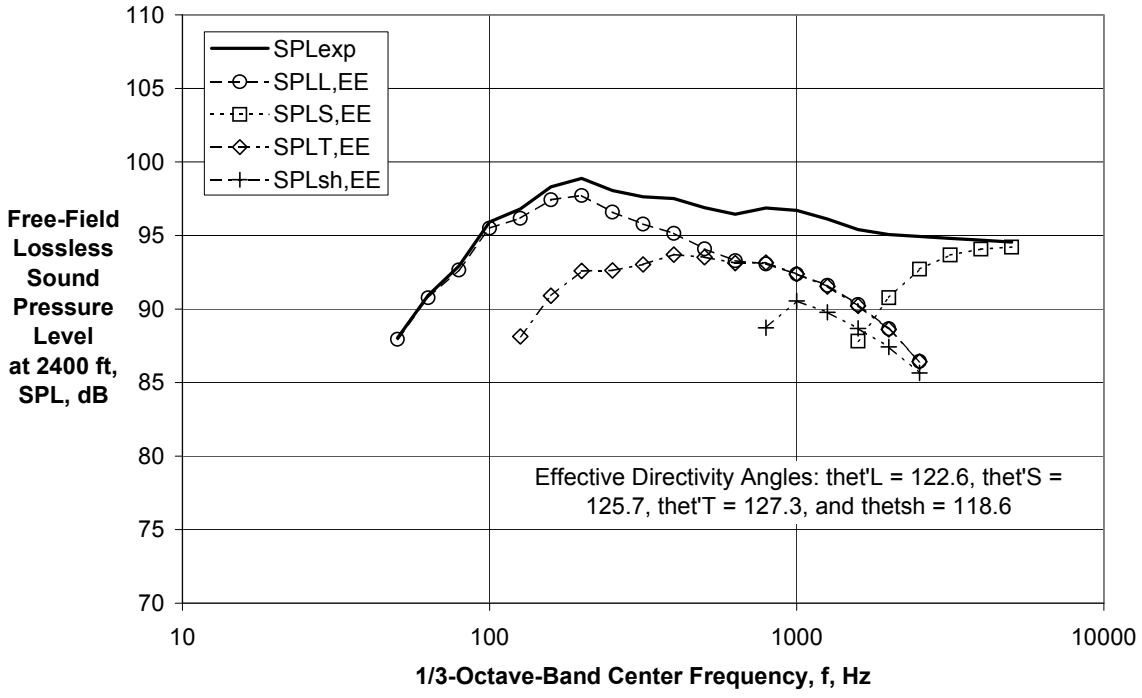

(d) Directivity Angle = 120 deg

Figure 7.—Continued.

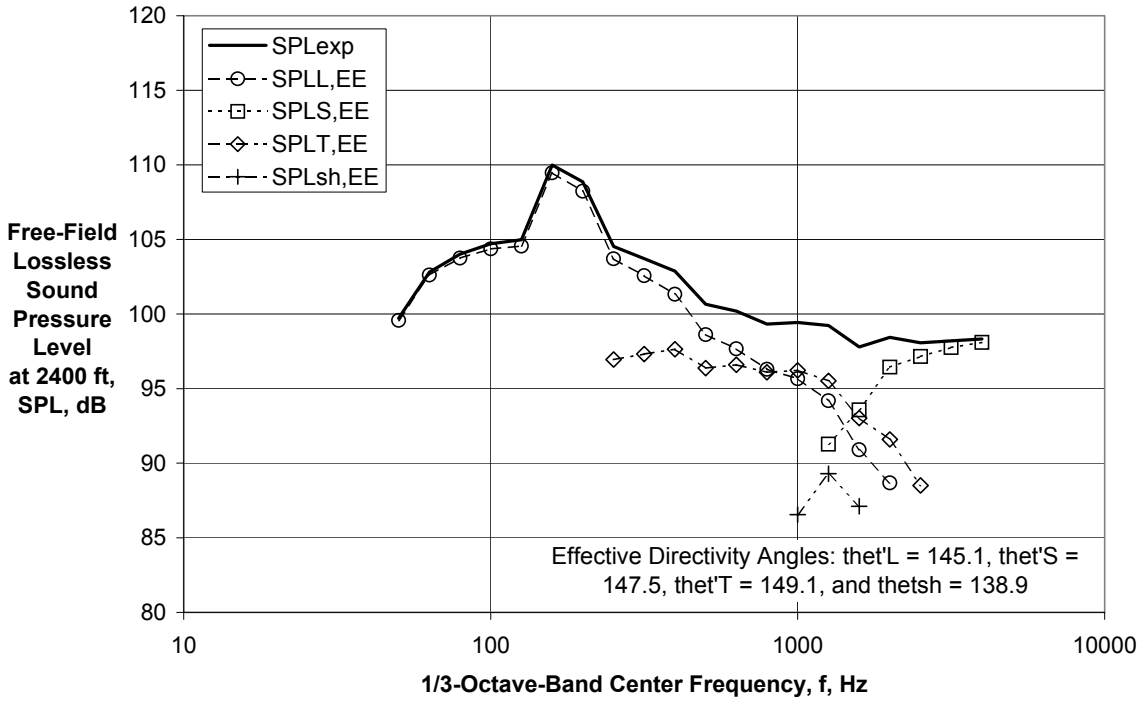

(e) Directivity Angle = 140 deg

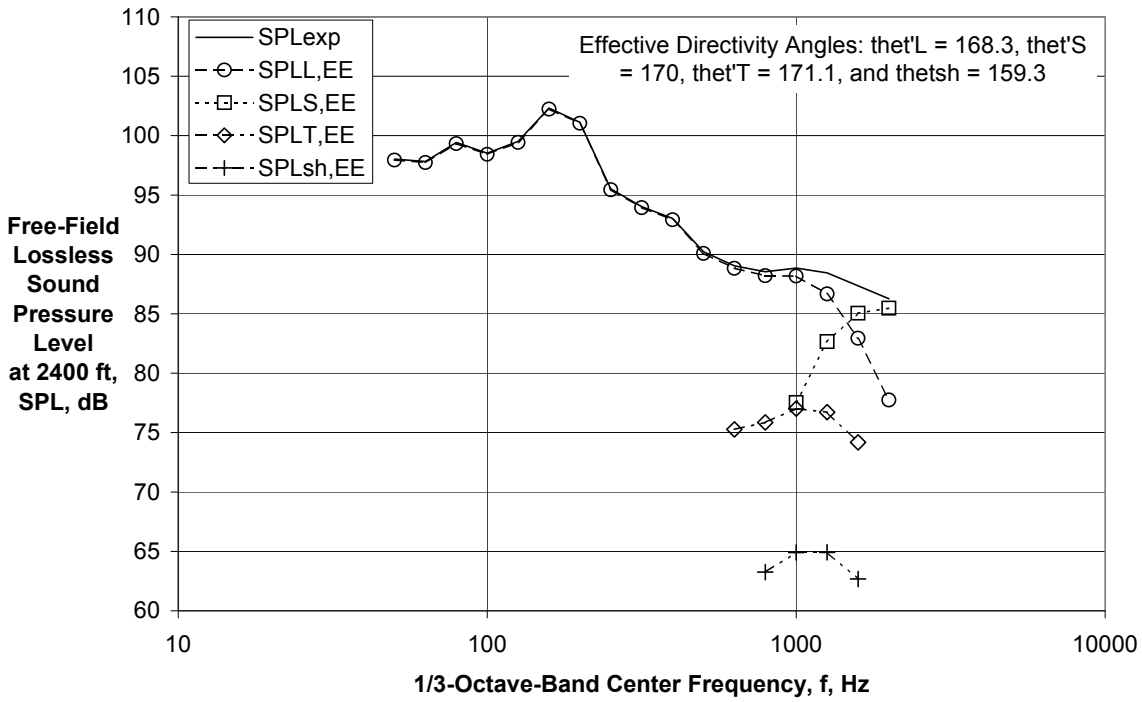

(f) Directivity Angle = 160 deg

Figure 7.—Concluded.

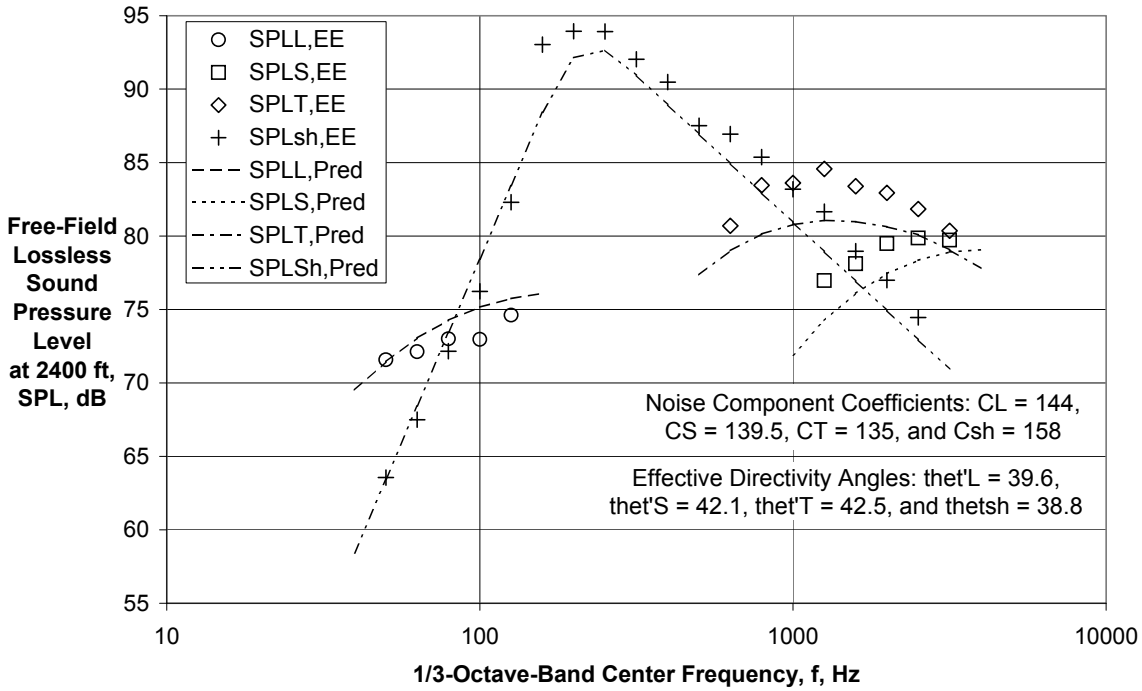

(a) Directivity Angle = 40 deg

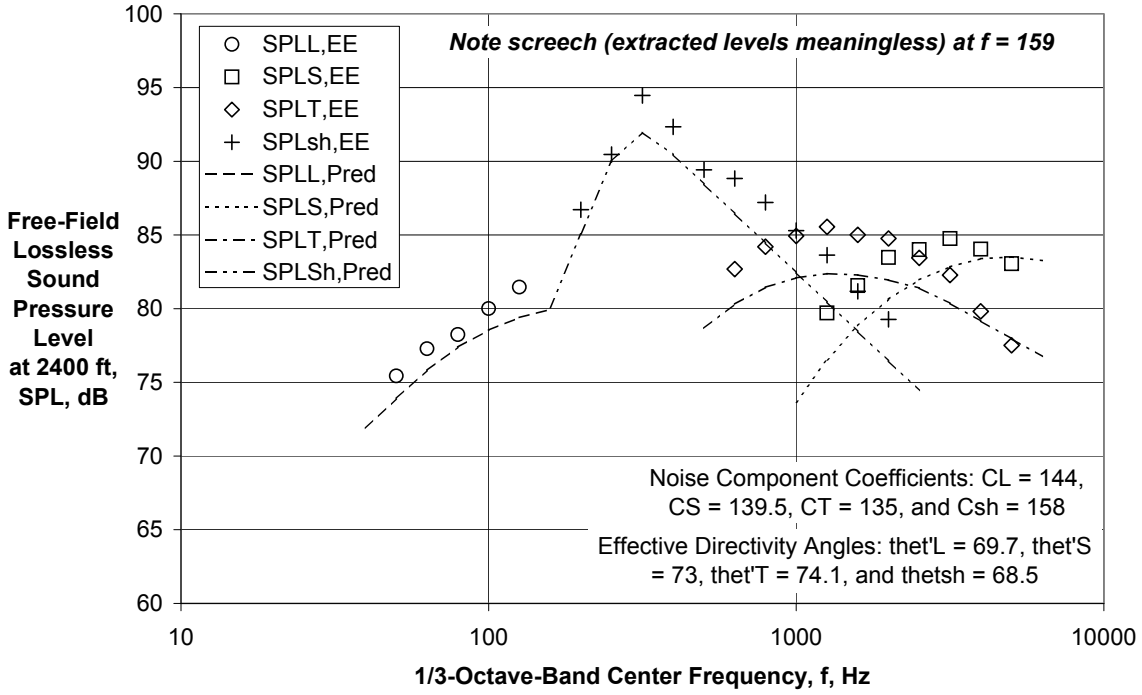

(b) Directivity Angle = 70 deg

Figure 8.—Comparison of Extracted and Predicted Component Spectral and Using Experimental Coefficients for Conical Nozzle with Vj/camb = 2.11 and Mf = 0.0 (Ref. 31).

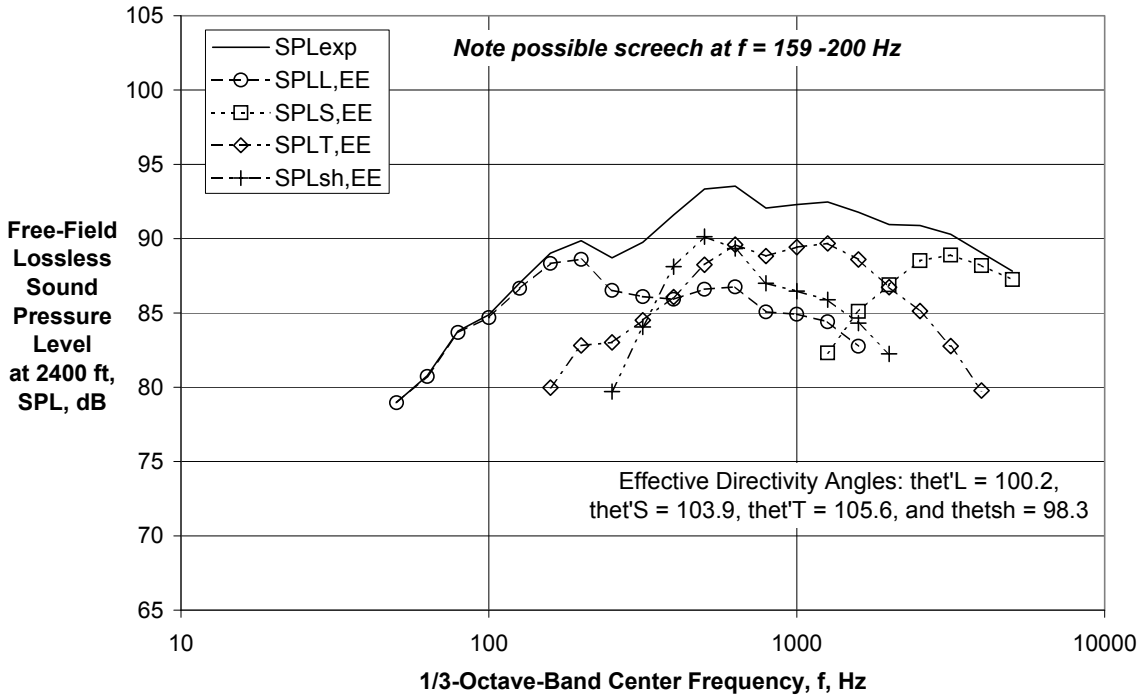

(c) Directivity Angle = 100 deg

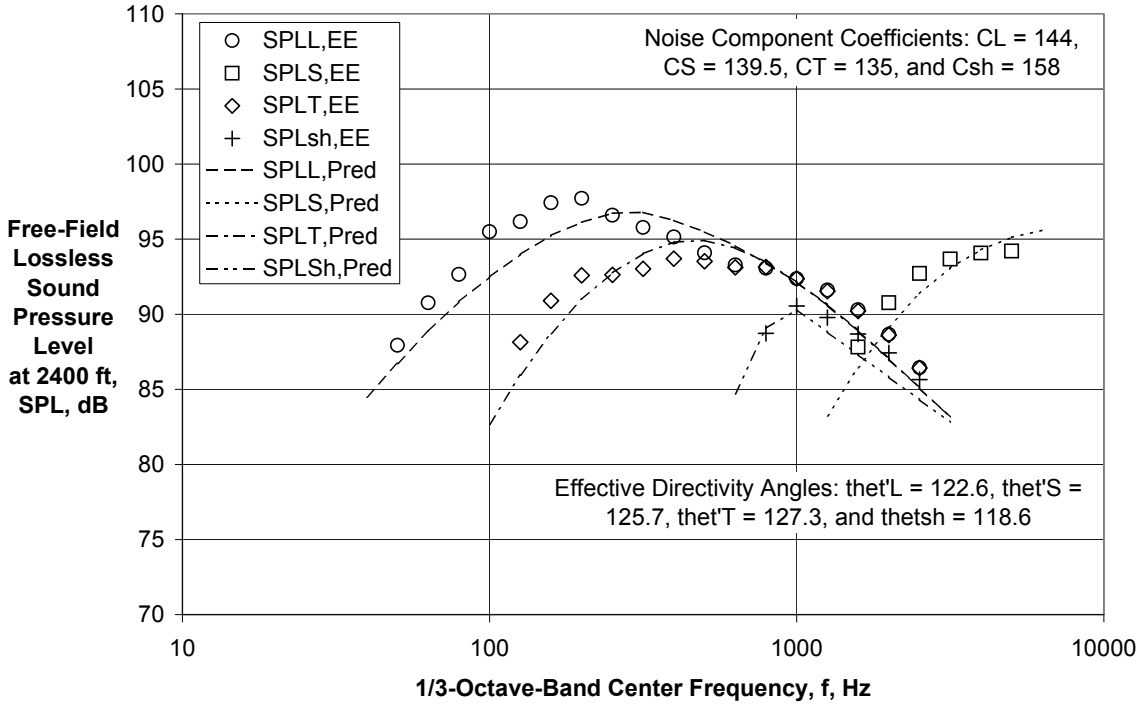

(d) Directivity Angle = 120 deg

Figure 8.—Continued.

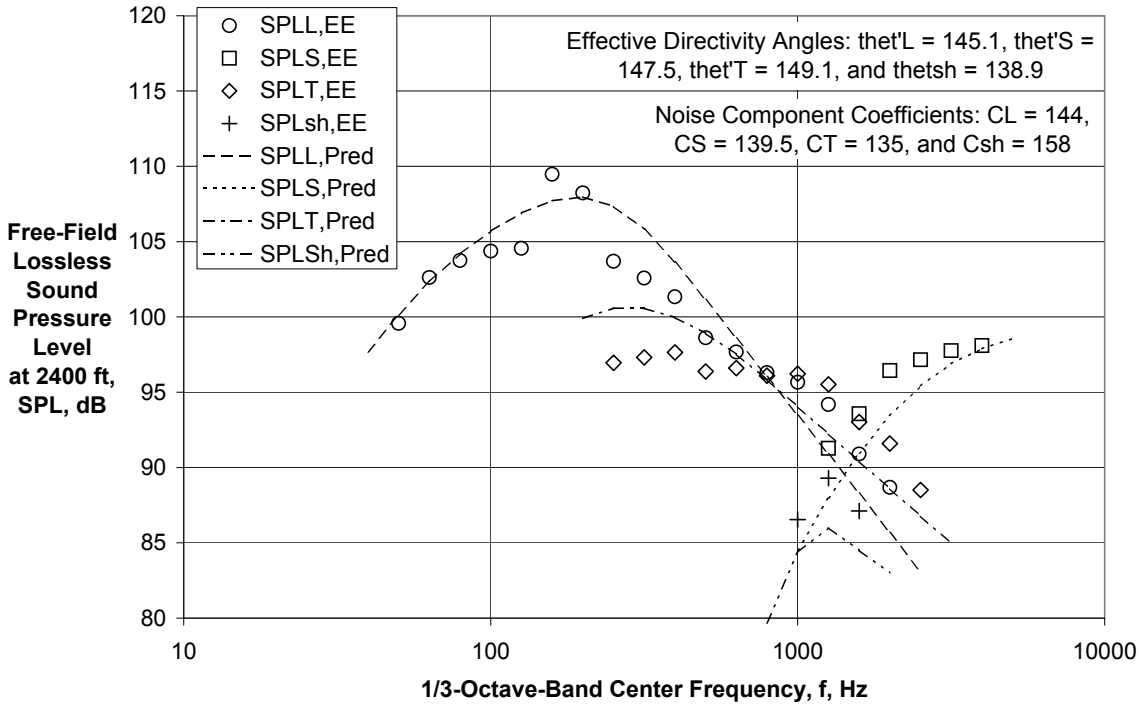

(e) Directivity Angle = 140 deg

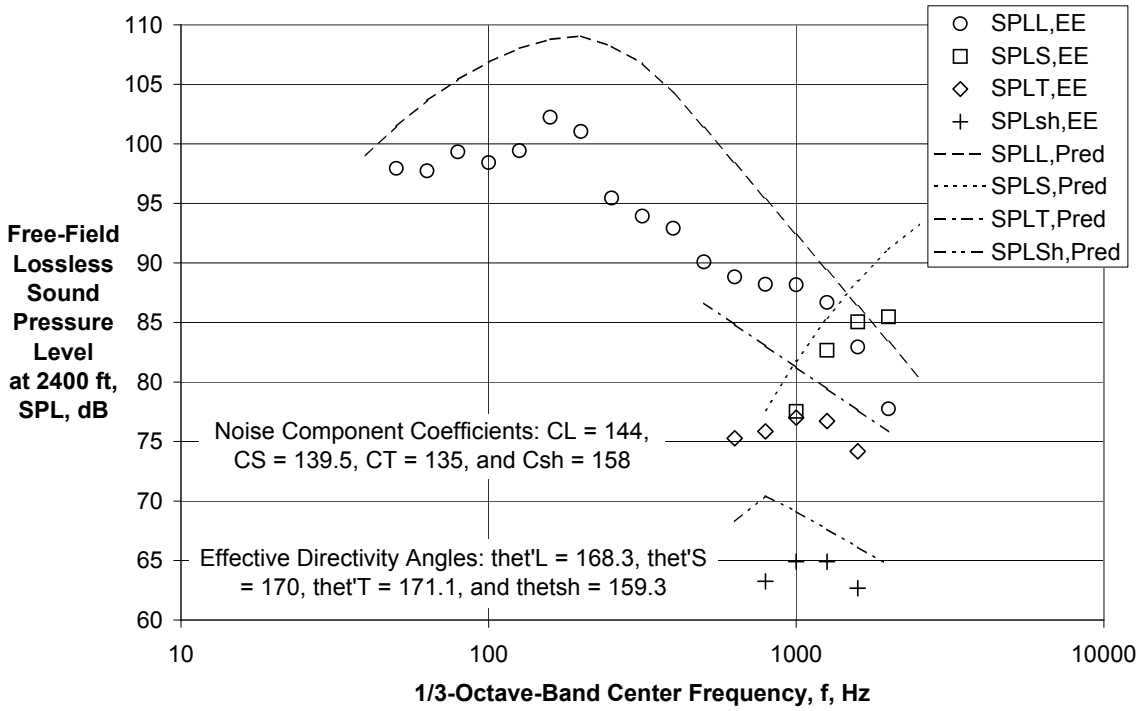

(f) Directivity Angle = 160 deg

Figure 8.—Concluded.

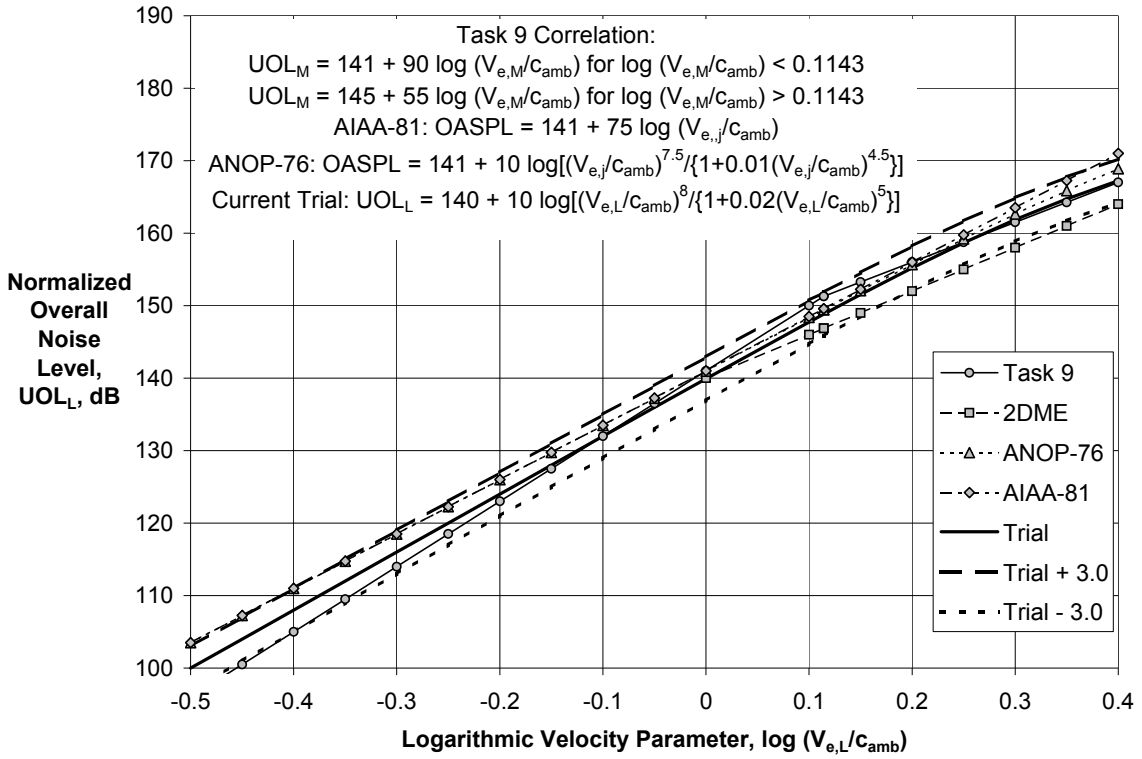

Figure 9.—Comparison of Unsuppressed Merged or Large Scale Mixing Noise Level and Overall Sound Pressure Level Correlations.

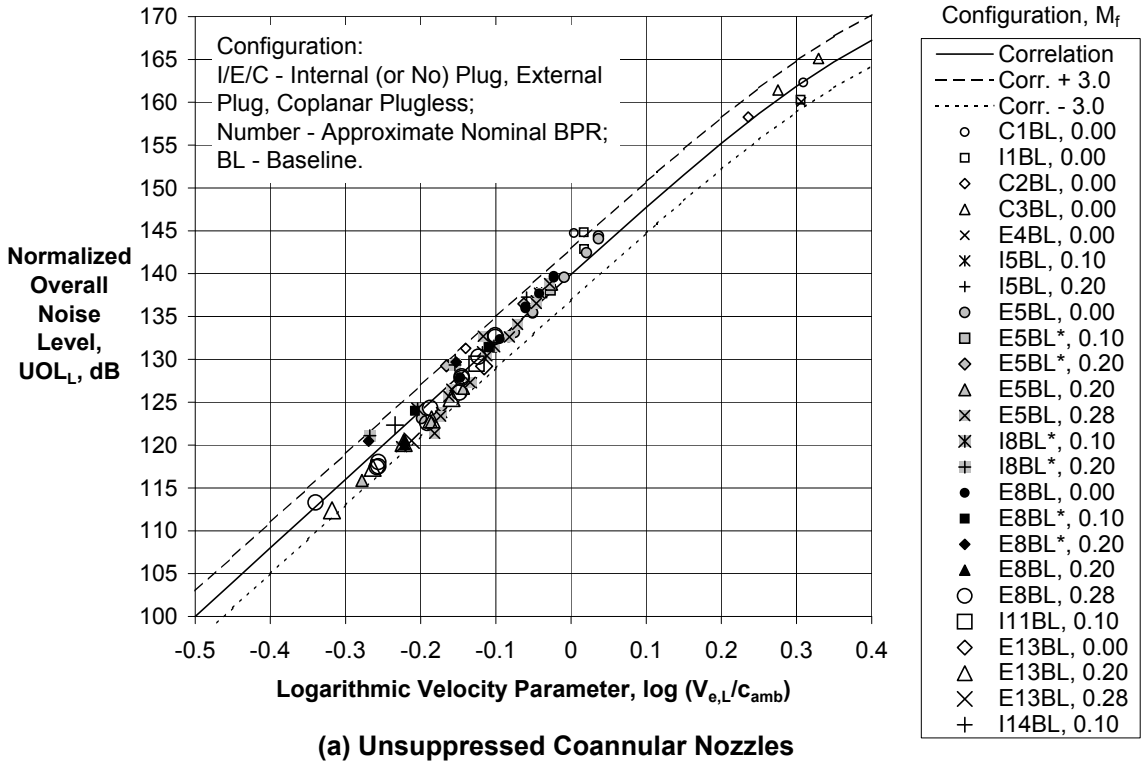

(a) Unsuppressed Coannular Nozzles

Figure 10.—Comparison of Experimental/Extracted Large Scale Mixing Noise with Correlation for Unsuppressed Configurations.

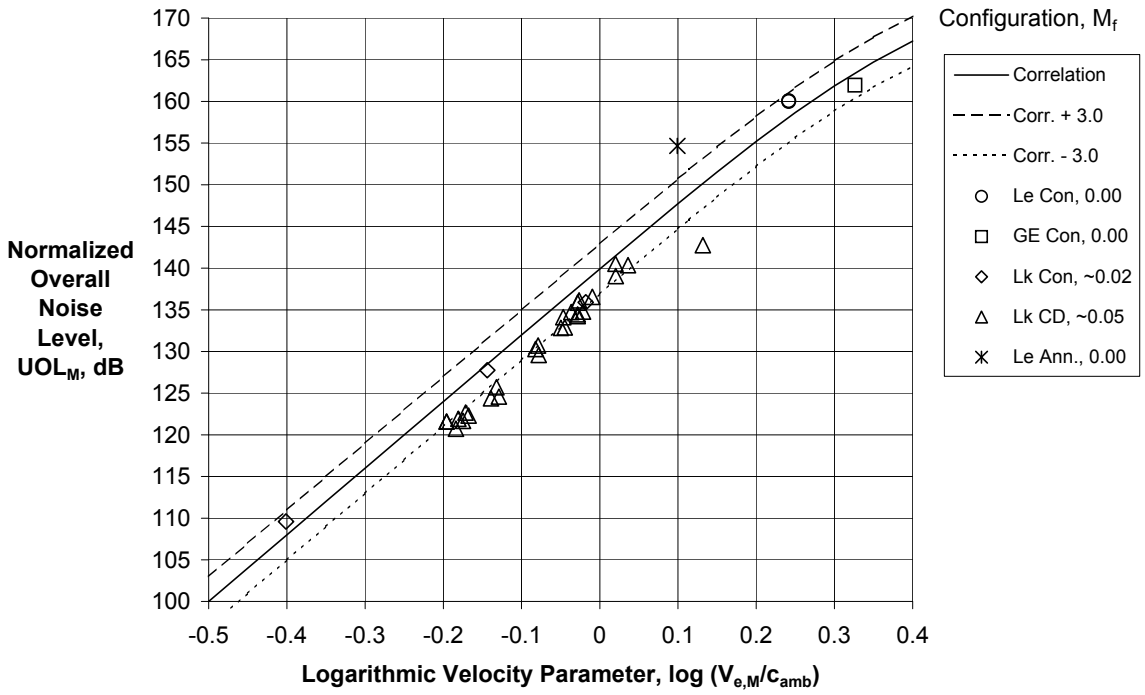

(b) Single Stream Unsuppressed Nozzles

Figure 10.—Concluded.

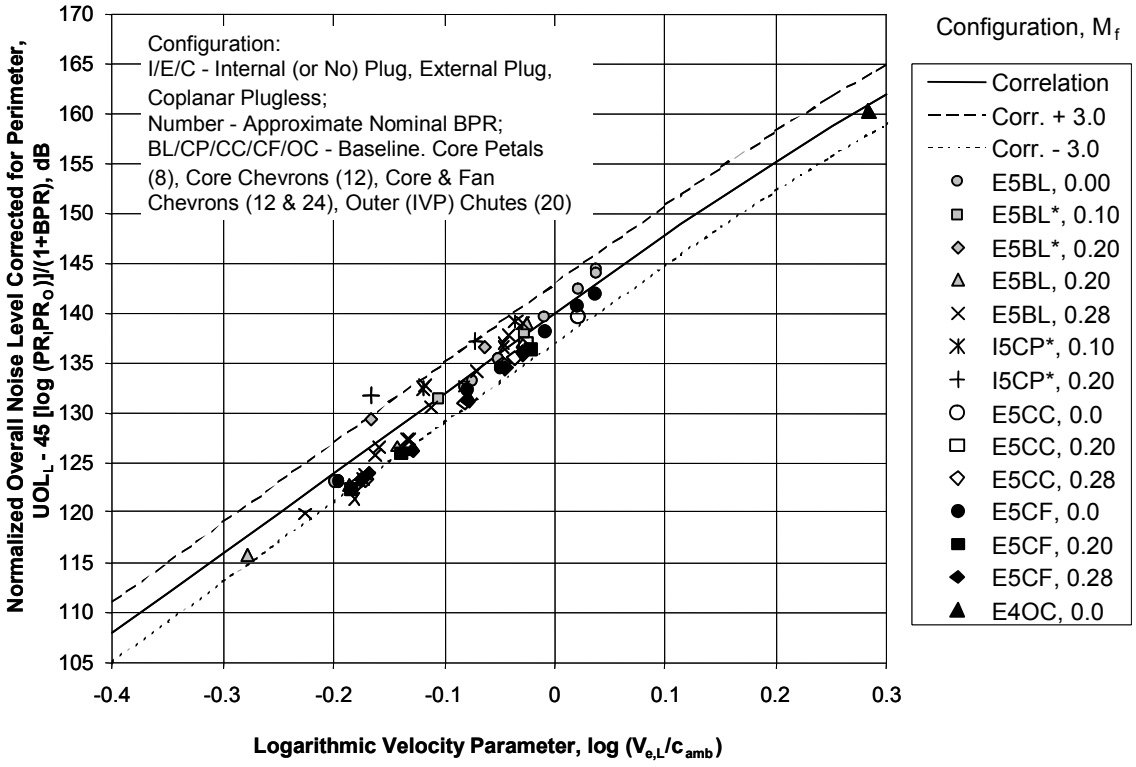

Figure 11.—Comparison of Experimental/Extracted Large Scale Mixing Noise with Correlation for Unsuppressed and Suppressed BPR ≅ 5 Configurations.

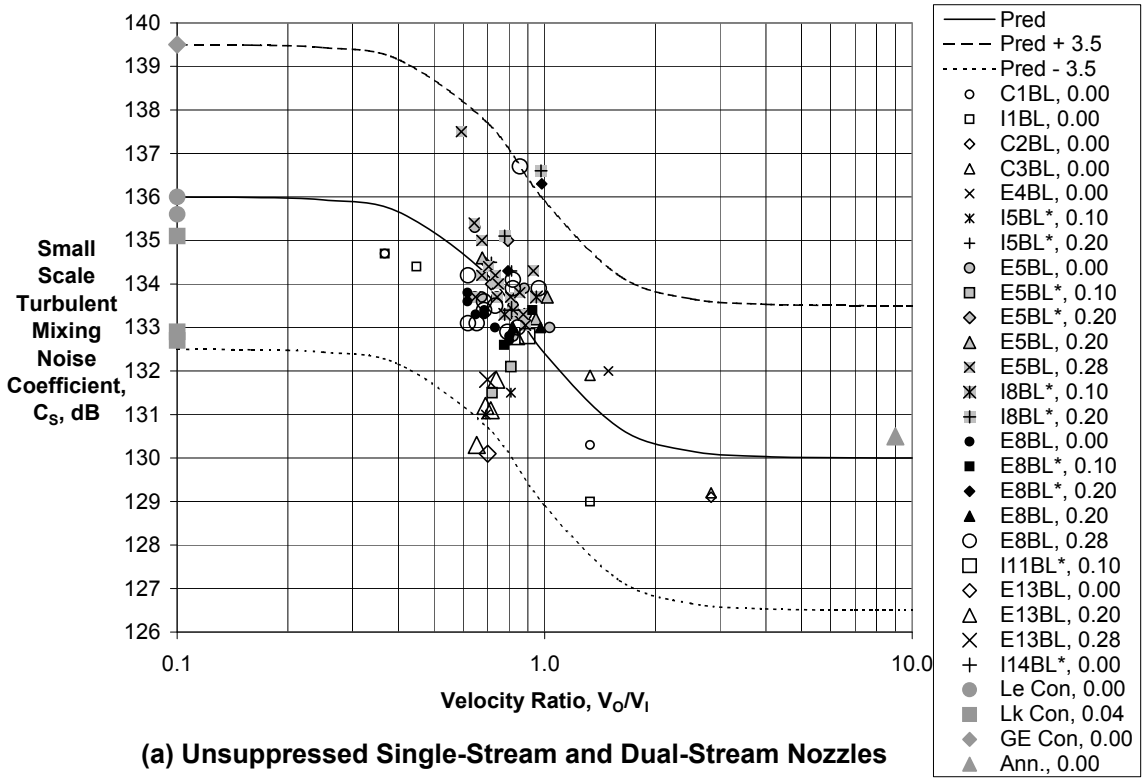

(a) Unsuppressed Single-Stream and Dual-Stream Nozzles

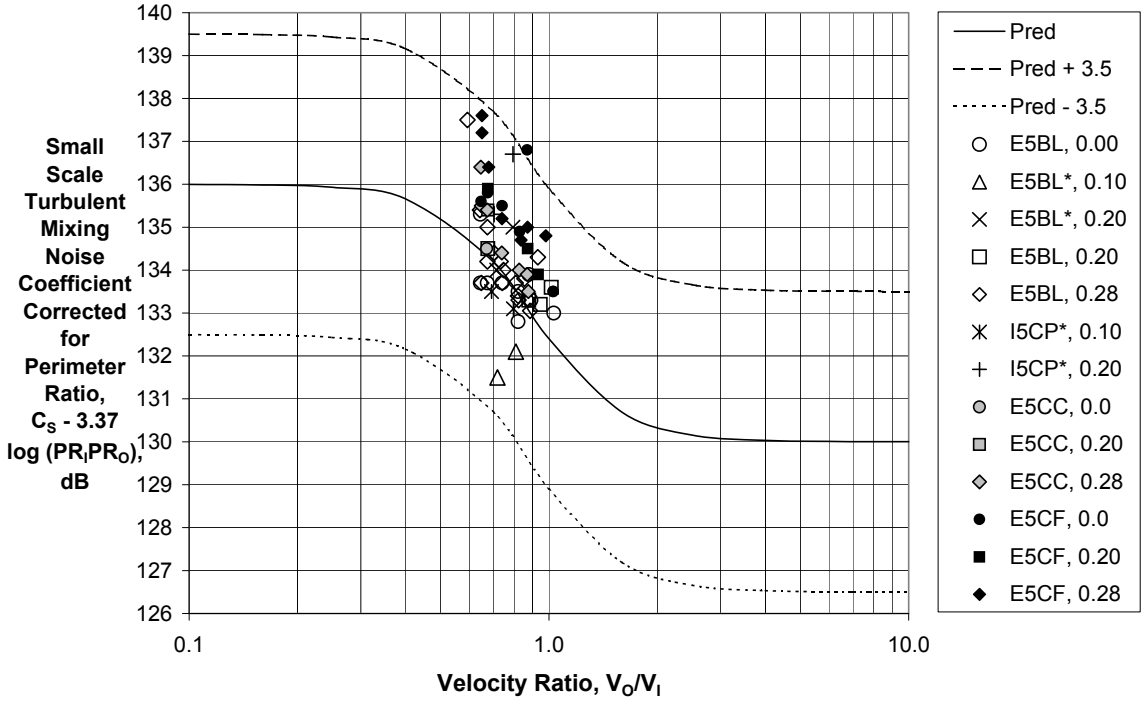

(b) Suppressed and Unsuppressed (BPR ~ 5) Dual-Stream Nozzles

Figure 12.—Correlation of Small Scale Mixing Noise Level.

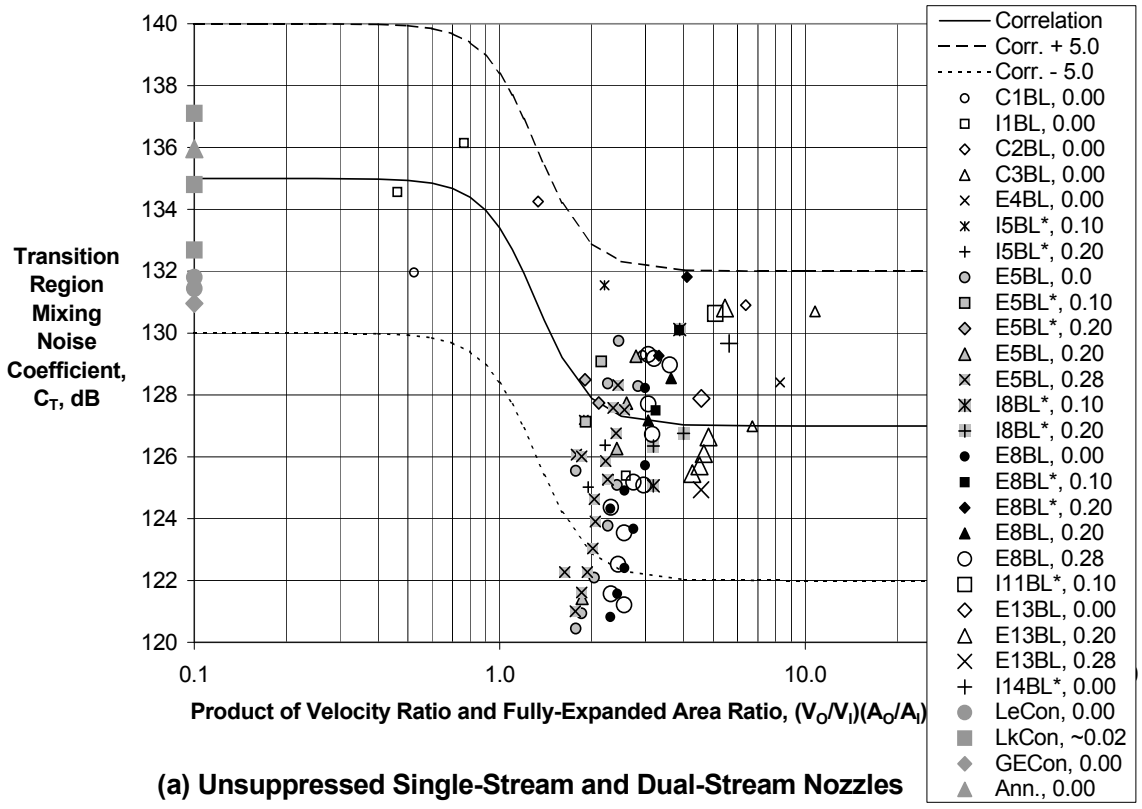

(a) Unsuppressed Single-Stream and Dual-Stream Nozzles

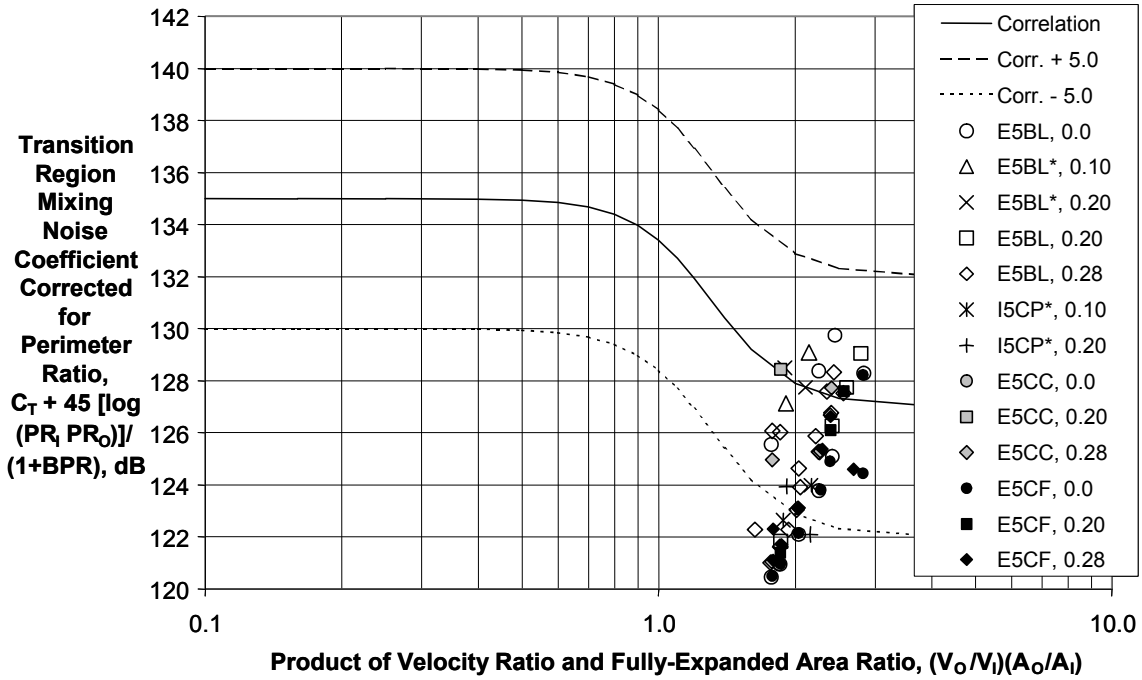

(b) Suppressed and Unsuppressed (BPR ~ 5) Dual-Stream Nozzles

Figure 13.—Correlation of Transitional/Intermediate Scale Mixing Noise Level.

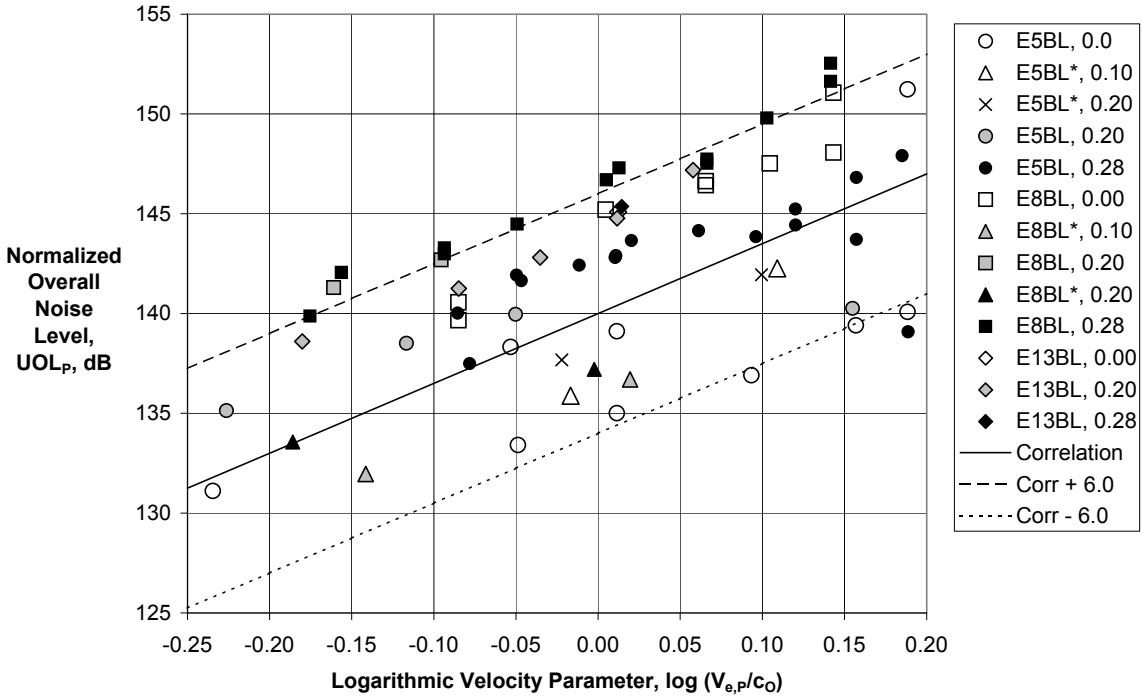

(a) Unsuppressed Nozzles in GRC and LaRC Facilities

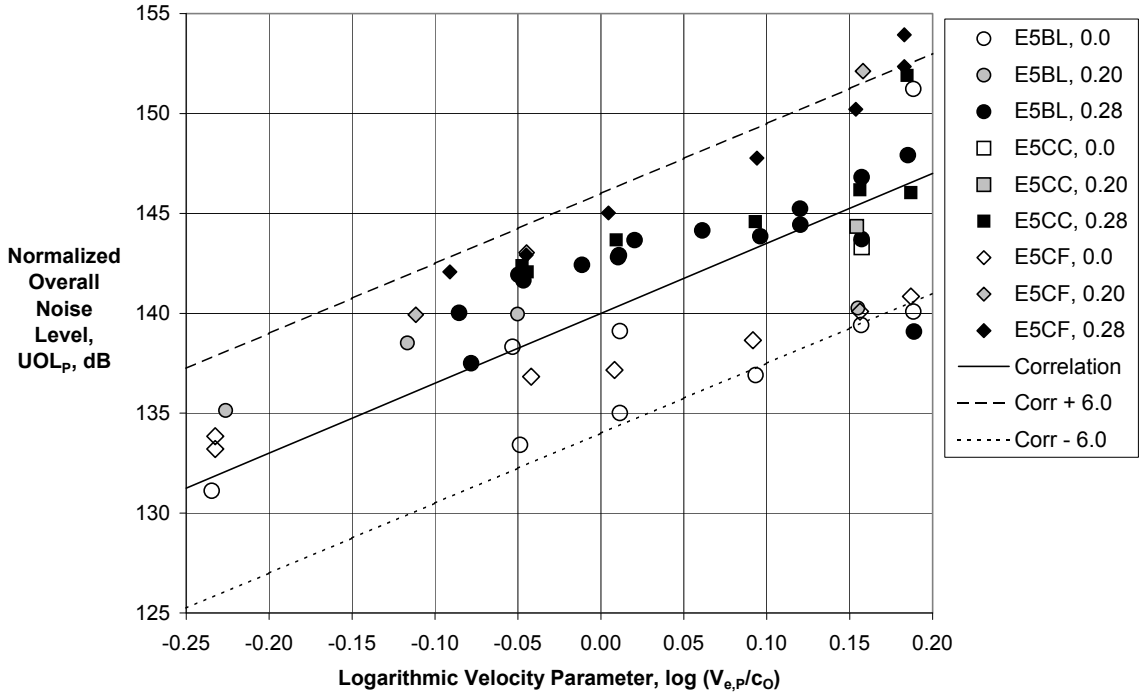

(b) Suppressed and Unsuppressed (BPR ~ 5) Nozzles in GRC Facility

Figure 14.—Correlation of Plug Separation Noise Levels.

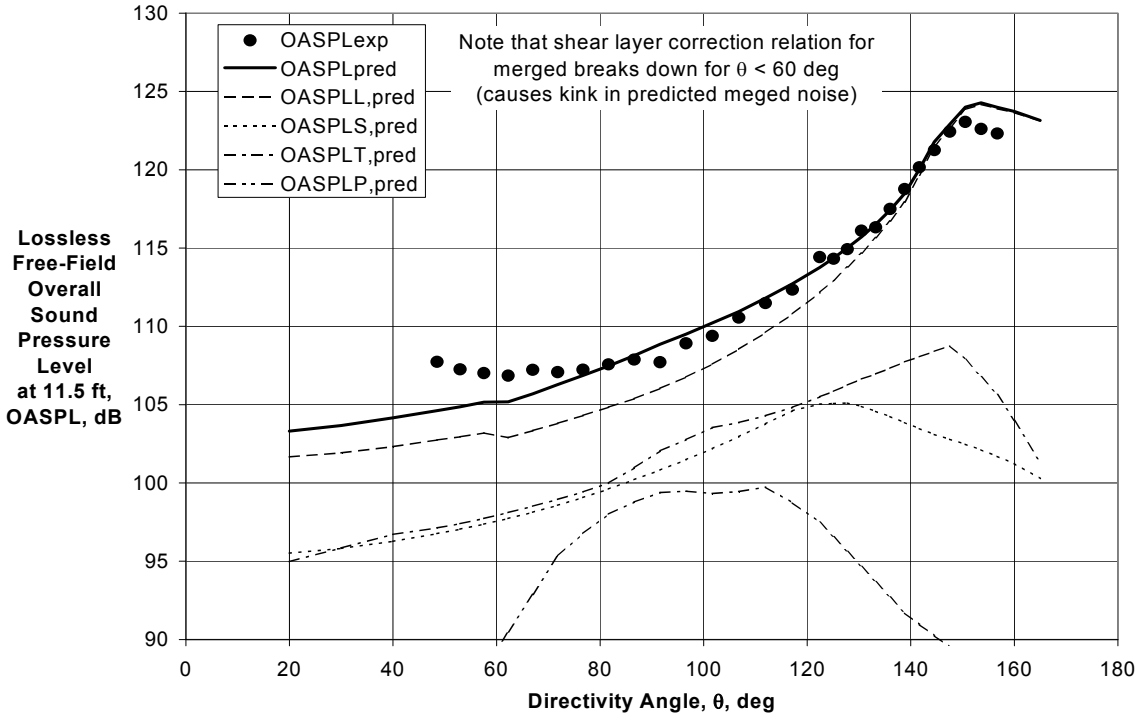

Figure 15.—Comparison of Experimental and Predicted Directivities for LaRC External Plug Nozzle with BPR ≅ 5 at V_{mix}/c_{amb} = 0.989 and M_f = 0.10.

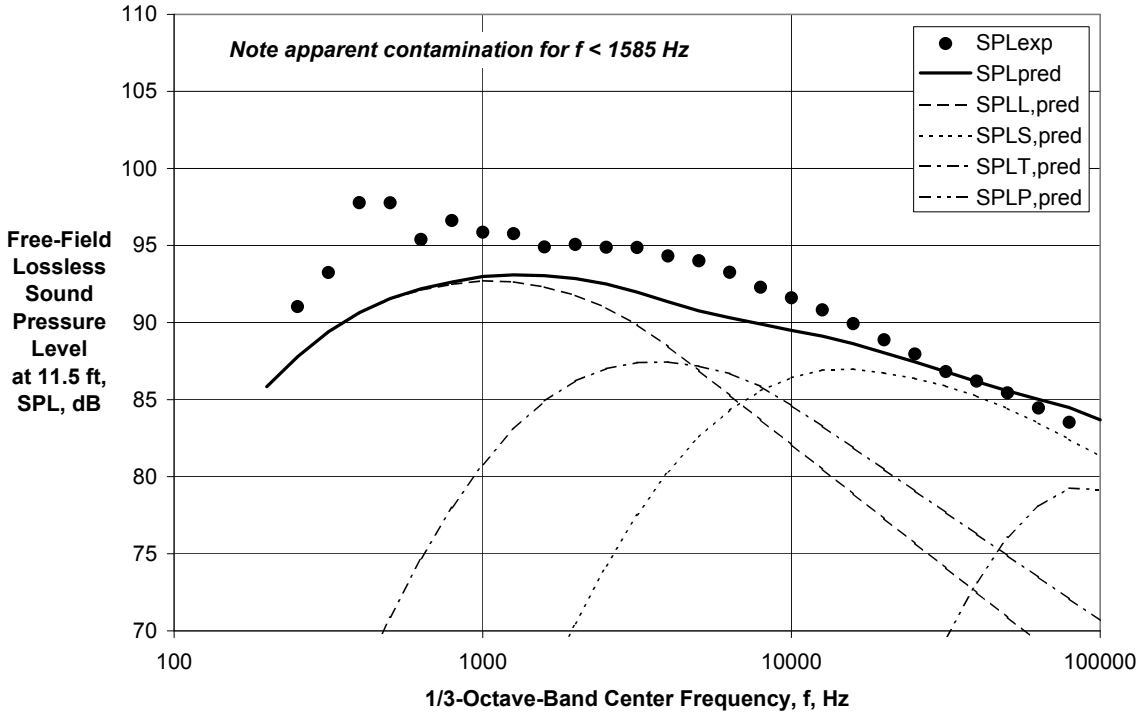

(a) Directivity Angle = 48 deg

Figure 16.—Comparison of Experimental and Predicted Spectra for LaRC External Plug Nozzle with BPR ≅ 5 at V_{mix}/c_{amb} = 0.989 and M_f = 0.10.

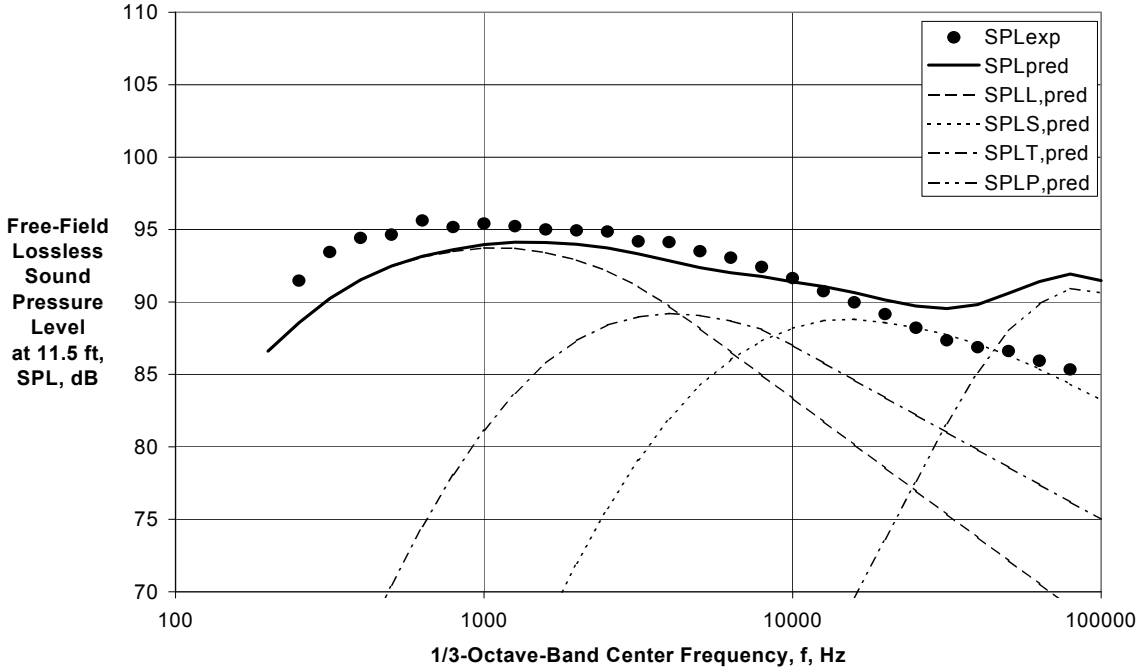

(b) Directivity Angle = 72 deg

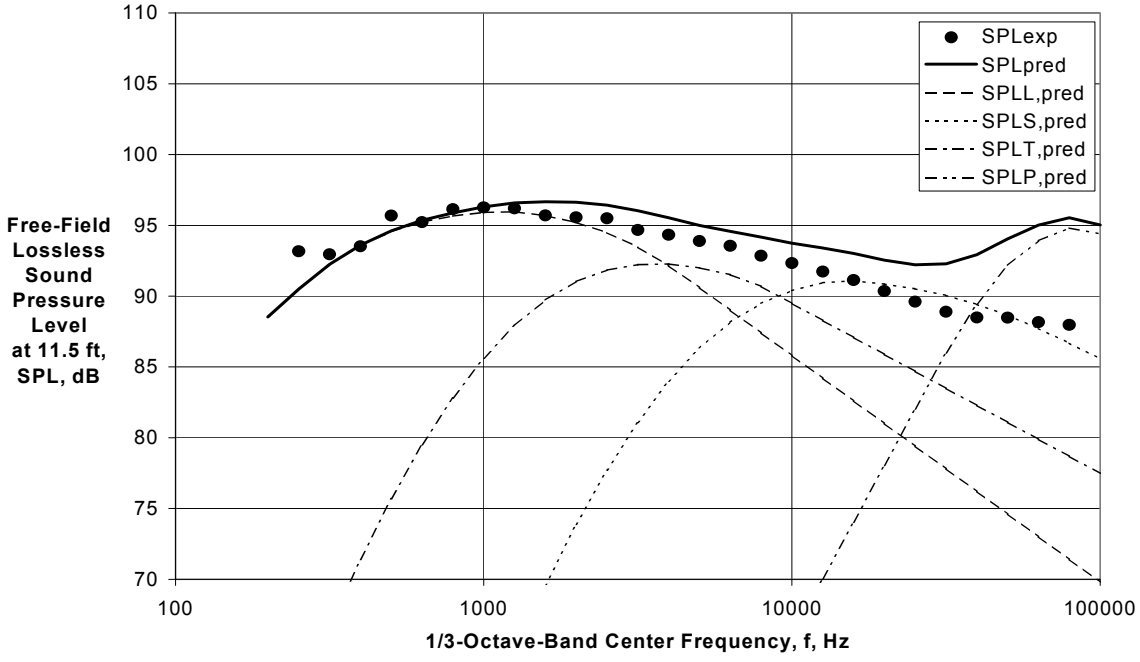

(c) Directivity Angle = 92 deg

Figure 16.—Continued.

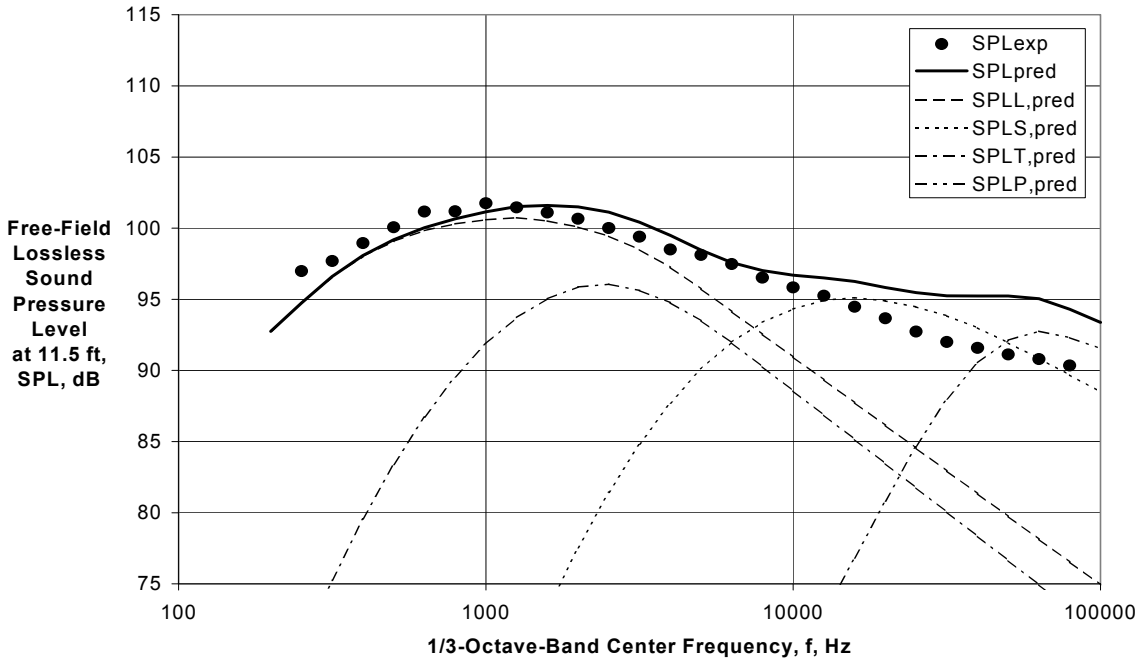

(d) Directivity Angle = 117 deg

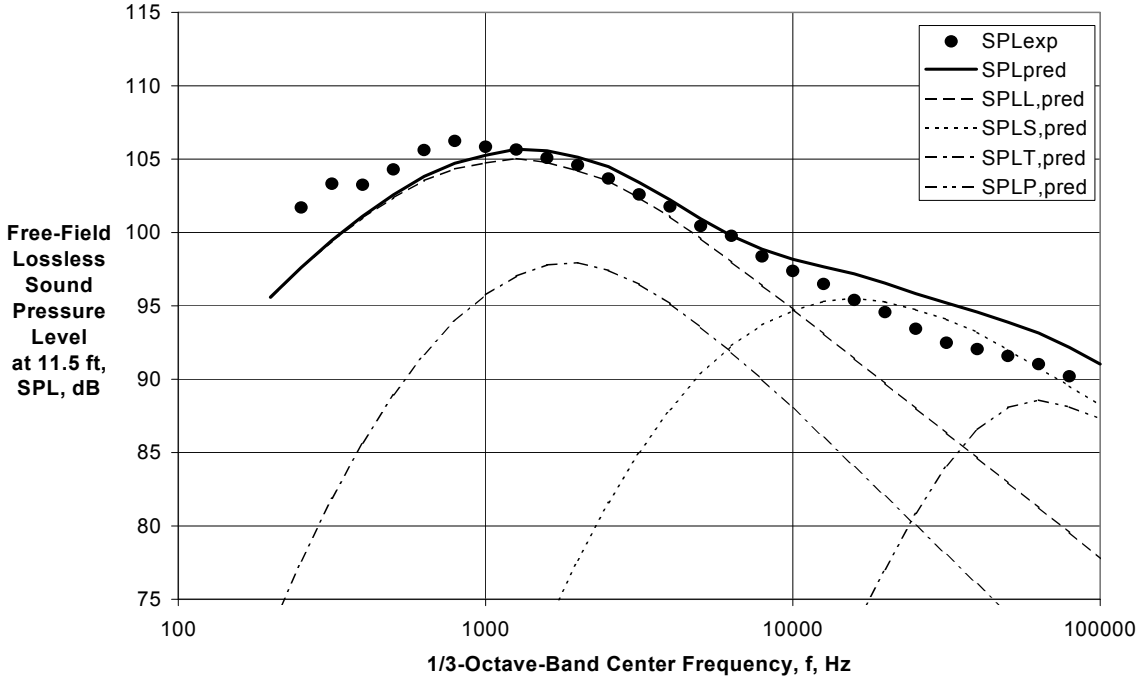

(e) Directivity Angle = 130 deg

Figure 16.—Continued.

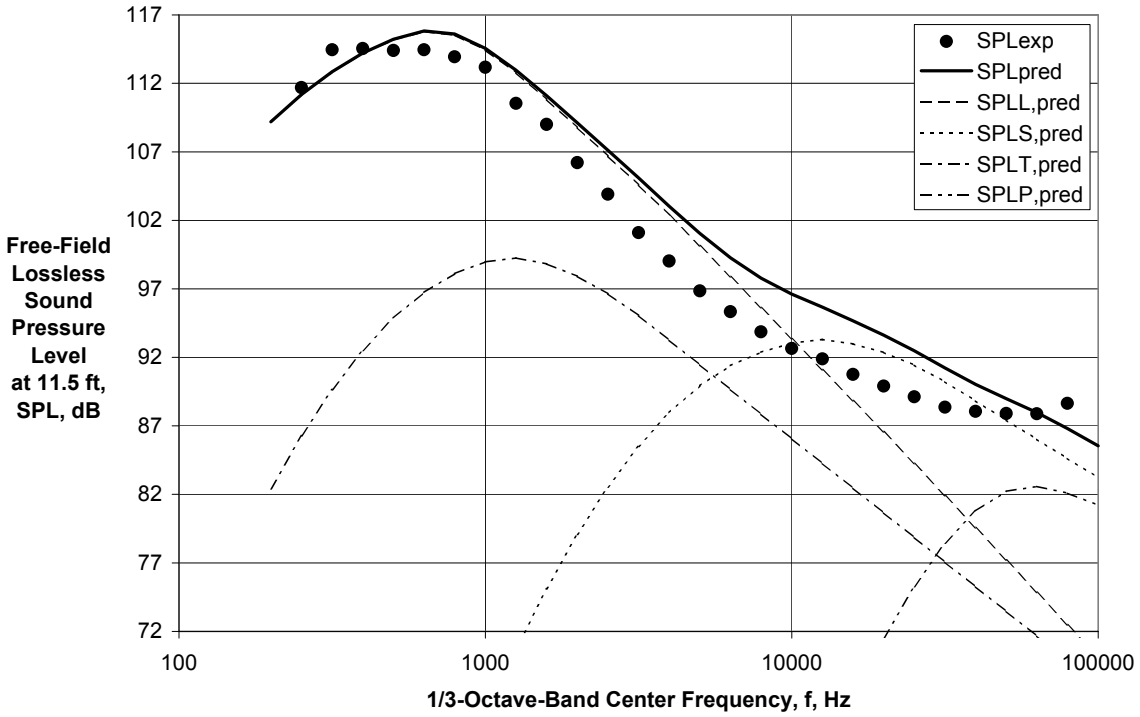

(f) Directivity Angle = 151 deg

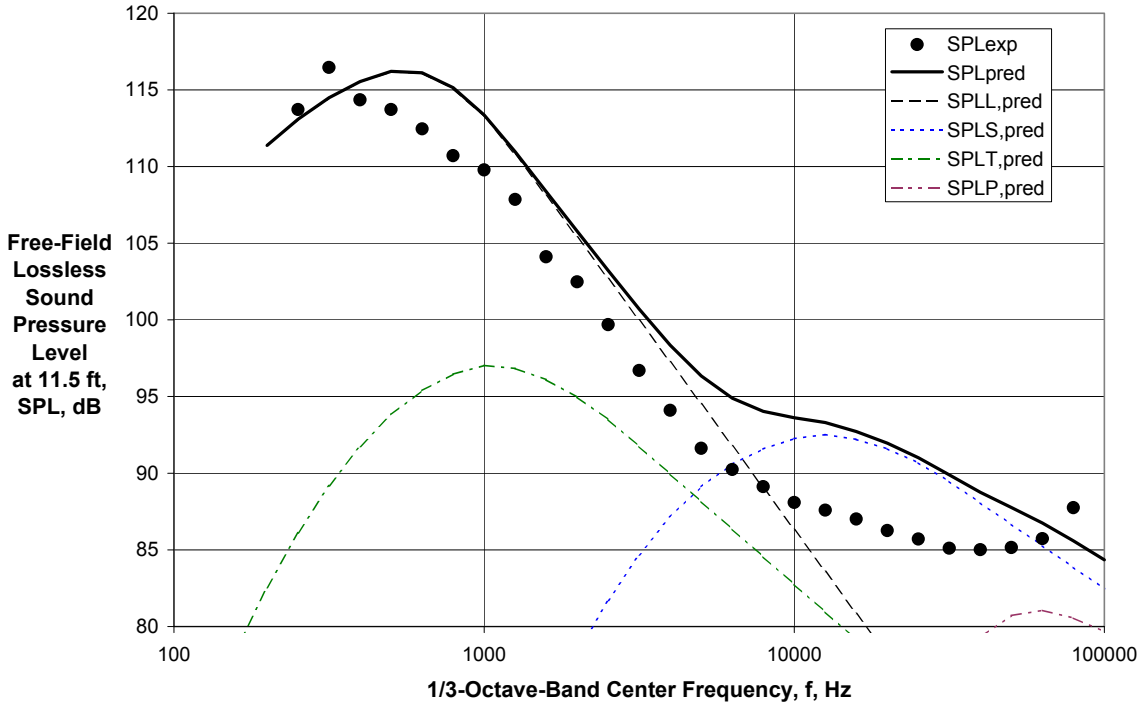

(g) Directivity Angle = 157 deg

Figure 16.—Concluded.

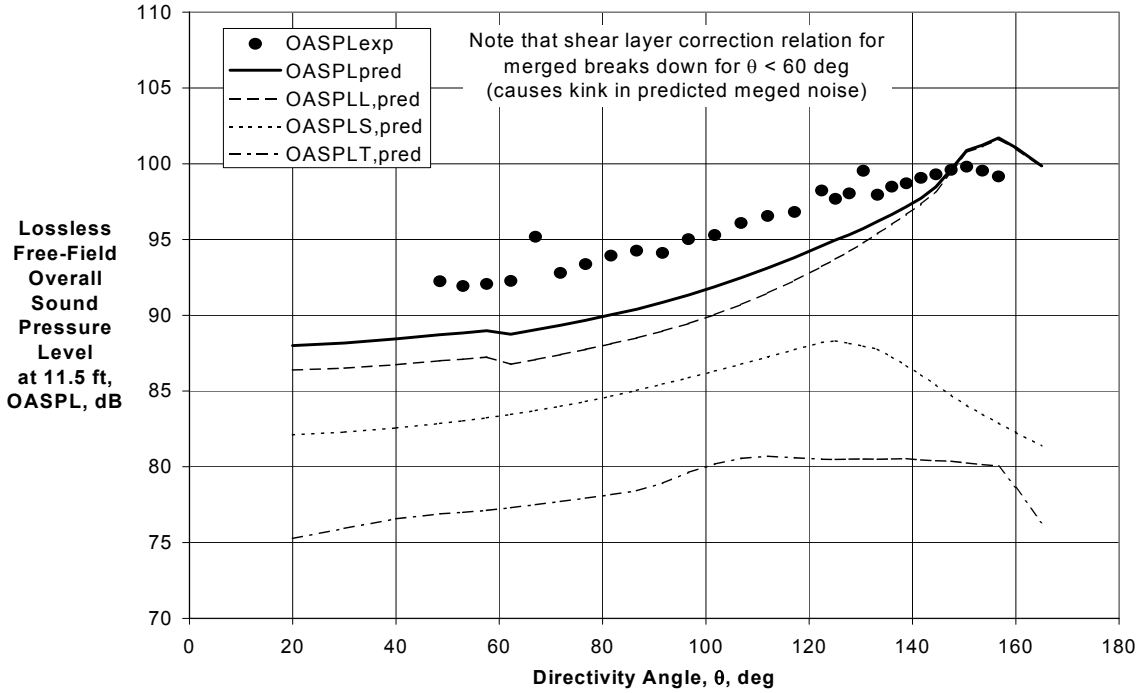

Figure 17.—Comparison of Experimental and Predicted Directivities for LaRC Internal Plug Nozzle with BPR ≅ 11 at V_{mix}/c_{amb} = 0.591 and M_f = 0.10.

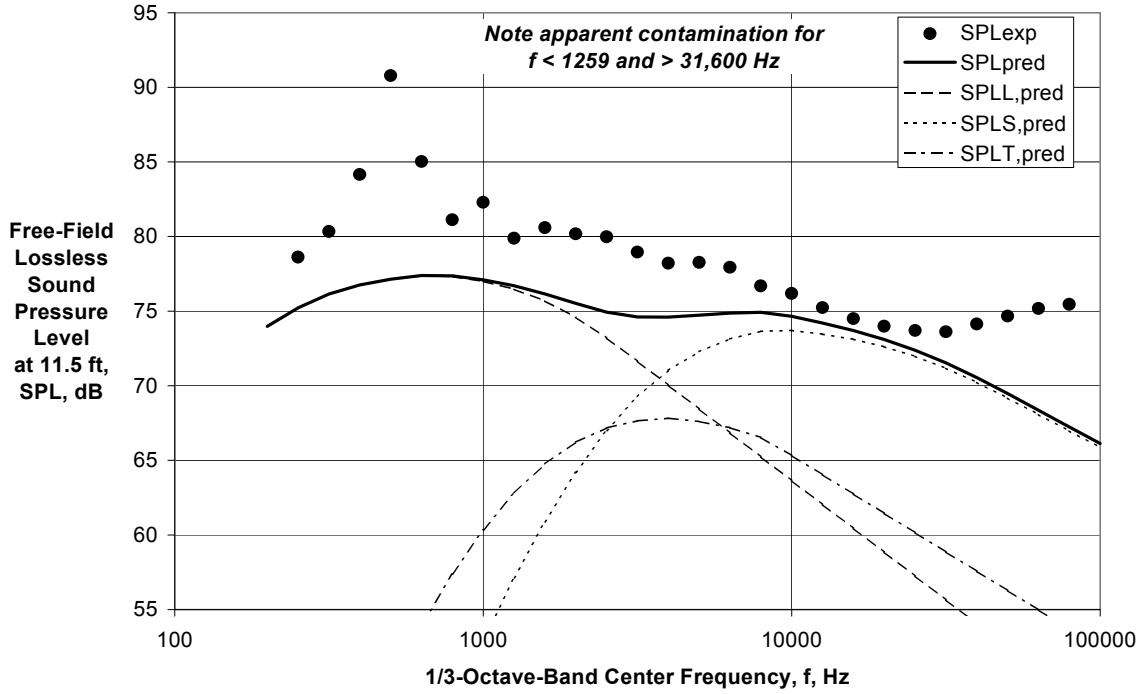

(a) Directivity Angle = 67 deg

Figure 18.—Comparison of Experimental and Predicted Spectra for LaRC Internal Plug Nozzle with BPR ≅ 11 at V_{mix}/c_{amb} = 0.591 and M_f = 0.10.

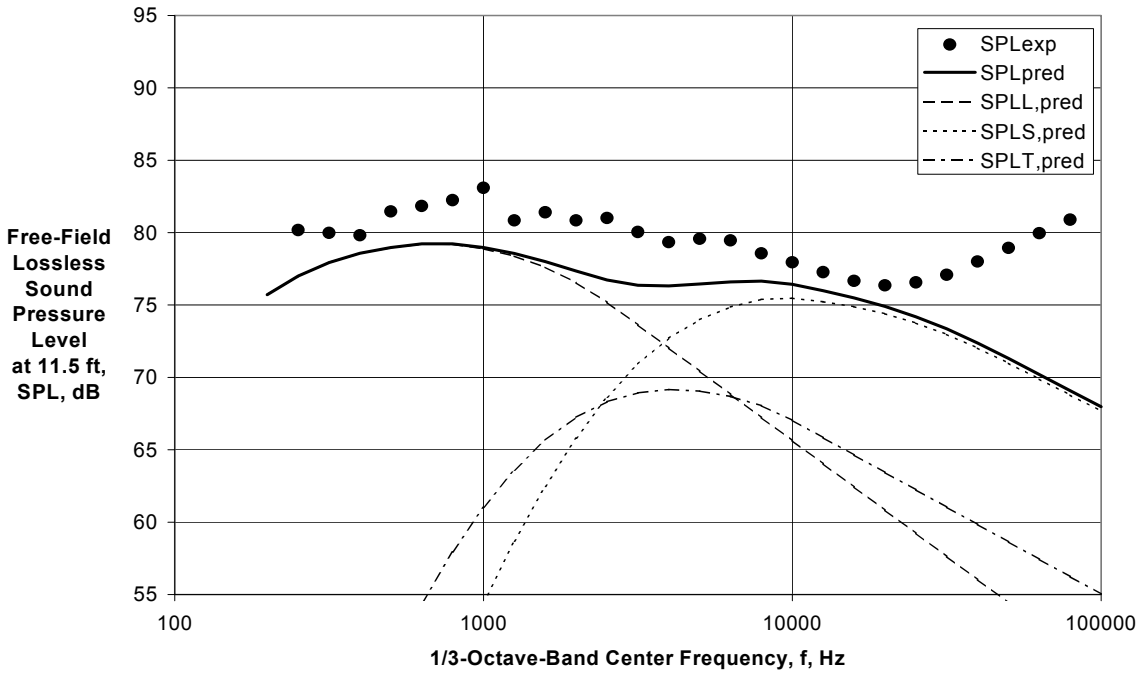

(b) Directivity Angle = 92 deg

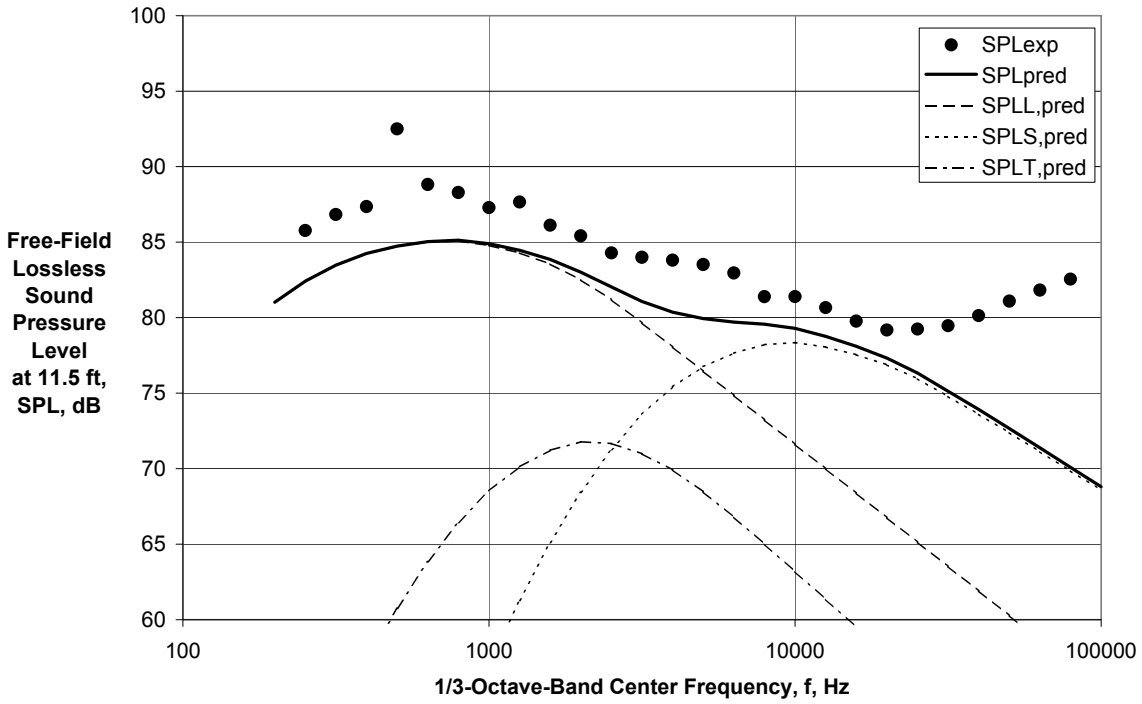

(c) Directivity Angle = 130 deg

Figure 18.—Continued.

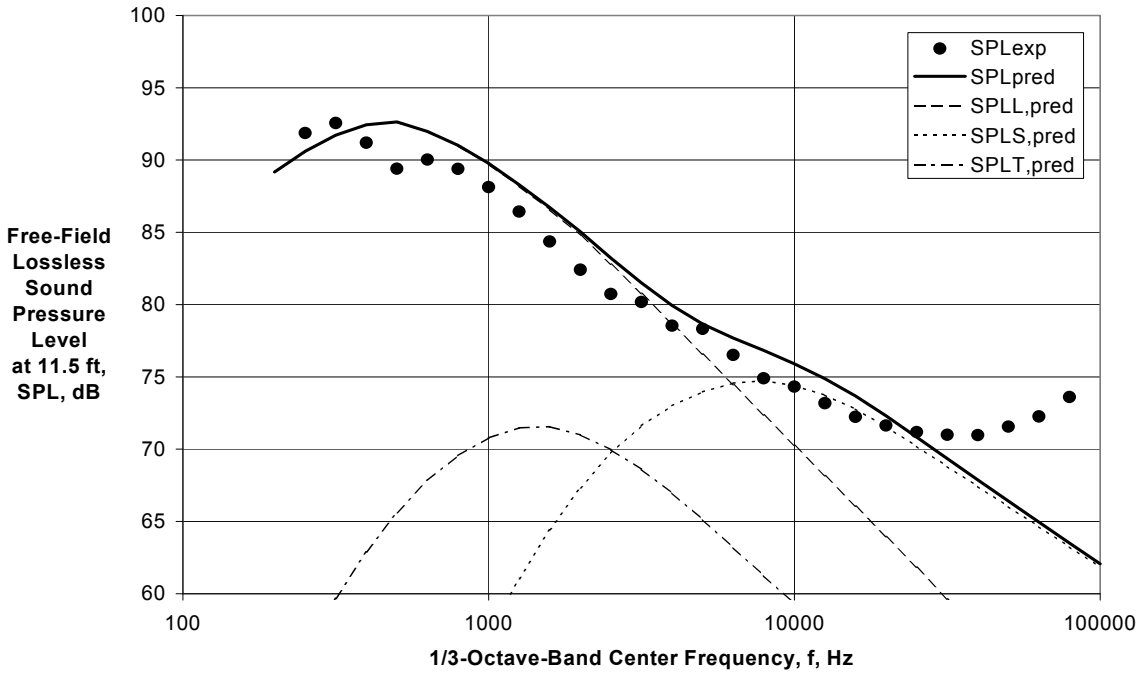

(d) Directivity Angle = 151 deg

Figure 18.—Concluded.

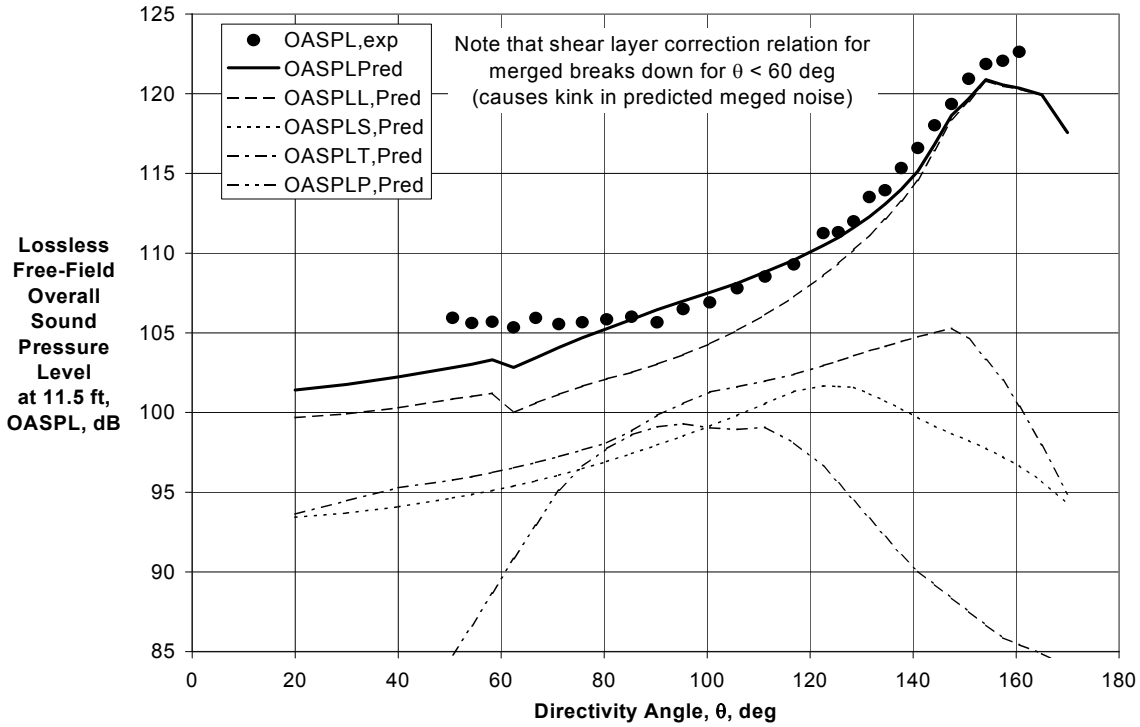

Figure 19.—Comparison of Experimental and Predicted Directivities for LaRC External Plug Nozzle with BPR ≅ 5 at V_{mix}/c_{amb} = 0.971 and M_f = 0.201.

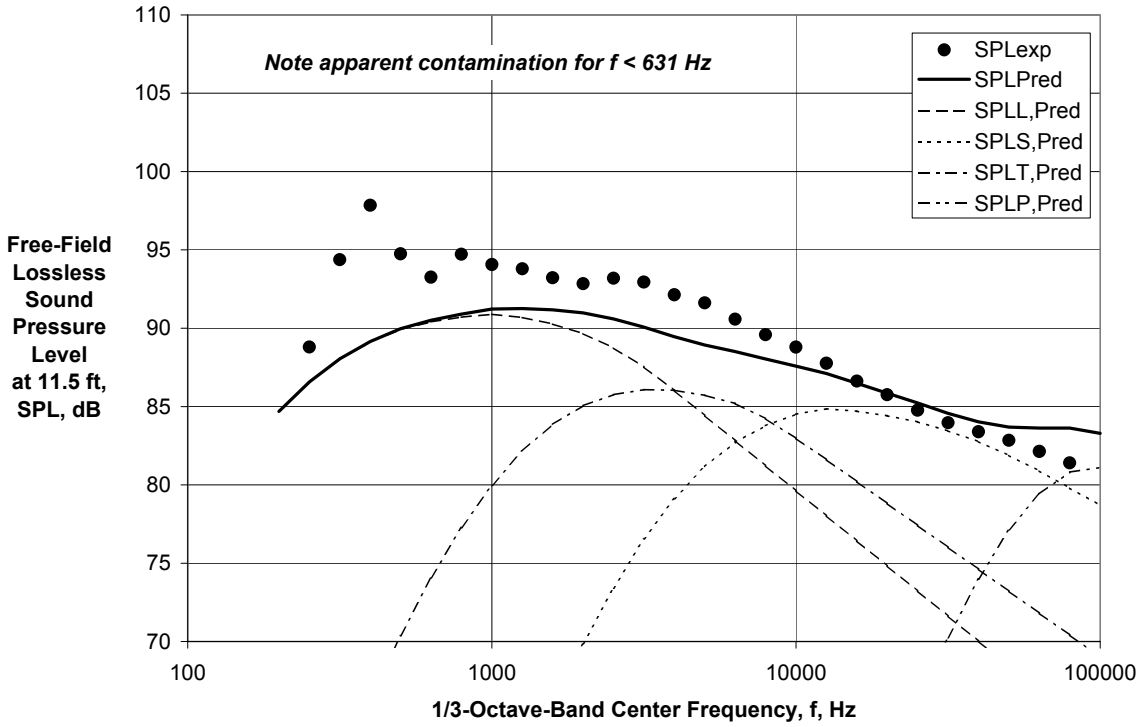

(a) Directivity Angle = 51 deg

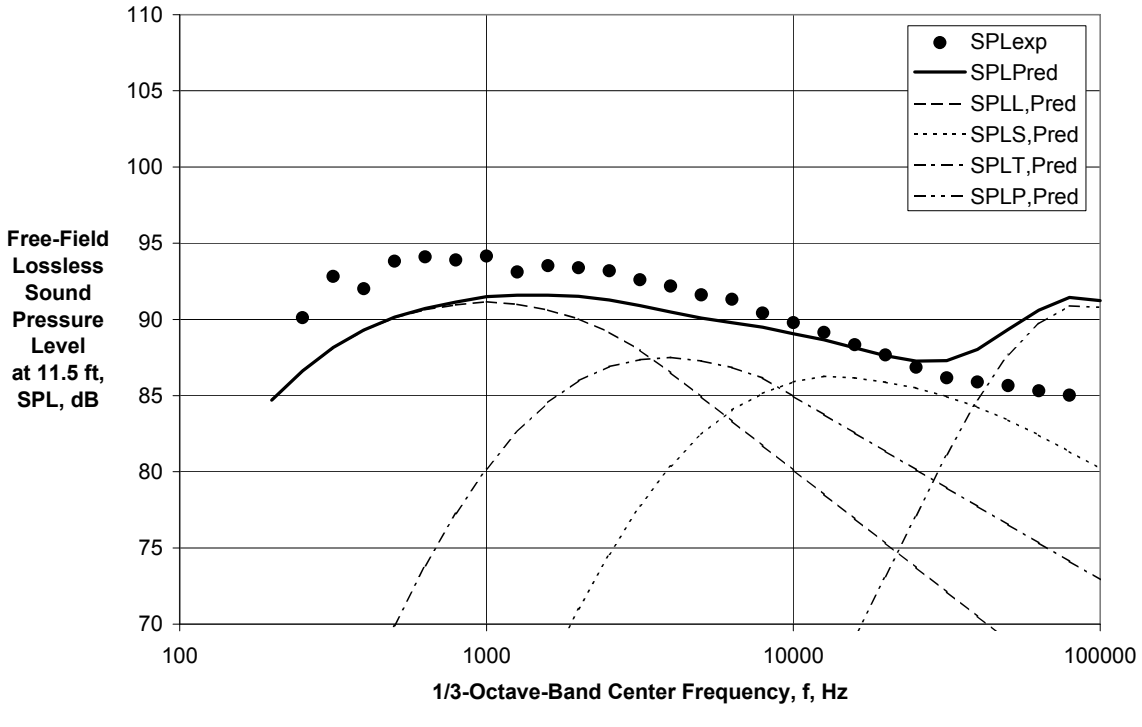

(b) Directivity Angle = 71 deg

Figure 20.—Comparison of Experimental and Predicted Spectra for LaRC External Plug Nozzle with BPR ≅ 5 at V_{mix}/c_{amb} = 0.971 and M_f = 0.201.

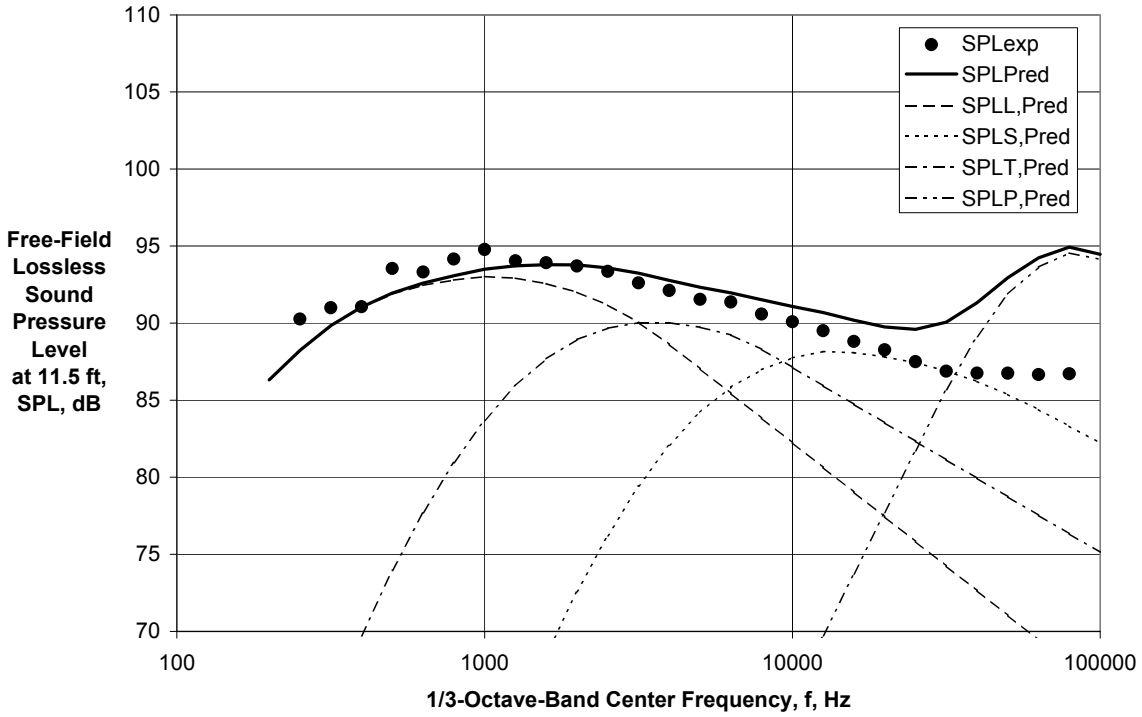

(c) Directivity Angle = 90 deg

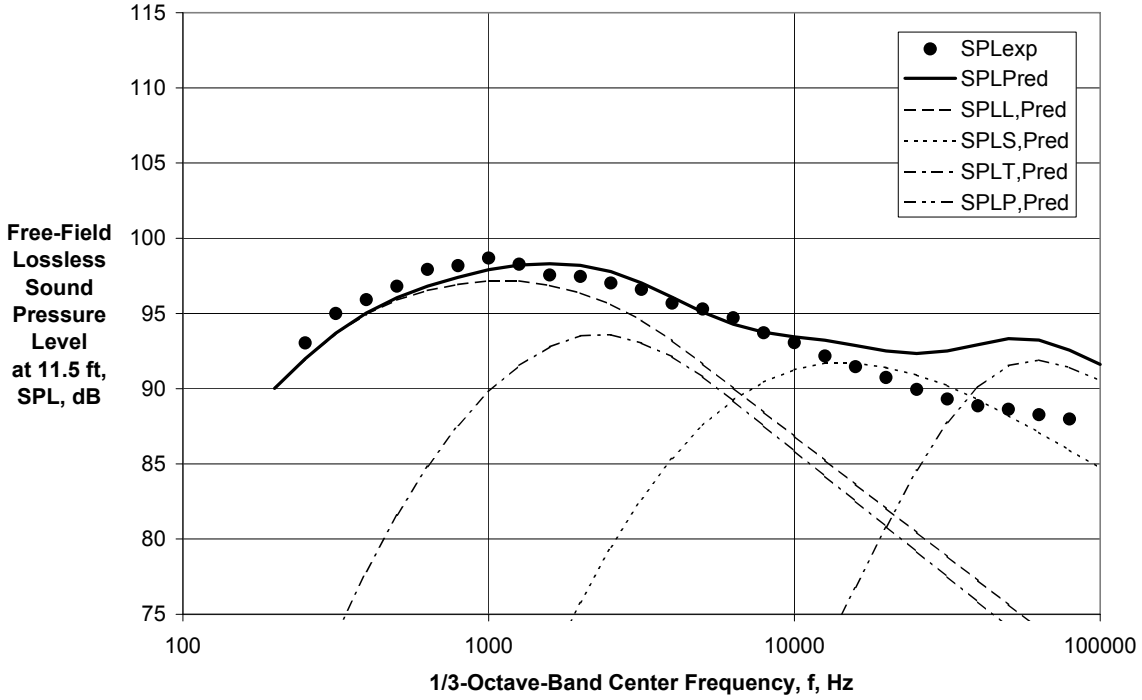

(d) Directivity Angle = 117 deg

Figure 20.—Continued.

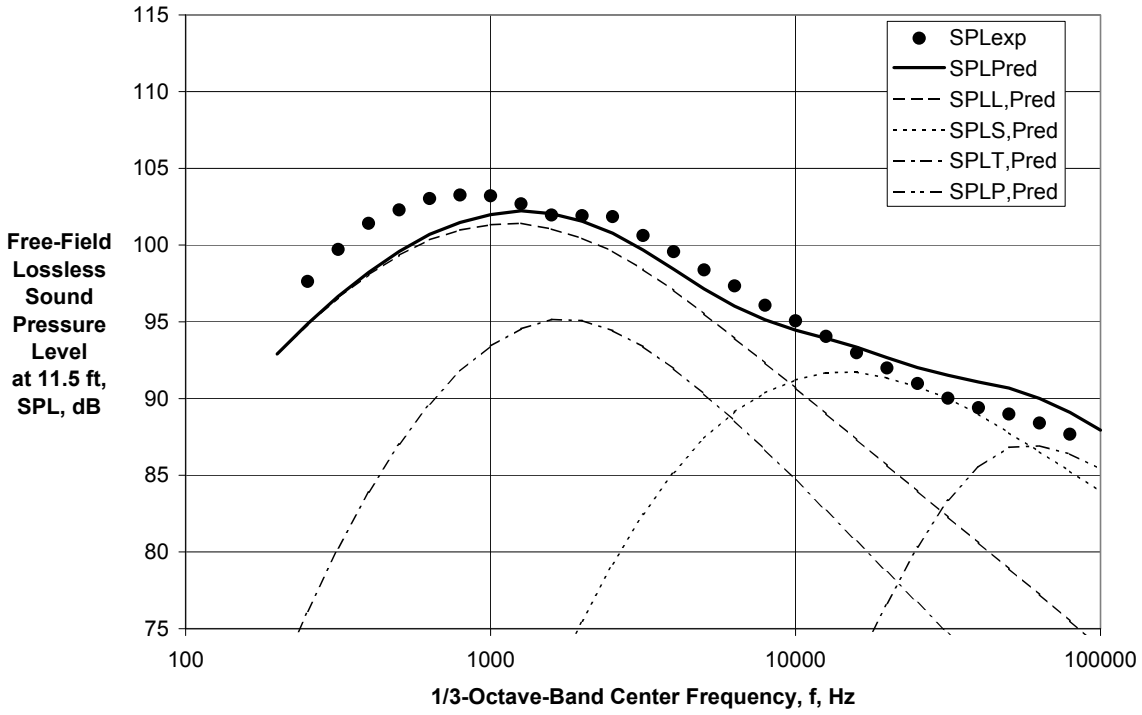

(e) Directivity Angle = 131 deg

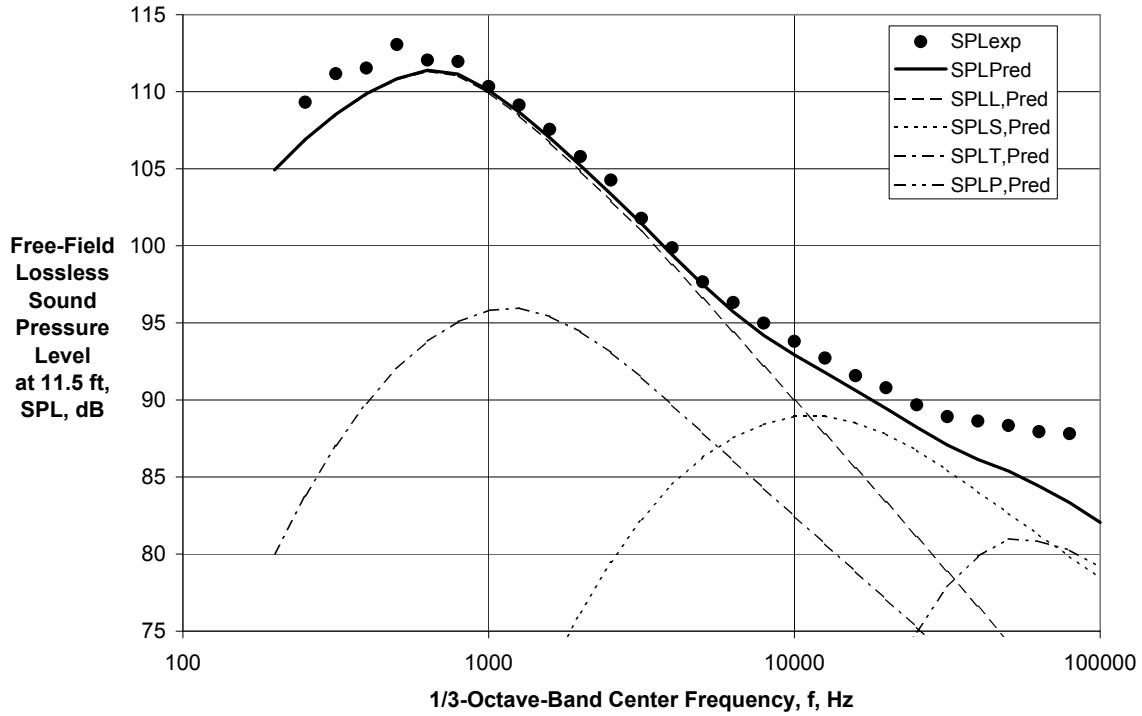

(f) Directivity Angle = 151 deg

Figure 20.—Continued.

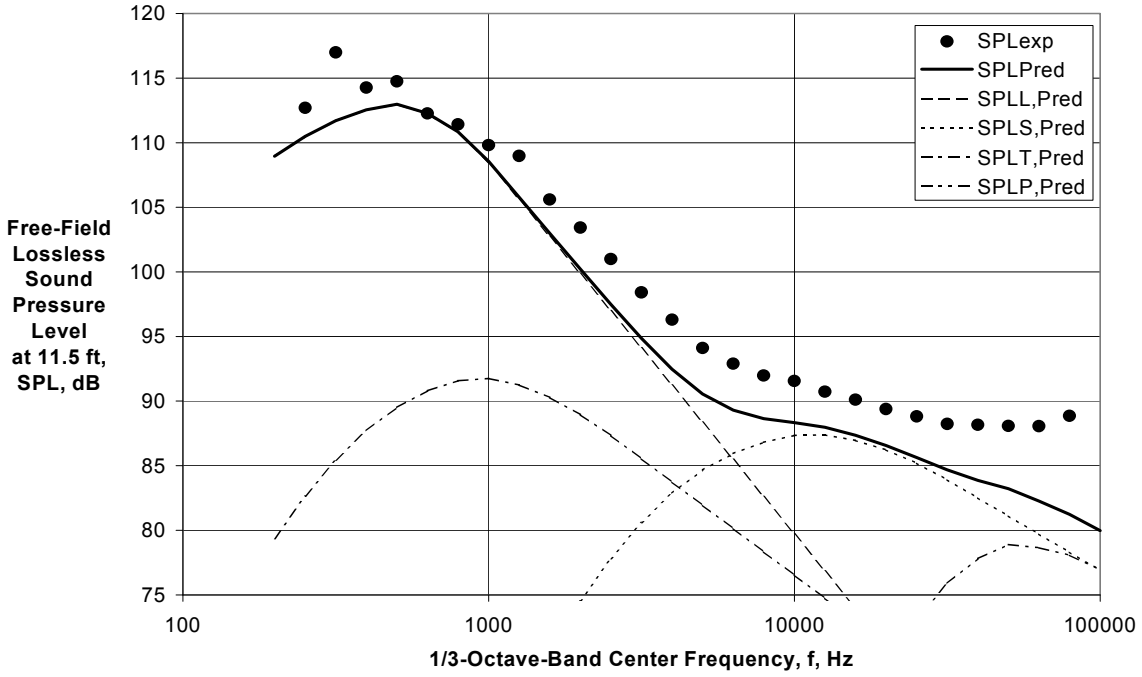

(g) Directivity Angle = 161 deg

Figure 20.—Concluded.

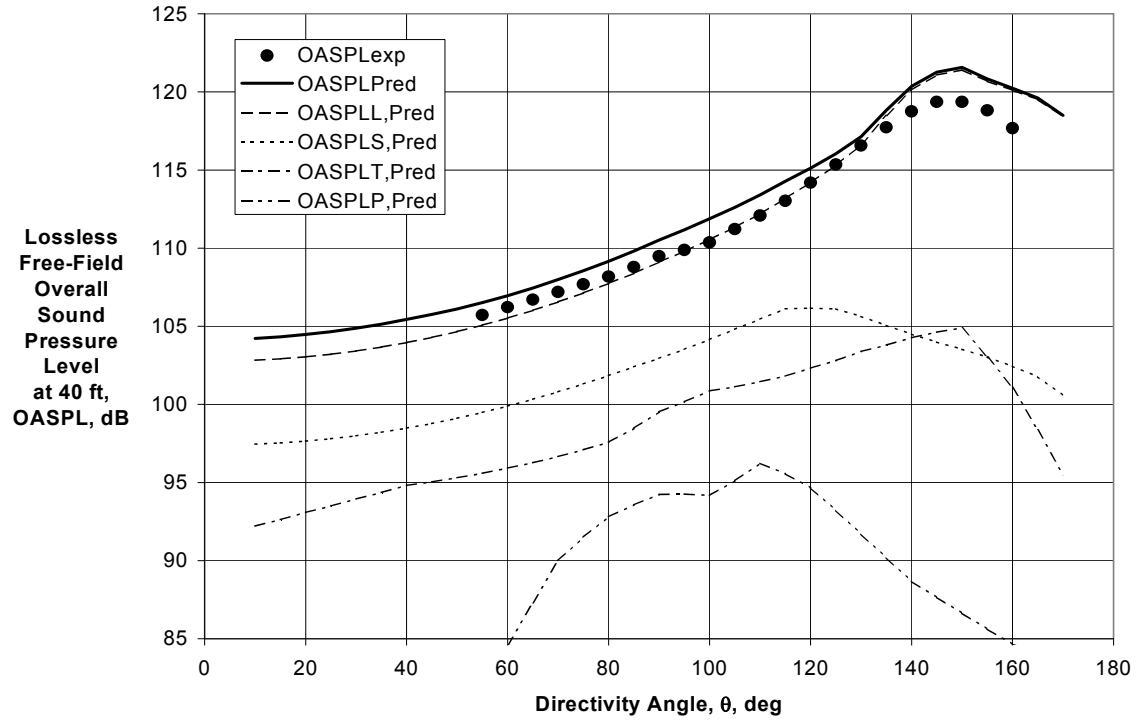

Figure 21.—Comparison of Experimental and Predicted Directivities for GE/GRC External Plug Nozzle with BPR ≅ 13 at V_{mix}/c_{amb} = 0.766 and M_f = 0.00.

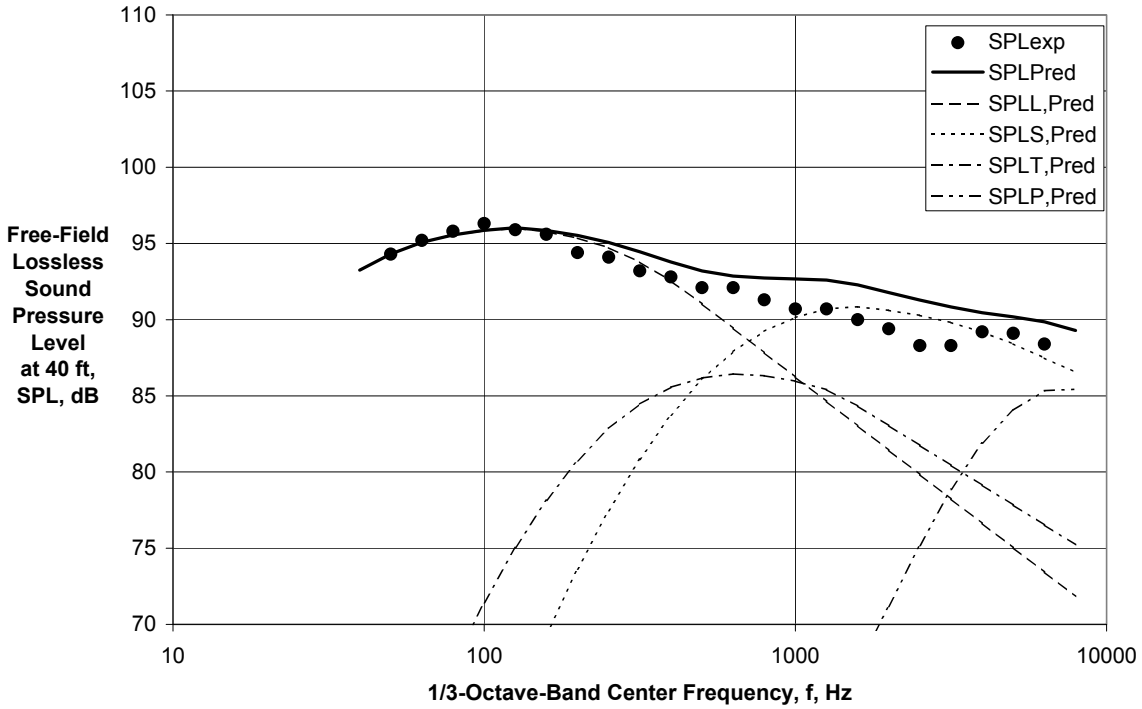

(a) Directivity Angle = 60 deg

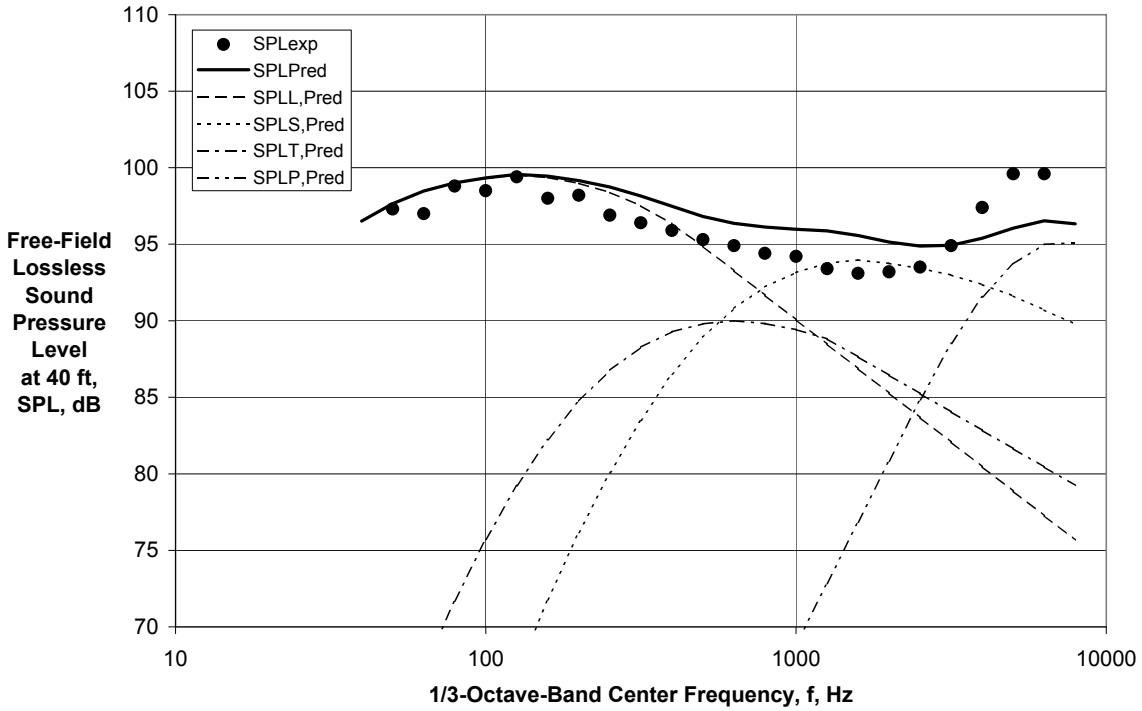

(b) Directivity Angle = 90 deg

Figure 22.—Comparison of Experimental and Predicted Spectra for GE/GRC External Plug Nozzle with BPR ≅ 13 at V_{mix}/c_{amb} = 0.766 and M_f = 0.00.

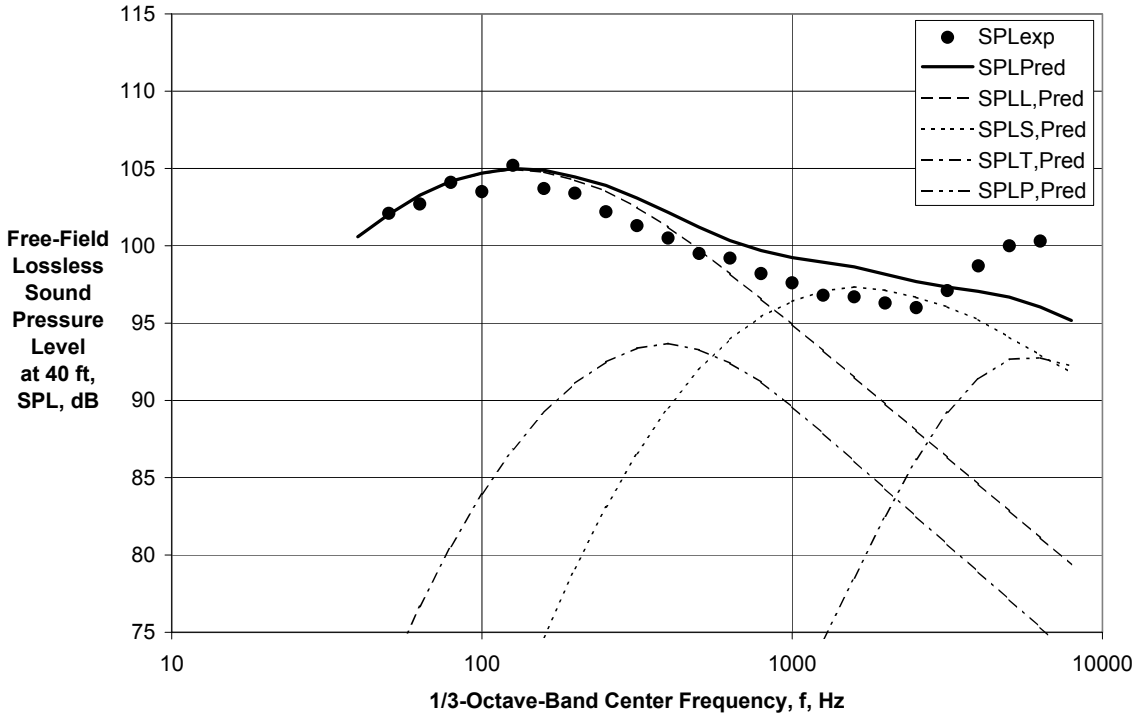

(c) Directivity Angle = 120 deg

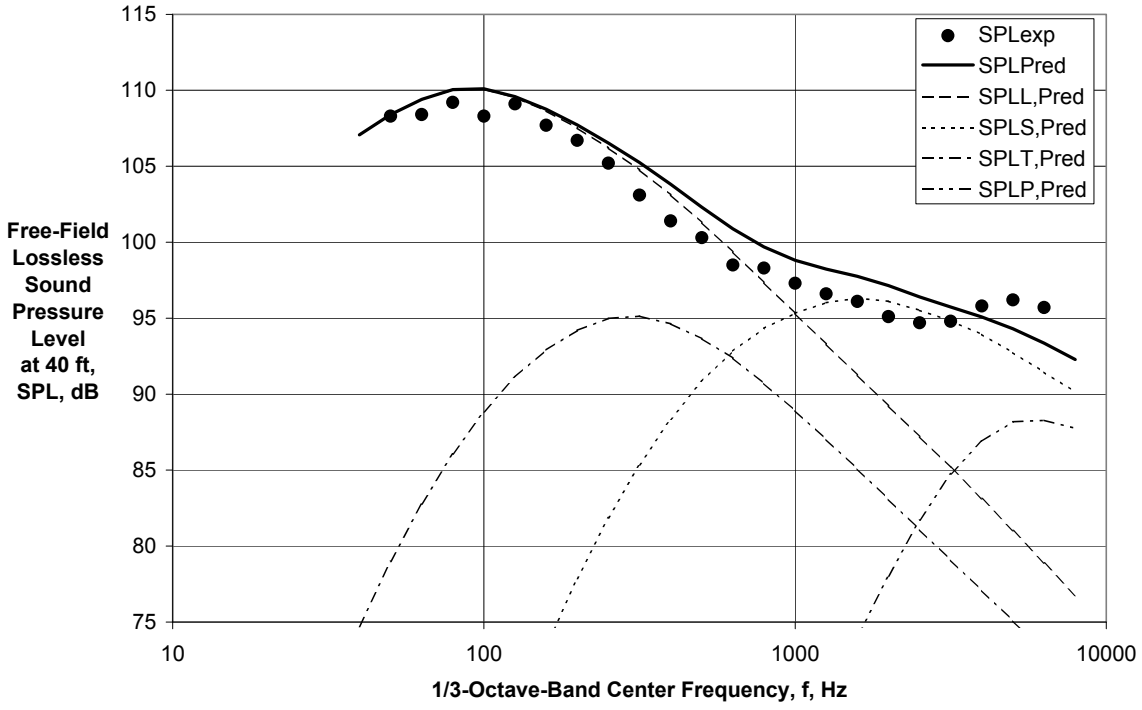

(d) Directivity Angle = 135 deg

Figure 22.—Continued.

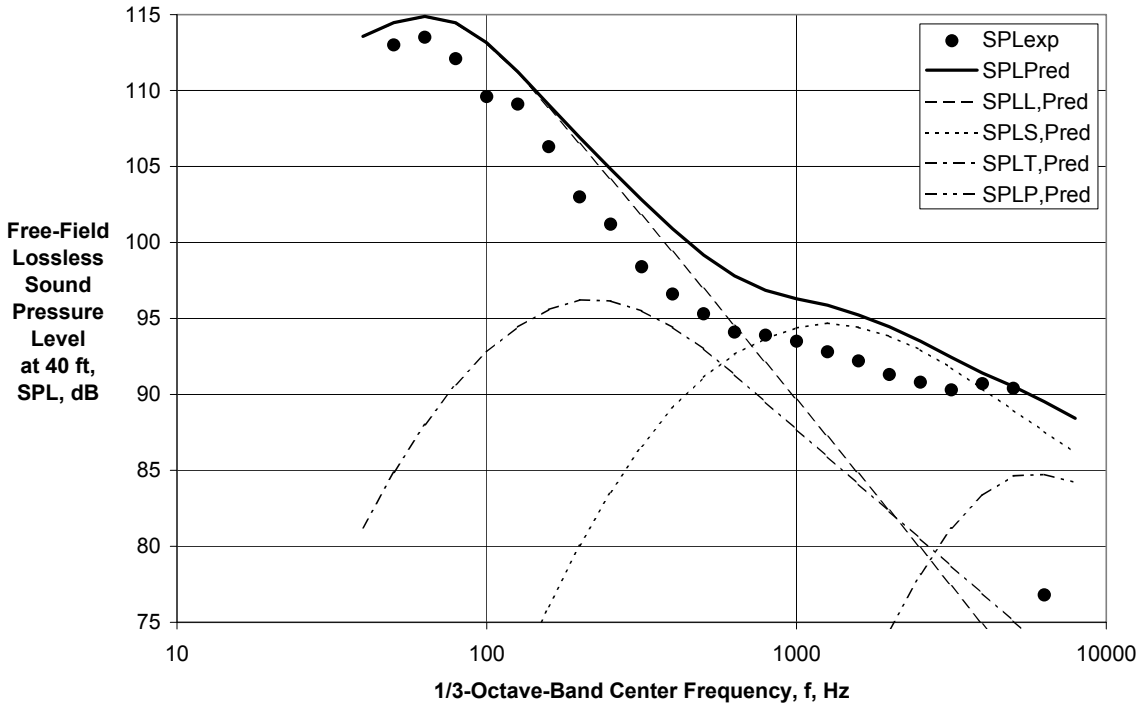

(e) Directivity Angle = 150 deg

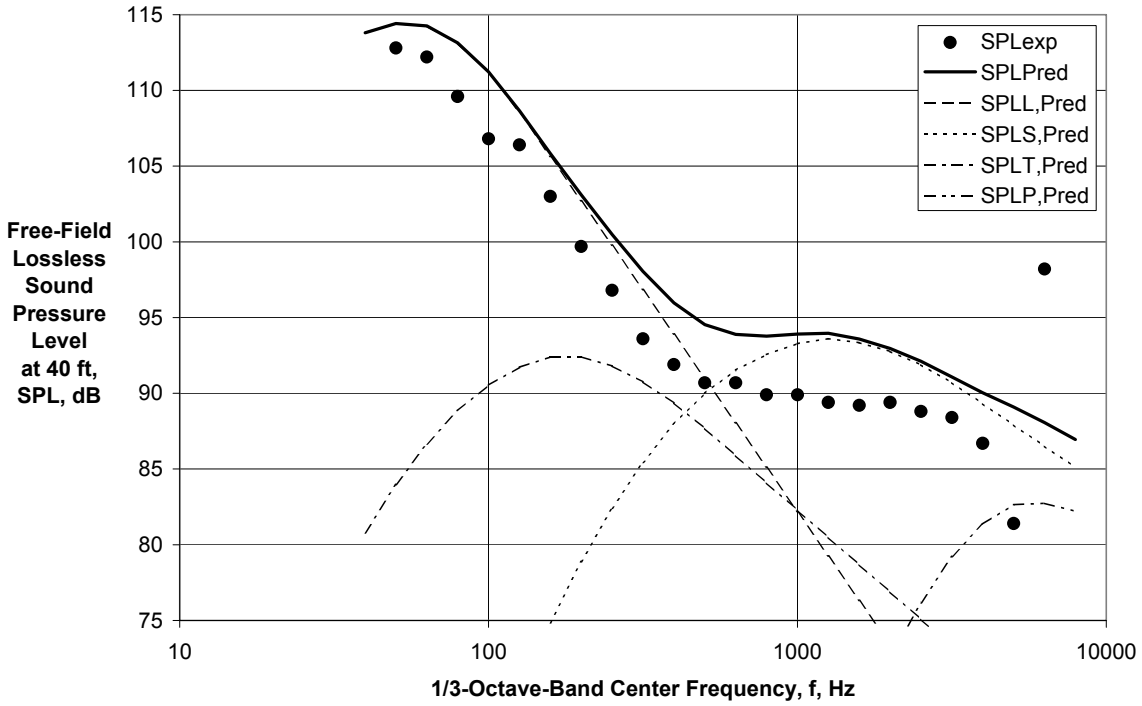

(f) Directivity Angle = 160 deg

Figure 22.—Concluded.

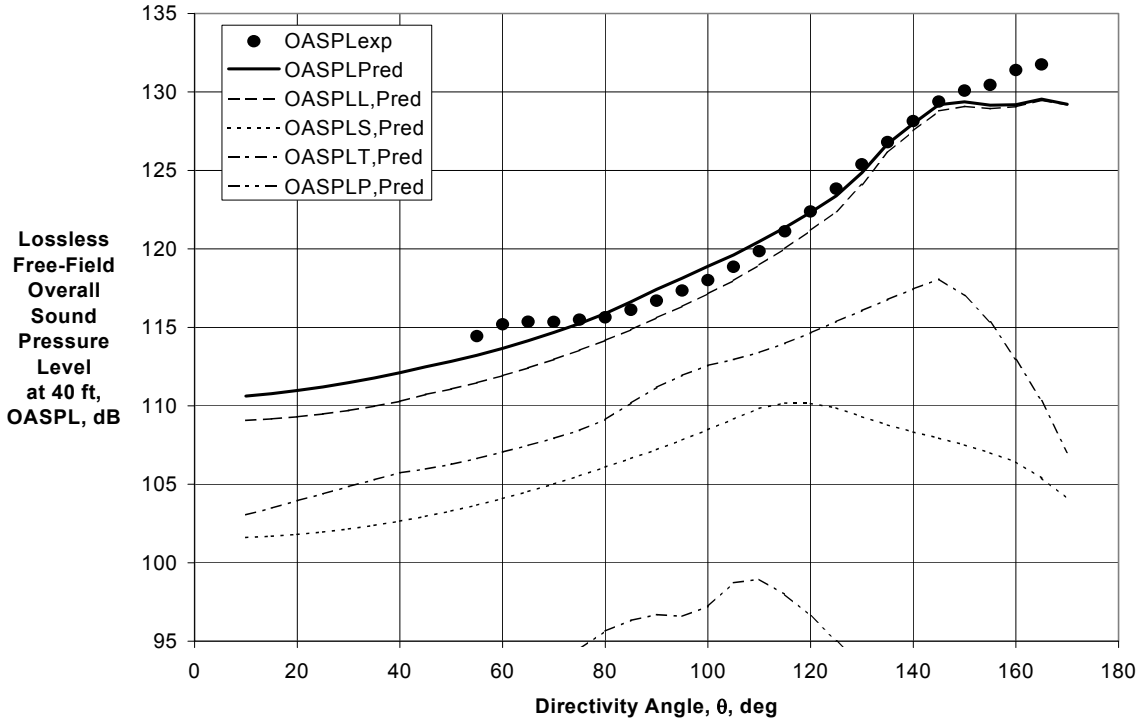

Figure 23.—Comparison of Experimental and Predicted Directivities for GE/GRC External Plug Nozzle with BPR ≅ 5 at V_{mix}/c_{amb} = 1.047 and M_f = 0.20.

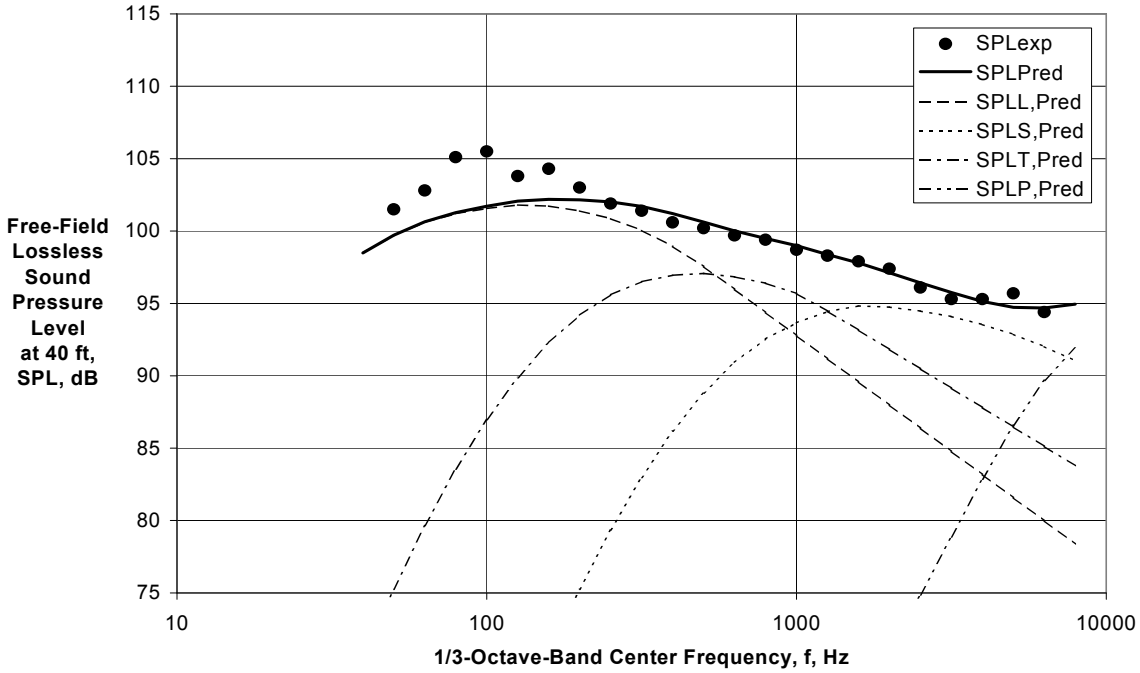

(a) Directivity Angle = 55 deg

Figure 24.—Comparison of Experimental and Predicted Spectra for GE/GRC External Plug Nozzle with BPR ≅ 5 at V_{mix}/c_{amb} = 1.047 and M_f = 0.20.

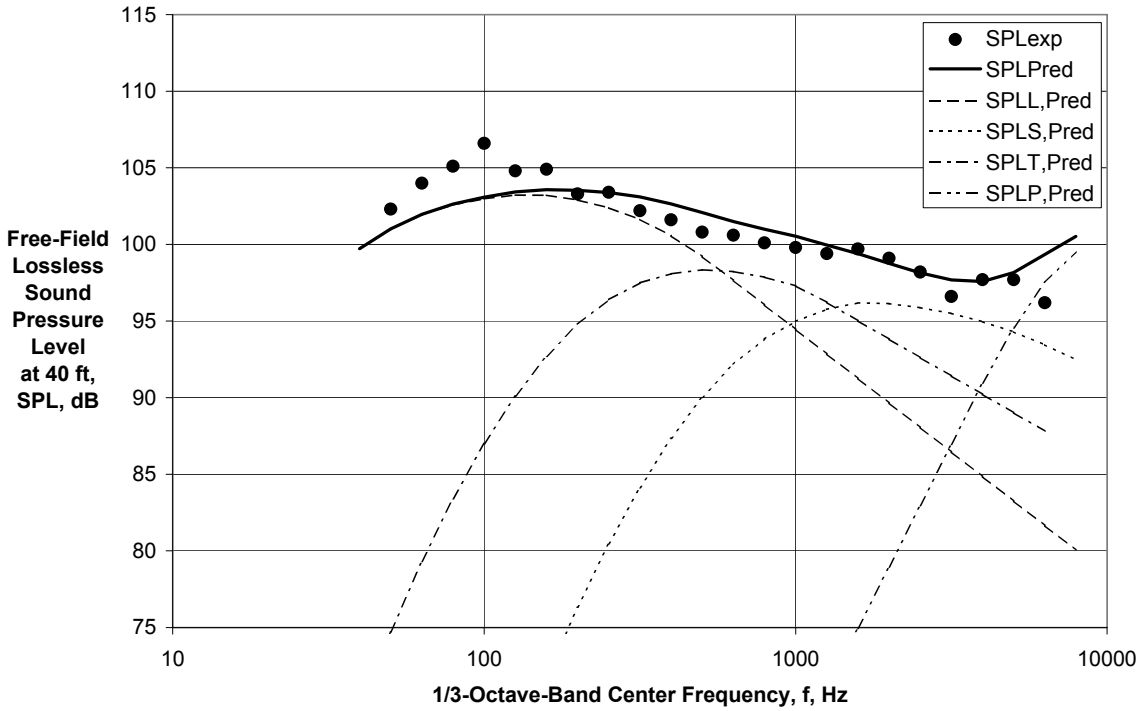

(b) Directivity Angle = 70 deg

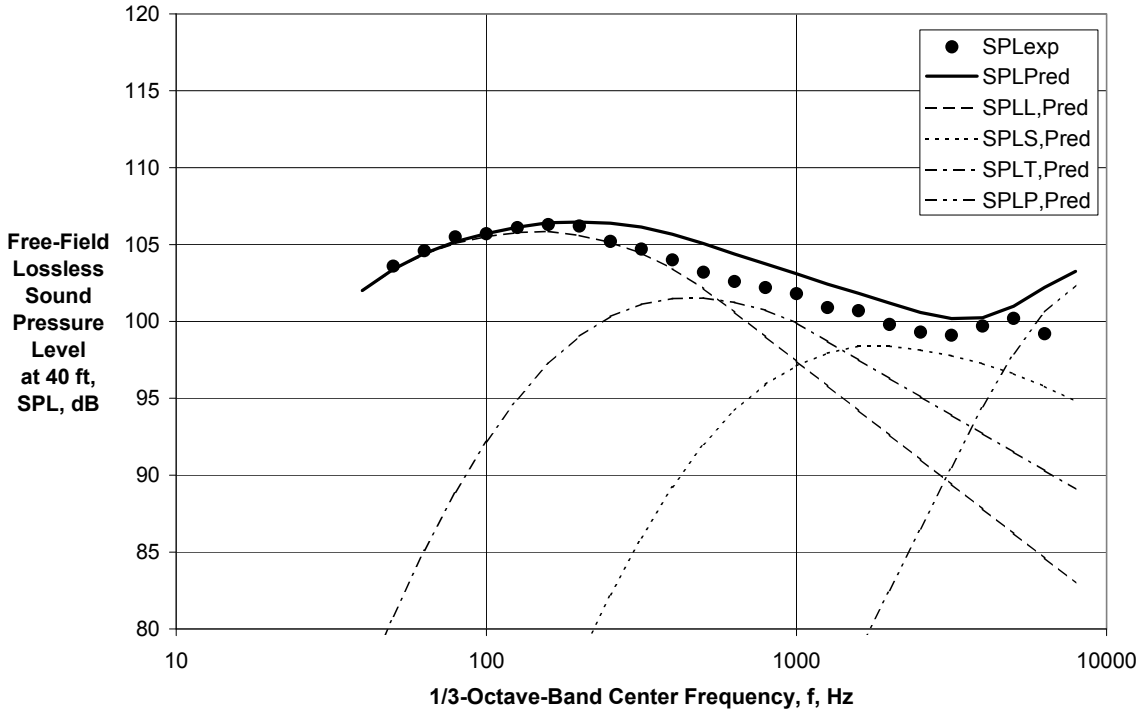

(c) Directivity Angle = 90 deg

Figure 24.—Continued.

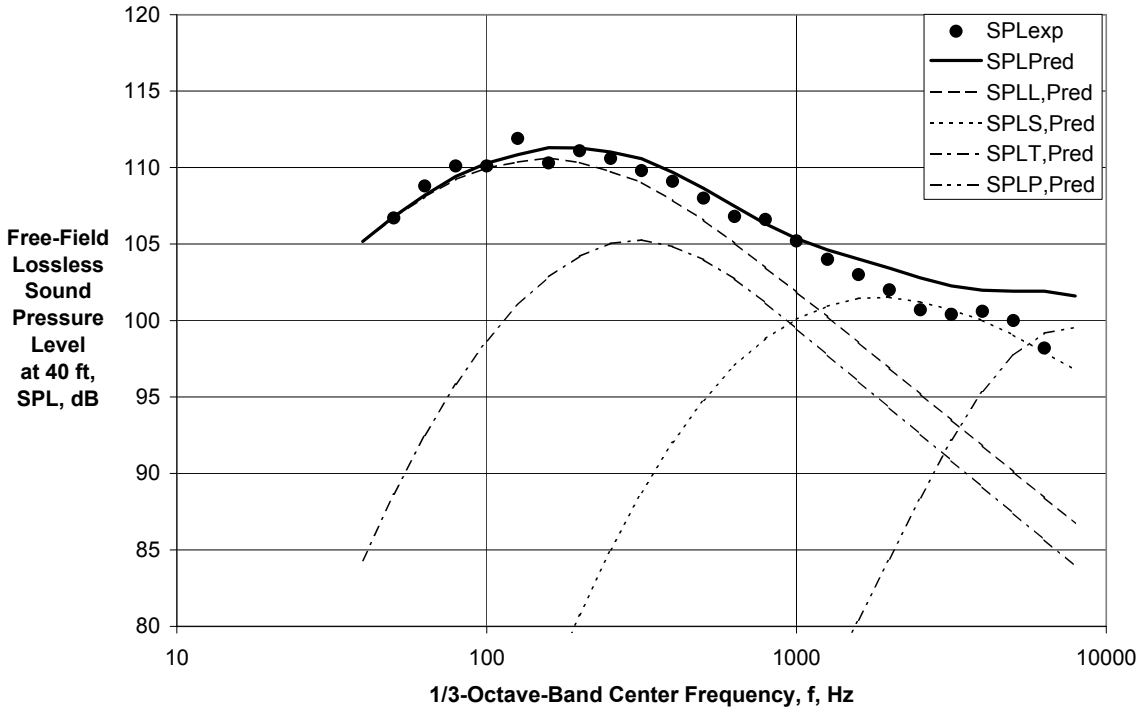

(d) Directivity Angle = 115 deg

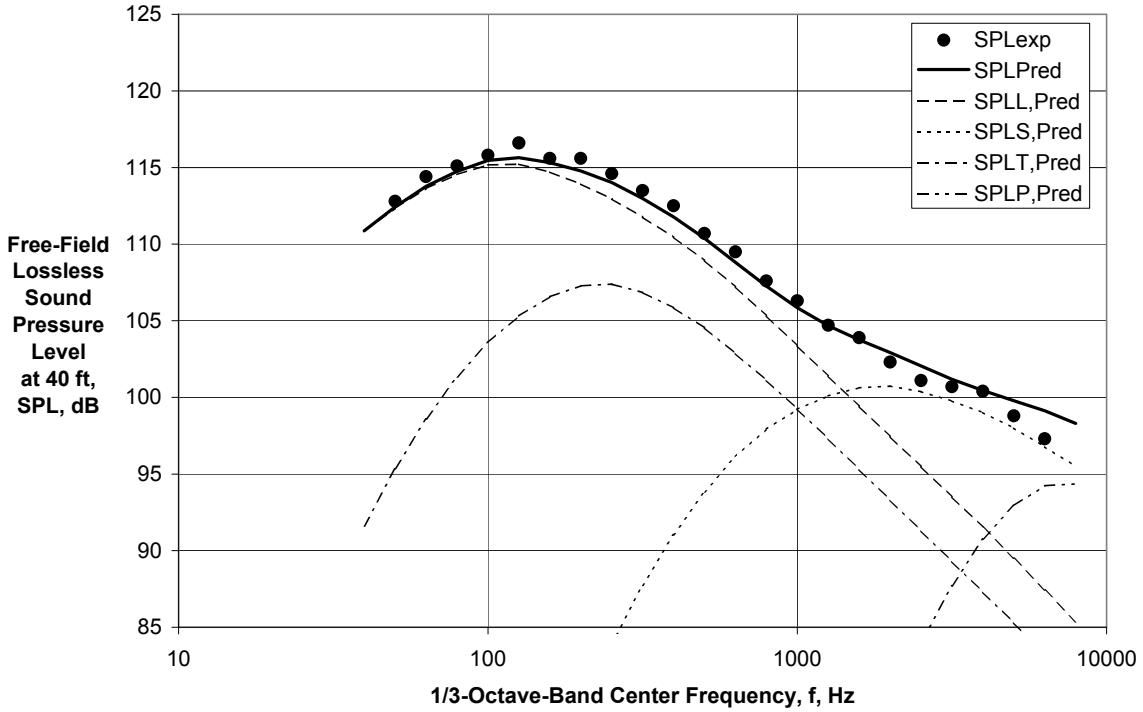

(e) Directivity Angle = 130 deg

Figure 24.—Continued.

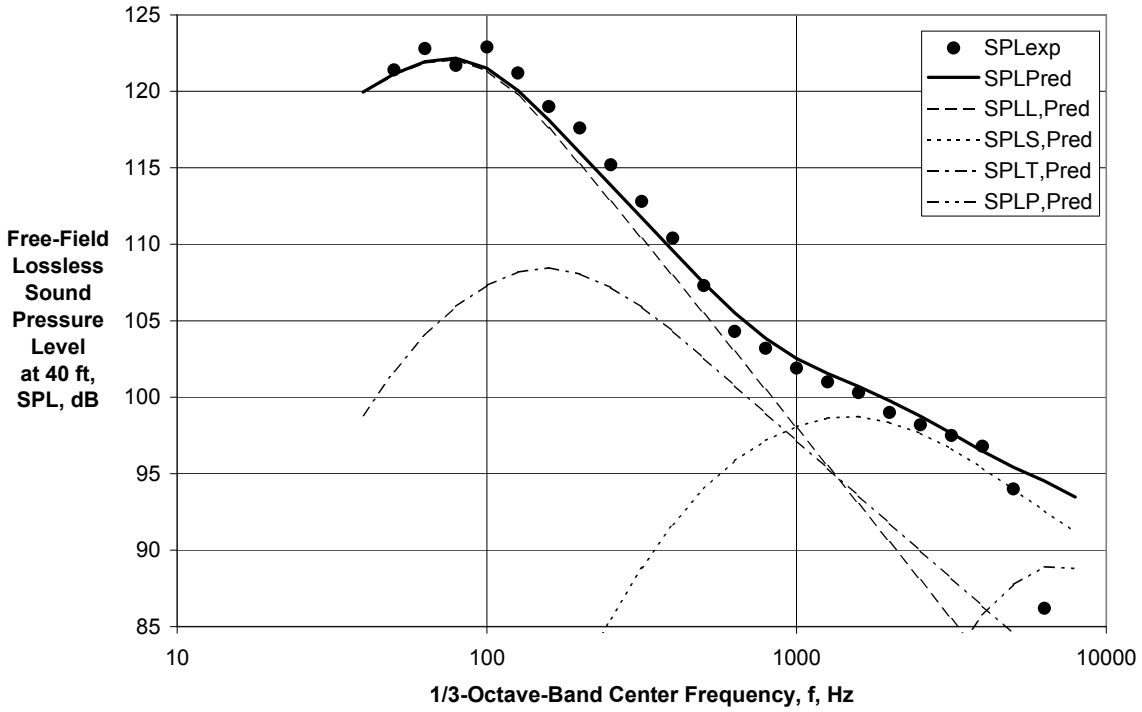

(f) Directivity Angle = 150 deg

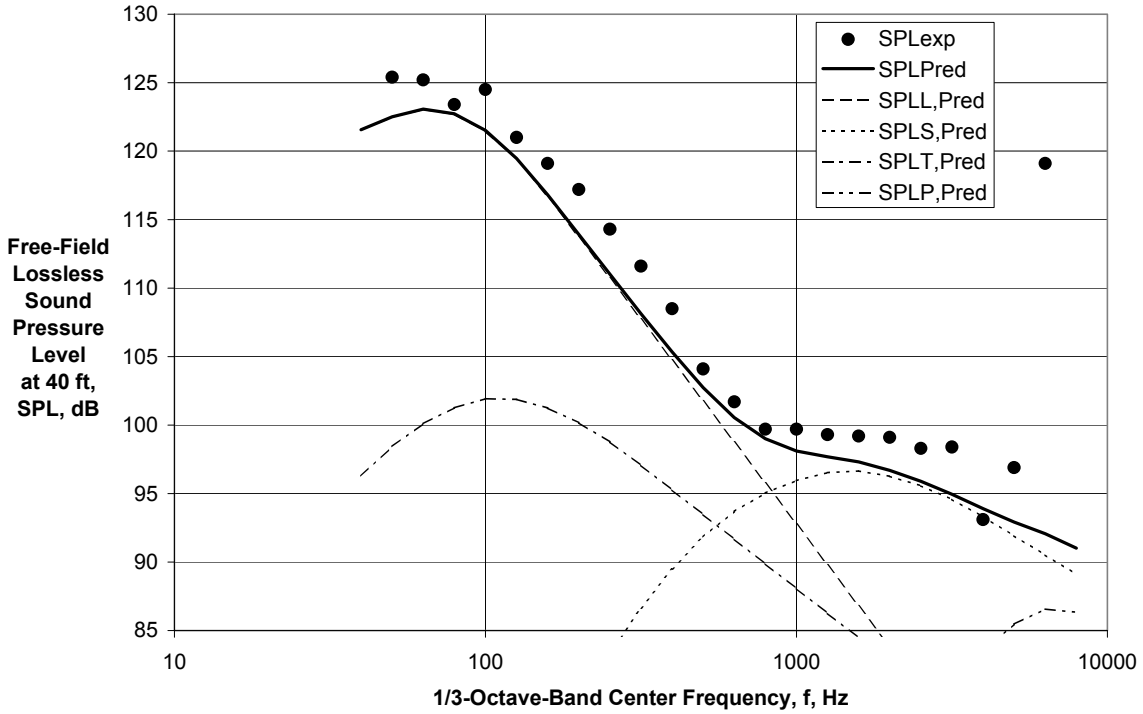

(g) Directivity Angle = 165 deg

Figure 24.—Concluded.

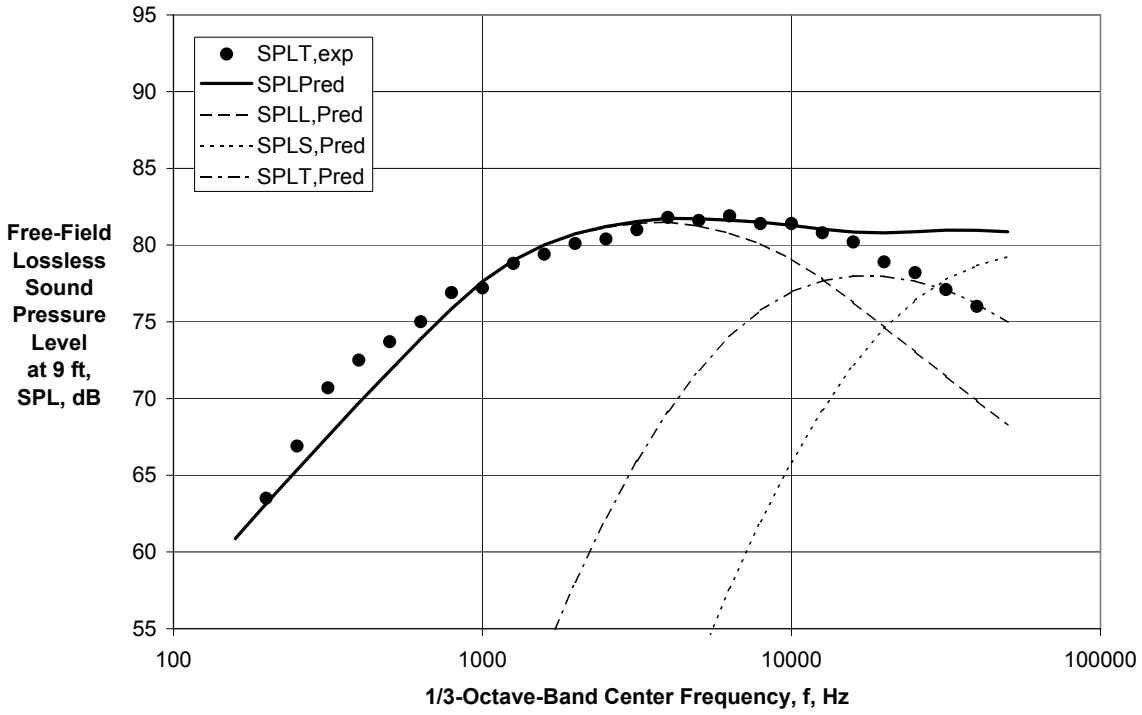

(a) Directivity Angle = 90 deg

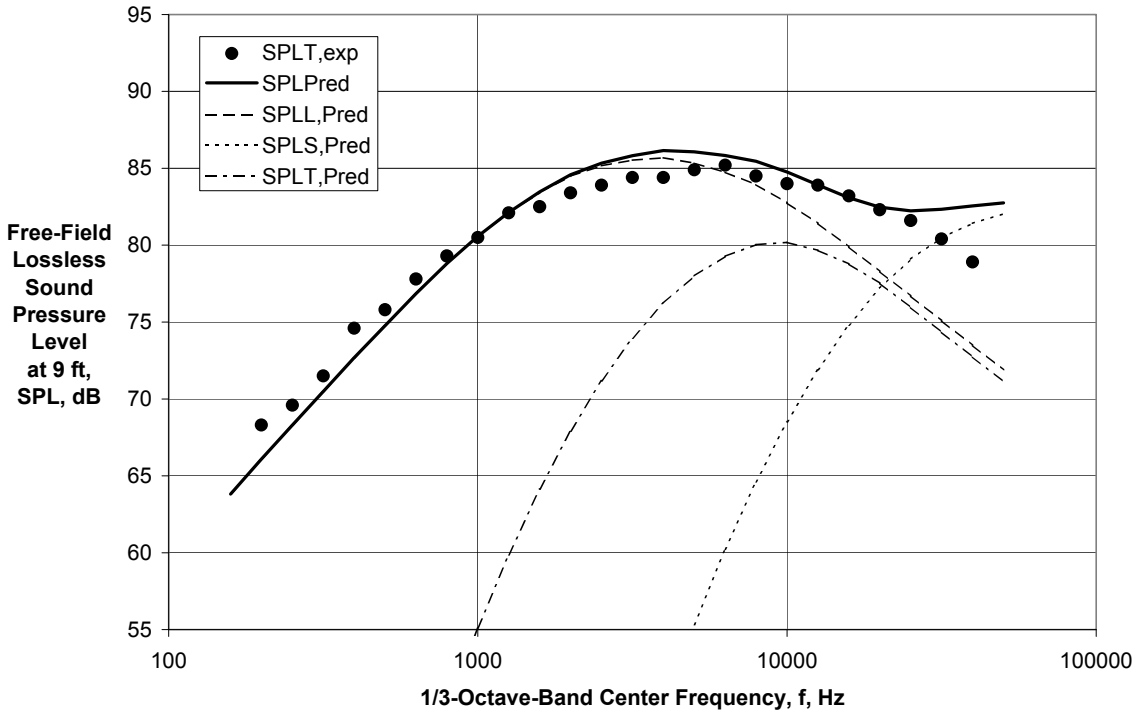

(b) Directivity Angle = 120 deg

Figure 25.—Comparison of Experimental and Predicted Spectra for Lockheed Georgia Conical Nozzle at V_j/c_{amb} = 0.740 and M_f = 0.036 (Pseudo-static).

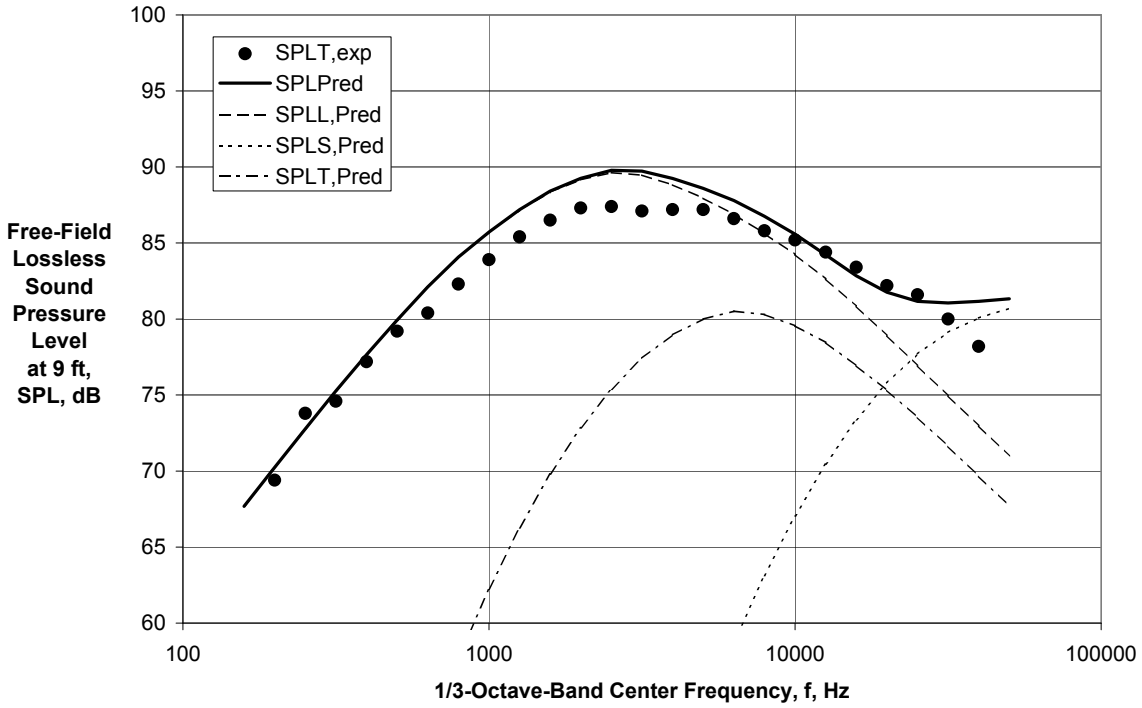

(c) Directivity Angle = 135 deg

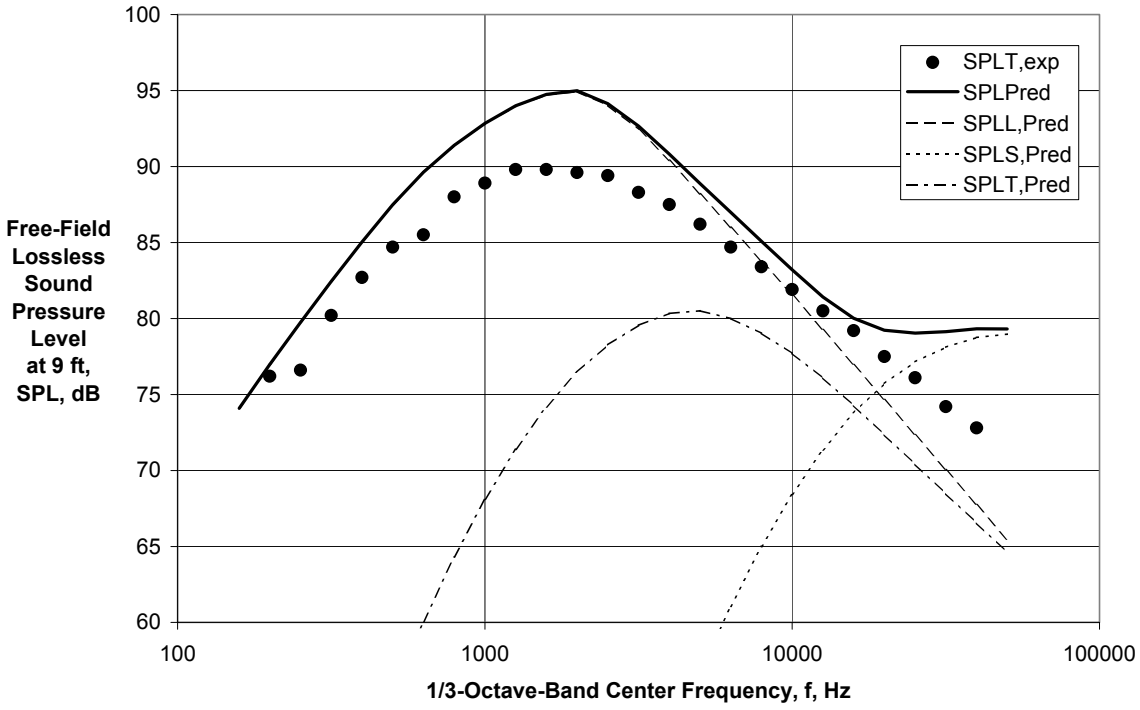

(d) Directivity Angle = 150 deg

Figure 25.—Concluded.

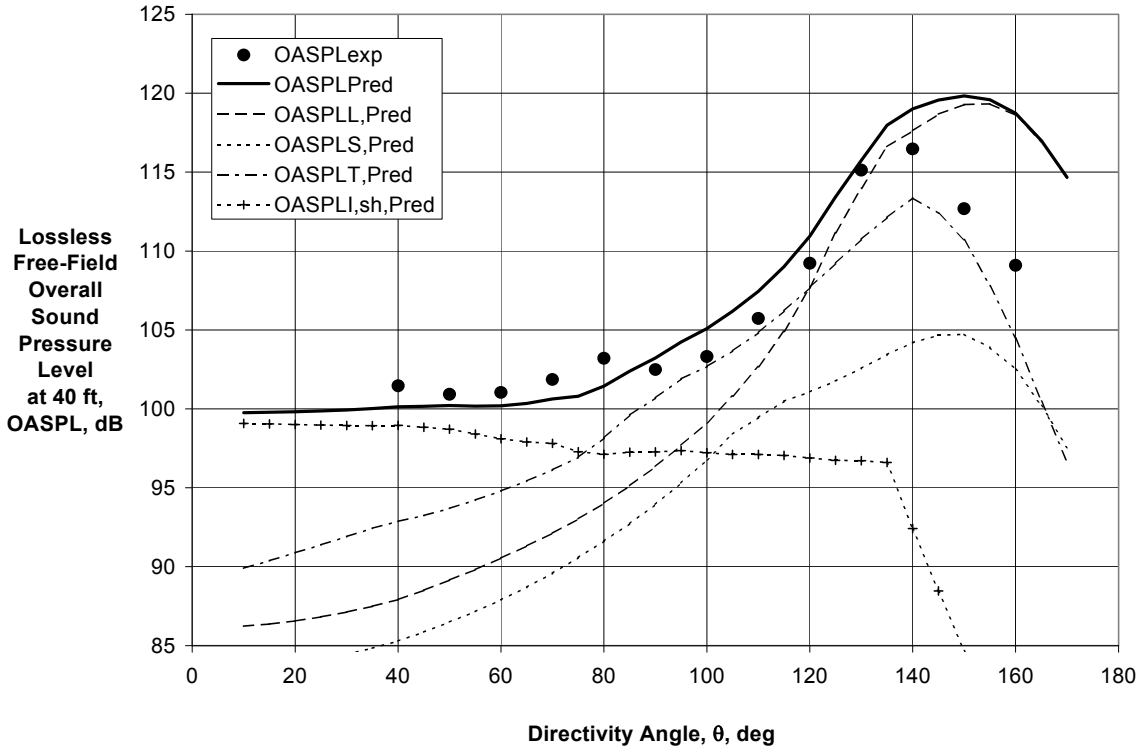

Figure 26.—Comparison of Experimental and Predicted Directivities for GE Conical Nozzle at V_j/c_{amb} = 2.11 and M_f = 0.00.

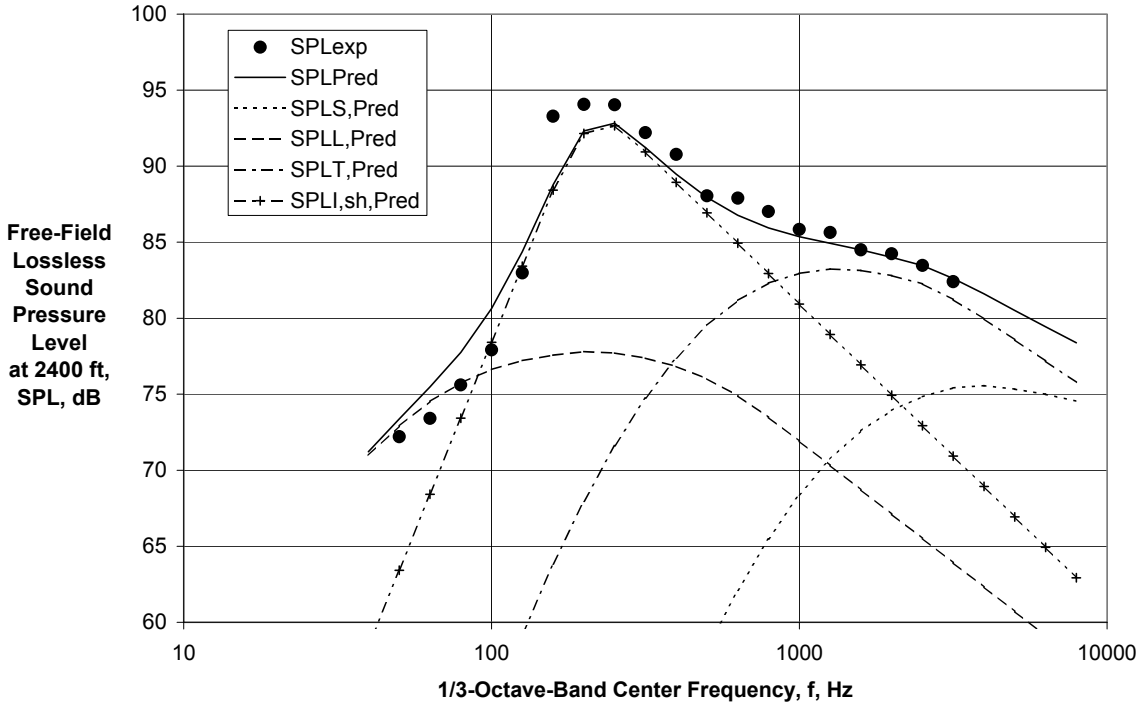

(a) Directivity Angle = 40 deg

Figure 27.—Comparison of Experimental and Predicted Spectra for GE Conical Nozzle at V_j/c_{amb} = 2.11 and M_f = 0.00.

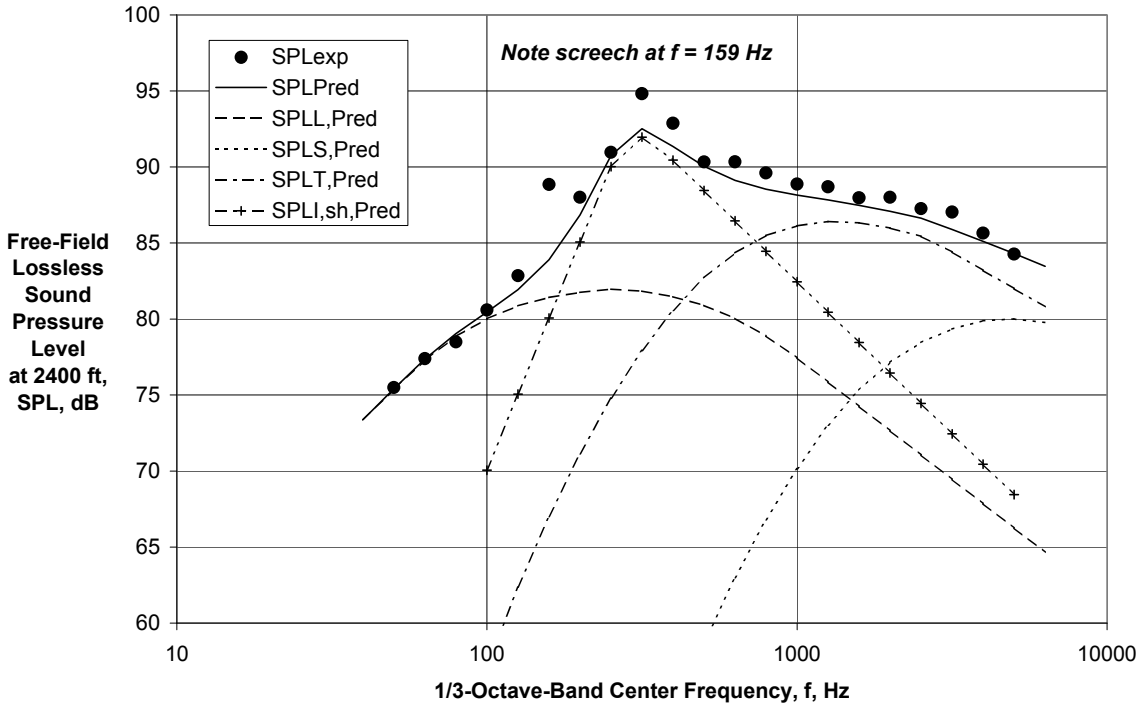

(b) Directivity Angle = 70 deg

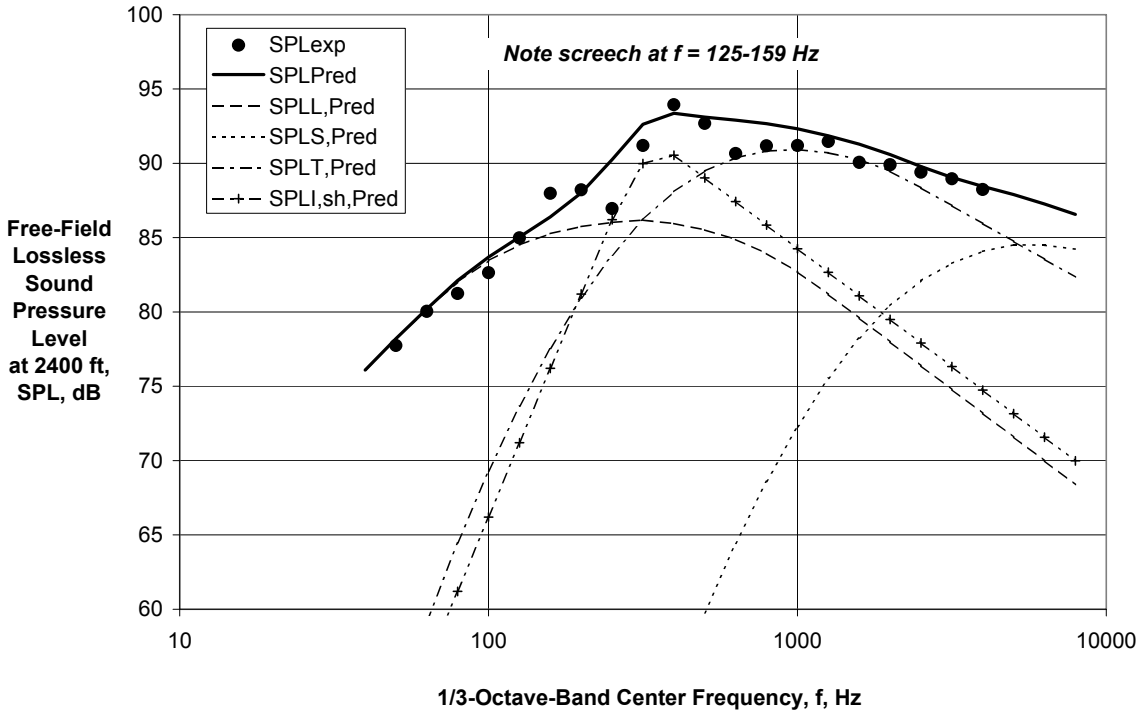

(c) Directivity Angle = 90 deg

Figure 27.—Continued.

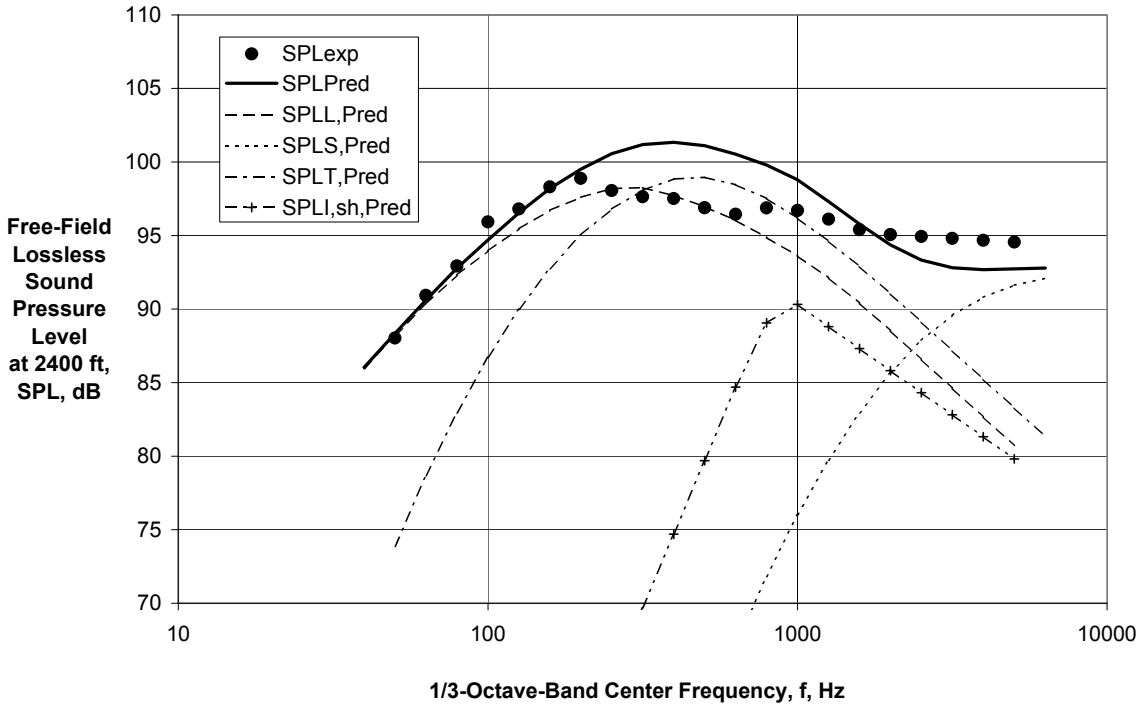

(d) Directivity Angle = 120 deg

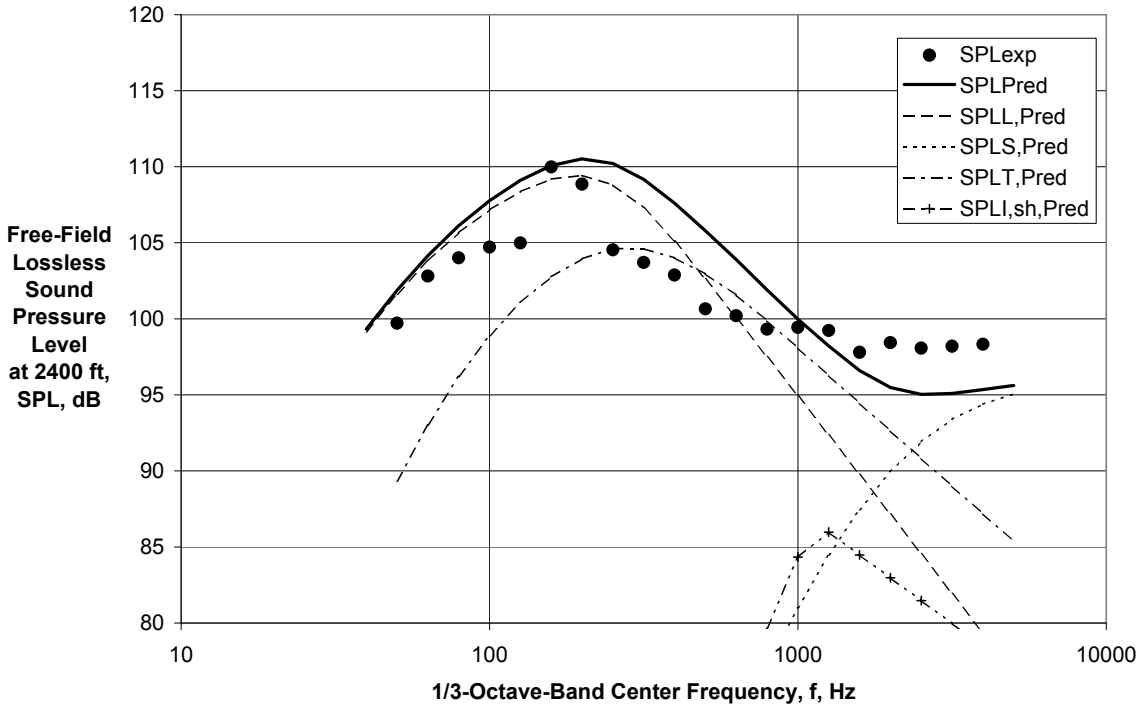

(e) Directivity Angle = 140 deg

Figure 27.—Continued.

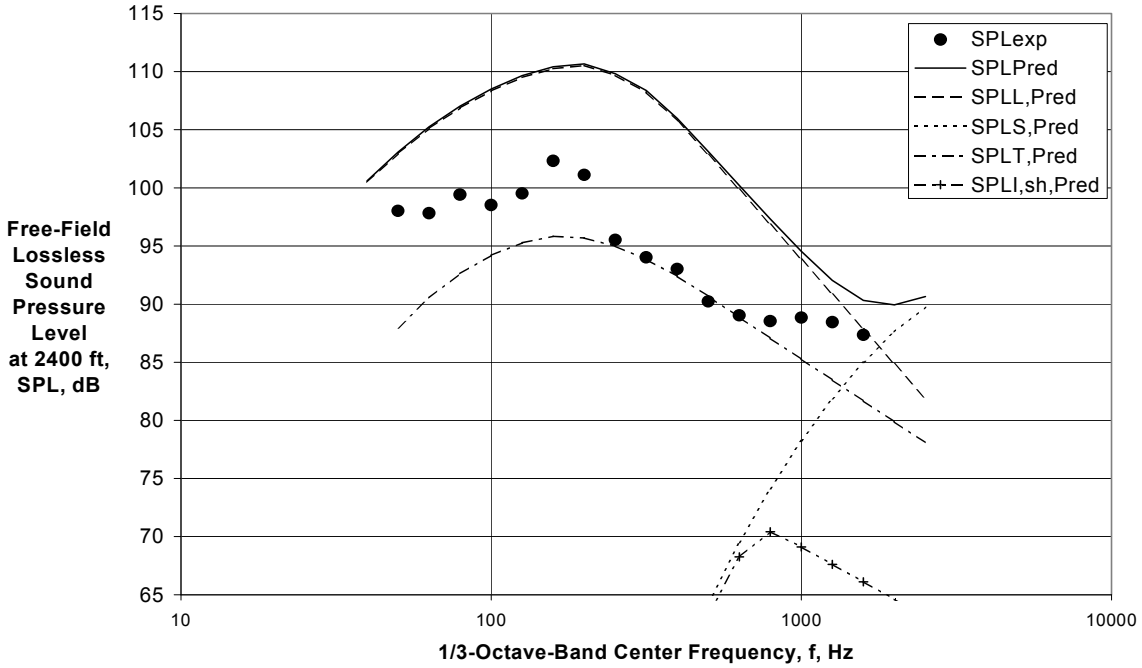

(f) Directivity Angle = 160 deg

Figure 27.—Concluded.

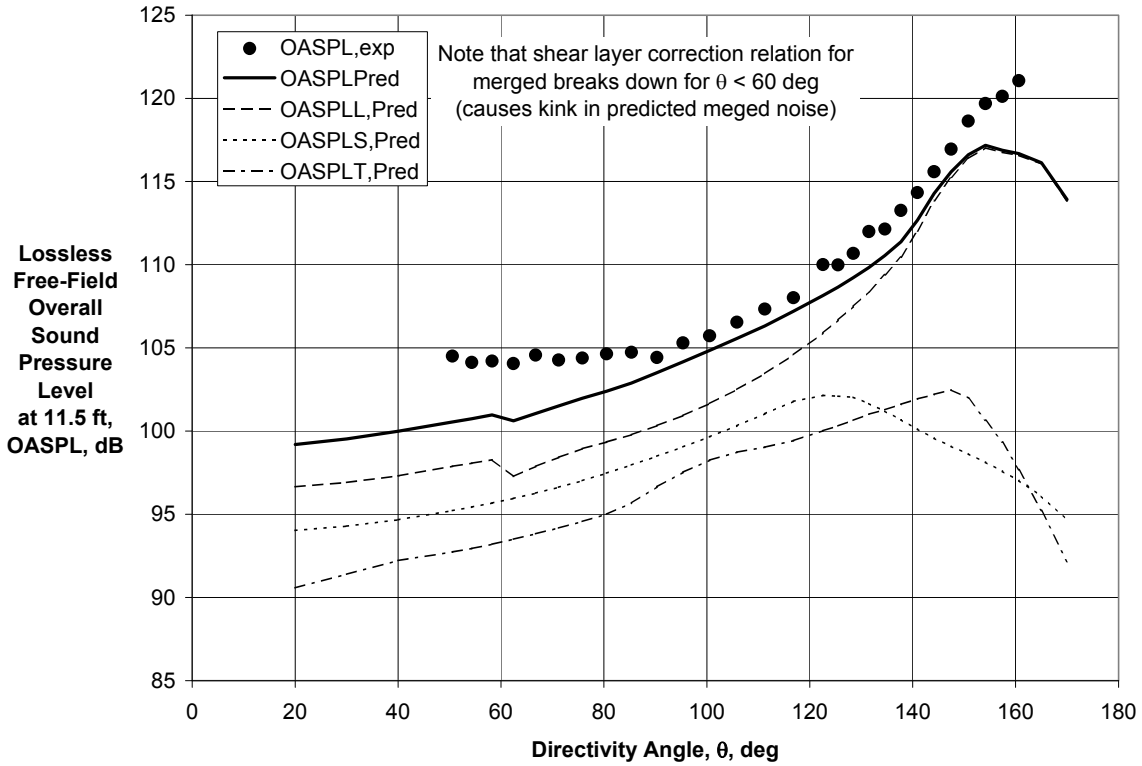

Figure 28.—Comparison of Experimental and Predicted Directivities for LaRC BPR ≅ 5 Internal Plug Nozzle with Core Petals at V_{mix}/c_{amb} = 0.954 and M_f = 0.201.

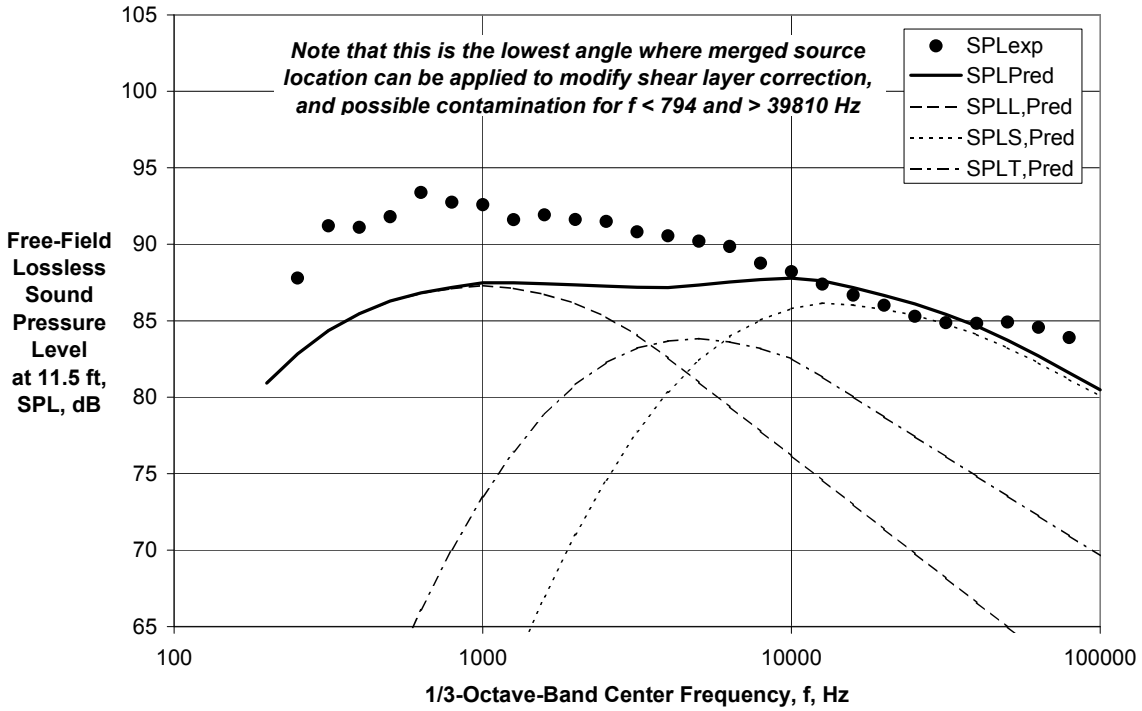

(a) Directivity Angle = 62 deg

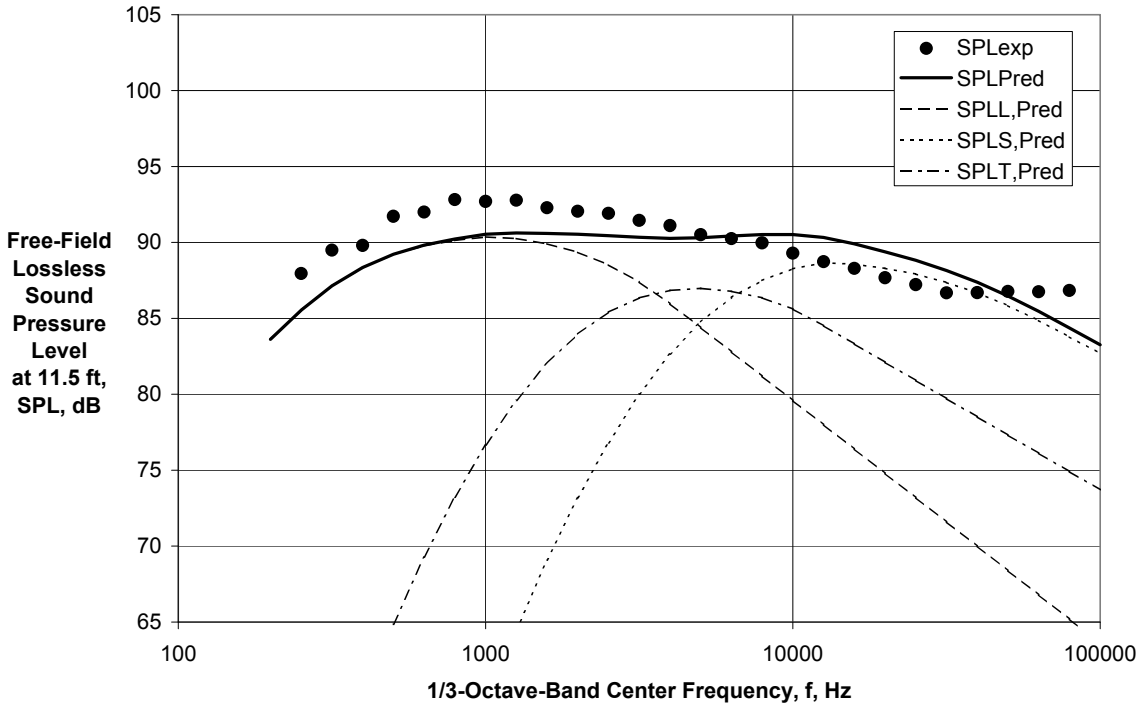

(b) Directivity Angle = 90 deg

Figure 29.—Comparison of Experimental and Predicted Spectra for LaRC BPR ≅ 5 Internal Plug Nozzle with Core Petals at V_{mix}/c_{amb} = 0.954 and M_f = 0.201.

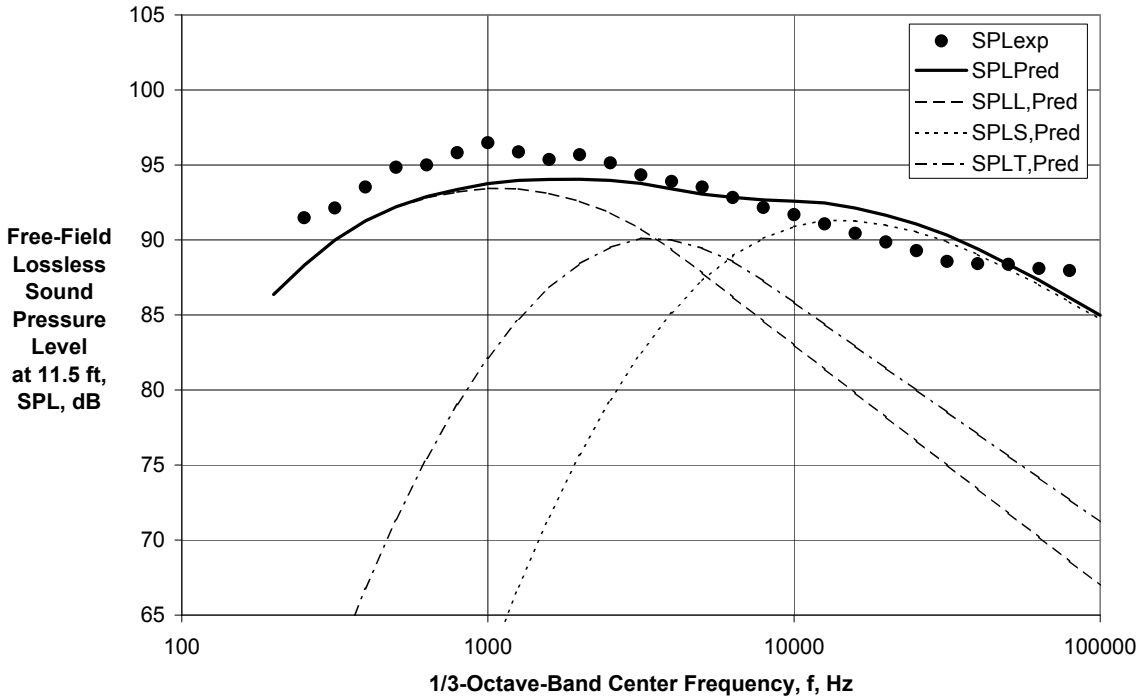

(c) Directivity Angle = 111 deg

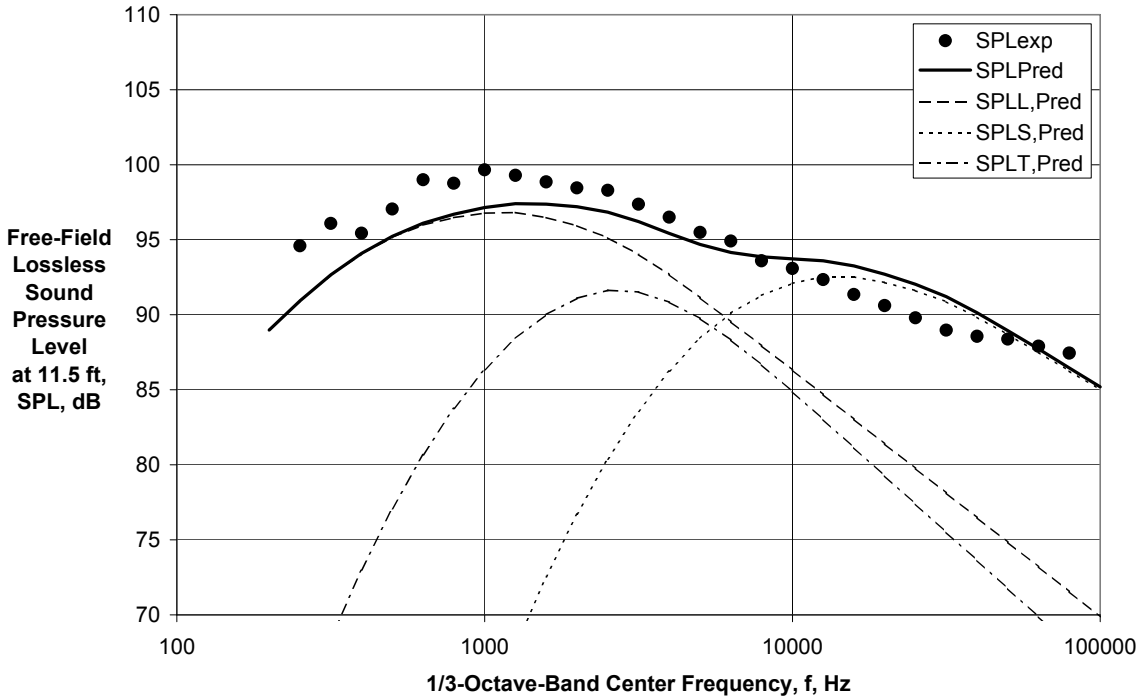

(d) Directivity Angle = 125 deg

Figure 29.—Continued.

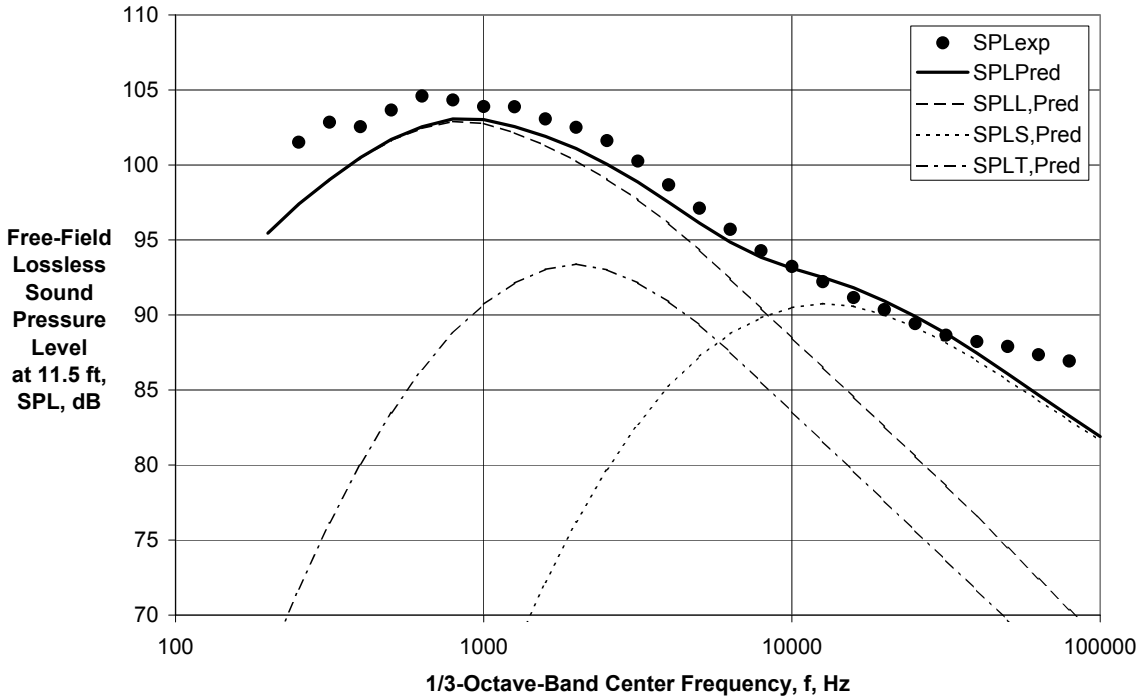

(e) Directivity Angle = 141 deg

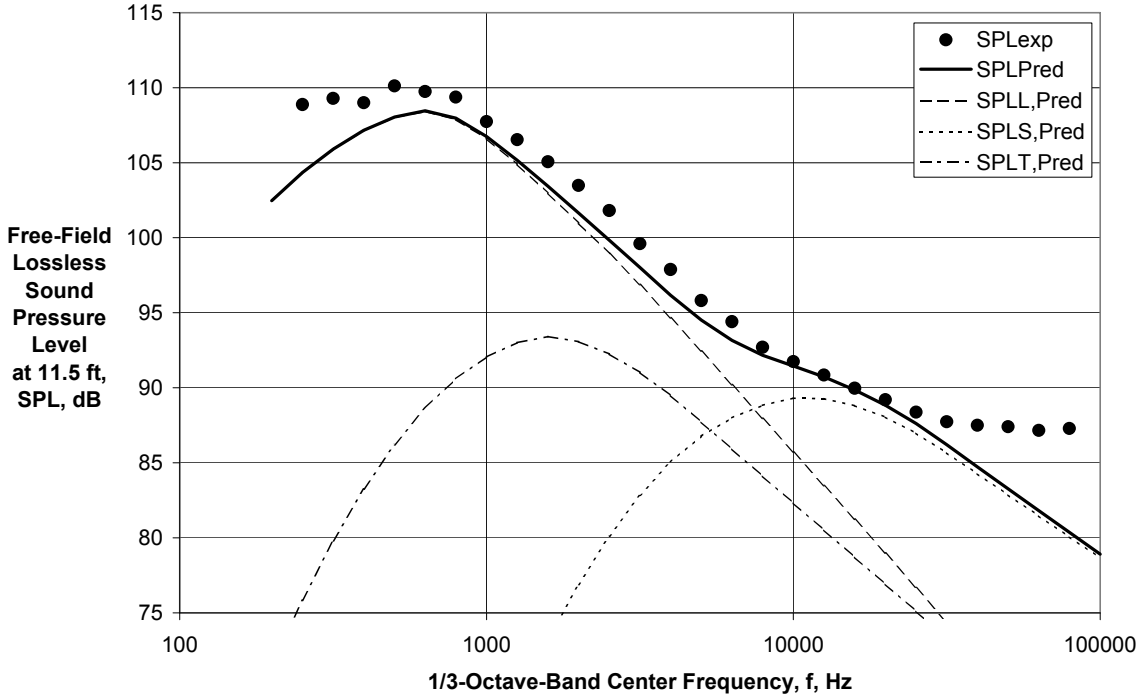

(f) Directivity Angle = 151 deg

Figure 29.—Continued.

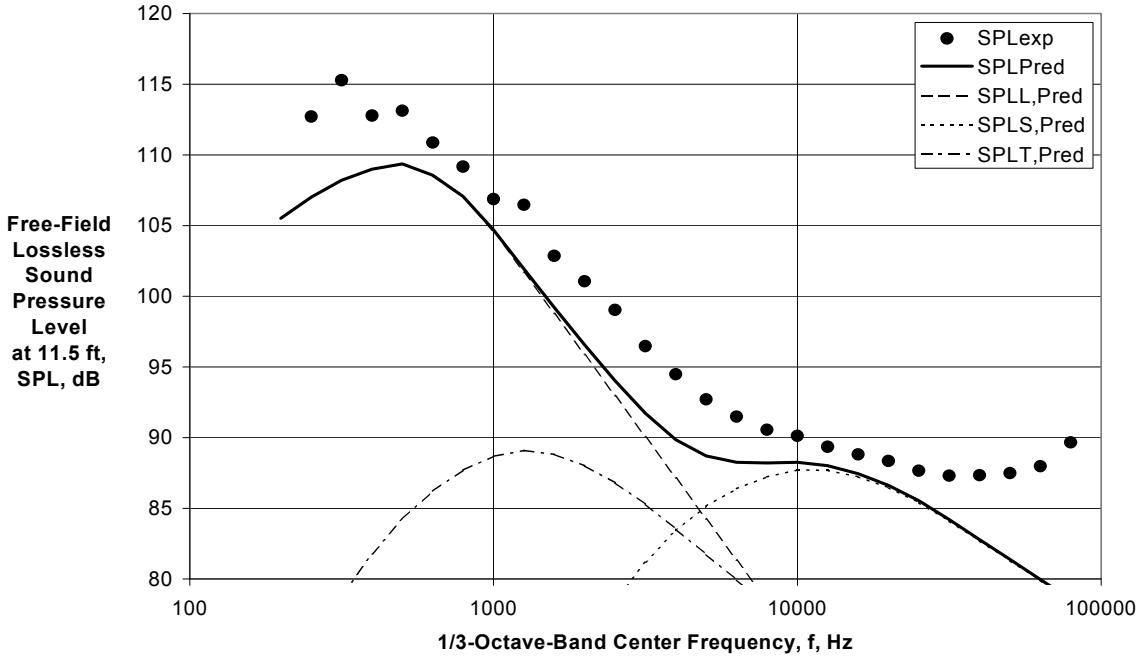

(g) Directivity Angle = 161 deg

Figure 29.—Concluded.

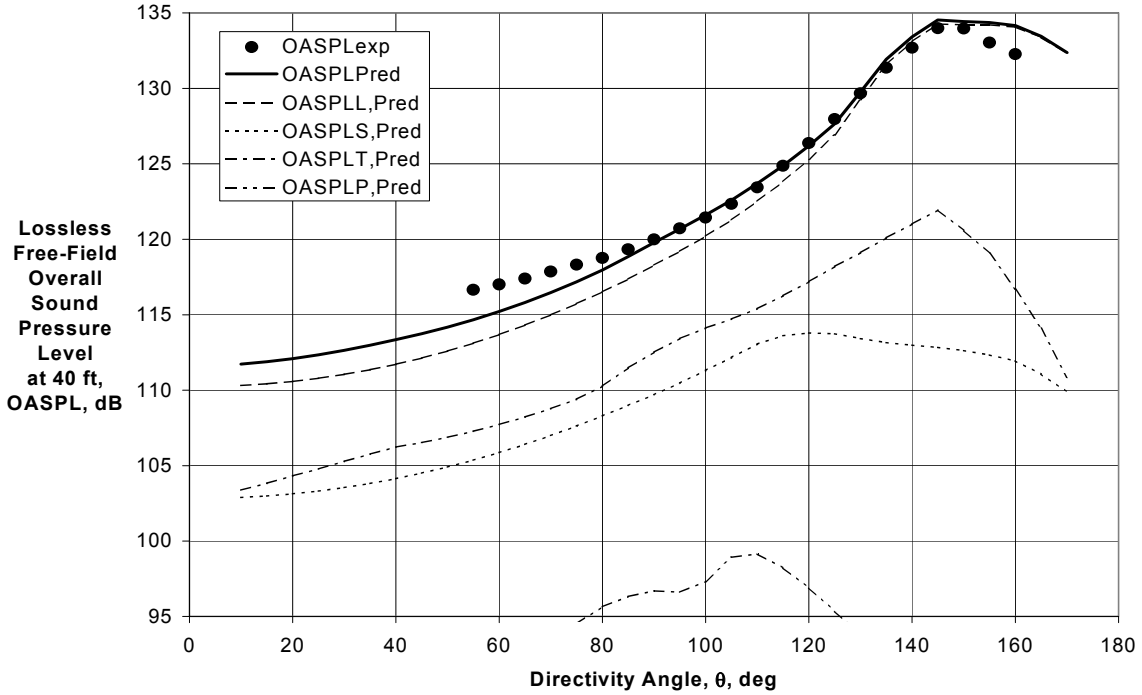

Figure 30.—Comparison of Experimental and Predicted Directivities for GE/GRC BPR ≅ 5 External Plug Nozzle with Core Chevrons; V_{mix}/c_{amb} = 1.047 and M_f = 0.00.

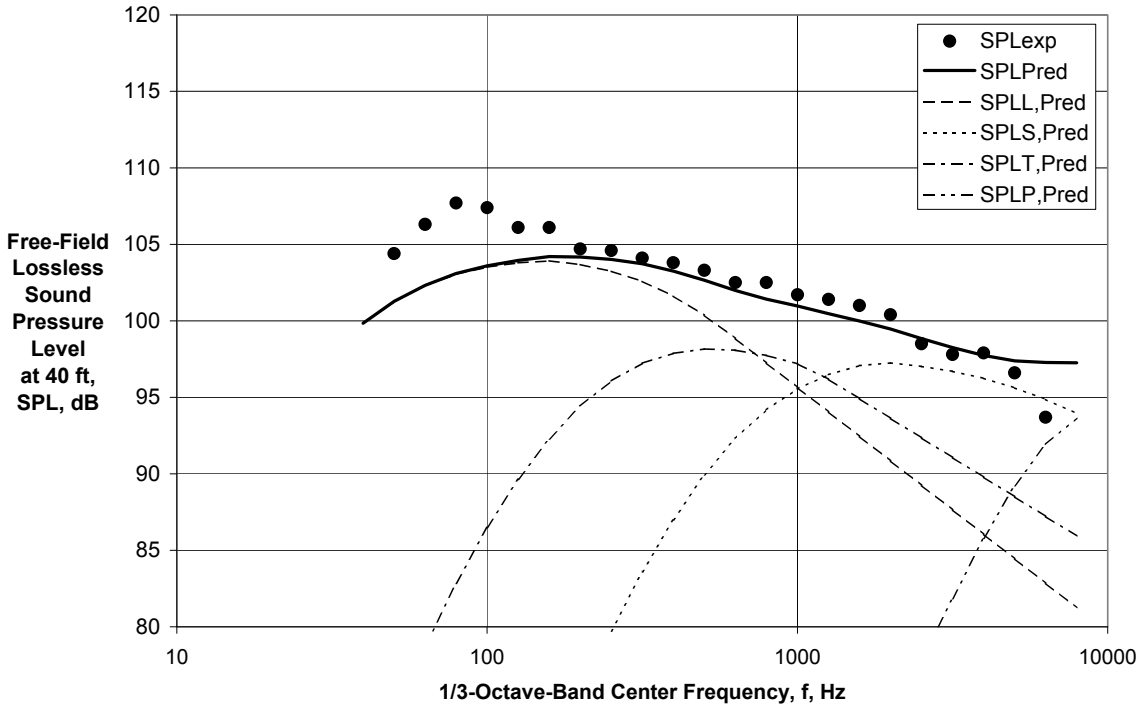

(a) Directivity Angle = 60 deg

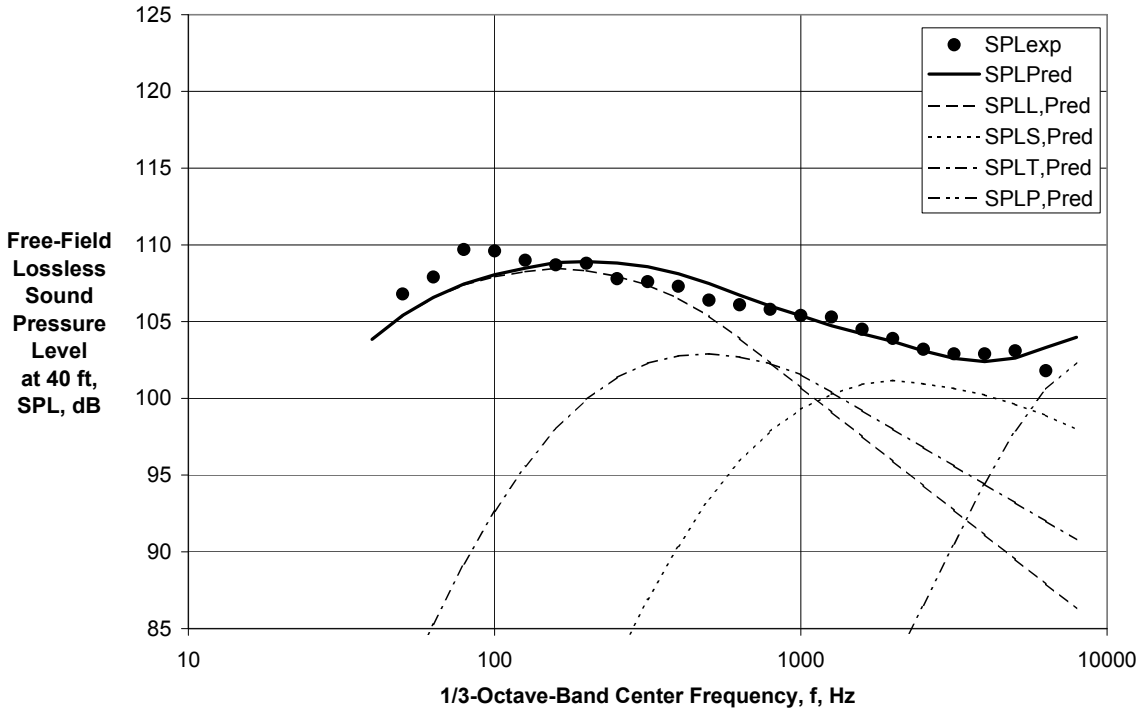

(b) Directivity Angle = 90 deg

Figure 31.—Comparison of Experimental and Predicted Spectra for GE/GRC BPR ≅ 5 External Plug Nozzle with Core Chevrons at V_{mix}/c_{amb} = 1.047 and M_f = 0.00.

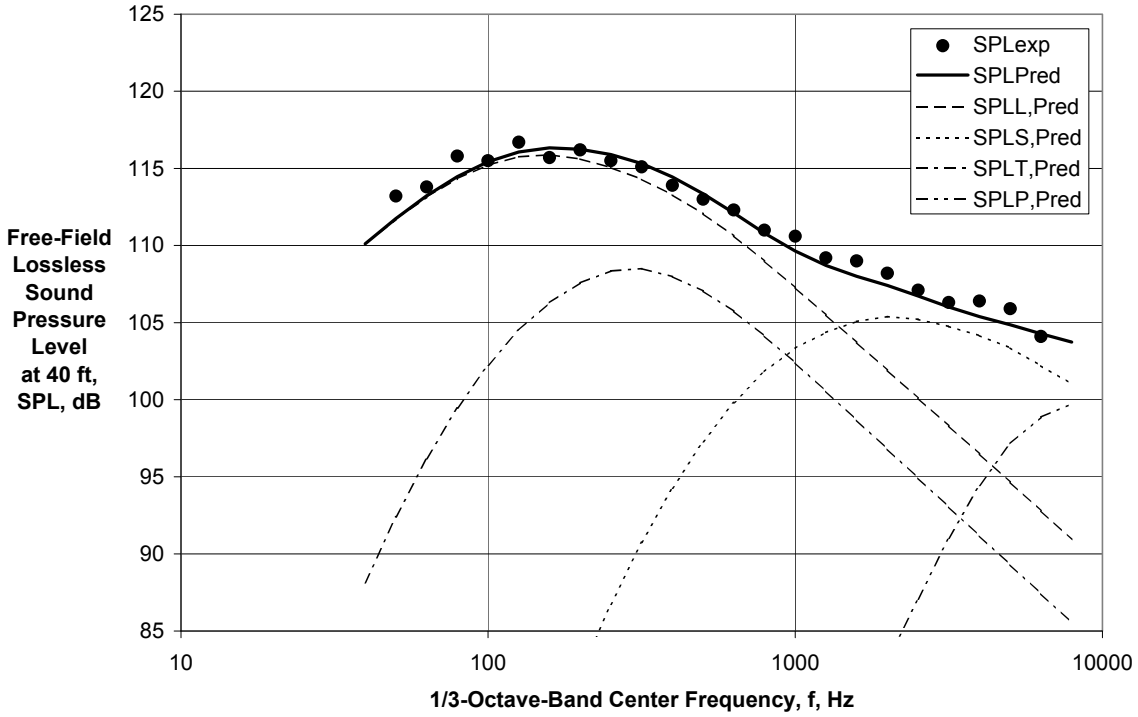

(c) Directivity Angle = 120 deg

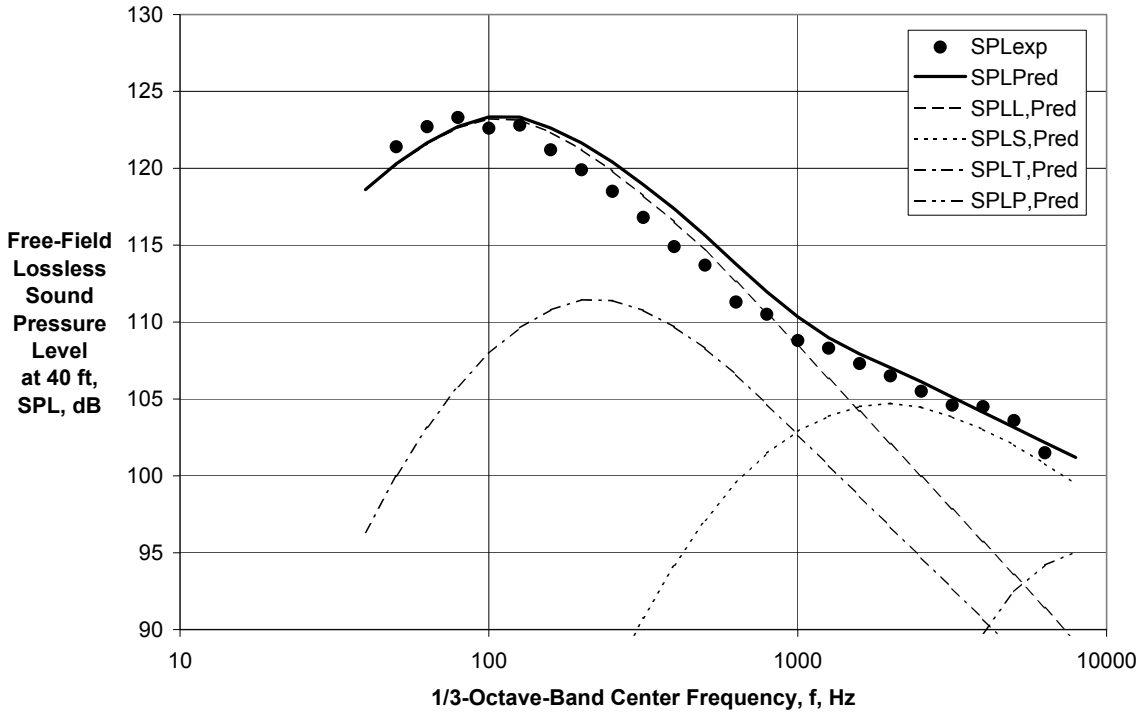

(d) Directivity Angle = 135 deg

Figure 31.—Continued.

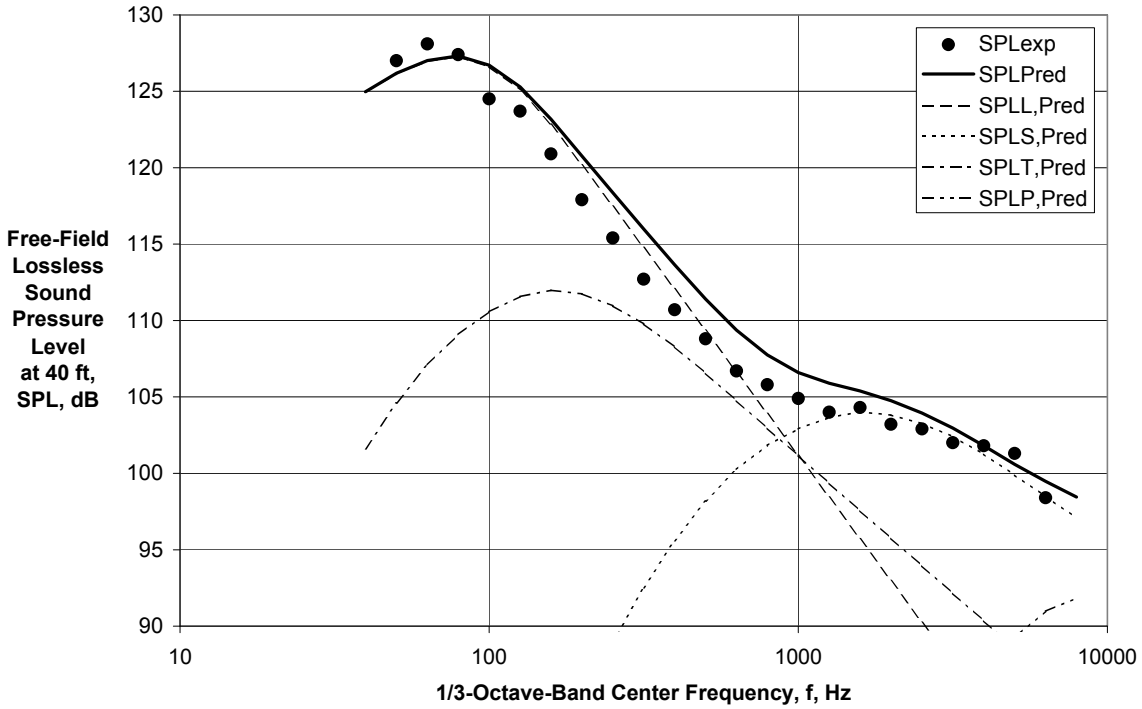

(e) Directivity Angle = 150 deg

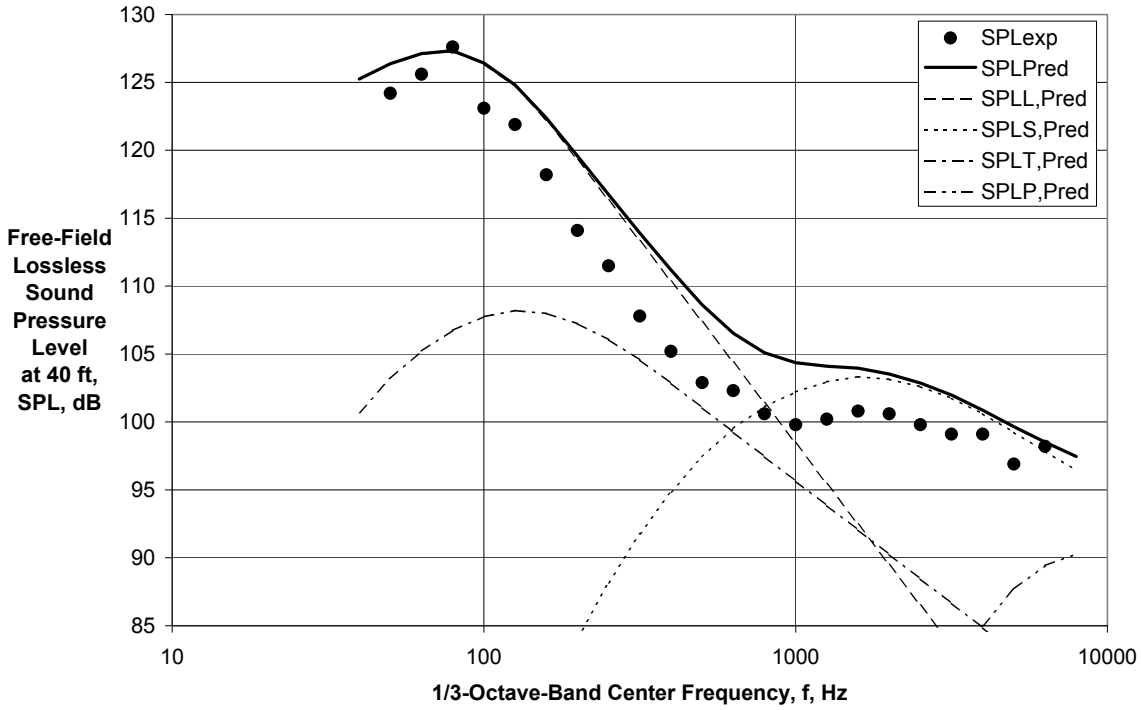

(f) Directivity Angle = 160 deg

Figure 31.—Concluded.

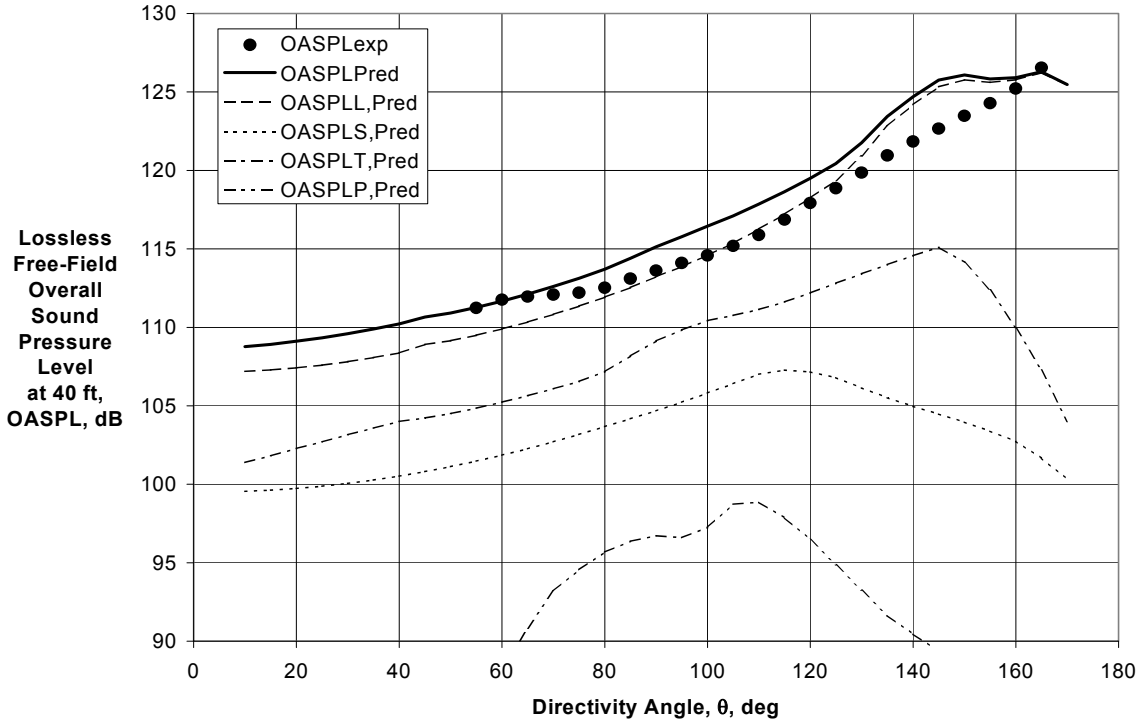

Figure 32.—Comparison of Experimental and Predicted Directivities for GE/GRC BPR ≅ 5 External Plug Nozzle with Core Chevrons; V_{mix}/c_{amb} = 1.049 and M_f = 0.28.

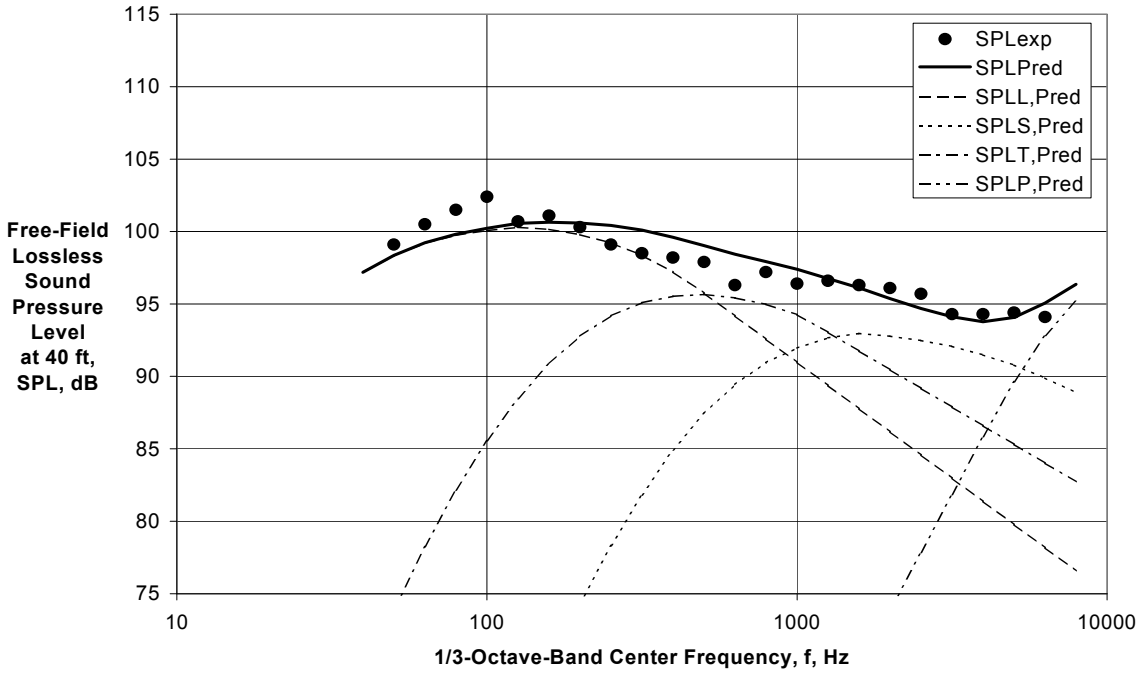

(a) Directivity Angle = 60 deg

Figure 33.—Comparison of Experimental and Predicted Spectra for GE/GRC BPR ≅ 5 External Plug Nozzle with Core Chevrons at V_{mix}/c_{amb} = 1.049 and M_f = 0.28.

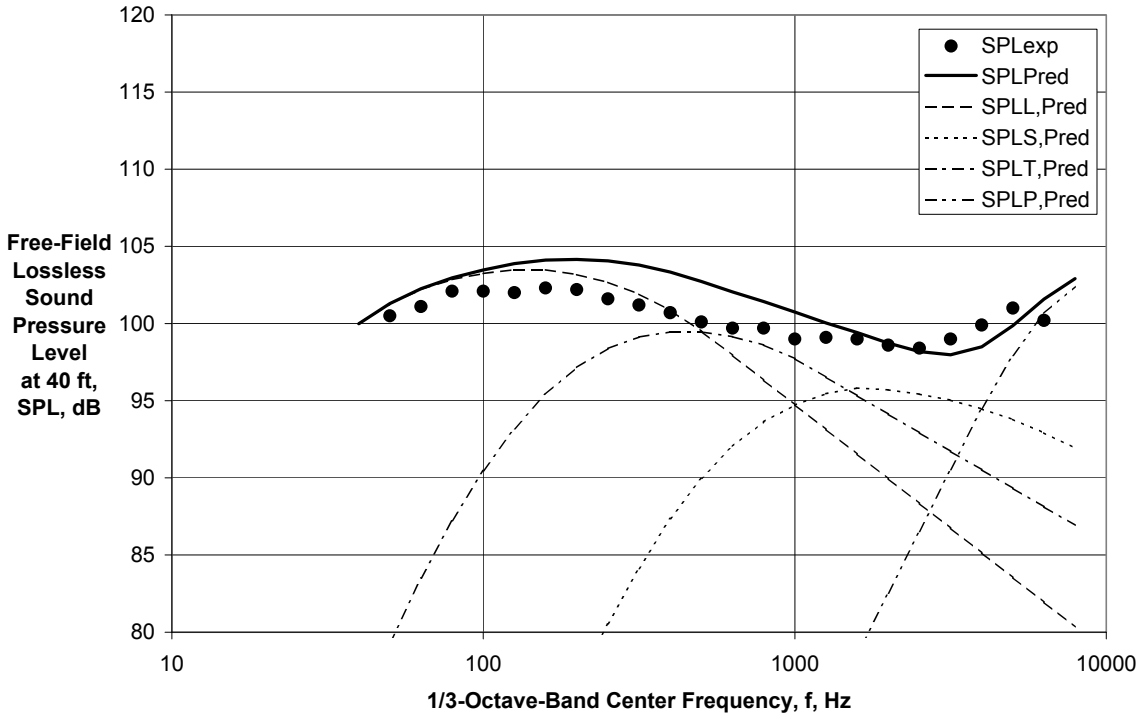

(b) Directivity Angle = 90 deg

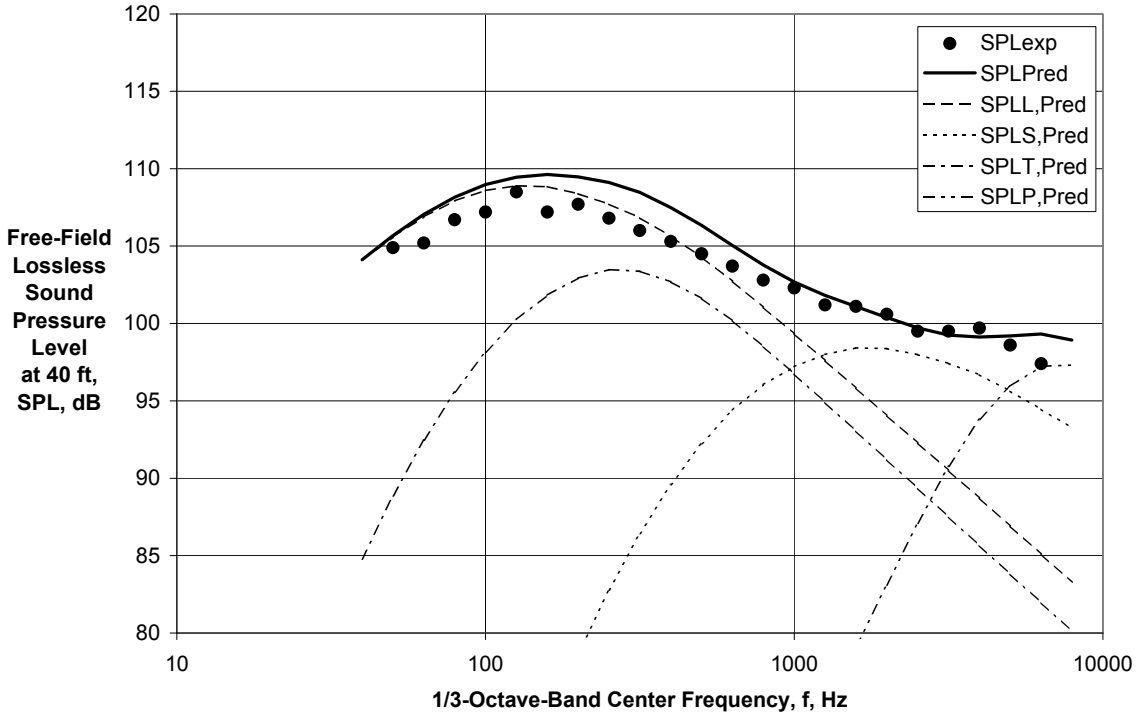

(c) Directivity Angle = 120 deg

Figure 33.—Continued.

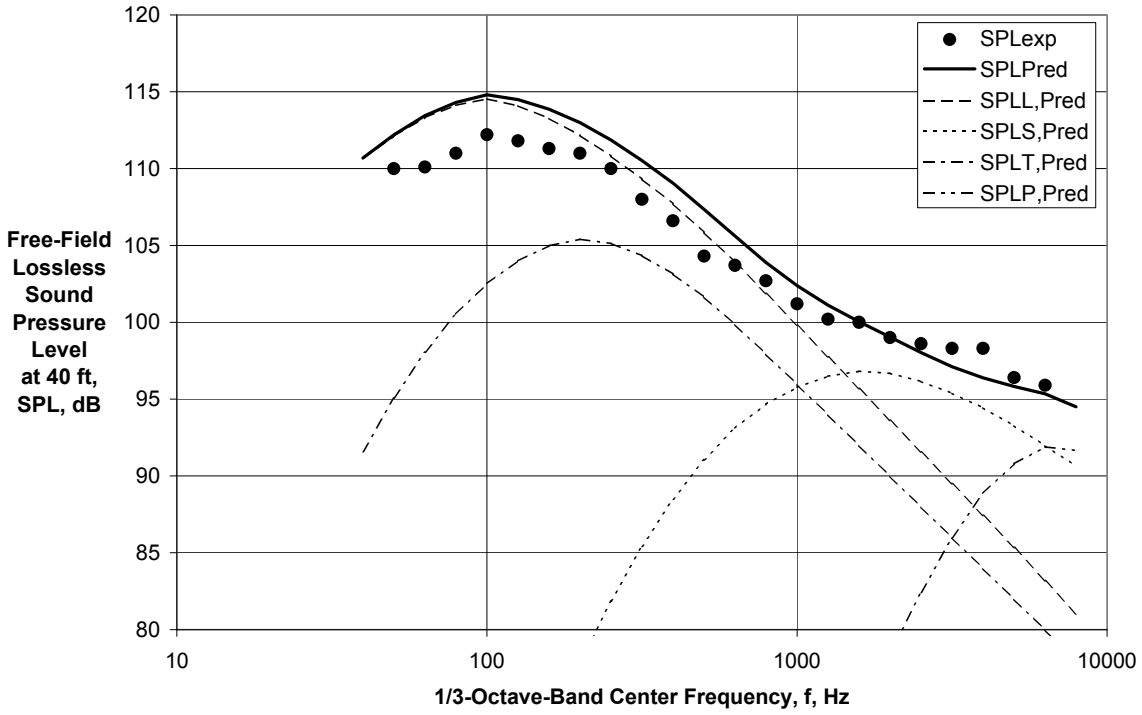

(d) Directivity Angle = 135 deg

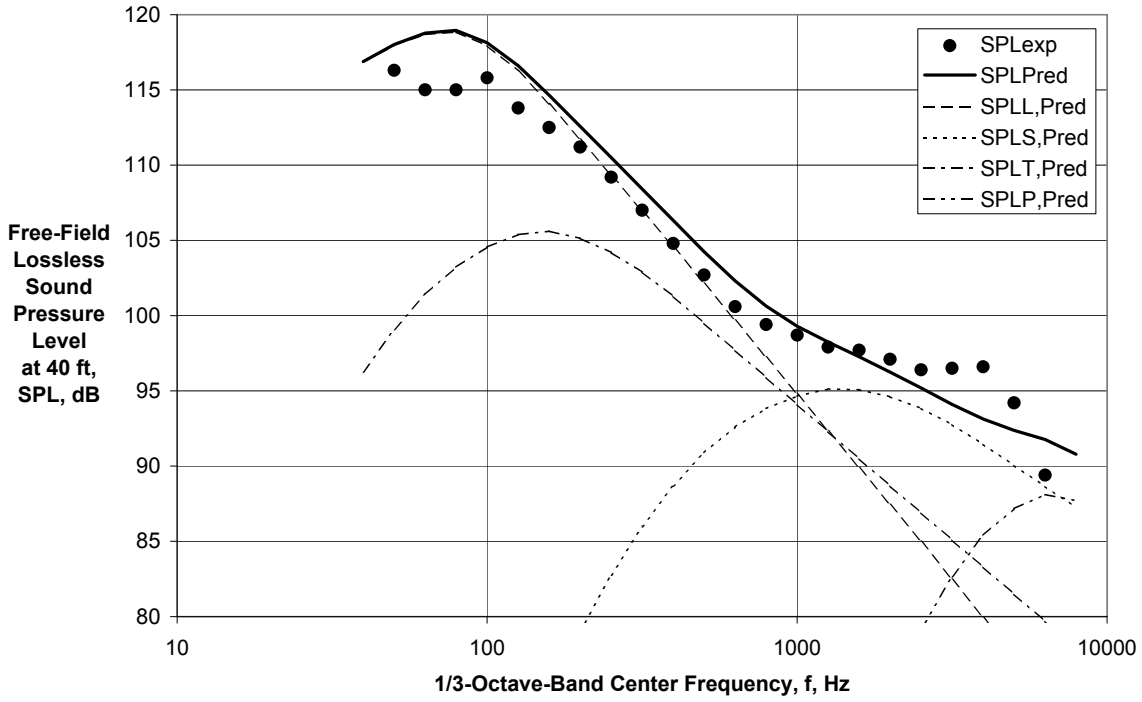

(e) Directivity Angle = 150 deg

Figure 33.—Continued.

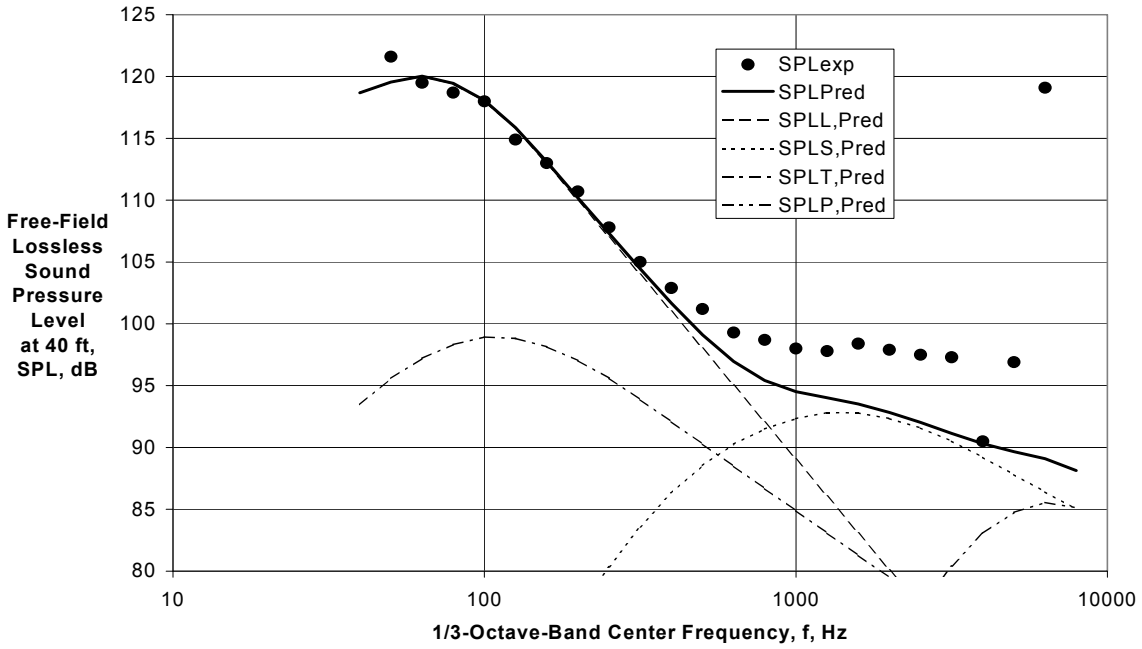

(f) Directivity Angle = 165 deg

Figure 33.—Concluded.

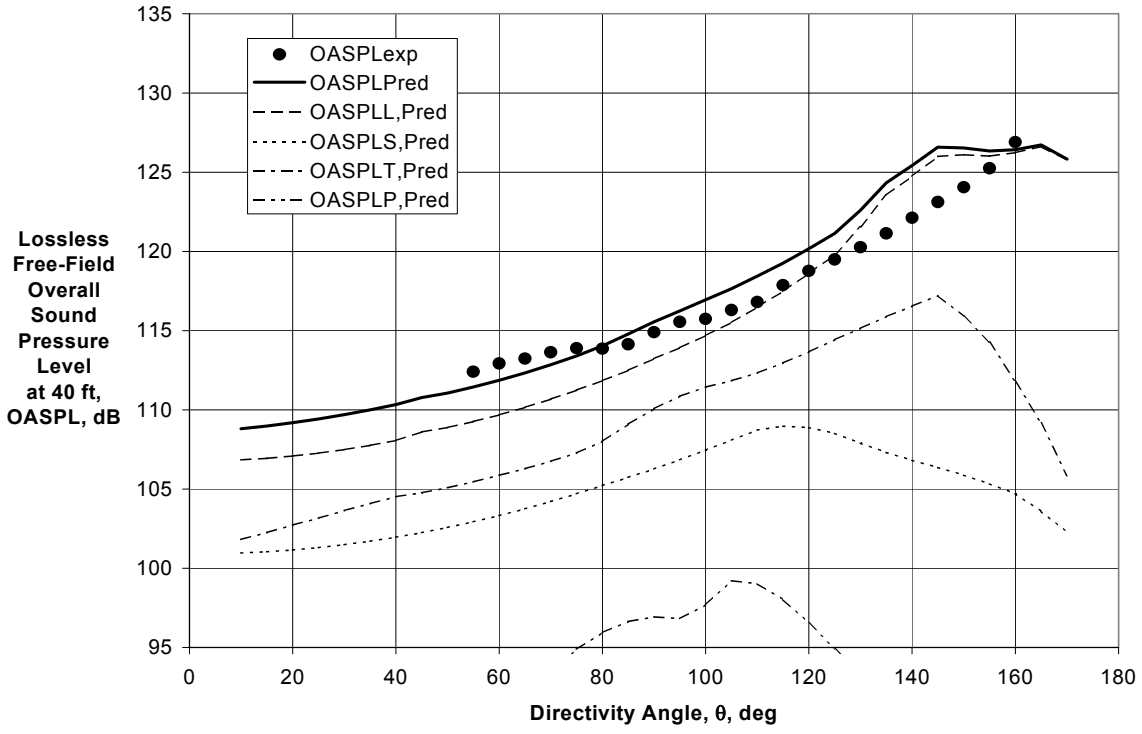

Figure 34.—Comparison of Experimental and Predicted Directivities for GE/GRC BPR ≅ 5 External Plug Nozzle with Core and Fan Chevrons at V_{mix}/c_{amb} = 1.087 and M_f = 0.28.

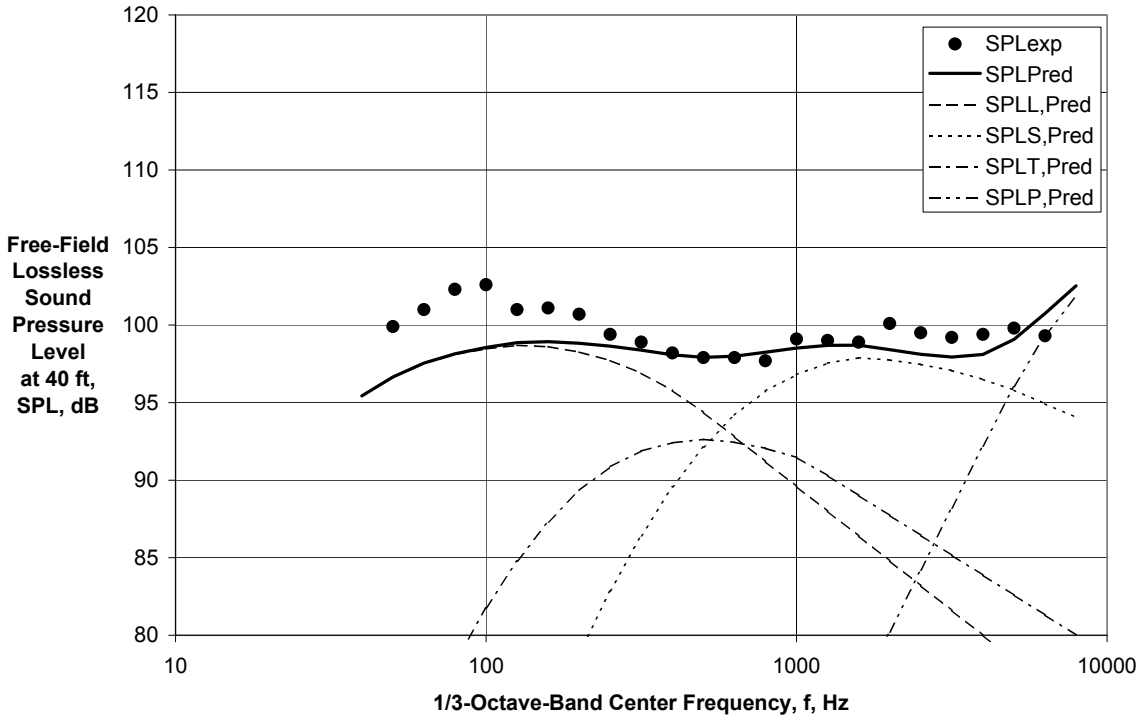

(a) Directivity Angle = 60 deg

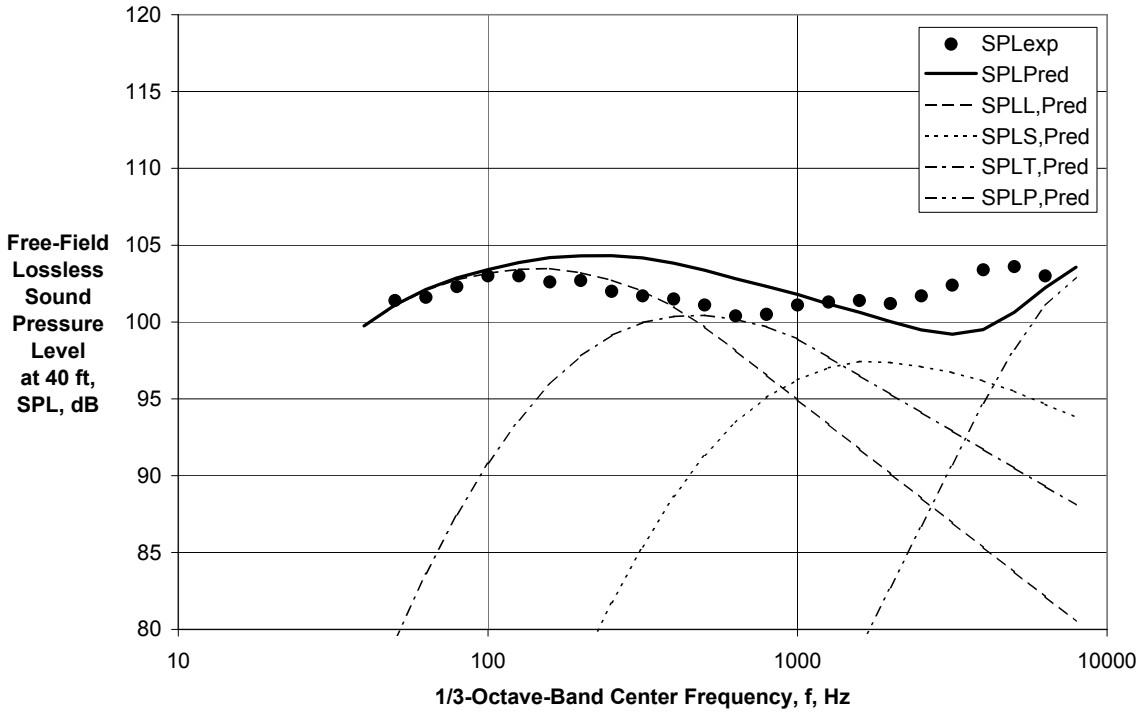

(b) Directivity Angle = 90 deg

Figure 35.—Comparison of Experimental and Predicted Spectra for GE/GRC BPR ≅ 5 External Plug Nozzle with Core and Fan Chevrons at V_{mix}/c_{amb} = 1.087 and M_f = 0.28.

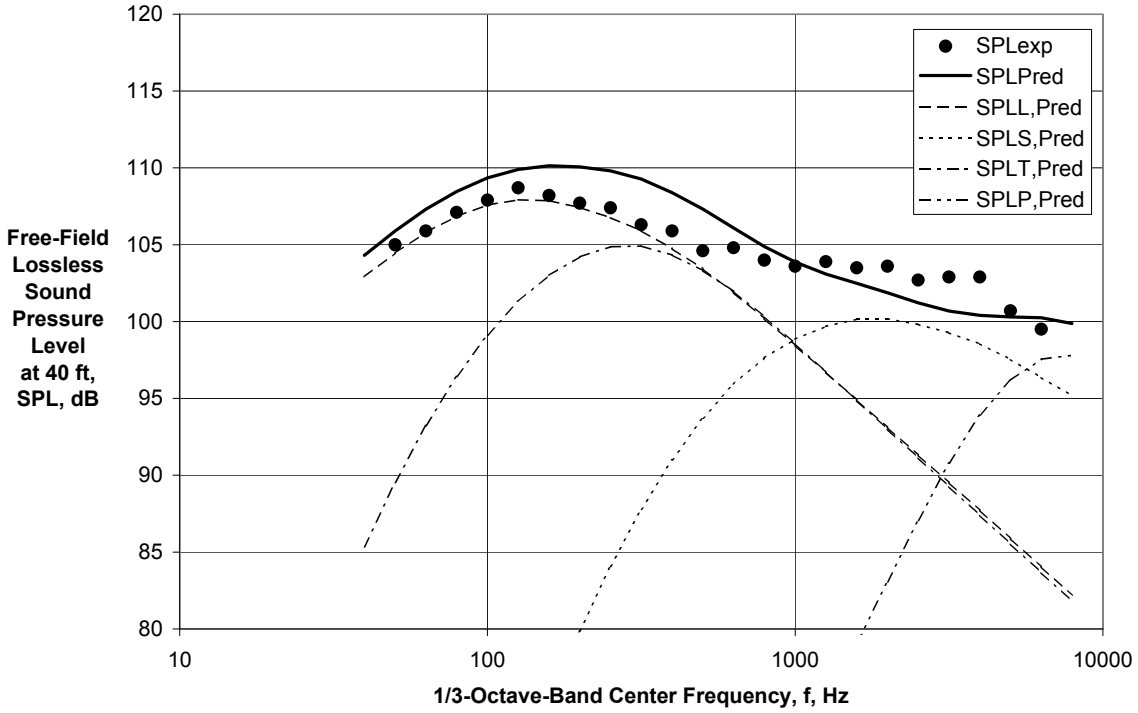

(c) Directivity Angle = 120 deg

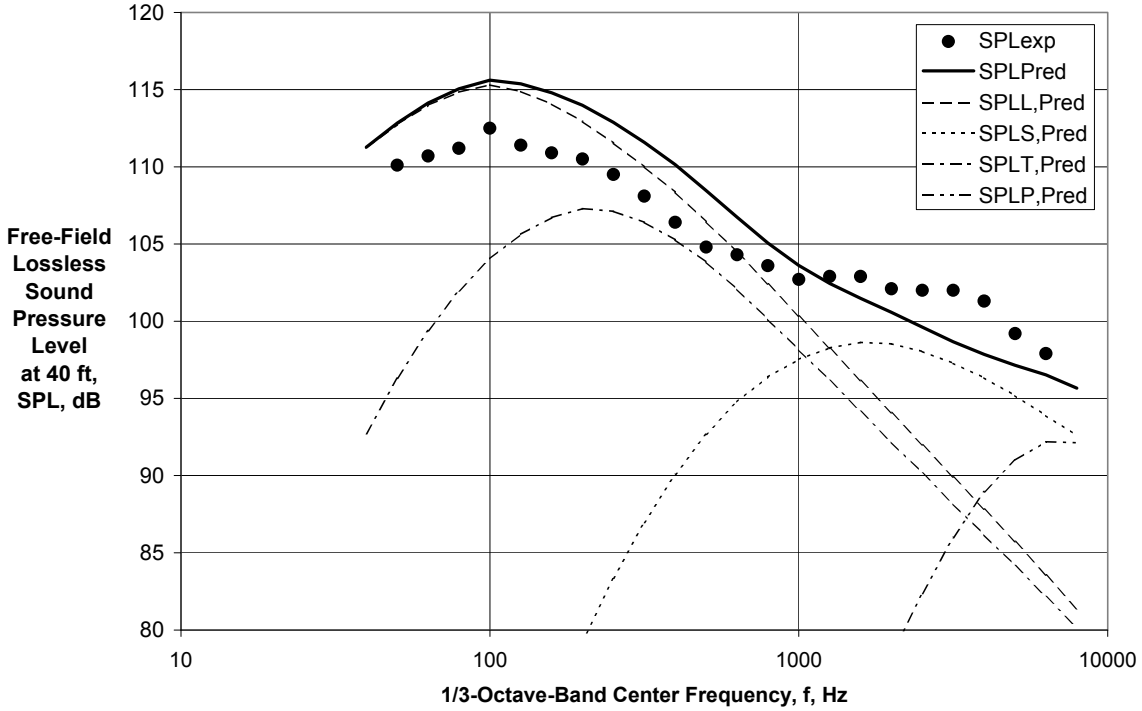

(d) Directivity Angle = 135 deg

Figure 35.—Continued.

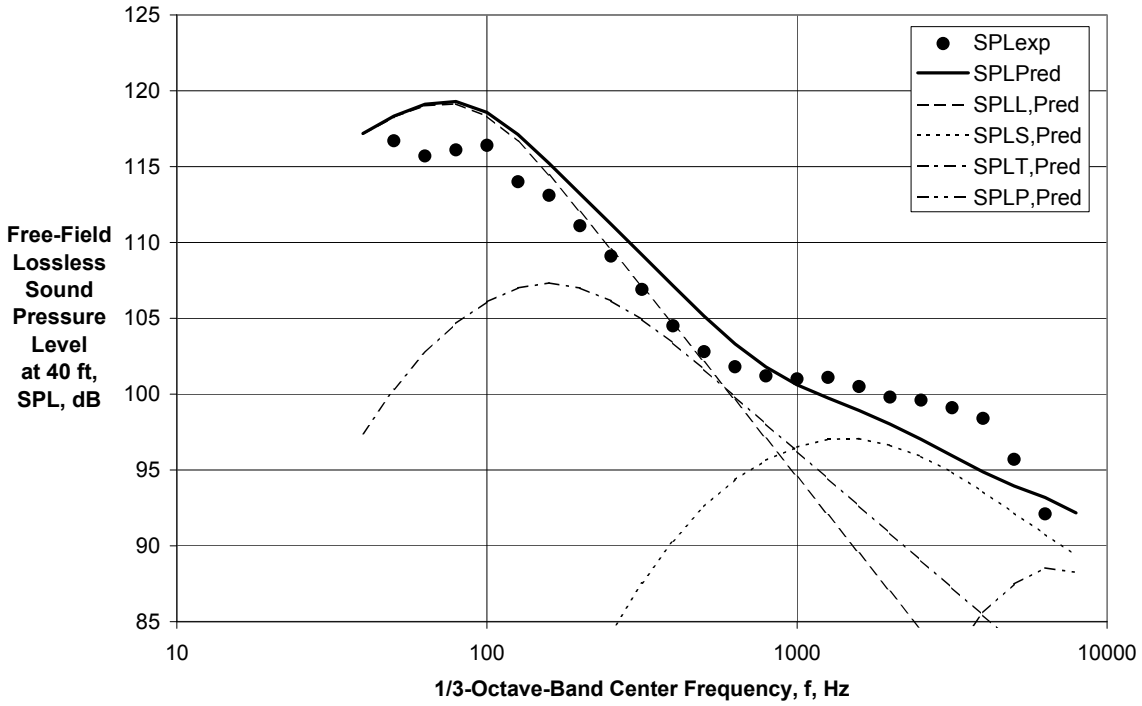

(e) Directivity Angle = 150 deg

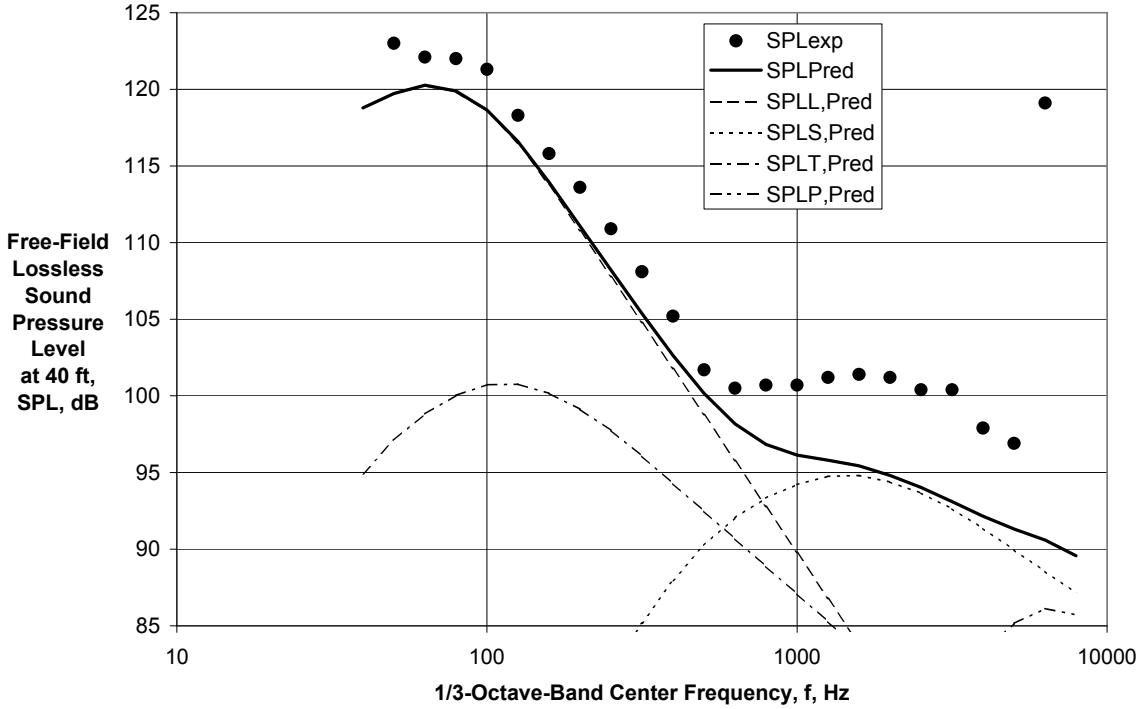

(f) Directivity Angle = 165 deg

Figure 35.—Concluded.

REPORT DOCUMENTATION PAGE	Form Approved OMB No. 0704-0188

1. REPORT DATE *(DD-MM-YYYY)*	2. REPORT TYPE	3. DATES COVERED *(From - To)*
01-03-2009	Technical Memorandum	

4. TITLE AND SUBTITLE
Jet Noise Modeling for Suppressed and Unsuppressed Aircraft in Simulated Flight

5a. CONTRACT NUMBER
NAS3-00178

5b. GRANT NUMBER

5c. PROGRAM ELEMENT NUMBER

6. AUTHOR(S)
Stone, James, R.; Krejsa, Eugene, A.; Clark, Bruce, J.; Berton, Jeffrey, J.

5d. PROJECT NUMBER

5e. TASK NUMBER
10

5f. WORK UNIT NUMBER
WBS 984754.02.07.03.12.02

7. PERFORMING ORGANIZATION NAME(S) AND ADDRESS(ES)
National Aeronautics and Space Administration
John H. Glenn Research Center at Lewis Field
Cleveland, Ohio 44135-3191

8. PERFORMING ORGANIZATION REPORT NUMBER
E-16805

9. SPONSORING/MONITORING AGENCY NAME(S) AND ADDRESS(ES)
National Aeronautics and Space Administration
Washington, DC 20546-0001

10. SPONSORING/MONITORS ACRONYM(S)
NASA

11. SPONSORING/MONITORING REPORT NUMBER
NASA/TM-2009-215524

12. DISTRIBUTION/AVAILABILITY STATEMENT
Unclassified-Unlimited
Subject Category: 07
Available electronically at http://gltrs.grc.nasa.gov
This publication is available from the NASA Center for AeroSpace Information, 301-621-0390

13. SUPPLEMENTARY NOTES

14. ABSTRACT
This document describes the development of further extensions and improvements to the jet noise model developed by Modern Technologies Corporation (MTC) for the National Aeronautics and Space Administration (NASA). The noise component extraction and correlation approach, first used successfully by MTC in developing a noise prediction model for two-dimensional mixer ejector (2DME) nozzles under the High Speed Research (HSR) Program, has been applied to dual-stream nozzles, then extended and improved in earlier tasks under this contract. Under Task 6, the coannular jet noise model was formulated and calibrated with limited scale model data, mainly at high bypass ratio, including a limited-range prediction of the effects of mixing-enhancement nozzle-exit chevrons on jet noise. Under Task 9 this model was extended to a wider range of conditions, particularly those appropriate for a Supersonic Business Jet, with an improvement in simulated flight effects modeling and generalization of the suppressor model. In the present task further comparisons are made over a still wider range of conditions from more test facilities. The model is also further generalized to cover single-stream nozzles of otherwise similar configuration. So the evolution of this prediction/analysis/correlation approach has been in a sense backward, from the complex to the simple; but from this approach a very robust capability is emerging. Also from these studies, some observations emerge relative to theoretical considerations. The purpose of this task is to develop an analytical, semi-empirical jet noise prediction method applicable to takeoff, sideline and approach noise of subsonic and supersonic cruise aircraft over a wide size range. The product of this task is an even more consistent and robust model for the Footprint/Radius (FOOTPR) code than even the Task 9 model. The model is validated for a wider range of cases and statistically quantified for the various reference facilities. The possible role of facility effects will thus be documented. Although the comparisons that can be accomplished within the limited resources of this task are not comprehensive, they provide a broad enough sampling to enable NASA to make an informed decision on how much further effort should be expended on such comparisons. The improved finalized model is incorporated into the FOOTPR code. MTC has also supported the adaptation of this code for incorporation in NASA's Aircraft Noise Prediction Program (ANOPP).

15. SUBJECT TERMS
Jet aircraft noise; Noise prediction; Noise reduction; Aeroacoustics

16. SECURITY CLASSIFICATION OF:			17. LIMITATION OF ABSTRACT	18. NUMBER OF PAGES	19a. NAME OF RESPONSIBLE PERSON
a. REPORT	b. ABSTRACT	c. THIS PAGE			STI Help Desk (email:help@sti.nasa.gov)
U	U	U	UU	113	19b. TELEPHONE NUMBER *(include area code)* 301-621-0390